Semiconducting Polymer Nanospheres
Organic Alternatives to Inorganic Quantum Dots?

Hashim, Zeina

Awarding institution:
King's College London

Title: Semiconducting Polymer Nanospheres

Organic Alternatives to Inorganic Quantum Dots?

Author: Zeina Hashim

KING'S COLLEGE LONDON
University of London

Semiconducting Polymer Nanospheres: Organic Alternatives to Quantum Dots?

by

Zeina Mohamed Abdullah Hashim

A thesis submitted in partial fulfilment for the degree of

Doctor of Philosophy

School of Physical Sciences and Engineering

Department of Physics

2013

Declaration of Authorship

I, Zeina Mohamed Abdullah Hashim, declare that this thesis titled 'Semiconducting Polymer Nanospheres: Organic Alternatives to Quantum Dots?' is the result of the work undertaken between October 2009 and June 2013 under the supervision of Dr Mark Green and Dr Lea Ann Dailey. I confirm that:

- This work was done wholly or mainly while in candidature for a research degree at this University.
- Where any part of this thesis has previously been submitted for a degree or any other qualification at this University or any other institution, this has been clearly stated.
- Where I have consulted the published work of others, this is always clearly attributed.
- Where I have quoted from the work of others, the source is always given. With the exception of such quotations, this thesis is entirely my own work.
- I have acknowledged all main sources of help.
- Where the thesis is based on work done by myself jointly with others, I have made clear exactly what was done by others and what I have contributed myself.

Signed:

Date:

Word Count

Number of Pages: 175

Number of Words: 57472

Abstract

Semiconducting polymer nanospheres are organic conjugated polymer nanoparticles which are synthesized from benign materials and exhibit excellent fluorescence properties. The nanoparticles are generally larger than inorganic quantum dots with a relatively broad size distribution. Quantum dots, on the other hand, which have extensively been developed and synthesized with precise and narrow distributions of a few nanometers in dimensions, are now being widely investigated as bio-imaging agents, despite the rising concerns about their toxic compositions. Therefore, advances in the synthesis of the organic nanoparticles and investigations into their suitability as alternatives to quantum dots need to be explored.

The 'size problem' of semiconducting polymer nanospheres – polymer particles are significantly larger than quantum dots – was first tackled in this work. With modifications to the miniemulsion-evaporation synthesis method, narrowly distributed quantum dot-sized nanoparticles with diameters as small as 2 nm were synthesized. These organic nanoparticles which were capped/entwined with poly(ethylene) glycol (PEG), a Food and Drug Administration (FDA) approved surfactant, were found to conserve most of the optical properties of their constituent polymers, and are therefore expected to be useful in bio-imaging applications similar to their larger counterparts.

A second nanoparticle system with a dual-modality was then prepared; semiconducting polymer nanospheres capped/entwined with three amphiphilic lipids one of which was gadolinium – diethylene triamine pentacetate, a Magnetic Resonance Imaging (MRI) active ligand. These bimodal nanoparticles also maintained their optical properties, were readily taken up by two cell lines, were distinguishable from the auto-fluorescence of animal tissue, and were found to be MRI-active as revealed by their MRI relaxivity measurements.

Finally, the optimized organic nanoparticles and similarly coated quantum dots were investigated for their potential to interact with human blood components, a physiological system which may be very relevant for semiconducting polymer nanospheres used as medical diagnostic agents. The preliminary *ex-vivo* studies performed revealed that similarly coated organic nanoparticles and quantum dots did not induce platelet aggregation or alter aggregation behaviour in response to a physiological agonist. Further, no evidence of platelet activation, neutrophil activation or increases in platelet-monocyte adhesion was observed. This implied that introduction of the nanoparticles to the blood stream at the concentrations tested may not elicit acute pro-inflammatory effects or alter normal coagulation pathways, although further rigorous evaluation in this area is still required. Fluorescence imaging showed that the organic nanoparticles were taken up by different blood cells and also showed some evidence of adhesion to their surfaces, a property which might find an application in the future. Ultimately, more short-term and long-term safety studies (*in-vitro*, *ex-vitro*, and *in-vivo*) must be conducted before deriving any further conclusions.

Acknowledgements

Many thanks to Allah, Whom can never be thanked enough.
Many thanks to Him for giving me life, health, and power to reach this level in my path towards PhD
"Alhamdu-li-llah"

Many thanks to my parents "Mohamed Hashim" and "Mona Baarma", my husband; "Ali Almadodi", both our sons "Malik" and "Hamza", and all members of our families for their support.

Many thanks to Dr Mark Green, who is by all means "a perfect supervisor".

Many thanks to King Abdulaziz Universtiy in Saudi Arabia for their Scholarship. Many thanks to Dr Zain Yamani, King Fahad University of Petroleum and Minerals in Saudi Arabia, for his encouragement and support.

Many thanks to Dr Lea Ann Dailey, my second supervisor, for her supervision and joint work on the "Nanoparticles' Interactions with Human Blood Studies". Many thanks for her enlightening ideas, her kindness, seriousness, and modesty.

Many thanks to Dr Philip Howes who guided me in my first experiments and who sincerely shared his knowledge with me and frequently enlightened me with his useful advice.

Many thanks to Raha Ahmadkhanbeigi, from the Pharmaceutical Sciences Division in KCL, who jointly worked with me on a daily basis on the "Nanoparticles' Interactions with Human Blood Studies" presented in this thesis. Many thanks for her effort, her company, and friendship.

Many thanks to all members of my group: Dr Melanie Bottrill, Dr Arunkumar Panneerselvam, Wijittra Wichiansee, Hassan Mirzai, and specially Dr Shohei Taniguchi, for their company and friendship during both easy and tough days.

Many thanks to KCL members; Dr Anthony Brain, Dr Fiona Winning, and Dr Alice Warley for TEM assistance, Dr Andrew Cakebread for mass spectrometry, and Mr David Parker for EPR measurements.

Many thanks to Dr Pei Hua Chung and Dr Klaus Suhling, from the physics department in KCL, Dr Andrea Protti, Dr Alkystis Phinikaridou, and Dr Rene Botnar from the Imaging Sciences Division in KCL, Dr Abhinav Kumar, Dr Maya Thanou, and Dr Simon Pitchford from the Pharmaceutical Sciences Division in KCL, Ms Agnieszka Siupa from NanoSight NTA Company, UK, and Ms Nicola J. Commander and Ms Jo Scott from DSTL Porton Down, Salisbury, UK, for their collaboration.

To the World

Table of Contents

List of Figures

List of Tables

Abbreviations

AA	:	Ascorbic acid
ADP	:	Adenosine diphosphate
ADS108GE	:	Poly((9,9-dioctyl-2,7-divinylene-fluorenylene)-alt-co-(2-methoxy-5-(2-ethyl-hexyloxy)-1,4-phenylene))
BEHP-PPV	:	Poly(2-(2′,5′-bis(2″-ethylhexyloxy)phenyl)-1,4-phenylenevinylene)
CCM	:	Cell culture medium
CD11b	:	α_M integrin chain; a cell surface receptor found on activated neutrophils
CD14	:	GPI-anchored cell surface glycoprotein expressed on monocytes
CD16	:	GPI-anchored integral membrane glycoprotein expressed on neutrophils
CD41a	:	GPIIb/IIIa glycoproteins on the surface of non-activated platelets
CD62P	:	P-selectin platelet alpha-granule membrane protein
CdSe/ZnS	:	A cadmium selenide core with a zinc sulphide shell
$CHCl_3$	:	Chloroform
cPS	:	Carboxylated polystyrene nanoparticles
cQD	:	Carboxylic quantum dot
CuO	:	Copper oxide
DAPI	:	4',6-diamidino-2-phenylindole
DCM	:	Dichloromethane
DLS	:	Dynamic Light Scattering
DMEM	:	Dulbecco's modified eagle's medium
DMPO	:	Spin trap (5-tert-butoxy carbonyl-5-methyl-1-pyrroline-N-oxide)
DPPC	:	1,2-Dipalmitoyl-sn-glycero-3-phosphocholine
DSPE-PEG2000 carboxylic acid	:	1,2-distearoyl-sn-glycero-3-phosphoethanolamine-N [carboxy(polyethylene glycol)-2000] (ammonium salt)
DTPA	:	Diethylene triamine pentaacetic acid
ELISA	:	Enzyme-linked immunosorbent assay
EPR	:	Electron paramagnetic resonance
FACS	:	Fluorescence-activated cell sorting in flow cytometry
F8BT	:	Poly[(9,9-di-*n*-octylfluorenyl-2,7-diyl)-*alt* (benzo[2,1,3]thiadiazol-4,8-diyl)]
FBS	:	fetal bovine serum
Gd-DTPA-BSA	:	(diethylenetriaminepentaacetic acid)-bis(stearylamide) (gadolinium salt)
Gd-SPNs	:	Bifunctional gadolinium semiconducting polymer nanospheres

(Gd-SPNs)-IgG	:	IgG antibody conjugated Gd-SPNs
GPIIb/IIIa	:	Glycoprotein IIb/IIIa
HCl	:	Hydrogen chloride
HeLa	:	A human epithelial cell line
IgG	:	Immunoglobulin G
MEH-PPV	:	Poly(2-methoxy-5-(2-ethylhexyloxy)-1,4-phenylene vinylene)
MRI	:	Magnetic Resonance Imaging
MW	:	Molecular weight
MWCO	:	Molecular weight cut off membrane
NaCl	:	Sodium chloride
NaOH	:	Sodium hydroxide
NaN_3	:	Sodium azide
NTA	:	Nanoparticle tracking analysis
PBS	:	phosphate buffered saline
PEG	:	Polyethylene glycol
PEG300	:	Polyethylene glycol with a molecular weight = 300
PEG2000-PE	:	1,2-dipalmitoyl-sn-glycero-3-phosphoethanolamine-N-[methoxy(polyethyleneglycol)-2000] (ammonium salt)
PEG-dithiol	:	Poly(ethylene glycol) dithiol
PPE	:	Poly[2,5-di(3',7'-dimethyloctyl)phenylene-1,4-ethynylene]
PPM	:	Parts per million
PPP	:	Platelet poor plasma
PPV	:	Poly(*p*-phenylene vinylene)
PRP	:	Platelet rich plasma
QD	:	Quantum dot
QY	:	Quantum yield
r_1	:	Relaxivity in T1–weighted Magnetic Resonance Imaging
R1	:	Relaxation rate in T1–weighted Magnetic Resonance Imaging
RCF	:	Relative centrifugal force
RPM	:	Revolutions per minute
SDS	:	Sodium dodecyl sulphate
SPNs	:	Semiconducting polymer nanospheres
TEM	:	Transmission Electron Microscopy
TiO_2	:	Titanium dioxide nanoparticles
VWF	:	Von Willebrand Factor

1 Introduction

The prefix “nano” is the Greek word that means “dwarf” [1]. The prefex “nano” is a scale of length and refers to 10^{-9} of a metre. i.e. 1 nm equals 0.000000001 m.

Although the concepts of nanotechnology were first referred to by Richard Feynman in 1958, the term “nanotechnology” was not introduced until 1974 [1-3]. By then, Taniguchi *et. al.* defined nanotechnology as “the processing, separation, consolidation, and deformation of materials by 1 atom or by 1 molecule” [3].

In 2004, “nanotechnology” was defined by the *Royal Society/Royal Academy of Engineering* in the United Kingdom as “the design, characterisation, production and application of structures, devices and systems by controlling shape and size at nanometre scale”, and “nanoscience” was defined as “the study of phenomena and manipulation of materials at atomic, molecular and macromolecular scales, where properties differ significantly from those at a larger scale”.[1]

Research in nanoscience and nanotechnology has combined many disciplines such as physics [4], chemistry [5], biology [6], engineering [7-9], and medicine [3, 10-12] into one identity. Scientists with different expertise, who previously worked only within the realm of their expertise, now work together and share their knowledge to achieve their multidisciplinary goals. Because of this multidisciplinary manner of such an emerging field, research is dramatically increasing, with the number of published documents, including articles and books, rising almost exponentially [13-14] over the years (Figure 1).

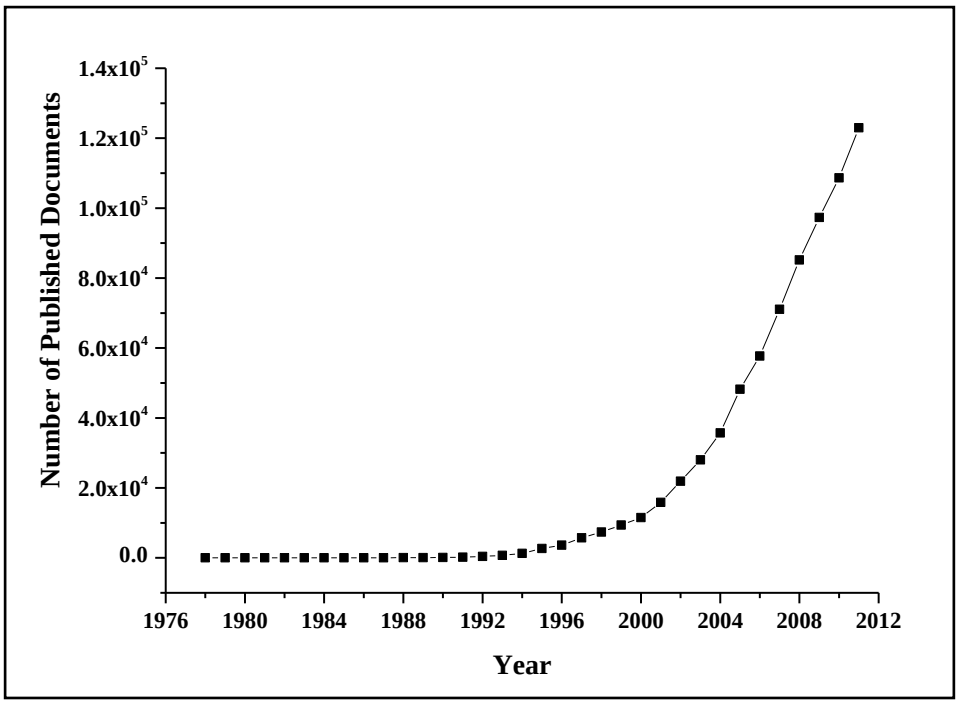

Figure 1 The number of published documents which are related to nanoscience and technology throughout the years. Data collected from the Web of Knowledge, All

Databases, King's College London's access, on 20 May 2012. Search done in English, on: (nanotechnolog* OR nanoscience OR nanomaterial* OR nanoparticle* OR nanotube* OR nanorod* OR nanosphere* OR "quantum dot"* OR nanosheet* OR nanowire*), under the (topic) category.

1.1 Nanoparticles

1.1.1 Definition and History

With the development of nanoscience and technology, official attempts to define the newly arising nanomaterials were also made. According to the *Royal Society/Royal Academy of Engineering*, July 2004, nanoparticles were defined as follows: "We classify nanoparticles to be particles of less than 100 nm in diameter that exhibit new or enhanced size-dependent properties compared with large particles of the same material" [1]. Another general definition was made by the British Standards Institution (BSI), in their PAS71:2011 document, describing a nanoparticle to be a material with its three external dimensions in the nano-scale, clarifying a nanoscale to be a size range between approximately 1 and 100 nm [15].

1.1.2 Nanoparticles Synthesis Routes in a Nutshell

Nanoparticles have existed on earth for thousands of years; nanoparticles have been produced by plants, natural erosion processes, and volcanic activities.[16-17] Man-made nanoparticles, however, were initially generated unintentionally for some time. Metal nanoparticles imbedded in glass, for example, were made by glass craftsmen in a process invented to produce light-induced changeable coloured glass such as that of the Lycurgus Cup which was dated back to the 4th century AD.[18]

The first reported synthesis of nanoparticles was in 1857 by Faraday, who synthesised and studied the colour of gold nanoparticles which he referred to as colloidal gold.[18] Since then, the syntheses of many nanoparticles, under various names, were reported, until the nomenclature "nanoparticle" was introduced.

Nowadays, the synthesis methods of nanoparticles usually follow a top-down or a bottom-up synthesis route [1] or a combination of both [19-20]. In the top-down approach, materials with large scales are reduced in size to smaller dimensions. Examples of well established synthesis methods that use this approach are nano-imprint lithography [21], photolithography [21], and e-beam lithography [22]. In the bottom-up approach, atoms, molecules, or smaller nanoparticles are used as the building blocks in the synthesis of the required nano-structures. Such an approach usually involves chemical reactions as in the syntheses of most quantum dots [23] or self-assembly as in the formation of polymer nanoparticles from ready-made polymers *via* emulsion-solvent

evaporation or precipitation techniques [24], self-assembly with the assistance of biological reactors as in the synthesis of antimony sulphide nanoparticles using microorganisms [25], or a combination of techniques as in miniemulsion polymerisations which involve both physical actions and chemical reactions [26]. The combined top-down and bottom-up approaches are sometimes used to overcome obstacles or to improve the outcomes of the synthesis of a certain type of nanoparticles using only one of the approaches [19-20].

Regardless of the synthesis method used, nanoparticles can be directly synthesised in solution, or they can be etched or formed by deposition on different surfaces.

1.1.3 Common Properties of Nanoparticles and their Applications in Biology

1.1.3.1 Common Properties of Nanoparticles

Nanoparticles can be synthesised in different shapes which, if specified, can be used to denote different nomenclatures to the nanoparticles. For example, spherical nanoparticles are interchangeably called “nanospheres”, rod-shaped nanoparticles are usually called “nanorods”, and polyhedron-shaped nanoparticles are sometimes called “nanoprisms”.

Nanoparticles can be organic or inorganic, they can exist as crystalline or amorphous structures [27], and they can be in a single core construction, or in a core/shell or core/multi-shell construction. Quantum dots and polymer nanoparticles are examples of such systems.

An important feature which distinguishes nanoparticles from bulk materials is the increase in their surface-to-volume ratio as their size decreases. This results in an increase in their surface-related properties, such as reactivity. Therefore, nanoparticles can be highly reactive, favouring aggregation or adsorption of certain molecules, and they can be extremely interactive with their surrounding environment. An example of a highly reactive surface is that of a crystalline nanoparticle which includes “dangling-bonds” from the atoms in the incomplete lattice units of its outer surface.

To stabilise the surface and reduce these bare-surface related phenomena, nanoparticles can be coated with different coatings which occupy and neutralize their reactive sites and sometimes produce an electrostatic repulsive force between the nanoparticles, especially those tending to aggregate. Examples of such coatings are silica shells, molecular ligands, amphiphilic polymers, or functionalized alkyl chains [28-30].

Capping of the nanoparticles also facilitates the functionalisation of their surfaces for specific applications such as molecular targeting. It can also be used to phase-transfer the nanoparticles and change their solubility which depends on the chemical structures of the nanoparticles’ capping agents. For example, nanoparticles which are not dispersible in water can be made aqueous by capping the particles with amphiphilic molecules which have a hydrophobic part that adsorbs on

the nanoparticles' surfaces and a hydrophilic part which assists their aqueous dispersion in water.

Another important feature is that they have unique properties which arise from their nanometre sizes. When the dimensions of materials are reduced to this scale, their properties are solely governed by quantum mechanics. These quantum mechanical effects are usually dominated when the nanoparticle's dimensions are below a specific value such as the excitonic Bohr radius in inorganic semiconductors [31] and the characteristic Weiss domain in superparamagnetic and magnetic materials [32].

Therefore, many nanoparticles have unique optical and electrical properties which are size and shape dependent. Examples are noble metal nanoparticles and inorganic semiconductor nanoparticles. Noble metal nanoparticles have changeable plasmonic properties which are observed as a change in the nanoparticles' colour with the change in their size or shape, while inorganic semiconductor nanoparticles have size and shape-dependent tuneable bandgaps which result in changeable electrical and fluorescence properties.

1.1.3.2 Biological Applications of Nanoparticles

Due to the above mentioned phenomena, nanoparticles found many applications and are being proposed as alternatives to many conventional materials in numerous research areas. In biology, nanoparticles are beings studied as medical diagnostic and therapeutic tools.[33] This is because they have comparable sizes to many biological species and are able to interact with their environment while conserving their properties of interest such as magnetism and fluorescence. Therefore, many nanoparticles are now being explored as fluorescence imaging probes [34-36], as magnetic resonance imaging contrast agents [37-41], as drug delivery vehicles [42-44], as radioactive agents for cancer treatment [45], and in many pathological studies [46].

Capping of the nanoparticles can be used to improve their bio-compatibility, increase their circulation time, decrease their non-specific binding to the contents of their environment, and phase-transfer them to aqueous media in preparation for their use within biology.[47]

Many nanoparticles have already proved efficient in cell imaging, enhancing the sensitivity and improving the resolution of many conventional diagnostic techniques, and increasing our current knowledge of the cellular interactions and processes.[48] With further developments, nanoparticles can be very powerful tools in medicine and can serve as effective imaging agents for more sophisticated methods such as multiphoton fluorescence imaging [49] and single molecule spectroscopy [50-51].

1.1.4 Nanoparticles as Fluorescence Bio-imaging, Labelling, and Tracking Agents

All materials absorb electromagnetic waves (photons) with certain energies and therefore have unique absorption spectra. These absorption spectra are associated with the energy levels of the

materials where electrons from the ground states absorb only the photons which have energies equal to the energy difference (gaps) between their ground state and excited states and therefore travel to the excited states. Those excited electrons decay to their ground state either radiatively or non-radiatively depending on the type of material. Radiative decay of the electrons results in the emission of a photon.

Fluorescence is the emission of light with a lower energy than that of the absorbed exciting energy. This is because both radiative and non-radiative processes occur where an excited electron first decays non-radiatively within its excited states reaching the excited state with the lowest energy, then decays radiatively to its ground state emitting the excess energy as a photon, as illustrated in Figure 2.

Because fluorescent materials emit light with a different wavelength than that absorbed, they were found to be useful in many applications such as biological imaging, labelling and tracking.

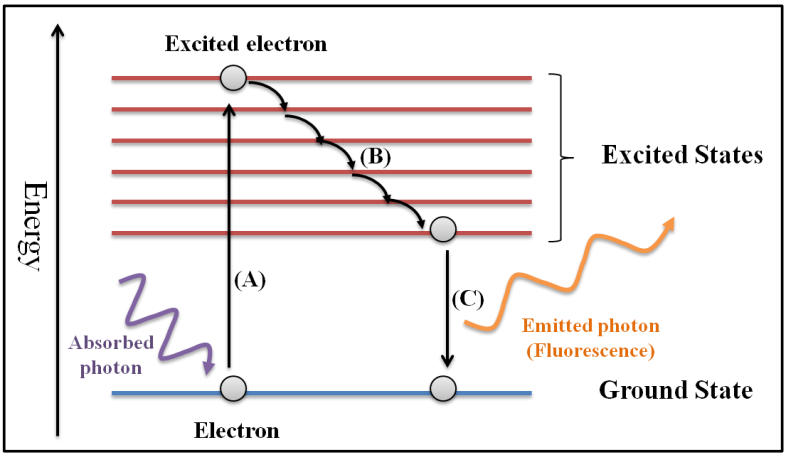

Figure 2 An illustration of the energy levels of a fluorescent material. During fluorescence, a photon with a suitable energy is absorbed and an electron is excited from its ground state to an excited state (path A). Then it decays non-radiatively within the excited states (path B), and finally decays radiatively and returns to its ground state (path C) emitting a photon with a lower energy than that of the absorbed photon.

Biological studies involve the experimentation with, and observation of, the biological samples in one or more of the following main settings; *in-vitro* (in a laboratory vessel), *in-vivo* (within the natural setting or living organism), and *ex-vivo* (outside the living organism).

The organelles of cells *in-vitro* are almost optically transparent, therefore, to distinguish between the different organelles some form of colour labelling is required.[52] This can be achieved by the use of suitable non-toxic fluorescent labels which can be excited with an undamaging tuned frequency of light and detected with conventional optical microscopes. In the imaging process, the natural fluorescence which is emitted from some parts of the cells under excitation, auto-fluorescence, is easily compensated for, and currently cell imaging using this fluorescence labelling technique is widely used. In more complex biological samples however, this

process is more complicated because the absorption of a substantial region of the light spectrum is present and auto-fluorescence of the biological samples is increased, therefore, special labels which absorb and emit in the available transparent optical window, such as the near-infrared region [53], are required.

Traditional organic fluorescent probes which are currently being used as cell imaging agents are organic fluorophores. The fluorophores' fluorescent property arises from their chemical structure (see section1.3.3 for further details on the relationship between the chemical structure of molecules and their optical properties). The functional groups of the fluorophores, which can be chemically modified prior to the imaging process, enable them to be directly attached to the biological sample under study, or to be attached to a targeting biomolecule such as an antibody which can then bind to the sample of interest.[52, 54]

Although these conventional imaging probes proved relatively safe and efficient, they have their limitations which restrict their use in many areas. For example, many fluorophores have wide emission spectra, a problem which limits their use in multicolour imaging.[55] Moreover, fluorophores are prone to fast photo-bleaching under exposure to prolonged optical excitations. Photo-bleaching is the weakening and eventual disappearance of fluorescence due to irreversible photo-induced reactions such as oxidation. Traditional fluorophores are also very sensitive to their environment; they change their conformation with the fluctuations of temperature, for example. Conformational damage causes a loss in fluorescence and conformational fluctuations induce fluorescence blinking. Fluorescence blinking is a phenomenon where the fluorescence of single molecules is switched "on" and "off", a phenomena which is not always desired.[52, 56]

Fluorescent nanoparticles were found to overcome many of these problems.[6, 57-59] Examples of such nanoparticles are some noble metal nanoparticles [60-61], fluorescent silica nanoparticles [62-63], fluorescently labelled micelles [64], quantum dots [56], and semiconducting polymer nanospheres which are the main focus of this thesis.

1.2 Quantum Dots

1.2.1 Definition and History

Quantum dots (QDs) are nano-sized crystals (nanoparticles) of inorganic semiconducting materials [46] which were first synthesised in the 1980s [14]. The nano-sizes of these inorganic semiconductor nanoparticles cause their electrons to be confined in all three dimensions so that they are localised in discrete energy levels controlled by quantum mechanical laws.[65] Due to the three dimensional confinement of electrons, these nanoparticles are often called zero-dimensional structures (0-D) [66], and because of their size-related arising quantum effects, they are also called quantum dots (QD) [14].

QDs not only exhibit unique electrical properties which make them useful in the semiconductor industries [67-68], but also fluoresce in the visible region when exposed to suitable higher energies which also makes them possible alternatives to conventional fluorophores in the bio-imaging and medical diagnostic fields.[14, 46, 54, 56, 69-70]

1.2.2 An Overview of the Physical and Chemical Properties of Quantum Dots

1.2.2.1 Composition and Physical Properties of Quantum Dots

QDs are crystalline in structure. i.e. their atoms are arranged in a three-dimensional periodic order so that their smallest repetitive unit is identified as a lattice with characteristic lattice constants.[71] The atoms which form these nanocrystals are those of the periodic table which are known to be compositions of bulk, elemental or compound, semiconductors in either an intrinsic [23] or extrinsic [72-74] form. Silicon [57, 75] and germanium [23, 76] QDs are examples of inorganic elemental semiconductor nanoparticles, while CdSe [74], CdTe [48], ZnSe [73] and HgSe [77] QDs (II-VI semiconductors), InP [48] and GaSb [78] QDs (III-V semiconductors), or PbS [68] QDs (IV-VI semiconductors) are examples of inorganic compound semiconductor nanoparticles. Furthermore, QDs can be synthesised from a single semiconductor such as silicon QDs [57, 75] and CdSe QDs [79], or from several semiconductors in core/shell or core/multi-shell structures such as CdSe/ZnS [80] and CdTe/CdSe/ZnSe [81] QDs. Depending on the QDs' synthesis parameters, they can be formed with specific shapes such as rods [65, 80], spheres [65], pyramids [82], or tetrapod-shaped heterostructures [80], etc, they can also be tuned [83] to different sizes, ranging between 1 – 20 nm [14] with very low polydispersities [81].

1.2.2.2 Chemical Stability, Surface Modifications and Coatings of Quantum Dots

QDs are typically stored in temperatures below 4 ^{o}C under light exclusion [84]. QDs are very sensitive and fragile nanomaterials. They can undergo rapid oxidation when exposed to different environments (e.g. PbSe nanocrystals oxidise rapidly when exposed to air [85]), their elemental ions can leach from their core materials [86], and they can be very reactive with their environment because of their increased surface areas. Such chemical instability can cause a rapid loss of their desired optical properties (quenching), with many non-chemically stable QDs reported to have a very short shelf life.[87]

Surface modifications were found to improve the QDs' chemical stability (decrease ionic leaching and prevent oxidation), conserve their optical properties, and improve their bio-compatibility.[88] Surface modifications were also performed to phase-transfer QDs from their usual organic solvents to aqueous media in preparation for their use in many applications such as bio-imaging. An example of such surface modifications is the addition of a ZnSe shell to

CdTe/CdSe core/shell QDs which acts as an electron-hole internaliser and a cadmium-leaching preventer.[81] Another example is capping CdS QDs with silica shells to improve their bio-compatibility and photostability and increase their shelf life.[88]

1.2.3 General Applications of Quantum Dots

Quantum dots, with their unique optical and electrical properties proved highly useful in many applications. Most importantly, in both electrical applications, such as transistors, light emitting devices, lasers, and photovoltaics [67-68, 72, 89-92], and in biological applications, such as cell imaging, and bio-labelling and tracking [46, 48, 54, 56-58, 69, 93-97].

As our focus in this work is on providing organic semiconducting polymer nanoparticles, which might be good alternatives to QDs for bio-imaging applications, the following sections will only consider relevant studies done using QDs.

1.2.4 Quantum Dots as Fluorescence Bio-imaging, Labelling, and Tracking Agents

The fundamental studies using quantum dots as fluorescence imaging agents were reported in 1998 by Bruchez *et al.* [55] and Chan *et al.* [98]. Both groups used CdSe/ZnS QDs, which were made aqueous by either coating them with silica shells or by attaching a linking molecule to their surfaces which made them water soluble.[81]

Since then, among all types of nanoparticles, quantum dots have received the most attention in this field.[29, 47, 49, 52, 94, 99-102] Before the emergence of alternatives to quantum dots, such as semiconducting polymer nanospheres, quantum dots were found to be the best imaging agents *in-vitro* and *in-vivo* exceeding conventional fluorophores in several aspects [52, 55]. Quantum dots have size and material-tuneable emission peaks (400 nm – 2 μm [55]) which are separated from their excitation peaks with considerable Stokes shifts. Their emission spectra are narrow and symmetric (typical emission widths of 20 – 30 nm in the visible region [55]) while they absorb light in a very wide range, facilitating multiplex detection [103] and conserving the characteristics of the emission peaks regardless to the excitation energy used [55]. They do not photo-bleach as fast as fluorescent dyes (typical CdSe/ZnS QDs are 100 times more stable against photo-bleaching than conventional organic dyes [98]), and are considered very bright. Also, quantum dots have tunable-surface properties which can be modified by functionalisation with a range of surfactants.[29, 52, 56, 96]

However, significant issues evolved regarding the safety of use of these materials in the biological and medical fields because many quantum dots contain toxic inorganic elements such as mercury and cadmium. These will be discussed in detail in section (1.2.5).

1.2.5 Limitations of Quantum Dots' use as Bio-imaging Agents

Until recently, the most suitable and commercially available quantum dots were cadmium-based. Cadmium is toxic in its ionic form [54, 103-104], therefore, many toxicity studies were conducted on those quantum dots and several issues were revealed.[104-109] Other than the toxic contents which were found to leach from the QDs into the biological environment [110], it has been reported that the surface interactions of the QDs with their surroundings can also cause a problem [111]. It has also been reported that QDs can cause DNA damage [112-113].

To prevent the surface interactions and leaching of the toxic contents of QDs and to increase their biocompatibility, QDs can be coated with effective coatings such as silica shells and polymers.[88, 110-111, 114-115] However, this gives rise to another problem, especially if used *in-vivo*, as their increased size disables them from being renal-cleared.[116] This can also give rise to long term toxicity issues.[103]

Another limitation which hinders the QDs' use as bio-imaging agents, other than their toxicity issues, is the high sensitivity of their optical properties to their structure. Any damage to part of their surface can cause a loss of fluorescence. Damage can occur with phase-transfer or with the capping treatments needed to increase their biocompatibility [117]. Damage of the QDs' optical properties can also occur during the procedures involved prior to the imaging of the biological samples.

With these limitations, the search for alternative nanoparticle probes, for *in-vivo* and *in-vitro* bio-imaging applications, with competing properties is now under study.[36, 70, 118-123]

1.3 Semiconducting Polymer Nanospheres

1.3.1 Definition and History

1.3.1.1 Polymers

The word "Polymer" is derived from two Greek words; "*Poly*" meaning "many" and "*meros*" meaning "parts". This Greek naming is directly related to a common property of these materials which is their huge chemical structure that is composed of many parts.

Polymers have occurred in nature since the beginning of life, in the form of proteins, fibres, and rubbers etc. After the development of polymer chemistry, these were given the name "naturally occurring polymers" or biopolymers. During the 19^{th} century, experimentalists tried to improve the properties of these natural materials by mixing them with different chemicals and exposing them to severe conditions.[124] The discovery of the first synthetic polymer was announced in 1907 by Leo Baekeland, given the name Bakelite.[124] During the 20^{th} century, extensive work was done to explore, experiment, and develop a theoretical understanding of these large molecules [124], and at

present, polymers have a well defined chemistry. They are easily synthesized and are used in a wide range of applications: in coatings, textiles and ceramics, electronic and optical devices such as LEDs, and in many other commercial products.

Polymers are composed of a chain of carbon atoms covalently bonded forming the back-bone of the polymer. The structure of a polymer can be described by a repeated unit, called a monomer, which is repeated many times. Figure 3 shows the chemical structure of a well known simple polymer, polyethylene (PE). The number of the repetition of the monomer unit is called the degree of polymerization (*n* in Figure 3). A small polymer is called an *oligopolymer* or *oligomer*, which has a very low degree of polymerization (less than 10 repeated units). There are many different types of polymers which can be grouped according to their chemical structure, constituents, or orientation.[125]

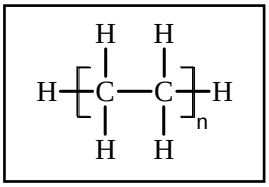

Figure 3 The chemical structure of polyethylene (PE). The polymer is synthesised from ethylene, the monomer, which is the structure between the square brackets but with a double bond between the carbon atoms. The degree of polymerisation is (n).

1.3.1.2 Conjugated (Semiconducting) Polymers

Conjugated polymers are polymers which have alternating multiple and single bonds along their backbone as illustrated in Figure 4. The length of uninterrupted conjugated chain segments in a polymer is called the conjugation length. The conjugation along the chains gives these polymers a bandgap which enables them to be thought of as alternatives to inorganic semiconducting materials and are therefore interchangeably called "semiconducting polymers". Also, many conjugated polymers have the potential to fluoresce when excited with a suitable energy, a property which is unobtainable with non-conjugated organic materials. These opto-electrical properties will be discussed in detail in section 1.3.3.

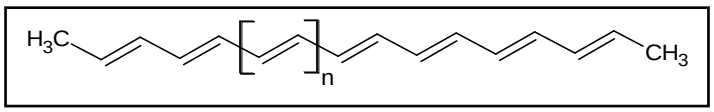

Figure 4 The backbone chain of a simple conjugated polymer.

The first conjugated polymer was discovered by mistake in 1974.[126] After that, extensive research in the synthesis of conjugated polymers with different properties started to take place, and numerous conjugated polymers were reported over the years. At present, many fluorescent conjugated polymers are synthesised and a large number of them is now manufactured and

commercially available. Taking this advantage, we used five of these polymers in this work: poly[2-(2',5'-bis(2''-ethylhexyloxy)phenyl)-1,4-phenylenevinylene] (BEHP-PPV, minimum MW 30000 g/mol), poly[2-methoxy-5-(2-ethylhexyloxy)-1,4-phenylenevinylene] (MEH-PPV, MW 40000 – 70000 g/mol), poly[(9,9-di-*n*-octylfluorenyl-2,7-diyl)-*alt*-(benzo[2,1,3]thiadiazol-4,8-diyl)] (F8BT, MW 5000 – 8000 g/mol), poly[2,5-di(3',7'-dimethyloctyl)phenylene-1,4-ethynylene] (PPE, MW 4122 g/mol), and poly[(9,9-dioctyl-2,7-divinylene-fluorenylene)-alt-co-(2-methoxy-5-(2-ethyl-hexyloxy)-1,4-phenylene)] (ADS108GE, MW 111000 g/mol). Their structures and their absorption and emission spectra are presented in Figure 5.

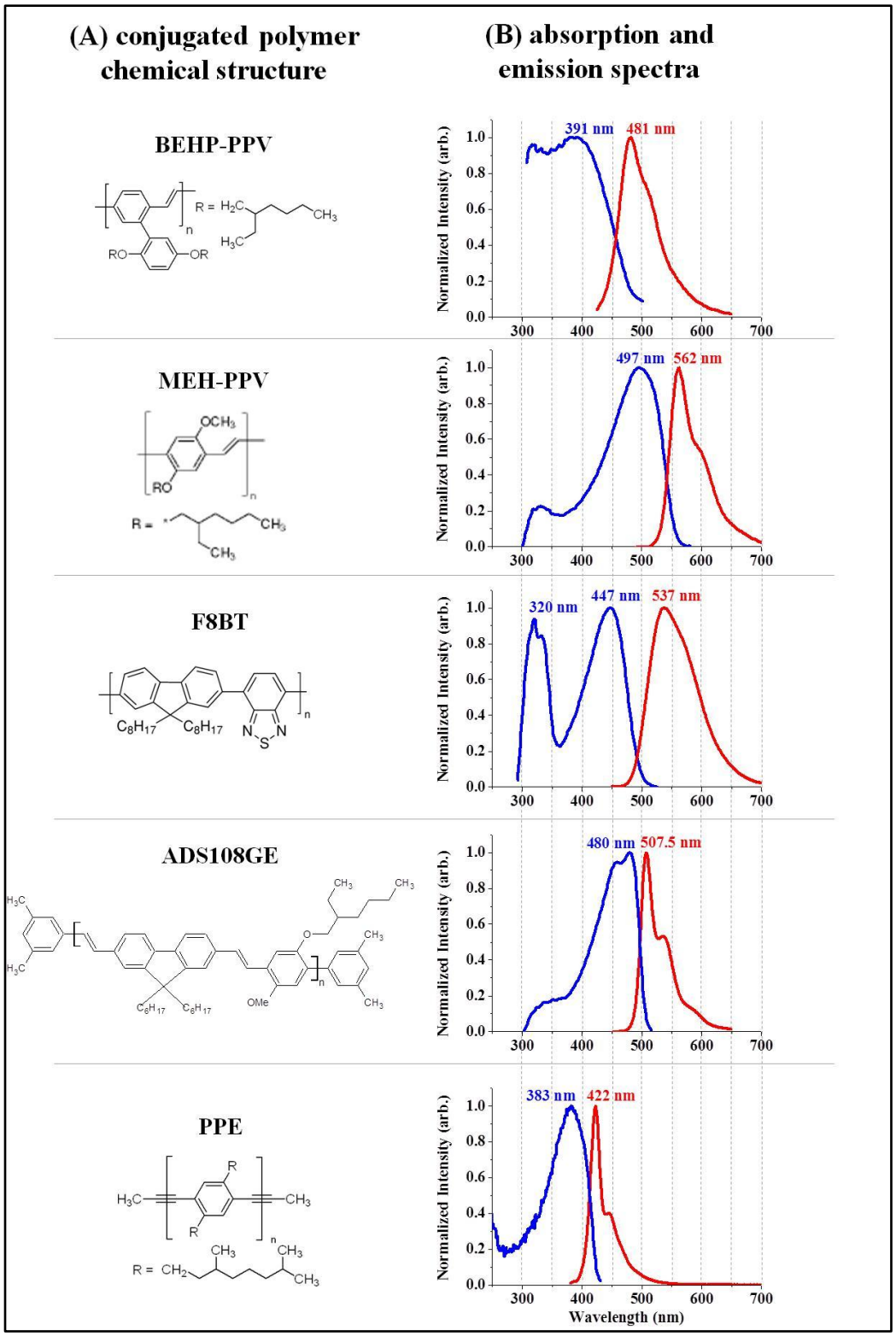

Figure 5 The chemical structures [127-129] and optical properties of five fluorescent conjugated polymers; BEHP-PPV, MEH-PPV, F8BT, ADS108GE, and PPE; (A) Their chemical structures, and (B) their absorption (blue line) and emission (red line) spectra in solution (dissolved in DCM).

1.3.1.3 Semiconducting Polymer Nanospheres

Semiconducting polymer nanospheres (SPNs) are spherical shaped nanoparticles composed of semiconducting polymers. Semiconducting polymer nanospheres are also called "conjugated polymer nanoparticles".

SPNs can be synthesised without any coatings [130], or they can be coated or entwined with different molecules[36]. The synthesis of SPNs will be discussed in section 1.3.6. An illustration of SPNs stabilised and coated with amphiphilic molecules is presented in Figure 6.

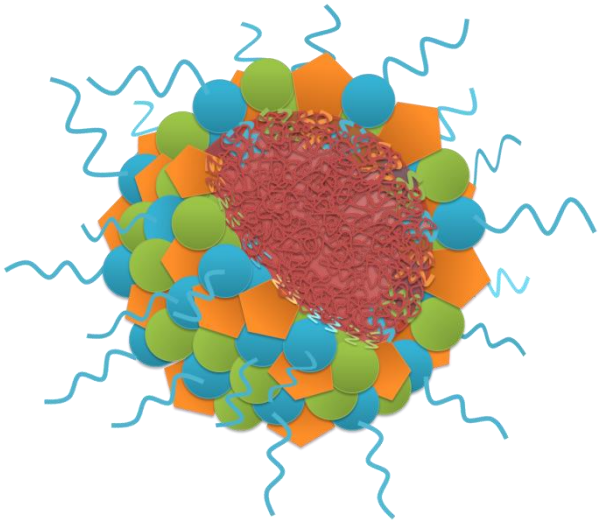

Figure 6 An illustration of a semiconducting polymer nanosphere stabilised by three different amphiphilic molecules.

1.3.2 Physical and Chemical Properties of Semiconducting Polymer Nanospheres

1.3.2.1 Composition and Physical Conformation of Conjugated Polymers in Good and Poor Solvents

As previously mentioned, conjugated polymers are composed of repeating monomers which are attached together to form a central back-bone chain of alternating single and double bonds. Many conjugated polymers also contain side chains which can be functionalised to give them different properties such as differing solubility. The solubility of a conjugated polymer in a specific solvent depends on the molecular structure of both solvent and solute, and it directly affects the polymer's physical conformation in that solvent. Solvents can therefore be categorised as good or poor for a particular conjugated polymer.

A good solvent is a solvent where the polymer chains are in an uncoiled conformation [131]. In this situation, the interactions between the polymer chains and the molecules of the solvent are energetically favourable. A poor solvent, on the contrary, is a solvent where the polymer chains form coils to minimise the non-favourable interactions between them and the molecules of the

solvent. An illustration of the conformations of the polymer chains in a good and a poor solvent is presented in Figure 7.

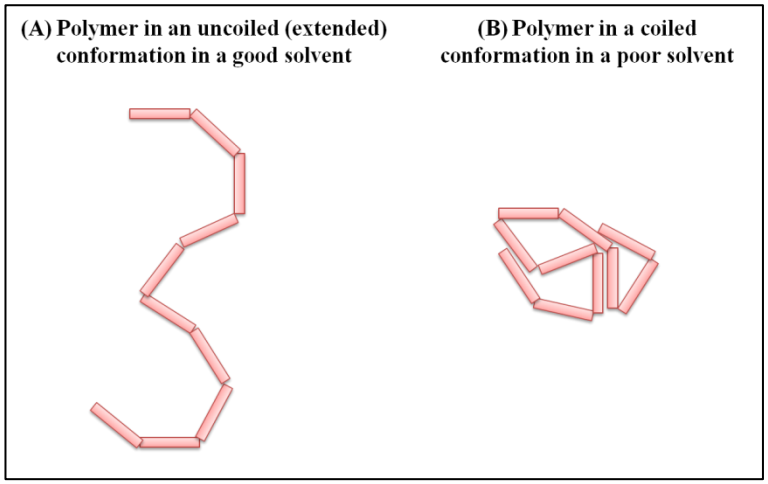

Figure 7 Polymer conformation when dissolved in (A) a good solvent and (B) a poor solvent. The polymer chains acquire an uncoiled conformation in a good solvent, while they prefer to collapse into a coiled conformation in a poor solvent.

For example, MEH-PPV has a non-polar aromatic backbone and slightly polar alkoxy side chains. In a non-polar solvent, the solubility of the aromatic backbone of MEH-PPV is favoured; therefore, the polymer maintains an extended conformation to increase the exposure of its backbone to the "good" solvent. In a polar solvent, the solubility of the backbone is unfavoured, therefore, its aromatic backbone chain coils up and collapses to limit its exposure to the "poor" solvent.[131]

1.3.2.2 Physical Conformation of Conjugated Polymers in Solid Films

The production of solid polymer films is important in electronic and optical device applications [132]. One way to produce solid polymer thin films is by drop-casting a solution containing the polymer onto substrates and evaporating the solvent.[133] It has been reported that polymers have a "memory effect" where their conformation in solid films adopt their original conformations in the solvents used.[134] Therefore, if drop-cast using a poor solvent, polymer films tend to have coiled-up and collapsed chains, while if drop-cast using a good solvent, they tend to have layers of polymer chains in an uncoiled conformation and minimum aggregation dependent upon concentration. The conformation of polymer chains in solid films was found to greatly affect the solid films' electronic and optical behaviour. This is discussed in detail in section 1.3.3.

1.3.2.3 Physical Conformation of Conjugated Polymers in Nanoparticles

The physical conformation of conjugated polymers in a nanoparticle form is not yet thoroughly explored. However, it was reported that conjugated polymers collapse in single or multiple chains

to form nanoparticles.[130] This implies an increase in folds and entanglements of the polymer chains which can be explained by the change in the electronic and optical behaviour of the nanoparticles in comparison to their behaviour in solution.[135]

1.3.2.4 Shape, Size, Chemical Functionalisation, Surface Morphology and Coatings of SPNs

Previously reported SPNs were always found to be approximately spherical in shape as suggested from TEM and AFM images, a property most probably influenced by the synthesis methods used. The spherical shape was reported by Moon *et al.* [136], Landfester *et al.* [26], and McNiell *et al.* [130, 137-138].

Different groups reported different diameters for their SPNs which had different coatings and were functionalised with different methods. For example, Landfester *et al.* reported the production of sodium dodecyl sulphate (SDS) stabilised SPNs with diameters ranging between 70 and 250 nm [139]. Moon *et al.* reported the production of uncoated functional SPNs as small as 25 nm in diameter. The chemical functionality was made by modifying the polymers used before synthesis [136, 140-141]. Chen *et al.* reported the formation of SPNs with sizes between 10 nm and 10 microns stabilised by different amphiphilic molecules which can be modified for different functionalities [142]. McNeill *et al.* reported the synthesis of non-coated, non-functionalised SPNs with diameters between 3 and 100 nm [143], they also reported the synthesis of silica capped SPNs functionalised with amine groups which were relatively large [137], and they recently reported the synthesis of bioconjugatable functionalised SPNs with diameters around 10 – 15 nm [144-145]. Our group reported the production of both PEG capped/entwined SPNs with diameters as small as 13 nm [118] and phospholipid capped/entwined SPNs with average diameters between 59 and 74 nm [36].

In general, most of the reported SPNs were substantially larger than the average diameters of QDs with relatively large size distributions. A few reports exist on the synthesis of QD sized fluorescent polymer nanoparticles, but either the method involved complicated methods with the use of toxic reagents, or the nanoparticles lacked surface functional groups which is an important feature for *in-vivo* administration [34, 130, 137, 146]. Therefore, further experimentations were needed with the use of one of the simplest, less toxic, synthesis routes to improve the sizes and size distributions of the produced SPNs to be comparable to QDs. The work reported in this thesis explored the preparation of QD-sized SPNs (Chapter 2).

1.3.3 Opto-electrical Properties of Semiconducting Polymer Nanospheres

Similar to quantum dots, the semiconducting and luminescent properties of semiconducting polymer nanospheres arise from their electronic structure which is similar to the electronic structure of their constituent polymers but is modified by the spatial configuration of their chains,

i.e. by the degree of packing of the chain segments and their folds and entanglements in solution, solid, or nanoparticle form.

1.3.3.1 Electrons in an Organic Molecule

Atoms in general are bound together by one or more of the different bonds: covalent, ionic, and/or metallic. These bonds cause the electrons of the solid/molecule to be delocalised to move in bands of energy instead of being highly localised in discrete energy levels as in the case of single atoms. In theory, each atom has a number of atomic orbitals where the probability of finding an electron is high. These atomic orbitals are described in quantum mechanics as electronic wavefunctions. Free atoms which are not full in their outer electronic orbitals tend to bond to other free atoms to reach a stable state where their outer orbitals are entirely full. We will first consider the H_2 molecule which is the simplest molecule to illustrate the molecular orbital model that leads to the band theory of materials. As shown in Figure 8, each hydrogen atom has a single electron in its atomic s-orbital. If two hydrogen atoms were brought together, at a certain distance, their atomic s-orbitals will begin to overlap and they will start to attract each other, and as they become closer the interactions between their orbitals increase until they combine and split into two molecular orbitals (MO); a bonding MO that corresponds to an inphase interaction of the atomic s-orbitals and has a lower energy than that of the individual atomic orbitals, and an anti-bonding MO that corresponds to an out-of-phase interaction and has a higher energy. In a non-excited state, i.e. when the H_2 molecule is in its ground state, both electrons of the two hydrogen atoms occupy and fill the bonding MO, and the molecule is said to be in its most stable condition.

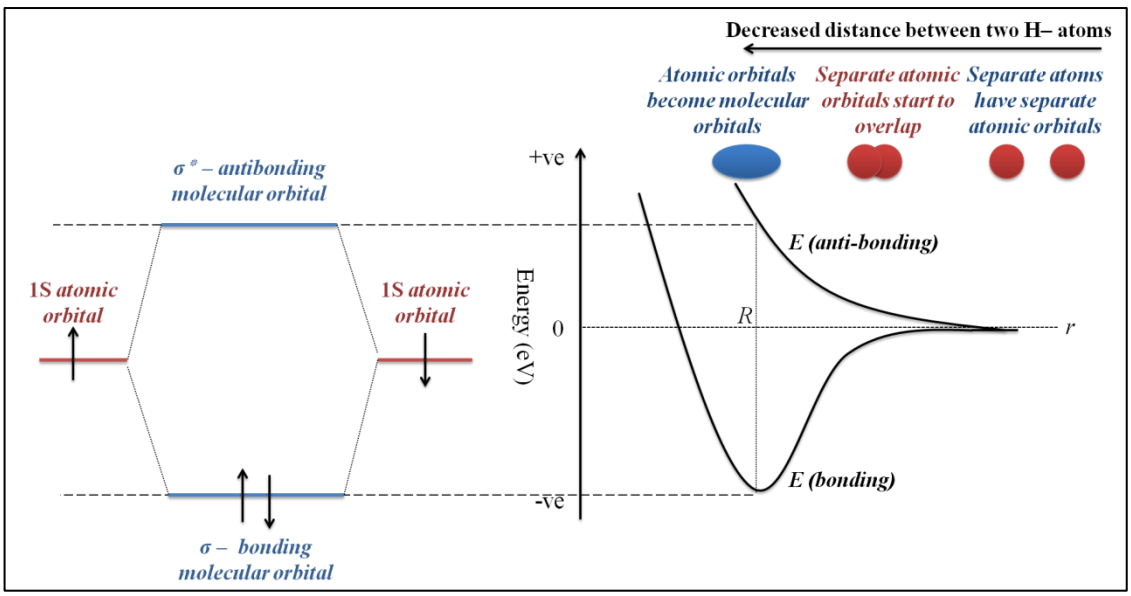

Figure 8 (right) The electronic energy levels of the H_2 molecule as a function of distance (r) between the nuclei of the two H-atoms. The curve (*E(bonding)*) is the energy of the bonding state, and (*E(anti-bonding)*) is the energy of the antibonding state. The

molecule is most stable when the distance between the atoms is (R). (left) A simplified molecular orbital diagram, representing the bonding and antibonding molecular orbitals in the stable H_2 molecule. The electrons (represented by arrows) occupy the lowest energy level of the system (the σ – bonding molecular orbital).[147]

As the backbones of polymers are typically composed of covalently bonded carbon atoms, a discussion of the electronic orbitals of two or more carbon atoms bonding together in an organic molecule applies here. Similar to hydrogen atoms in a hydrogen molecule, each carbon atom has a number of atomic orbitals where the probability of finding an electron there is high. If two carbon atoms were put together, their atomic orbitals interact to form molecular orbitals (MO) which can be bonding or antibonding. Figure 9 (A) shows the formation of the 1s and 2s molecular energy levels of molecules composed of two multi-electron atoms such as two carbon atoms. The highest occupied molecular orbital in a molecule is called the HOMO, and the lowest unoccupied molecular orbital is called the LUMO. The HOMO and LUMO are separated by an energy gap that is characteristic of the atoms, their quantity, and the type of bond forming that molecule. If the molecule is excited with an energy equivalent to or more than that of the energy gap, an electron will absorb that energy and set off from the HOMO to the LUMO.

If more than two carbon atoms form a molecule (Figure 9 (B)), other energy levels appear so that the number of molecular orbitals of the system equals the addition of the number of atomic orbitals of the constituent atoms, and if the number of atoms forming this molecule becomes very large (Figure 9 (C)), as is the case of polymers, the energy levels become bands.[148-149]

The energy gap between the bands is a forbidden area for electrons. An electron cannot jump a gap from one band to the other except if it is excited with an amount of energy that is equal to or more than that of the band gap. However, the bands are not always separated by a band gap, some bands can overlap so that the highest level in one band is above the lowest level in its upper neighbour.

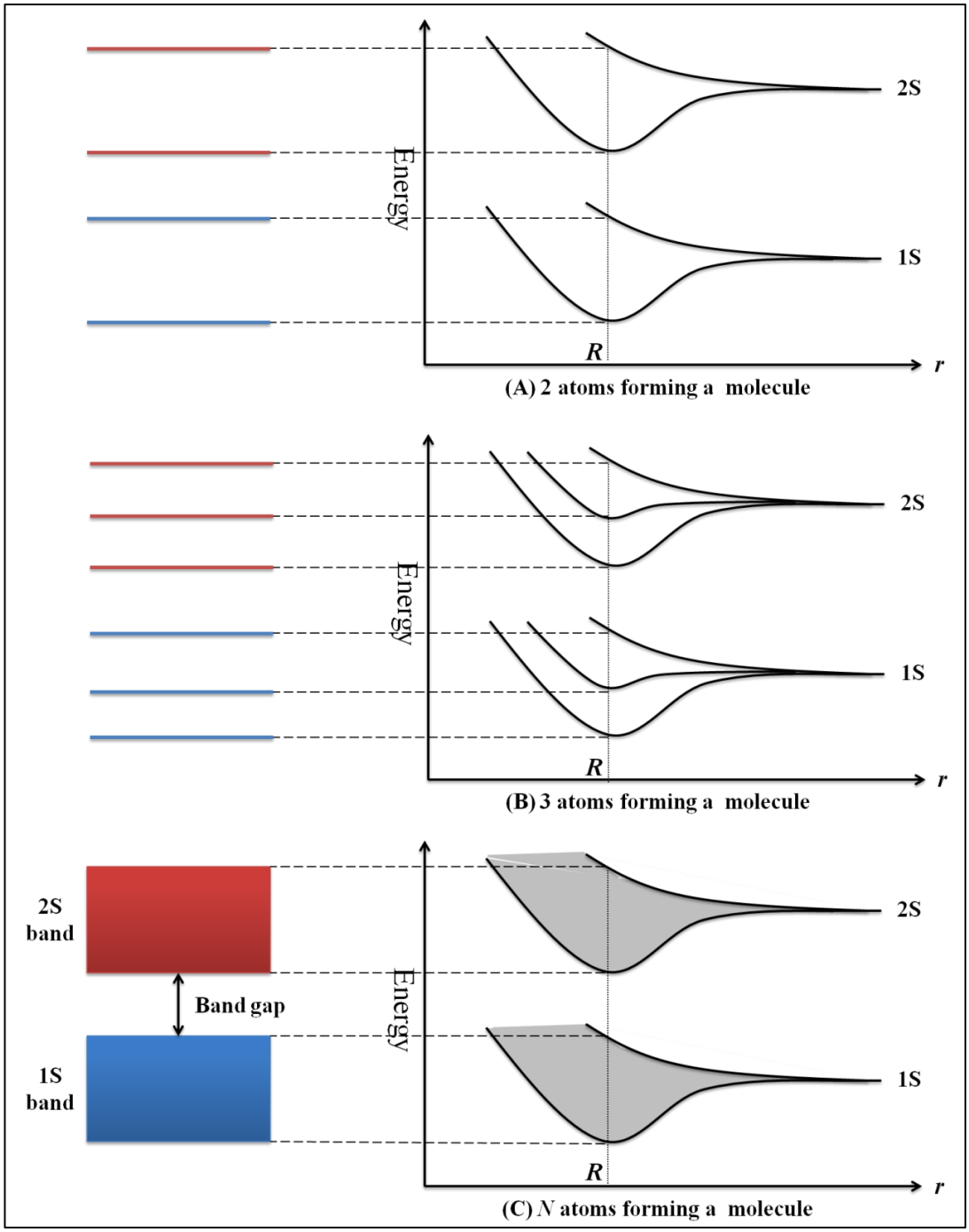

Figure 9 (right) The electronic energy levels of molecules formed from multi-electron atoms as a function of distance (r) between the nuclei of the atoms. (left) A corresponding simplified electronic energy diagram. Only the (1s) and (2s) orbitals are shown. The combination and splitting of the atomic orbitals happens when molecular orbitals are formed in (A) a two-atom molecule and (B) a three-atom molecule. The molecular electrons occupy and fill the lowest available energy states first before filling available states in higher energy levels. The spacing between the split molecular orbitals is reduced as the number of atoms in the molecule is increased and (C) with an infinitely large molecule the energy levels become bands.[147]

1.3.3.2 Optical and Electrical Properties of Conjugated Polymers in Free Spatial Configuration

Like inorganic solids, polymers can be insulators, conductors, or semiconductors. If we consider non-conjugated, single-bond chained, polymers, the molecular orbitals of such systems do not overlap because they are orbitals that emerge from the sigma bond which has a large separation between its bonding and antibonding states. Therefore, the electrons in such systems are highly localised around their atoms. This gives rise to a very wide bandgap between the HOMO and LUMO levels and gives the polymers an insulating electronic structure. The molecular orbitals of double or even triple bonded polymers, on the other hand, emerge from a sigma bond and a pi bond (or two pi bonds in the case of triple bonded polymers). In contrast to sigma bonds, pi bonds do not have a large separation between their bonding and antibonding states. Therefore, the relatively weaker pi bonds extensively overlap delocalising their electrons along their double- or triple-bonded chains. The bandgaps, here, decrease with the increase of chain-lengths, and with very long chains, the polymers become conducting. However, when the double and single bonds alternate, developing conjugation along the chains, a midpoint between the two situations takes place, and small bandgaps similar to the bandgaps of inorganic semiconductors are formed. Such a conjugated polymer, therefore, has a semiconducting property and is called an organic semiconductor.[148, 150]

Organic semiconductors exhibit changes in their energy levels with the presence of “defects”. Defects are interruptions of the conjugation along the polymers’ chains which were argued to arise from bending and twisting of their chains in non-free, i.e. real, configurations. However, it was recently proved by a quantum chemical approach that only chemical defects cause such interruptions.[151] Electrons in organic semiconductors are therefore confined in a one-dimensional quantum well, with the potential barrier of the well changing with the change in the conjugation length. The average un-interrupted conjugation lengths in conjugated polymers are called “effective conjugation lengths”, and these are the conjugated segments which define the semiconducting polymers’ electrical and optical properties.[127, 152]

For an organic semiconductor to fluoresce, its carbon skeleton should be conjugated, it should have a separation between its ground state and first excited state, and it should have a good separation between its excited singlet and triplet states with a relatively stable singlet state.

The un-interrupted conjugated segments which are responsible for the fluorescence property of the polymers are called “chromophores”. Because these chromophores have different chain lengths, the absorption spectra of the fluorescent conjugated polymers are usually wide and featureless. This, however, is not the case with the emission spectra of the polymers because excited electrons tend to travel to the chromophores with the lowest energy before decaying radiatively especially when the polymer chains are in near proximity from each other.[153]

1.3.3.3 Optical and Electrical Properties of Conjugated Polymers in Different Dilute Solutions

The conformation of the conjugated polymer, and therefore its optical and electrical behaviour, is governed by the medium which surrounds the polymer such as the pH of the sample, its temperature, and most importantly, the influence of other molecules also present in the sample such as the molecules of the solvent.[154]

Conjugated polymers dissolved in a good solvent have an uncoiled conformation. In a dilute solution, there is little interaction between the different polymer chains, i.e. interchain interactions, and little interaction between the chromophores of the same chain, i.e. intrachain interactions. In this situation, excitons mostly form from the excitation of electrons of the chromophores to higher energies in the same chromophores and radiatively decay in the same manner.

Conjugated polymers dissolved in a poor solvent have a coiled up and collapsed conformation. Therefore, the chromophores of the polymer chains have an increased contact and both interchain and intrachain interactions happen. The site where such interactions happen is called an aggregation site. Aggregation sites are not always emissive. Excitons formed in an aggregation site of two chromophores situated in a parallel position to each other tend to decay radiatively, however, they tend to have lower energies than those excitons created in non-aggregation sites due to the increased delocalisation of the electrons there. Therefore, such excitons from those new emissive species contribute to a new red shifted emission peak in the emission spectrum of the conjugated polymer. An example of MEH-PPV dissolved in a good and a poor solvent is presented in Figure 10.

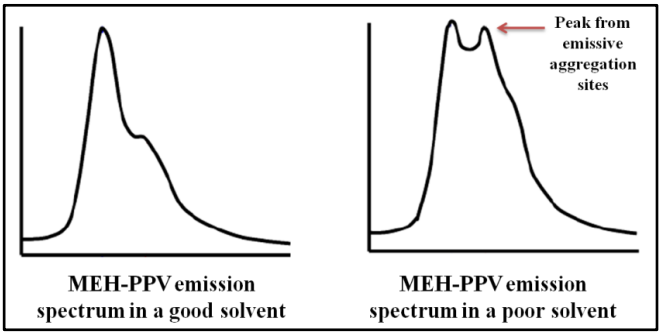

Figure 10 The emission spectra of MEH-PPV dissolved in (left) a good solvent and (right) a very poor solvent. (Modified image from [135])

1.3.3.4 Optical and Electrical Properties of Conjugated Polymers in Concentrated Solutions and in Solid Films

The conformations of conjugated polymers in amorphous solid films were reported to be similar to their conformations in the solutions they were cast from. This also contributes to a similar optical and electrical behaviour to the polymers in solution. An increase in the concentration of the

solution causes the polymer chains to entangle. Therefore, if cast from a good solvent for example, the spatial gap between different polymer chains in the solid film decreases while the polymer chains remain in an extended conformation. This causes an increase in interchain interactions.[134] In such interactions, electrons tend to migrate from the chromophores of higher energies to near-by chromophores of lower energy before decaying to emit photons. Therefore, the emission spectra of conjugated polymers tend to be skewed towards the red emissive species of the sample causing an over-all shift and narrowing of the emission peaks but maintaining the same emission profile. Figure 11 illustrates this phenomenon in the emission spectra of MEH-PPV in a solid film (right) cast from a good solvent (left).

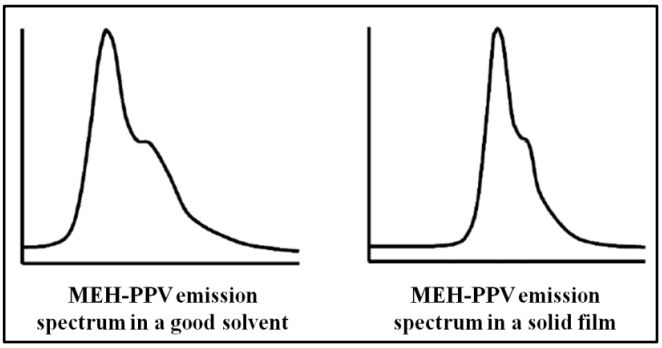

Figure 11 The emission spectra of MEH-PPV (left) dissolved in a good solvent and (right) as a solid film cast from a good solvent. (Modified image from [135])

1.3.3.5 Optical and Electrical Properties of Conjugated Polymers in Nanoparticle Form

The optical and electrical behaviour of conjugated polymers in nanoparticle form was reported by Grey *et al.* and Howes *et al.* [36] to be similar to their optical and electrical behaviour in solid films [155] with the emission entirely red-shifting [135]. This was observed in MEH-PPV SPNs ranging between 10 nm and 100 nm in diameter.[155] Another group reported that SPNs with sizes ranging between 70 nm and 160 nm did not have a size dependent change in their photoluminescence properties.[156] As those nanoparticles are relatively new, further experimental and computational optical and electrical studies need to be conducted to further understand their behaviours.

1.3.4 General Applications of Semiconducting Polymer Nanospheres

Polymers in general have found many applications within nanoscience.[157-158] Research is ongoing in incorporating polymers in nanolithography [157], nanoelectronics [159], light-emitting devices and solar cells [132], nano-based cancer treatments [160], MRI signal enhancement [161], drug delivery [162-163], and nanocomposites for food packaging [164]. This is mainly due to their wide-ranging well controlled properties associated with their nanoscale lengths, configurations, and chemical functionalities.[124, 157]

Conjugated polymers, in particular, were found to be useful in many applications. For instance, conjugated polymers were good candidates for the emergence and development of molecular electronics [165]. This included both organic light emitting devices (O-LEDs) [153] and organic solar cells [132, 166]. Conjugated polymers in their nanoparticle form were also investigated and were found to be useful specifically in O-LEDs fabrication. In such devices, SPNs were deposited from an aqueous suspension to form an active layer of light emitting nanoparticles which had a bandgap that is the same as that of the nanoparticles' [139, 167].

With their functionalisable side chains [168], their high brightness [137], and their composition being benign [169], conjugated polymers were also found to be good materials in the biological and medical fields. This will be discussed in detail in the next section.

1.3.5 Semiconducting Polymer Nanospheres as Bio-imaging, Labelling, and Tracking Agents

Polymers have many desirable properties which made them attractive in the biological and medical fields from as early as the 1980s [169]. Conducting polymers, for example, were used in bio-sensing [170] and enzyme entrapment [171]. They were found to change cellular activities [172], transfer charge in biomedical processes, and electrically interact with cardiac and nerve cells.[169]

Semiconducting polymers, which also share the property of being benign with many conducting polymers [169], exhibit stable and high fluorescence brightness [137]. This allows them to be considered as possible fluorescent probes. However, many conjugated polymers are hydrophobic in nature. This was overcome by chemically modifying their side chains [173]. Despite the fact that this process significantly agitated their fluorescent properties, such conjugated polymers were able to be used as oxygen sensors [174], as bacteria detectors [175], and in DNA assays [176-178].

As described in section 1.3.3, most of the optical properties of semiconducting polymers can be reserved by incorporating them into nanoparticles [139]. This also enables them to be functionalised as desired. SPNs are therefore being developed and studied as bio-imaging and sensing agents [36, 179] such as multiphoton fluorescence imaging [143] and oxygen sensing [180]. They are also being developed as bioconjugates for specific cellular targeting [144] and were used in targeting tumour cells [145]. They were also found to be good tracking agents for tracking cellular processes with nanoscale 3D tracking methods [181]. By doping the SPNs with singlet oxygen photosensitizers, the SPNs were able to damage DNA, and are therefore proposed as promising materials for cancer treatment by photodynamic therapy [138]. SPNs were also modified to incorporate more than one property to be used in more than one imaging technique. An example is imbedding iron oxide nanoparticles inside the polymeric core of the SPNs for both fluorescence and magnetic resonance imaging [182]. With this rapid increase in experimentation with such

recent nano-materials especially in the biological and medical fields, it is therefore important to develop their synthesis methods to be as effective as possible and as green as possible as well as to conduct toxicity and safety assessment studies to estimate how safe they are for use in their proposed applications.

1.3.6 Synthesis Routes of Semiconducting Polymer Nanospheres

The synthesis of semiconducting polymer nanospheres (SPNs) for biological applications is relatively new.[36, 183] In general, two approaches can be taken here. Synthesis can be performed using pre-formed polymers, or by in-situ polymerization.[130, 146, 184-186] Polymerization of dispersed monomers in-situ is problematic because of toxic residues of monomers, oligomers or catalysts [187], while polymerization with dendritic routes is complicated and lengthy [186]. Therefore, methods for nanoparticle preparation from ready-made, well studied, and non-toxic synthetic-polymers have subsequently been developed.[184, 187-188] Notably, Landfester *et al.* produced SPNs from three preformed polymers by a miniemulsion – solvent extraction method. The miniemulsion – solvent extraction method is described in detail in chapter 2, but briefly, it involves the mixing/stirring of a water immiscible solvent, which contains the polymer chains, in water under high shear. Under these conditions, nanodroplets containing some polymer chains form. The polymer nanoparticles are then formed by extracting the solvent from these nanodroplets. In Landfester's work, the nanoparticles were stabilised using sodium dodecyl sulphate (SDS), and exhibited diameters in the range of 70 – 250 nm, with their main applications envisaged to be film formation for electronic devices such as organic-light-emitting diodes (OLEDs) as SDS is toxic.[139, 167, 189] Landfester *et al.* mostly focused on miniemulsion polymerisation of monomers, but recently reported the use of pre-formed polymers again using the same method used by McNeill *et al.* [190].

McNeill *et al.* concentrated mainly on the use of commercially available polymers, with a similar method to the miniemulsion method which they referred to as a reprecipitation method. In the reprecipitation method, a water miscible solvent, such as tetrahydrofuran (THF), which contains the polymer chains is injected/stirred/mixed with water, then the solvent is extracted. The polymer chains, which must be hydrophobic, collapse with the contact with water to form polymer nanoparticles. The miscible solvent is then removed in various ways. McNeill *et al.* used the reprecipitation method to first prepare surfactant-free polymer nanospheres of diameters between 3 and 100 nm. The fluorescent nanoparticles were envisaged to be useful in photovoltaics as well as biological applications. Although the resulting polymer nanoparticles were of a medically-desired diameter, they initially lacked a surface functionality which limited their biological applications.[34, 130, 191] To improve fluorescence and stability of the polymer nanoparticles as well as allowing functionalisation, the nanoparticles were encapsulated with silica shells, to which,

for example gold nanoparticles could be attached.[137] However, this step contributed significantly to the particle diameters and has not, to date, been developed any further by this group. McNeill *et al.* further developed their method to prepare functionalised polymer nanoparticles by adding functionalised amphiphilic polymers to their polymer mixtures before synthesis. These 10 to 15 nm sized functionalised SPNs which were prepared at the same time as the research presented in this thesis were able to be bioconjugated with streptavidin or antibodies and were used in labelling specific human cells [144-145]. The same idea was used to dope their SPNs with tetraphenyl porphyrin (TPP) for photodynamic therapy applications [138].

Moon *et al.* used the same method as McNeill *et al.* but they called it a phase-inversion method [136, 140-141]. Moon *et al.* used a preformed, but modified, polymer to synthesise nanoparticles which they measured to be as small as 25 nm (dynamic light scattering). Larger nanoparticles, with an average of 70 nm in diameter, were observed by TEM but the group stated that the smaller nanoparticles which they believed were the majority of the population were not able to be imaged due to a technical difficulty. Modification of the polymer was essential to make the nanoparticles useful in biological applications. Such modified polymers are not commercially available, thus a separate polymerization step was needed before the nanoparticles' formation process.

Chen *et al.* reported the formation of water-soluble fluorescent nanoparticles which contain fluorescent polymers entangled with amphiphilic molecules.[142] The polymers used were commercially available, and the resulting nanoparticles formed were of sizes between 10 nm and 10 microns in size. These particles were suggested to be useful as probes for cell imaging and similar biological applications.

In previous work, our group used a miniemulsion – solvent extraction route to produce BEHP-PPV and MEH-PPV fluorescent nanoparticles capped/entwined with poly(ethylene glycol) molecules, which were in some cases as small as 13 nm (BEHP-PPV) as measured from TEM images [118, 192]. With some modification to the synthesis method and the addition of several phospholipids to the polymer mixture, which are amphiphilic in nature, phospholipid capped/entwined SPNs were also produced. These SPNs were slightly larger than the PEG capped/entwined SPNs with average diameters ranging between 59 and 74 nm as measured from TEM images [36], but both SPN systems were found to be extremely good fluorescent probes in cell imaging.[36, 118, 192] For a dual-modality, iron oxide nanoparticles were embedded in the phospholipid capped/entwined SPNs. The produced nanoparticles were found to be MRI active as well as fluorescent [182]. However, the fluorescence of the nanoparticles was significantly quenched due to the iron oxide nanoparticles' absorption, and their sub-micron sizes were significantly larger than the other two SPN systems. Further work was needed to provide bimodal SPNs with better properties to compete with QDs prepared for similar applications.

1.3.7 Semiconducting Polymer Nanospheres – still young in comparison to quantum dots but can they be greener?

Semiconducting polymer nanospheres can be synthesised in simple ways in comparison to QDs. When prepared from pre-formed conjugated polymers, SPNs do not need to undergo any chemical reaction. SPNs can be synthesised and stored in ambient conditions with most of their properties being conserved for a relatively long time. There is a good range of solvents which can be used to initially dissolve the conjugated polymers in the synthesis process. This gives one the option to use one of the least toxic solvents such as dichloromethane (DCM) making the synthesis process less toxic than the processes usually used in the preparation of QDs.

In terms of functionalisation, conjugated polymers can be functionalised with different side groups before nanoparticle synthesis. These can give the conjugated polymers different solubilities. Also with pre-functionalised conjugated polymers, SPNs can be prepared with different functionalities such as carboxylation for further bioconjugation.[144] Functionalities can also be introduced by using functional capping agents such as carboxylated amphililic molecules.[36]

The fact that SPNs are prepared from benign conjugated polymers [114] gives the SPNs the potential to be less toxic than QDs with the same fluorescent properties. However, this cannot be certain without proper safety assessment experiments as the nanosizes of nanoparticles in general are also an arguable issue.

Another drawback which hinders the investigation of SPNs use in bio-medical applications is that, up to the time of this research, SPNs were usually prepared with larger diameters than QDs with relatively larger size distributions. With a less monodispersed population of nanoparticles, SPNs could not compete with QDs in such studies. Therefore, the synthesis methods of these SPNs need to be developed to produce better, smaller, more monodispersed populations.

Also, many QDs are already commercially available. This makes them easily obtainable by research groups in the biological and medical fields, pushing research using QDs forward despite the fact that most of these QDs contain toxic materials and are still under study in nanotoxicology.

Conjugated polymer nanoparticles were reported to be roughly 15 times brighter than QDs with similar properties.[145] The nanoparticles were also reported to be highly efficient in energy transfer.[193] With such competing optical and electrical properties, and with established studies pointing towards the toxicities of many QDs, SPNs stand a chance to be effective alternatives to QDs especially if they are optimised to have similar diameters. However, extensive toxicological studies have to be made on both nanoparticle species before a solid conclusion such as the above can be made. The question raised in the title of this thesis and the research presented here are therefore a few steps towards achieving this goal.

1.4 The Current Work

1.4.1 Scope and Objectives

Our first objective was to synthesis PEG capped/entwined semiconducting polymer nanospheres with diameters similar to those of QDs, i.e. around 10 nm and less, using a miniemulsion-evaporation method and pre-prepared, commercially available, conjugated polymers. Then, with modifications to the surface capping agents of the SPNs, we aimed to produce bi-modal nanoparticles (Gd-SPNs) which are proposed to be suitable for fluorescence bio-imaging and as MRI contrast agents.[97, 194-195] These bi-modal Gd-SPNs are proposed to be alternatives to similar bimodal QDs [97]. Finally, to be suitable alternatives to QDs, monomodal and bimodal SPNs need to be proven to be both safe and efficient. Therefore, our third and final objective was to conduct some preliminary investigations about the interactions between nanoparticles both SPNs and Gd-SPNs and cells in comparison to QDs with similar surface coatings. This study, which was the first nanoparticle-cell interactions study reported on such organic nanoparticles was aimed to investigate the nanoparticles' behaviour in synthetic and biological media and their interactions with human blood components as they will most likely be administered intravenously if used as medical diagnostic and bio-imaging tools.

1.4.2 Overview of Thesis

An introduction to the basic scientific background information, definitions, properties, applications, and syntheses of quantum dots and semiconducting polymer nanospheres was presented in this chapter. The work done for the completion of this thesis is presented in the next chapters where the PEG capped/entwined SPNs are presented in chapter 2, followed by the bimodal gadolinium containing SPNs (Gd-SPNs) in chapter 3, and the preliminary nanoparticle-cell interaction investigations of the SPNs and Gd-SPNs in comparison to similarly coated QDs and carboxylated QDs in chapter 4. The experimental methods which include chemicals, equipment, characterisation techniques, and detailed synthesis descriptions are included in chapter 5. A conclusions chapter, which summarises the work presented in the three core chapters of this thesis and proposes routes for future work, is presented in chapter 6, followed by all the references, and finally some complimentary information (chemical structures and definitions) are added in two appendixes attached at the end of the thesis.

2 Quantum Dot Sized PEG Capped/Entwined Semiconducting Polymer Nanospheres

Conjugated polymers are organic semiconductors which exhibit strong photo- and electroluminescence. They can undergo intense fluorescence under excitation with suitable electric or electromagnetic stimulation, with high quantum yields and improved fluorescence properties compared to many other organic materials.[196-197] Many conjugated polymers are biocompatible and environmentally benign.[114] These properties have brought them to the attention of groups trying to synthesise fluorescent nanoparticles.[130]

Ideally, for any fluorescent material to be used for biological labelling applications and function as desired, it should be non-toxic, non-immunogenic, non-aggregating, and should not accumulate in the body, decompose in ambient conditions, or adsorb non-specifically to other biological molecules. It has been proposed that for inorganic quantum dots (QDs), there is a diameter threshold of *ca.* 5.5 nm, above which renal clearance from the body will not be possible.[116] Quantum dots can be synthesized with such small diameters, less than 5 nm, but are typically composed of toxic materials, such as cadmium. For this reason, quantum dots are encapsulated with biocompatible materials for use in biological applications.[110-111, 114-115] However, this addition substantially increases the hydrodynamic diameter of the particles. Additionally, the risk from the presence of non-capped quantum dots, or the aggregation and decomposition of the particles in the body cannot be neglected, and long term toxicity will always be a concern.

The synthesis of semiconducting polymer nanospheres for biological applications is relatively new.[183, 194] While synthesised from benign materials, most of the methods reported until now resulted in nanoparticles with relatively large diameters when compared to QDs. A few reports exist on the synthesis of QD-sized fluorescent polymer nanoparticles, but either the method involved polymerization or the nanoparticles lacked surface functional groups which is an important feature for *in-vivo* administration.[34, 130, 137, 146]

In this chapter, we introduce our work in controlling and optimising the miniemulsion-evaporation method to produce QD-sized poly(ethylene glycol) (PEG) capped/entwined SPNs from ready-made polymers. This method was previously used by our group to prepare SPNs with larger diameters. In the introduction of this chapter, the miniemulsion-evaporation method is explained in detail, and then the previously prepared larger SPNs are briefly described. This is followed by the results and discussion sections which describe the work towards the synthesis and characterisation of QD-sized SPNs and finally an investigation into the role PEG, the capping agent, played.

2.1 Introduction

2.1.1 The Miniemulsion – Evaporation Method for Nanoparticle Formation

The miniemulsion method is a method derived from the well established emulsion process [198]. In an emulsion, two immiscible liquids are mixed together to form liquid droplets (the dispersed phase) dispersed in a liquid medium (the continuous phase), as illustrated in Figure 12. To stabilise the dispersion a third component, an emulsifier, is usually used and is initially dispersed in one of the liquids before they are combined. The final emulsified systems can be classified according to the types of liquids used (oil in oil (O/O), oil in water (O/W), water in oil (W/O), or water in oil in water (W/O/W), etc), and/or the nature of the emulsifier (small molecules, surfactants, non-ionic polymers, solid droplets, mixed emulsifiers, etc). Figure 13 shows examples of emulsified systems. The emulsifier is also responsible for the long-term stability of the emulsion, however, other factors can also cause emulsion breakdown and are well reported in the literature.[199]

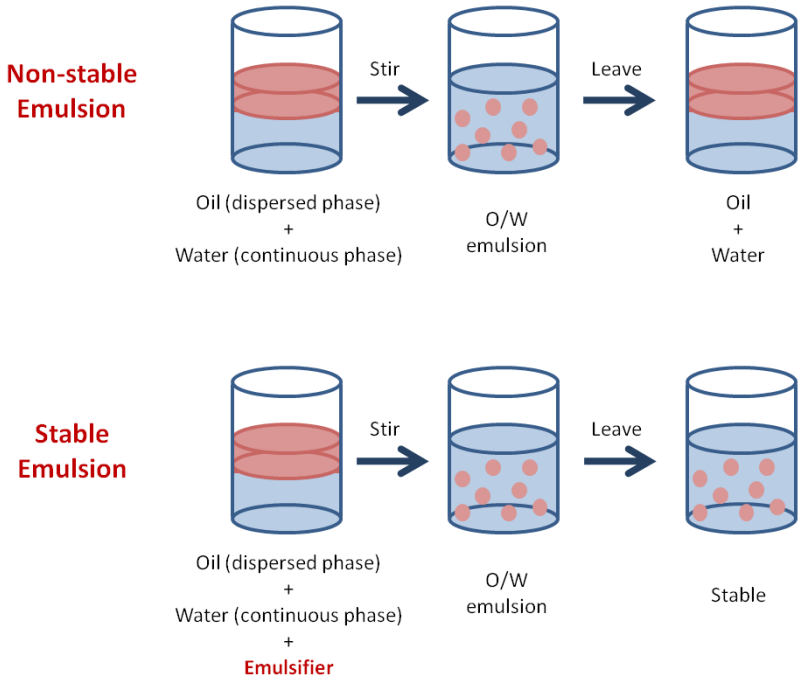

Figure 12 The emulsion process.

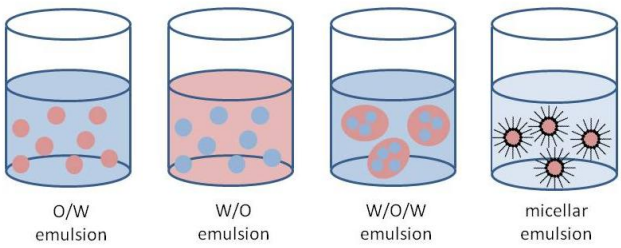

Figure 13 Different emulsified systems.

In the emulsion process, normal shear is used to mix the liquids such as stirring with a magnetic bead. This produces droplets with micrometre sizes. In miniemulsion, high shear is used, such as ultrasound or a high-pressure homogenizer, and a nanometre-size-droplets dispersion is obtained.[26] See Figure 14.

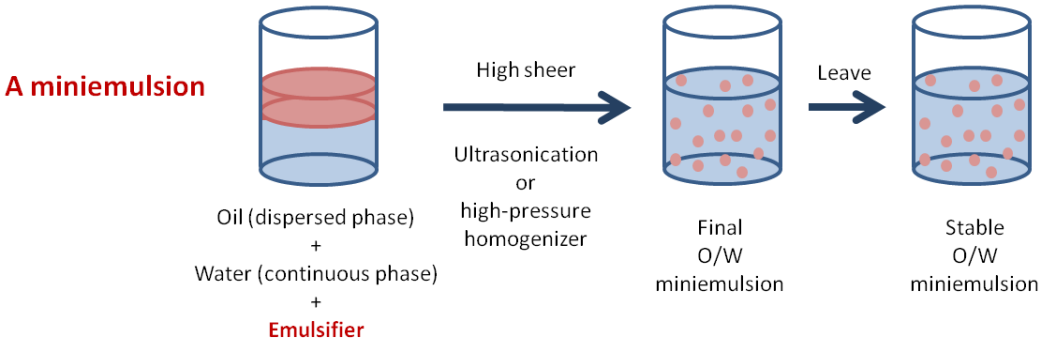

Figure 14 An illustration of a miniemulsion.

For nanoparticle formation (nanocapsules, nanoshells, or solid nanospheres, etc.), the nanoparticle constituents are initially dispersed in the emulsified solvent which forms the droplets of the system. The emulsion or miniemulsion process is then followed by a solvent extraction technique, such as evaporation, which transforms the droplets into particles after the extraction of the emulsified solvent from the micro- or nano- droplets, as illustrated in Figure 15. Miniemulsions were used to synthesise nanoparticles composed of various organic and inorganic materials, such as metals [200-201], ceramics [202], different biomolecules [203], and polymers [204-205]. For polymer nanoparticles formation in particular, two types of miniemulsions can take place: an active miniemulsion or a passive miniemulsion. In an active miniemulsion, the droplets initially contain monomers which are then activated by a chemical reaction within the droplets, the nanoreactors [198, 206], to create polymer nanoparticles in a process called miniemulsion polymerization [26, 184-185, 198, 202, 207]. In a passive miniemulsion no chemical reaction takes place and the droplets initially contain preformed polymers which are then transformed into nanoparticles [118, 139, 184, 192, 208]. Due to limitations and complexity of the active form as described in section 1.3.6, the relatively simple route of polymer nanoparticles formation, the passive form, was used in our syntheses.

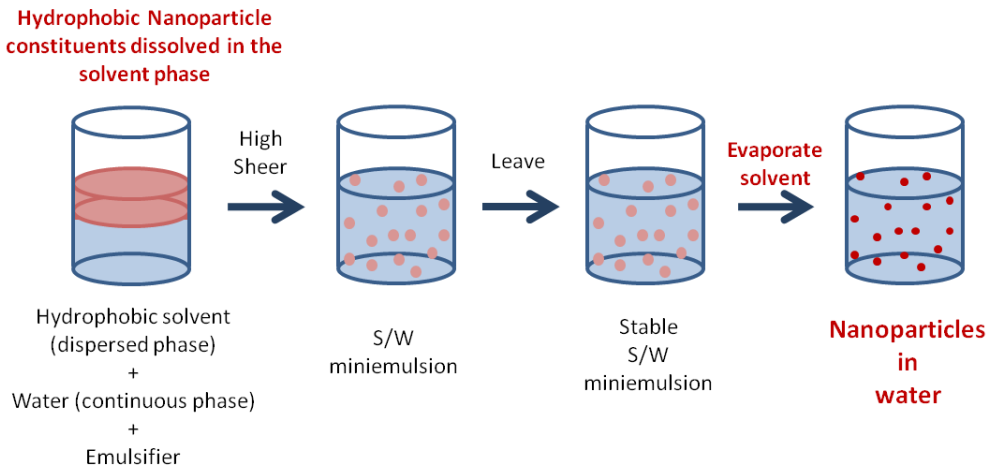

Figure 15 Nanoparticle formation with a miniemulsion-evaporation technique.

2.1.2 The Synthesis of PEG Capped/Entwined Semiconducting Polymer Nanospheres with Large Diameters

The first synthesis of PEG capped/entwined SPNs in water was reported by our group [118, 192]. In a typical synthesis, dichloromethane (DCM) containing 20 ppm (by weight) of hydrophobic conjugated polymer was added to water containing PEG8000. The beaker holding the combined solutions was exposed to ultrasound in a heated water bath for 25 minutes. The high shear caused the production of a miniemulsion while the heating promoted DCM evaporation. The reaction turned clear by the end of the exposure indicating the full evaporation of DCM and the formation of aqueous SPNs with diameters as small as 13 ± 5.4 nm [192]. A centrifugation and filtration step was also included to remove the large particles and any dispersed bulk material. The same method was also used with a higher polymer concentration and resulted in nanoparticles with a mean diameter of 100 nm.[118]

In the above synthesis, DCM was chosen as the polymer medium because it is immiscible with water, is a good solvent for many hydrophobic conjugated polymers, and has a low boiling point (40 °C) which enabled its evaporation after the formation of the miniemulsion droplets.

Also, PEG with a molecular weight of 8000 g/mol was used as an emulsifier which enabled the two immiscible solutions, DCM and water, to be emulsified. Figure 16 shows the chemical structure of PEG. PEG is a polymer used as a surfactant in many industries. It was selected in this synthesis instead of an initially used toxic emulsifier; sodium dodecylsulphate (SDS) [118], used in reference to similar work done by Landfester *et al.*[139]. PEG is an extremely useful capping agent especially if the nanoparticles are aimed to be used in biological applications such as fluorescence bio-labelling. This is because PEG is non-toxic, non-immunogenic, soluble in most solvents including water, and approved for human use [209], whilst exhibiting a wide range of chemistries which could be exploited to allow further functionalisation with biological materials. PEG has also

been shown to significantly reduce nonspecific binding of the surrounding biological molecules to nanoparticles, which is essential for successful *in-vivo* applications.[210] Thus, the use of PEG in the syntheses produced SPNs with biologically desirable properties, and provided a potential route for bio-functionalisation.

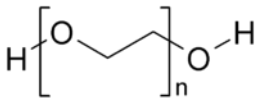

Figure 16 The chemical structure of PEG.

Although particles as small as 13 nm were obtained using the above described synthesis procedure and parameters, the miniemulsion was not fully controlled and a considerable volume of the non-aqueous phase remained separated from the aqueous phase while the mixture was under high shear.[135] This resulted in the precipitation of a large amount of polymer which was discarded in the purification step.

Our group further refined the above synthesis to be as follows; 16 mL of dichloromethane containing 40 ppm (by weight) of hydrophobic conjugated polymer was added to 30 mL of water containing 0.5 mg PEG300. The mixture was stirred for 10 minutes, then it was ultrasonicated for 10 minutes at room temperature or at 30 °C, and finally the miniemulsion was stirred on the bench until DCM had fully evaporated and the nanoparticles had formed. The nanoparticle solution was then centrifuged and filtered through filter paper.[135]

The increase in the volume ratio of water to DCM, the use of PEG with a lower molecular weight, and the incorporation of a stirring step before the exposure of the mixture to the high shear all contributed to a better emulsion and therefore a better reaction yield. It is believed that this also contributed to a better size distribution of nanoparticles. This will be discussed in detail in section 2.2.

2.2 Factors to Consider for a Reproducible, Narrow Size Distribution, of QD-sized PEG Capped/Entwined SPNs

At the beginning of this work, the synthesis technique was studied thoroughly and according to research and first experimental observations it was concluded that to achieve a reproducible, good, and possibly narrow size distribution of SPNs, the following need to be considered:

1. The emulsion needs to be fully controlled.
2. The solvent used to dissolve the polymer needs to be a “good” solvent [135].
3. The evaporation of the solvent in the droplets needs to be avoided until the emulsion/miniemulsion is complete.

However, to produce significantly smaller nanoparticles, other factors need to be considered:

1. The initial polymer concentration in the solvent [118, 192].
2. The high shear used.
3. The amount [199, 211] and type [212-213] of emulsifier.

The above listed factors are discussed in detail in the following subsections.

2.2.1 Factors Affecting Reproducibility and Broadening of the SPNs' Size Distributions

Two droplets in an emulsion lead to two nanoparticles with different diameters following one of two scenarios: either the droplets were of different diameters but contained the same concentration of nanoparticle constituents, or the droplets had the same size but contained different concentrations of nanoparticle constituents, as illustrated in Figure 17 (A and B). The former scenario is supported by the reported observation that with smaller droplets, due to high shear in a miniemulsion for example, the emulsion produces smaller nanoparticles [206], while the latter is supported by the reported observation that a change in polymer concentration leads to a change in the nanoparticles average diameters [118, 192]. Therefore, to achieve a monodispersed nanoparticle system, ideally, the droplets of the emulsion need to be of the same size and they should contain the same concentration of nanoparticle constituents. This ideal situation could be true if no other factors affecting the final nanoparticles' diameters took place in the solvent evaporation step, and if the final density of the nanoparticles was the same. Although the droplets of an emulsion cannot reach the ideal situation discussed above, the distribution of their diameters can be controlled and practically reproduced by obtaining a successful emulsion that is well controlled. The polymer concentration in the droplets, on the other hand, can be fairly equalised by using a good solvent and by prohibiting its evaporation during the emulsification step.

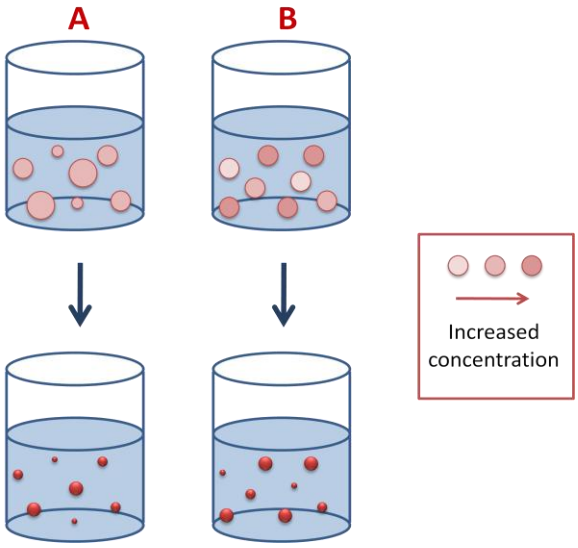

Figure 17 Different nanoparticle sizes obtained from (A) droplets with different droplet sizes having the same polymer concentration, and (B) droplets with the same size but containing different polymer concentrations.

2.2.1.1 Obtaining a Successful, Well Controlled, and Reproducible Emulsion

A successful emulsion is obtained when the dispersed solution is fully dispersed in the continuous solution. If the high shear is not enough to obtain this condition, then a stirring step is required before the high shear to initiate the full emulsion. We therefore introduced 10 minutes of stirring as a pre-miniemulsion step mentioned at the end of section 2.1.2.

A well controlled and reproducible emulsion can be obtained by using a non-changeable shear; i.e. stirring two separate emulsions with the same speed and placing them at the same height and position in the same ultrasound bath, and by not changing the exposure times, the glassware, the size and shape of the magnetic stirring beads, and the volumes of the solutions, etc. The above measures become very important in such a synthesis method because it involves a physical reaction rather than a chemical reaction. Therefore, the physical aspects such as the size, shape, volume, viscosity, and force become the ultimate controllers of the outcomes of an emulsion.

2.2.1.2 Using a Good Solvent

The conformation of polymer chains in a solvent depends on their solubility. As discussed in section 1.3.2.1, a polymer in a good solvent acquires an uncoiled (extended) conformation, while a polymer in a poor solvent tends to aggregate and acquire a coiled conformation. This behaviour affects the homogeneity of concentration of the polymer chains in the solvent used. With an extended conformation in a good solvent, the polymer is evenly distributed so that the concentration of the polymer in the solvent is homogeneous with minimum aggregation. A homogeneous concentration of polymer in the solvent is very important in the synthesis of the SPNs especially if a reproducible narrow size distribution is desired, as described at the beginning of this section (section 2.2.1). Also, the type of solvent used (good or poor) affects the electrical and optical characteristics of the polymer and can therefore affect the luminescence properties of the SPNs. This was described in detail in section 1.3.3.

DCM is a good solvent for many hydrophobic polymers and is therefore used in our syntheses.

2.2.1.3 Controlling DCM Evaporation in the Emulsion/Miniemulsion Steps

If DCM is allowed to evaporate while the emulsion/miniemulsion is incomplete, a significant amount of polymer will precipitate as observed in our first syntheses [118, 192]. The quick evaporation of DCM can also lead to droplets with different polymer concentrations and therefore to a broader size distribution of nanoparticles. DCM has a very low boiling point (40 ºC). It can evaporate at room temperature with a steady, relatively low, speed of stirring. Therefore, to avoid its evaporation in the synthesis of the SPNs, the reaction's temperature must be decreased by decreasing the solutions temperatures before the synthesis and adding ice cubes to the ultrasound bath. DCM evaporation can also be restricted by using a flask with a narrow neck and closing it

with a suitable lid throughout the emulsion and miniemulsion processes. It can also be restricted by controlling the speed of stirring and changing the position of the flask in the ultrasound bath to avoid splashing of the mixture.

2.2.2 Factors Affecting the Average Size of the SPNs

The nanoparticles' sizes can be reduced by decreasing the droplets diameters. This can be achieved by increasing the shear such as using high shear instead of normal shear, by controlling DCM so that it does not evaporate until such small droplets are formed, and by increasing the amount of surfactant so that the increased surface area of the droplets can be stabilised [199, 211].

Another way to reduce the nanoparticles sizes is by using shorter surfactants, such as using PEG with a molecular weight of 300 g/mol instead of 8000 g/mol [212-213]. This reduces the diameter of the surfactant shell, while maintaining the same diameter of the polymer core.

A third way to reduce the nanoparticles sizes is by reducing the initial concentration of the polymer in DCM which results in smaller polymer cores [118, 192].

Landfester *et al.* reported that some parameters were shown not to have a systematic affect on the particles' size in the miniemulsion process such as the variation of the system's temperature from 0 to 60 ºC. However, in their investigations, they used different solvents which had boiling points varying between 80 and 291 ºC [211]. In our syntheses however, DCM which evaporates rapidly (boiling point = 40ºC) is used. So, the temperature in our systems has to be decreased if smaller, reproducible, and narrow size distributions of nanoparticles are targeted. Also, when working with fluorescent molecules, such as the conjugated polymers we used, it is advisable to keep the temperature to a minimum to preserve their emission intensities and avoid any temperature-related quenching.

With the consideration of all the above factors, the method described in section 2.1.2 was further refined, and a narrow size distribution of QD-sized SPNs was prepared.

2.3 Synthesis of Quantum Dot Sized Semiconducting Polymer Nanospheres

2.3.1 First Synthesis of QD-sized SPNs using 40 ppm of BEHP-PPV

The first synthesis was performed using a blue/green fluorescent conjugated polymer: poly[2-(2',5'-bis(2''-ethylhexyloxy)phenyl)-1,4-phenylenevinylene] (BEHP-PPV). The polymer was dissolved in DCM to form a 40 ppm (by weight) solution. 8 mL of the polymer in DCM solution was added to 20 mL of water containing 0.5 mg PEG300 in a beaker. The beaker was covered with filter paper and the solutions were stirred for 10 minutes to initiate the emulsion. Then they were ultrasonicated at room temperature for 10 minutes to form the miniemulsion droplets, and finally

the miniemulsion was stirred at room temperature until the solution became clear indicating the full evaporation of DCM and the formation of the nanoparticles. The nanoparticle solution was filtered through filter paper to remove any bulk material but was not centrifuged.

The physical characteristics of the resulting nanoparticles were analysed by transmission electron microscopy (TEM) and dynamic light scattering (DLS), while their optical properties were analysed by absorption and emission spectroscopies. The aqueous nanoparticles' solution was found to contain nanoparticles with polymer cores as small as 4 nm in diameter as measured from TEM images. Figure 18 shows two TEM images of the spherical nanoparticles. Because PEG is not TEM visible, the dark spots in the images show the polymer cores of the nanoparticles without any indication of PEG.

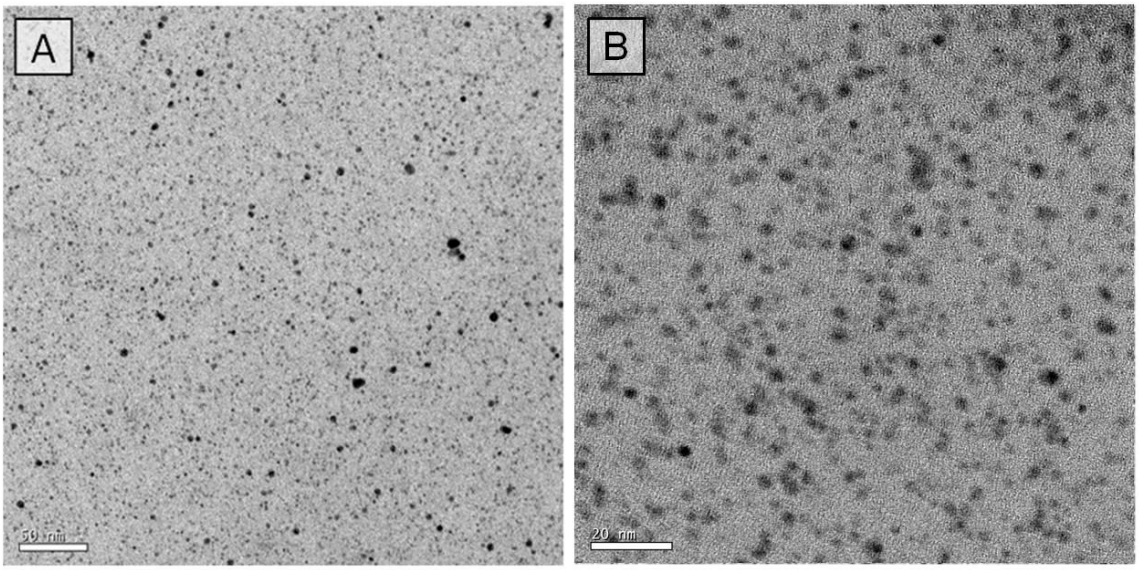

Figure 18 TEM images of the first synthesis of QD-sized SPNs using 40 ppm BEHP-PPV in DCM. Scale bars are (A) 50 nm and (B) 20 nm.

The other sizing method, DLS, was used to determine the hydrodynamic diameters of the nanoparticles in water. The hydrodynamic diameter is a measure of the diameter of the nanoparticle core, any capping agents or molecules which are attached to it, and the electronic cloud that surrounds it as shown in Figure 19. With limited characterisations of the newly produced SPNs, the DLS measurements could not be executed without the assumption that the SPNs are similar to polystyrene beads and therefore have the same parameters. The average diameter determined by the DLS intensity distribution was considered here instead of the commonly reported cumulants diameter because the samples did not undergo excessive purification as they were not centrifuged to remove any large particles. The large particles were found to skew the cumulants results towards the larger diameters giving a faulty determination of a significantly larger population than that of the actual. The average hydrodynamic diameter determined by the DLS intensity distribution therefore cannot be directly linked to the average diameter measured from TEM images. However,

it can give an indication of the range of hydrodynamic diameters in the sample if, and only if, the assumption made above is true. This is discussed in detail in the methods chapter (section 5.7.2). The hydrodynamic diameters of the nanoparticles in the above sample were found to range between 60 nm and 400 nm with their average diameter being around 179.3 ± 68.1 nm.

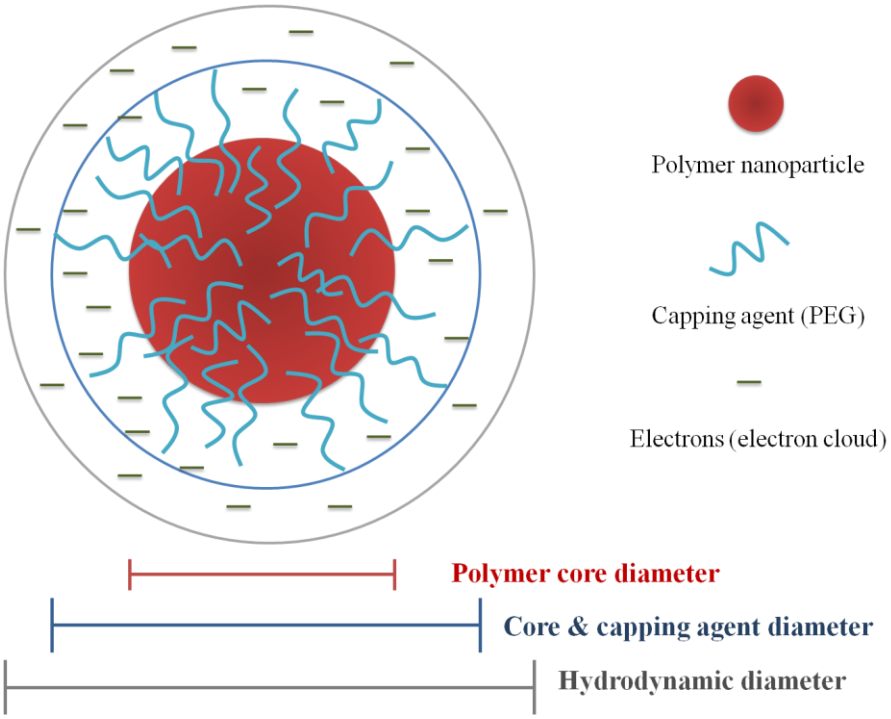

Figure 19 The hydrodynamic diameter of a nanoparticle.

Absorption spectroscopy is one of many chemical analysis methods used to determine the chemical composition of any sample. It is also a direct indicator of the concentration of those chemical constituents. Absorption spectroscopy was used here to determine the presence and preservation of the polymer in the aqueous nanoparticles sample after synthesis. Emission spectroscopy was used to determine the fluorescence of the nanoparticles. Figure 20 shows the absorption and emission spectra of the BEHP-PPV SPNs solution compared to the absorption and emission spectra of BEHP-PPV in DCM. The absorption peak around 400 nm was conserved when the polymer chains were converted from an extended conformation in DCM to aqueous nanoparticles. This indicates that the chemical structure of the polymer was conserved. The emission spectra were also similar and no significant shift in the emission's peak of BEHP-PPV was observed. However, there was an increase in the intensity of the second optical transition (around 520 nm) and an increase in the intensity of the tail of the spectrum between that optical transition and 720 nm. These attribute to a slight increase in the emissive aggregates which indicate an increase in the interchain interactions due to the folds and entanglements of the polymer chains. This also indicates that the chain segments of the same polymer became of near proximity to each other which means that the nanoparticles were formed from one, or a few, polymer chains.

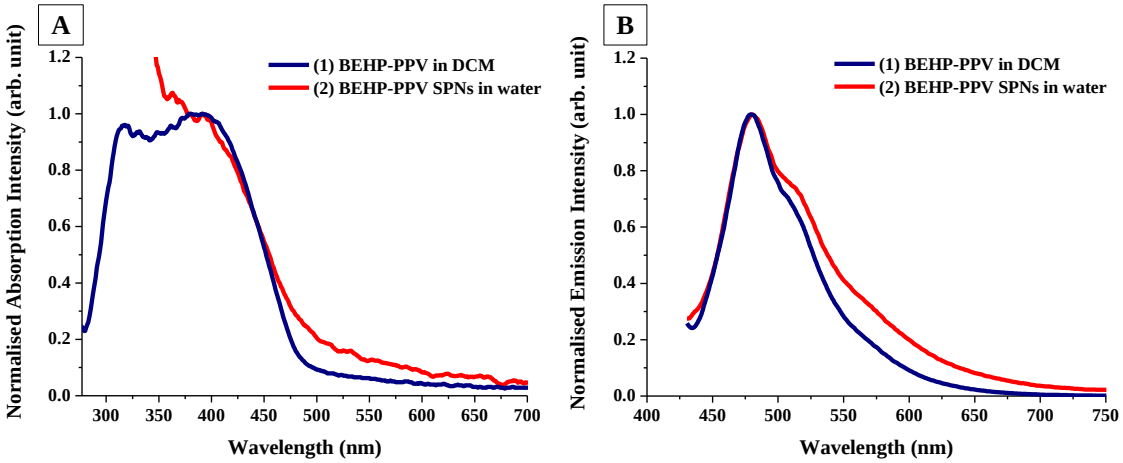

Figure 20 The normalised (A(1)) absorption and (B(1)) emission spectra of the first synthesis of QD-sized SPNs using 40 ppm BEHP-PPV in DCM compared to the normalised (A(2)) absorption and (B(2)) emission spectra of BEHP-PPV in DCM. Emission was under λ_{ex}= 400 nm excitation.

2.3.2 Syntheses using Different BEHP-PPV Concentrations

In an attempt to study the effect of polymer concentration on nanoparticle size, four different polymer concentrations were used in the synthesis method described above (in section 2.3.1); 40, 10, 5, and 1 ppm, and four aqueous SPN solutions were obtained.

Figure 21 shows TEM images of the BEHP-PPV SPNs prepared using 40 ppm and 1 ppm of polymer concentration. Both images show the presence of small nanoparticles, whilst the SPNs prepared from the 1 ppm solution were observed to be generally smaller with a mean diameter of only 2 nm compared to 4 nm for the SPNs prepared using 40 ppm.

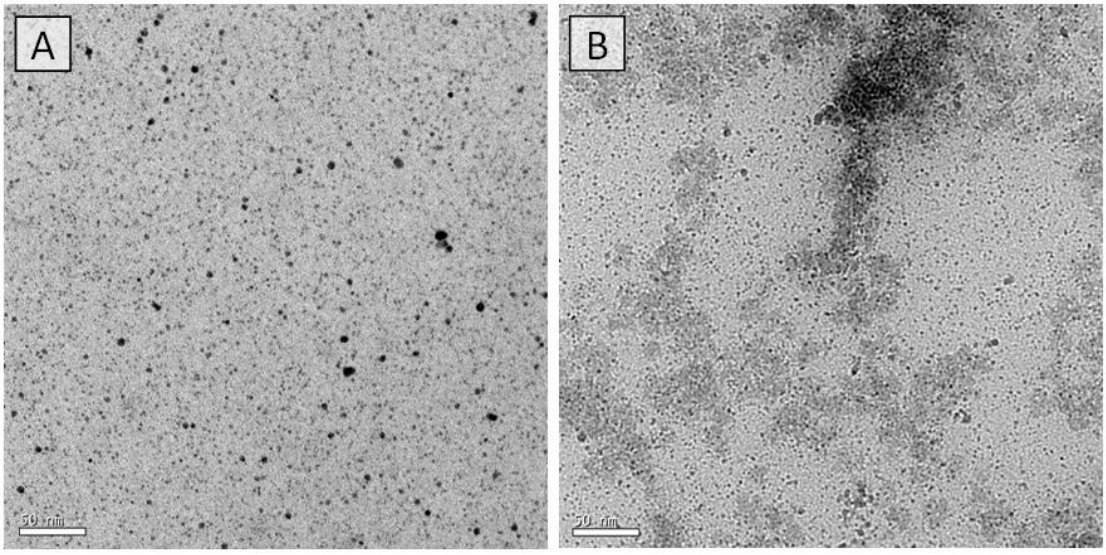

Figure 21 TEM images of BEHP-PPV nanoparticles synthesised using (A) 40 ppm, and (B) 1 ppm of polymer in DCM. Scale bars are 50 nm.

The average hydrodynamic diameters of the nanoparticles determined from the nanoparticles DLS intensity distributions were also found to decrease as the polymer concentration decreased. Table 1 shows the average diameters determined by DLS intensity distribution for each concentration. This is a direct indicator of the decrease in the average diameters of the QD-sized nanoparticles as discussed earlier.

Table 1 BEHP-PPV initial concentrations and their resulting nanoparticles hydrodynamic diameters and standard deviations as determined by their DLS intensity distributions:

BEHP-PPV Concentration before Synthesis (ppm)	DLS Intensity Distribution Average Diameter (nm)	DLS Intensity Distribution Standard Deviation (nm)
40	179.3	68.1
10	146.1	50.5
5	138.5	60.3
1	123.3	54.1

The emission spectra of the SPN solutions are shown in Figure 22. The sequential blue shift in the emission peaks of the SPNs in Figure 22 suggests an increase in the bandgap of the system with the decrease in nanoparticles diameters, most probably arising from a decrease in effective conjugation length. This occurred probably because of the intense aggregation of the polymer chains when they were confined in smaller structures.

With this increase in physical defects in the smaller nanoparticles, a considerable amount of fluorescence quenching is proposed. The quantum yield (QY), which is the measure of fluorescence efficiency of the system calculated as the number of photons emitted divided by the number of photons absorbed, could not be measured for the four SPNs due to the extremely dilute solutions. However, this phenomenon was investigated previously using a high polymer concentration of four different conjugated polymers [135]. The QY was measured before and after centrifugation, which removed the larger particles, and was found to drop for all four SPN solutions. This consistent drop in QY with the decrease in the SPNs average size suggests an increase in fluorescence quenching in the smaller SPNs.

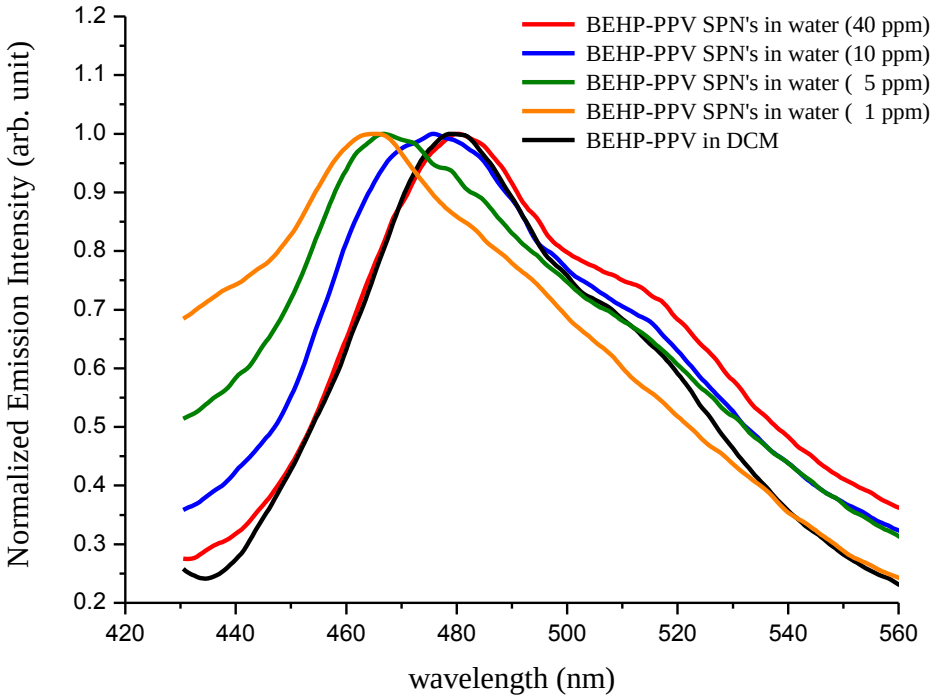

Figure 22 The normalised emission spectra of four BEHP-PPV aqueous nanoparticle solutions synthesised using polymer concentrations = 40 ppm, 10 ppm, 5 ppm, and 1 ppm, under λ_{ex}= 400 nm.

2.3.3 Synthesis using Prolonged Ultrasound Exposures

The synthesis of the nanoparticles using 1 ppm BEHP-PPV was repeated with a modification of the ultrasound exposure time from 10 minutes to 45 minutes. The produced nanoparticles were also of QD-sizes as shown in the TEM images in Figure 23. The average hydrodynamic diameters of the nanoparticles prepared using 45 min of ultrasound exposure was 133.5 ± 47.6 nm as suggested by the DLS intensity distribution. This was not significantly different than that of the nanoparticles prepared under 10 minutes exposure (123.3 ± 54.1 nm). However, the ultrasound exposure was not modified further and no further characterisations were made, therefore no systemic effect was studied.

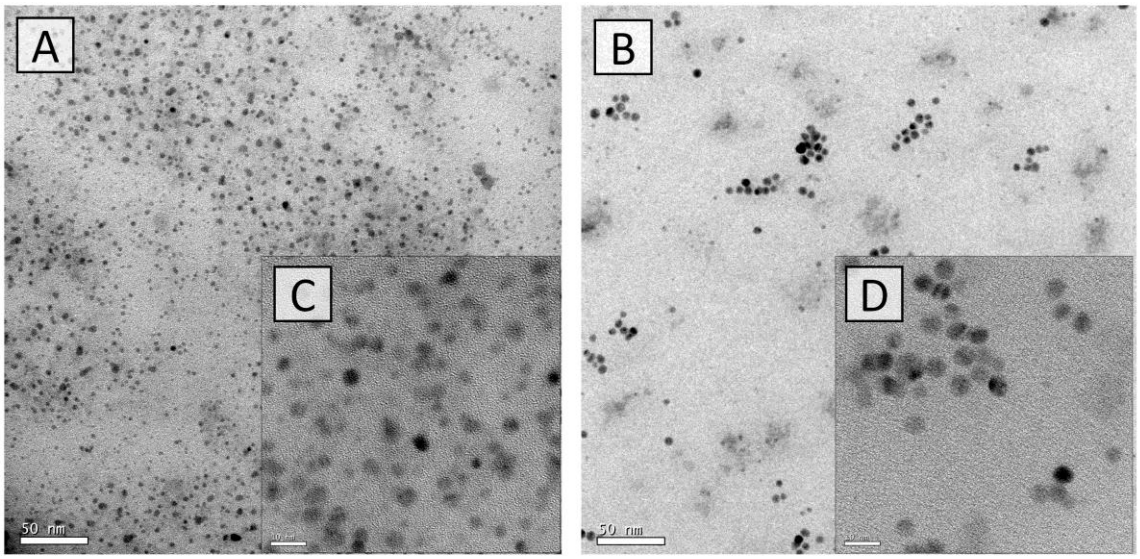

Figure 23 TEM images of BEHP-PPV nanoparticles synthesised using 1 ppm of polymer in DCM under 45 minutes ultrasound exposure. Scale bars are (A, B) 50 nm and (C, D) 10 nm.

2.3.4 The Role of PEG in the Synthesis, and the Effect of Changing its Concentration and Molecular Weight

For the emulsion preparation to be fully successful and stable, the presence of PEG was essential. This was observed when performing the same experimental procedures described previously but using a red emitting polymer; poly[2-methoxy-5-(2-ethylhexyloxy)-1,4-phenylenevinylene] (MEH-PPV) in DCM with/without PEG in water. Both experiments performed with and without PEG resulted in the formation of SPNs. This was confirmed with the observation of a homogeneous suspension of clear, red coloured, aqueous solution after DCM evaporation, and both had similar absorption and fluorescence spectra. However, mixing the conjugated polymer solution in water at the beginning of the synthesis was problematic in the absence of PEG, and the resulting emulsions were not fully stable after the ultrasonication step, while the systems containing PEG formed a relatively stable, milky coloured, emulsion.

To study the effect of the PEG concentration and molecular weight, a series of experiments using BEHP-PPV were undertaken with different quantities and different molecular weights of PEG. The change in the amount of PEG or molecular weight resulted in a consistent change in polymer yield and fluorescence intensity of the produced SPNs. For example, in syntheses using 8 mL/40 ppm BEHP-PPV in DCM in 20 mL of deionised water, the use of very low amounts of PEG300 (below 0.005 g) or very high amounts of PEG300 (above 0.01 g) resulted in low reaction yield, while using an amount of PEG300 between the above mentioned values enhanced the formation of SPNs and increased the final absorption and emission intensities as shown in Figure

24 (A). However, the change in the amount of PEG did not contribute to any change in the SPNs size. This was concluded from comparisons of the normalised fluorescence spectra which did not show any shifts (Figure 24 (B)).

As mentioned earlier, the presence of PEG facilitated the formation of a stable emulsion. However, when the concentration of PEG in the water was substantially increased, the stirring rate was observed to decrease, suggesting that the solution became more viscous. This had a negative effect on the stability of the emulsion, changing the rate at which DCM is emulsified in water, and therefore increasing the percentage of its non-emulsified portion. Consequently, we suggest the majority of the conjugated polymer in the non-emulsified portions of DCM precipitated onto the walls of the reaction vessel after DCM evaporation. This resulted in a lower yield of SPNs in water. Similarly, using a very low concentration of PEG in water resulted in a partially successful emulsion and the same argument applies. The stirring rate also decreased with the increase in the molecular weight of PEG, leading to the same effects. As a result, the final concentration of the QD-size SPNs was found to be controlled by the amount and molecular weight of PEG in water, and the SPNs synthesised using the optimum amount of PEG were found to be more concentrated than the SPNs synthesised without PEG. This was also observed with the use of a high concentration of conjugated polymer (by Dr Philip Howes [135]) (*ca.* 1000 ppm), PEG was essential in obtaining a high yield of SPNs, which approached 100%. Without PEG in the system, the vast majority of the polymer precipitated. These results indicate that PEG has a direct influence on the formation yield of the SPNs.

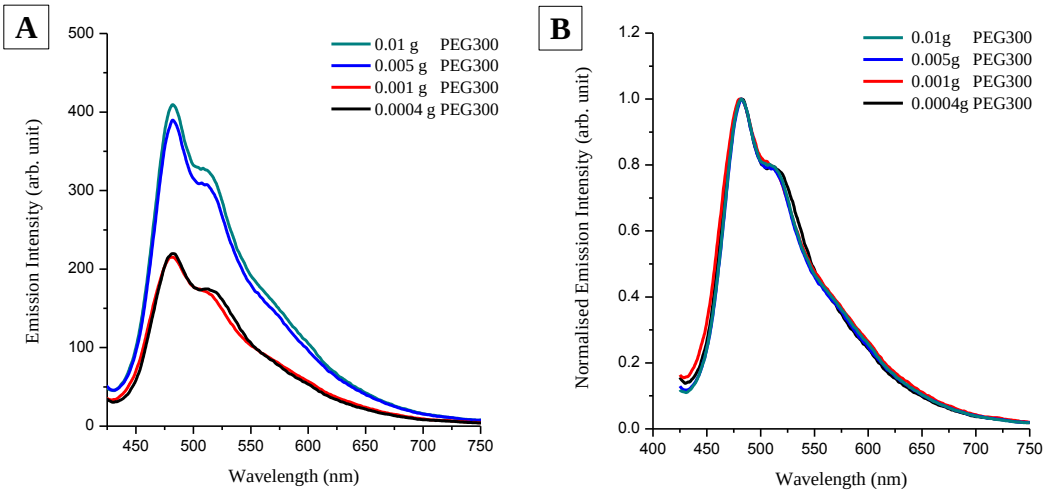

Figure 24 The emission spectra of BEHP-PPV SPNs prepared using 8mL/40ppm polymer solution and different amounts of PEG300 (A) Not normalised, (B) Normalised.

2.3.5 The Refined and Final Synthesis of QD-sized SPNs using BEHP-PPV

The synthesis described in section 2.3.1 was further refined and the following changes were made: a conical flask was used instead of a standard beaker which was covered throughout the

emulsification process to discourage DCM evaporation. The ultimate amount of PEG300 which was found to give the highest reaction yield as described in section 2.3.4, in this case 0.01 g, was used instead of an excessive amount of PEG300 (0.5 g in the first synthesis). The addition of the polymer in DCM solution to the water solution was further controlled by adding it drop-wise to the water solution while stirring. The stirring speed and the position of the flask in the ultrasound bath were adjusted to avoid splashing of the mixture. After 5 minutes of ultrasound exposure, the miniemulsion droplets were assumed to be formed and the lid was removed to enable some DCM evaporation. The solution was kept under high shear for another 15 minutes to encourage the droplets to stay separated in this process. This was because a very small amount of PEG was used compared to previous syntheses. The solution remained opaque throughout the 20 minutes of ultrasound exposure which indicated a decrease in the rate of DCM evaporation with the modifications done in this synthesis. Finally, the emulsion was transferred to a beaker and stirred rapidly to evaporate the remaining DCM. The resulting SPNs solution was then filtered through filter paper and centrifuged to remove any large nanoparticles or bulk materials. (See chapter 5 for full description of the synthesis procedure)

The sizes of the resulting nanoparticles were found to be similar to those of the nanoparticles in the first synthesis, as shown by TEM images of both syntheses (see Figure 25). However, with the above modifications; the reaction yield was higher, and the reproducibility of the refined synthesis was achieved.

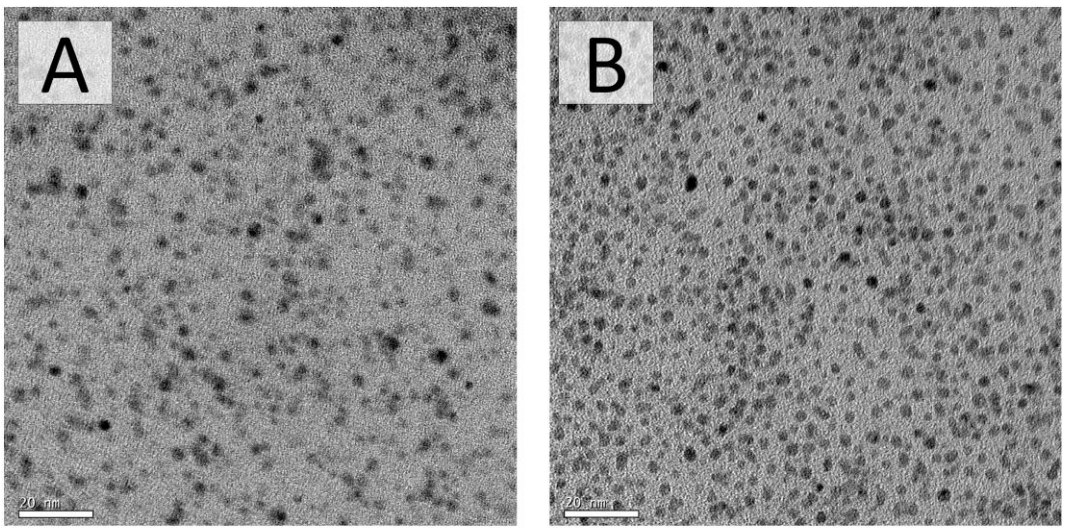

Figure 25 TEM images of BEHP-PPV SPNs prepared using (A) the first synthesis of QD-sized SPNs and (B) the refined and final synthesis. Bar-scales are 20 nm.

2.3.6 The Final Synthesis using Polymers Emitting in Different Colours

Five polymers were used in this work; poly[2,5-di(3’,7’-dimethyloctyl)phenylene-1,4-ethynylene] (PPE) which emits in the blue region of the visible light, BEHP-PPV which emits in

the blue/green region, poly[(9,9-dioctyl-2,7-divinylene-fluorenylene)-alt-co-(2-methoxy-5-(2-ethyl-hexyloxy)-1,4-phenylene)] (ADS108GE) which emits in the green region, poly[(9,9-di-n-octylfluorenyl-2,7-diyl)-alt-(benzo[2,1,3]thiadiazol-4,8-diyl)] (F8BT) which emits in the yellow region, and MEH-PPV which emits in the orange region.

The polymers were dissolved in DCM to form 40 ppm (by weight) solutions. 8 mL of each polymer solution was used independently in syntheses identical to the synthesis described in section 2.3.5. The resulting purified aqueous QD-sized SPN solutions were stable at room temperature for months.

2.3.6.1 Optical Properties

The absorption and emission spectra of the five aqueous SPN solutions are presented in Figure 26 (A, B), and a photograph of the SPNs, under light exclusion and excitation with a 365 nm UV lamp, is shown in Figure 26 (C). Summaries of the optical properties of the produced SPNs and their constituent polymers in dichloromethane (DCM) are presented in Table 2 and Table 3.

The peaks of absorption and emission spectra of the SPN solutions were shifted compared to the spectra of the constituent polymers in DCM (Table 2 and Table 3). This was attributed to the aggregation of the conjugated polymer chains when transferred from the DCM solution into a solid particle, similar to previous reports of polymer aggregation in solution [214-216] and thin-films [134, 217]. Both MEH-PPV and PPE SPNs showed a significant red-shift in their emission relative to the polymer in DCM (31 and 48 nm respectively). This was partially attributed to the aggregation of the chains, resulting in π-orbital overlap and delocalisation of electronic charge across several chains. This resulted in a reduced bandgap when comparison with the polymer in DCM is considered. However, F8BT, ADS108GE, and BEHP-PPV SPNs did not exhibit a significant red-shifted emission, which is as a result of the manner in which these polymers pack into a solid. Previous reports studying polyfluorenes have suggested that tight packing of the chromophores would not necessarily lead to rearrangement of energy levels.[218] All of the polymers (except F8BT) exhibited broadening in their emission tails, and PPE and BEHP-PPV SPNs also exhibited an increased intensity of their secondary (lower energy) emission peak. This is indicative of the formation of emissive aggregates due to the close proximity of chains.[218] It is likely that aggregates also formed in the other SPNs, but these did not contribute strongly to the lower energy emissions. The absorption spectra also tended to broaden. This broadening is demonstrative of the distribution of the electronic charge between the different chain segments in the nanoparticles due to the π-orbital stacking (intrachain and interchain).[131]

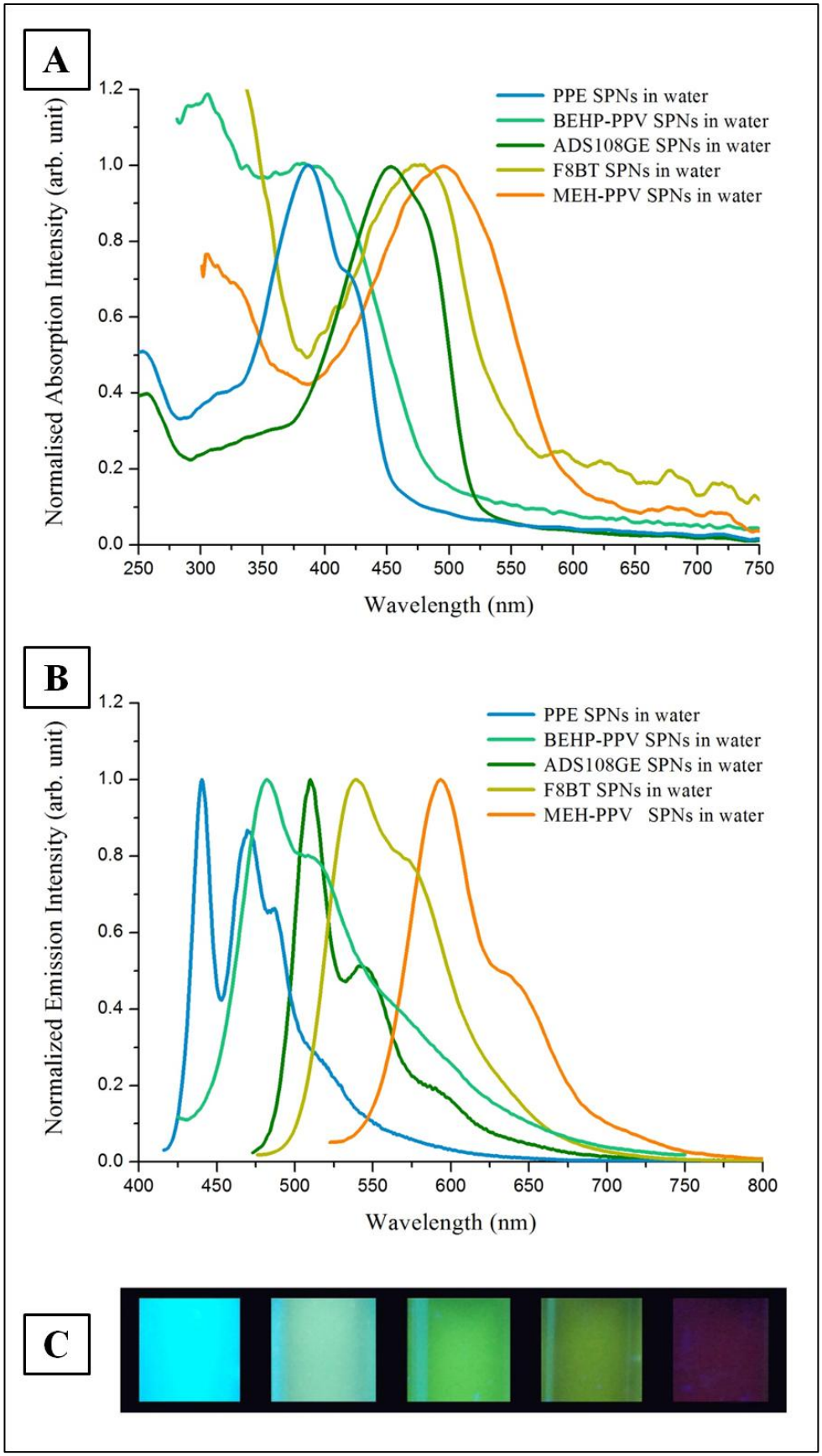

Figure 26 The (A) absorption and (B) emission spectra of the five aqueous SPN solutions, and (C) a photograph of the SPN solutions under 365 nm UV-lamp exposure.

Table 2 A summary of the optical properties of the aqueous SPNs:

Property	PPE SPNs	BEHP-PPV SPNs	ADS108GE SPNs	F8BT SPNs	MEH-PPV SPNs
Fluorescence colour under 363 nm UV-Lamp	Blue	Blue/green	Green	Yellow	Orange
Absorption Peak (nm)	388	400	451	475	496
Emission Peak (nm)	470	482	510	539	593
Quantum Yield (%)	5.9 ± 1.7	0.6 ± 0.1	1.7 ± 0.1	11.6 ± 1.5	0.8 ± 0.1
Extinction coefficient range ($L.g^{-1}.cm^{-1}$)	$18.3 \leq \varepsilon \leq 1830$	$10.47 \leq \varepsilon \leq 1047$	$7.49 \leq \varepsilon \leq 749.9$	$0.707 \leq \varepsilon \leq 70.7$	$1.556 \leq \varepsilon \leq 155.6$

Table 3 A summary of the optical properties of the polymer solutions in DCM before synthesis:

Property	PPE in DCM	BEHP-PPV in DCM	ADS108GE in DCM	F8BT in DCM	MEH-PPV in DCM
Absorption Peak (nm)	383	391	480	447	497
Emission Peak (nm)	422	481	507	537	562
Quantum Yield (%)	59.2	5.0	92	68.6	15.9
Extinction coefficient ($L.g^{-1}.cm^{-1}$)	56.47	9.9	113.07	59.84	85.05

Table 2 and Table 3 also show the quantum yields of the QD-size SPNs and of their constituent polymers in DCM (refer to section 5.6.4 for quantum yield measurements method). A reduction in quantum yield was observed with the SPNs in water as compared to their constituent polymers in DCM. This was attributed in part to the formation of non-radiative species across the polymer chains because of their tight packing in the particles, and has been observed previously in thin-films of MEH-PPV [217]. Excitons can move to structural defects where they decay nonradiatively to the ground state, and increased overlap of π-orbitals can result in the formation of electronic species, such as excimers and aggregates, which quench emission.[134, 217, 219] However, it seems that the final quantum yield was strongly dependent on the initial quantum yield of the polymer, and when polymers with high quantum yields were used, nanoparticles with relatively high quantum yields were obtained.

Due to the nature of the reaction we were unable, at that time, to calculate an exact reaction

yield which therefore hindered our calculations of extinction coefficients. Therefore, the extinction coefficients of the SPNs were estimated to range between two extremes; 100% and 1% reaction yields (refer to section 5.6.5 for extinction coefficients calculations method). The lowest estimated possible values of the extinction coefficients are still considered high (*ca.* 0.7 $Lg^{-1}cm^{-1}$) and comparable to QDs (CdSe extinction coefficients 1.31 – 2.72 $Lg^{-1}cm^{-1}$) [220], with the theoretical maximum significantly higher (1830 $Lg^{-1}cm^{-1}$). Observations of the syntheses suggest they are likely to be nearer the higher values of these ranges. The extinction coefficients of the polymers in DCM were also measured and were found to be within those ranges. The high extinction coefficients compensated for the low quantum yields, and our SPNs were observed to be of high brightness under UV excitation (365 nm).

2.3.6.2 Nanoparticles Size Distributions

TEM images of the SPNs are shown in Figure 27. Diameter measurements from these images showed a range of 0.5 – 6 nm for BEHP-PPV, MEH-PPV, and PPE. Larger nanoparticles were present in the ADS108GE and F8BT samples, with the largest being 21 nm and 14.4 nm in diameters, respectively. However, most of the SPNs of all five polymers were less than 5 nm in diameters, averaging between 2 and 3 nm as shown in the number distribution presented in Figure 28. The number distribution graph also shows that the number of larger nanoparticles in F8BT is significant. TEM examination confirmed that there were no large clusters, suggesting that the synthesis method produces very well defined and QD-sized nanoparticles only.

The average SPNs diameters as determined by TEM and the average diameters of the same samples as suggested by DLS (intensity distributions) are presented in Table 4. The diameters determined by the intensity distribution of DLS were substantially higher than the diameters determined by TEM. However, it is not possible to compare the two values especially that the DLS intensity distributions are considered here and not the DLS number distributions. The average DLS diameters presented in Table 4 give an insight of the presence of nanoparticles in the samples, however they do not represent their average hydrodynamic diameters. The latter should be obtainable from the DLS number distributions of the samples, however, accurate and reproducible number distributions of the SPNs were not obtainable (see section 5.7.2 for further details).

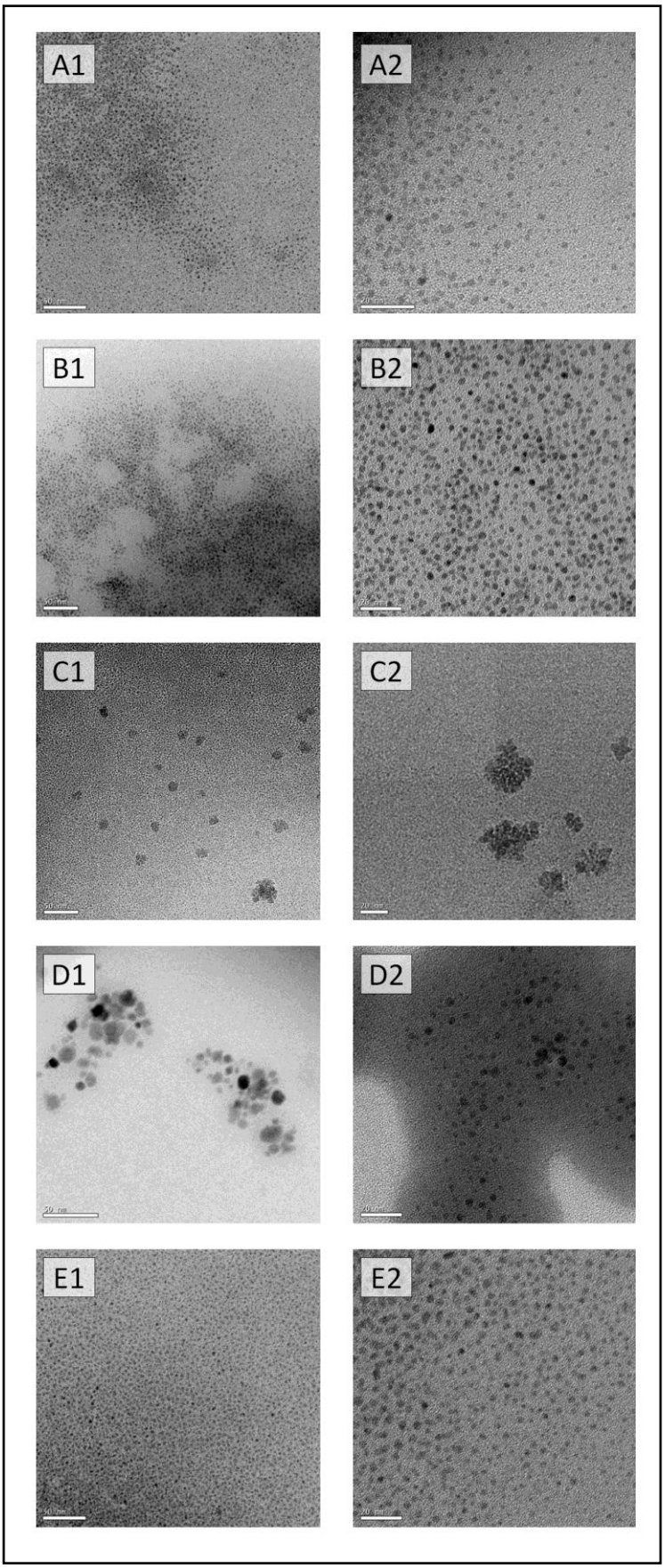

Figure 27 TEM images of (A) PPE SPNs, (B) BEHP-PPV SPNs, (C) ADS108GE SPNs, (D) F8BT SPNs, and (E) MEH-PPV SPNs. Scale bars are (1) 50 nm, and (2) 20 nm.

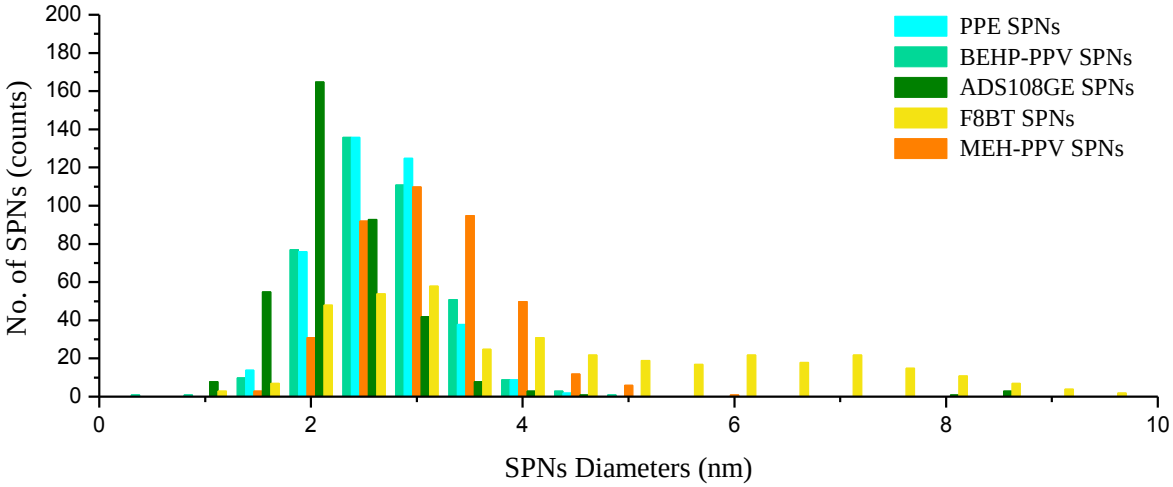

Figure 28 The five SPNs' number distributions measured from TEM images.

Table 4 A summary of the average SPNs' core diameters as measured from TEM images, and the average intensity distribution diameters of the same samples as measured by DLS:

Property	PPE SPNs	BEHP-PPV SPNs	ADS108GE SPNs	F8BT SPNs	MEH-PPV SPNs
TEM average diameter ± standard deviation (nm)	2.92 ± 0.55	2.93 ± 0.62	3.16 ± 2.90	4.78 ± 2.42	3.33 ± 0.76
Average hydrodynamic diameter (intensity distribution in DLS)	194.1	199.13	184.1	273.86	323.53

2.3.7 Investigations about the Capping Agent after Synthesis

Determining the identity of purely organic "capping agents" in organic nanoparticles presents numerous problems. To this end, in one variant of the synthesis, we employed thiolated PEG in our systems, allowing sulfur to be a reporter group that could be detected by mass spectrometry. The synthesis was performed exactly as the refined synthesis described above (section 2.3.5). The PEG-dithiol capped/entwined SPNs were extensively purified by a dialysis method ensuring that no free PEG-dithiol molecules were present in the purified solution (section 5.2.2 and section 5.3 for experimental details). The water used to wash the samples during dialysis was examined and no trace of emission was observed although mass spectrometry detected the presence of PEG-dithiol, therefore we can suggest that the nanoparticles did not pass through the dialysis membrane in contrast to the free PEG-dithiol molecules. Mass spectrometry of the purified sample detected a

sulfur concentration of 297.4 µg/L (compared to 11337.3 µg/L before dialysis), suggesting that, even after the excessive purification process, a ratio of more than 12 PEG-dithiol molecules to 1 polymer chain were present. We conclude that although a significant amount of PEG is needed for a high yield synthesis, not all of PEG molecules were capping or entwined with the SPNs. It is possible that a number of PEG molecules were initially loosely entwined with the polymer particle but then preferably diffused out. However, the loose PEG molecules were dialysed away and the SPNs were still found to be capped/entwined with a considerable amount of PEG.

2.4 Conclusions

The size and surface morphology of a nanoparticle play an important role in its properties and applications. This is because a decrease in size leads to a substantial increase in surface area, and therefore leads to a considerable increase in the nanoparticles' surface related properties. Also, nanoparticles with specific sizes and usually with the lowest size distribution available are preferred in many applications such as to facilitate renal clearance at the end of the nanoparticles use in medical applications. Therefore, if one nanoparticle type is to be proposed as an alternative to another, it has to have competing properties as well as a similar shape and size distribution.

Semiconducting polymer nanospheres are fluorescent nanoparticles which were previously reported to be significantly brighter than quantum dots, with their optical properties being conserved for relatively longer periods of time. However, SPNs were always reported to have relatively larger diameters and a relatively larger size distribution.

In this chapter we report the synthesis of SPNs with diameters similar to those of QDs in an attempt to improve organic SPNs to the level of inorganic QDs when size is concerned. With modifications to the miniemulsion-evaporation method used previously by our group, reproducible PEG functionalised QD-sized SPNs were successfully prepared from five commercially available conjugated polymers. The SPNs had narrow size distributions with average diameters between 2 and 5 nm, and were fluorescent across the visible spectrum. PEG was found to control the concentration of SPNs in water without a significant contribution to their size, providing a new feature which, to our knowledge, was not previously reported.

Control of the miniemulsion-evaporation synthesis method was vital for the production of such small nanoparticles with a high yield. This included the use of PEG, the emulsifier, with a certain molecular weight and a certain concentration, the use of a high shear which is preceded by an initiated emulsion through stirring, the use of a good solvent, DCM, and preventing the solvent's evaporation until the miniemulsion is complete. Another factor was the initial polymer concentration in DCM, with a decrease in polymer concentration leading to a decrease in the nanoparticles' average diameters.

The final SPNs were found to be capped/entwined with PEG as suggested by mass spectrometry

of a purified sample. Their quantum yields were measured and extinction coefficients estimated. The particles were found to be considerably bright and are expected to be effective in various fluorescence applications.[181]

3 Bimodal Gadolinium-Containing Semiconducting Polymer Nanospheres – For MRI and Fluorescence Bio-Imaging

The search for bimodal nanoparticles that act as molecular imaging agents recently began to increase [221-223]. Bimodal nanoparticles in this context refer to nanoparticles which have two probing properties and can be used simultaneously in two bio-imaging techniques such as fluorescence imaging, magnetic resonance imaging (MRI), X-ray computerised tomography (CT), or positron emission tomography (PET). In any diagnosis, more than one bio-imaging technique may identify the problem in hand and each imaging technique can provide complementary information. Imaging agents or probes are usually used to enable, enhance, or improve the contrast of the images obtained by these techniques, or to probe the environment [224-225]. The use of two techniques to probe one species therefore ideally requires a single imaging agent which has the two required probing properties for both techniques, i.e. requires a bimodal imaging agent.[222] The use of nanoparticles as imaging probes has several advantages over conventional imaging agents. Loadability is one of the advantages where the concentration of the imaging agent can be controlled within each nanoparticle during the synthesis process. Another advantage is the tunability of the surface of the nanoparticles which can extend the circulation time of the agent in the blood or target a specific location within the body [70]. With a bimodal nanoparticle system, all the above advantages can be integrated into one system.

In this chapter, we introduce our work in the synthesis of bimodal gadolinium-containing semiconducting polymer nanospheres (Gd-SPNs) which were both fluorescent and MRI active. In the introduction of this chapter, the science behind magnetic resonance imaging and gadolinium as a contrast agent is briefly introduced, followed by a literature review on bimodal nanoparticles. Then, our experimental work towards the synthesis and characterisation of reproducible Gd-SPNs is thoroughly discussed. This is followed by their use in cell imaging and cellular uptake, preliminary tests towards their potential use *in-vivo*, and a measure of their MRI activity.

3.1 Introduction

3.1.1 T1–weighted Magnetic Resonance Imaging and Contrast Agents

Magnetic resonance imaging (MRI) is a medical diagnostic technique which uses signals from the nuclei of hydrogen atoms present in the sample to generate an image.

When a hydrogen atom is placed in an external magnetic field, the magnetic momentum (spin) of its proton aligns with the direction of the field while undergoing precession. Precession, which is a change (wobbling) in the orientation of the proton's rotational axis occurs in a certain frequency called the Larmor frequency (given by Equation 1) that depends on the strength of the external

magnetic field and the type of spinning system involved (the proton in this case).

$$\omega_o = \gamma_o \times B_o$$

Equation 1 Larmor frequency equation, where ω_o is the Larmor frequency in megahertz (MHz), γ_o is the gyromagnetic ratio and is specific to the particular nucleus involved, and B_o is the strength of the magnetic field in tesla (T). The gyromagnetic ratio of protons is 42.58 MHz/T.

In a magnetic field, a proton's spin is aligned either parallel or anti-parallel to the direction of the magnetic field with more spins energetically favouring the parallel alignment resulting in a net longitudinal magnetisation. When an electromagnetic wave with a frequency equivalent to the Larmor frequency is applied to this stable spin system in the form of an exciting radiofrequency pulse, the longitudinal magnetisation is rotated 90º to the transverse plane and is now called transverse magnetisation. The transverse magnetisation undergoes precession (rotation) about the longitudinal axis generating an alternating voltage in a receiver coil which has the same frequency as the Larmor frequency. This MR signal is then collected and processed to generate the MR image. However, the MR signal is short lived and the excited spin system decays to its pre-excited state, i.e. undergoes relaxation, by two independent but simultaneous processes; spin-lattice interactions causing a T1 longitudinal relaxation, and spin-spin interactions causing T2 or T2* transverse relaxation.

In a T1 relaxation process, the excited nuclei of the hydrogen atoms in the system return to their ground states by dissipating their excess energy to their surroundings (lattice) decreasing the system's transverse magnetisation and restoring its longitudinal magnetisation. The time constant for this recovery (T1) is therefore dependant on the Brownian motion of the surrounding molecules and on the strength of the external magnetic field.

In a T2 relaxation process, the protons' spins lose their phase coherence and become out of phase cancelling each other's effects resulting in a decrease and finally a disappearance of their net transverse magnetisation without any energy dissipation to their surroundings. Spin de-phasing is caused either by energy transfer between the spins which interact with each other under the influence of their small magnetic fields causing a transverse relaxation with a time constant (T2) that is independent of the external magnetic field's strength, or by the intrinsic inhomogeneities of the external magnetic field which is due to the magnetic field generator and the imaged object/person (tissue borders, and local magnetic fields generated by paramagnetic objects/particles present) causing a faster transverse relaxation with a time constant (T2*).

T2 relaxation occurs within the first 0.1 – 0.3 seconds of exposure, while T1 relaxation and full longitudinal magnetisation recovery takes 0.5 – 5 seconds.

To generate a T1–weighted MR image, the tissue/body slice is excited many times and the MR signals are collected each time. The time interval between two successive excitations is called the

repetition time (TR). If TR is short (less than 0.6 sec), tissues with a short T1 have enough time to relax and restore much of the longitudinal magnetisation before the next excitation. With most of the longitudinal magnetisation restored, the second excitation results in a large MR signal. Therefore, these tissues appear bright in the MR image. On the other hand, tissues with a long T1 do not experience much relaxation and not a lot of the longitudinal magnetisation is restored before the next excitation. With small longitudinal magnetisation available for the second excitation, a small MR signal is obtained. Tissues with a long T1 therefore appear dark in the MR image.

If TR is fairly long, all tissues including those with long T1 values have enough time to relax and restore the longitudinal magnetisation and therefore they all give similar signals and result in an image with a very poor contrast. Because the different T1 values of the different tissues do not contribute much to the contrast of the image it is said that the measurement has low T1–weighting. Therefore, to obtain a T1–weighted image with a high contrast between the different tissues, strong T1–weighting has to be used by the use of a short TR. The contrast of the image is therefore dependent on the intrinsic properties of the tissues and on the pulse sequences of the MR scanner.

To further enhance the natural contrast of an MR image, pharmaceutically prepared contrast agents are sometimes administered prior to and/or during the MRI measurements. Contrast agents are also used to determine pharmacokinetic information.

Contrast agents alter the contrast of the obtained image either directly by changing the density of protons in the tissue, or in-directly by changing the local magnetic field or the resonance properties of the tissue and hence the tissues T1 and/or T2 values.

The relaxation efficiency of an MR contrast agent, *relaxivity* (r_1 in T1–weighted imaging, and r_2 in T2–weighted imaging), is defined as the reciprocal of the relaxation time T1 (or T2) in a one-molar solution at a temperature of 20 ºC and a given Larmor frequency/field strength. The higher the relaxivity, the better the interaction of the contrast agent with its nearby water protons, and therefore the more efficient the contrast agent is in speeding up their relaxation (in the example of T1–weighted imaging) and hence increasing the MR signal.[226]

The relaxivity of a contrast agent also depends on other factors such as its rotational correlation time associated with its Brownian motion (with a higher correlation time corresponding to a more efficient contrast agent), the number of water–agent interaction sites, and the water residence time (which is the time the water molecule stays bound and interacting with the contrast agent).[227]

3.1.2 Gadolinium as a Contrast Agent in MRI

3.1.2.1 Gd-DTPA as a T1–weighted MRI Contrast Agent

Gadolinium (as well as manganese, chromium, and iron) is a paramagnetic metal ion. It contains 7 unpaired electrons, and therefore its paramagnetic moment is relatively high. Paramagnetic ions

were found to affect the contrast of MRI images indirectly by decreasing the T1 relaxation time of the surrounding hydrogen protons in water, resulting in a brighter area in the image.

However, most of these ions are extremely toxic and cannot be used in MRI imaging of live cells without a reduction of their toxicity. One way to reduce the toxicity of gadolinium was found by chelating the gadolinium atoms with diethylene triamine pentaacetic acid (DTPA, see Appendix 1 for chemical structure) and forming what is known as a water soluble Gd-chelate called gadopentetate dimeglumine (Gd-DTPA). Gd-DTPA has a high binding constant, therefore the probability of finding free Gd radicals is significantly low which is considered an advantage.[228] The first trial of experimenting with Gd-DTPA in human volunteers was in 1983 which was followed by future trials [229], and now, the clinical use of Gd-DTPA is approved.[230]

Gd-DTPA is a low molecular weight chelate, has a short rotational correlation time (τ_r) associated with its Brownian motion, and a low energy exchange rate since it has only one water coordination sight. Therefore, for a considerable contrast, a very high concentration of Gd-chelates should be present in the imaged tissue. This is far from ideal, and the efficiency of using Gd-chelates in imaging is significantly low (several % of what is theoretically predicted). Several approaches were encountered to circumvent this problem, one of which is by increasing the number of active ions per particle by incorporating many Gd-chelates in dendrimers, micelles, liposomes, or nanoparticles.[230-231]

3.1.2.2 Gd-DTPA-BSA as a T1–weighted MRI Contrast Enhancing Bipolar Lipid

As mentioned in the previous section, one of the solutions for a better MRI contrast agent using Gd-DTPA is by attaching multiple Gd-chelates to one particle. One route to achieve this is by synthesising Gd-DTPA bipolar lipids to form liposomes or to coat readily made nanoparticles.[231-232] Bipolar lipids (also called amphiphilic molecules) are molecules which have hydrophilic heads and hydrophobic tails. When dispersed in water, their hydrophobic tails tend to aggregate together pointing their hydrophilic heads towards the surrounding water forming micelles, liposomes, or bilayer sheets as illustrated in Figure 29.

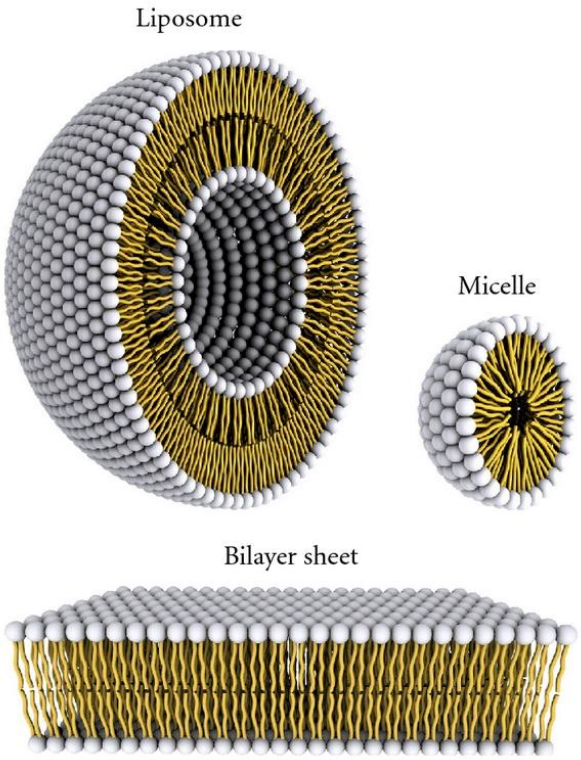

Figure 29 A schematic of a micelle, a liposome, and a bilayer sheet. The white spheres represent the hydrophilic parts of the amphiphilic molecules (heads), while the yellow lines represent the hydrophobic parts of the amphiphilic molecules (tails).[233]

Bipolar lipids were also found to be useful in stabilising emulsion systems. In an oil-in-water emulsion, for example, lipids favourably aligned themselves on the interface between oil bubbles and the surrounding water, pointing their tails towards the bubbles and their heads towards water, forming well dispersed micelles which contained the hydrophobic solution in their cores. In water-in-oil emulsions, however, they align themselves the other way around, forming what are known as inverse micelles which stabilise the water bubbles in oil. This simple principle allowed the formation of drug containing liposomes and micelles in drug delivery studies [234], and facilitated the dispersion of hydrophobic nanoparticles in water.[194]

The first bipolar lipid formed using Gd-DTPA is Gd-DTPA-bis(stearylamide) (Gd-DTPA-BSA).[235-236] Its structure is presented in Figure 30. Liposome agents made using Gd-DTPA-BSA were found to be large MR signal enhancers in T1–weighted MRI, and were found suitable for imaging several organs such as the liver and bone marrow.[231, 236] Other Gd-DTPA lipids were synthesised after that [231], however, since we used Gd-DTPA-BSA in our syntheses, which was already commercially available in contrary to many others, we did not consider the other Gd-DTPA lipids any further.

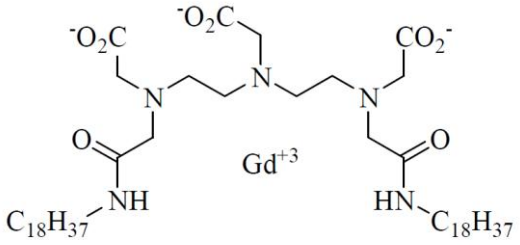

Figure 30 The chemical structure of Gd-DTPA-BSA.[237]

3.1.3 Bimodal Nanoparticles

Different bimodal nanoparticles which act as fluorescent probes for optical imaging and contrast agents in MRI have been reported. For the fluorescence property, either inorganic quantum dots [38, 97], fluorescent dyes [119, 238], or fluorescently labelled lipids [239] were used. As MRI contrast agents, either superparamagnetic agents such as iron oxide (Fe_3O_4) nanoparticles [38, 240] or paramagnetic agents such as gadolinium (in the form of Gd-lipids [97] or as doping atoms [241]) were used. Different methods of synthesis have produced various modes for incorporating multiple imaging agents. For example, one component of the system may be coating the other or they may be covalently attached [38], both agents may be embedded in a carrier such as a silica [238, 242] or a polymer [119, 243] nanoparticle, one agent may be embedded in a carrier which is coating the second agent [243], or both agents may be incorporated together into a micelle or liposome [122, 239]. Several articles have been published recently reviewing fluorescent and MRI active bimodal nanoparticles' properties, their synthesis, and applications [70, 221-223, 243].

As introduced at the beginning of this thesis, conjugated polymer nanoparticles or semiconducting polymer nanospheres (SPNs) are fluorescent organic nanoparticles which are synthesised from benign conjugated polymers [114]. These nanoparticles may be used in similar applications to QDs and may even be superior to QDs due to their high fluorescence stability and enhanced biocompatibility [34, 36, 136, 196, 244]. The use of conjugated polymers in bimodal systems was reported previously, however, the systems were composed of aqueous conjugated polymers which were covalently bound to gadolinium containing molecules [245-246]. These systems therefore lacked the advantages of nanoparticle systems and limit the syntheses to hydrophilic conjugated polymers only.

Bifunctional (bimodal) phospholipid capped/entwined SPNs embedded with iron oxide nanoparticles were reported previously by our group [182]. The SPNs had diameters ranging between 160 and 380 nm after centrifugation, and they had very low fluorescence quantum yields in comparison to non-iron oxide phospholipid encapsulated SPNs [36, 182]. The strong iron oxide nanoparticles' absorption of the wavelengths of light used to excite the nanoparticles contributed significantly to the final quantum yields of the SPNs, a problem which can be avoided by using less

light absorbing MRI active components. These bimodal iron oxide containing SPNs compare non-favourably to similar bimodal quantum dots due to their larger diameters, lower QYs, and higher polydispersity [97].

Bimodal, MRI active and fluorescent, systems containing Gd-DTPA-BSA in the form of dye-labelled liposomes were synthesised and were found useful for both probing techniques [93, 121-122, 230, 247-249]. Recently, the same group used quantum dots for the source of fluorescence and coated them with Gd-DTPA-BSA and PEGylated lipids to form bifunctional nanoparticles [97]. Inspired by their work, the work of our group [36, 135], and the work of others [250], we investigated a new bimodal SPN system comprised of SPNs coated/entwined with a layer of mixed phospholipids including Gd-DTPA-BSA as the MRI active lipid. The work towards the synthesis of these Gd-SPNs is presented in the following section.

3.2 Towards the Synthesis of Reproducible MEH-PPV Gd-SPNs

3.2.1 Non-Reproducible Synthesis Attempts of MEH-PPV Gd-SPNs

First attempts to produce Gd-SPNs were carried out using the same synthesis method described by Howes *et al.*[36]. The same materials were also used but with the modification of the lipids' contents to incorporate Gd-DTPA-BSA instead of 1,2-dipalmitoyl-sn-glycero-3-phosphocholine (DPPC, see Appendix 1 for chemical structure of DPPC) while conserving the same total number of lipids used.

In the first synthesis, 7.6 mg 1,2-dipalmitoyl-sn-glycero-3-phosphoethanolamine-N-[methoxy(polyethyleneglycol)-2000] (ammonium salt) (PEG2000-PE, see Appendix 1 for chemical structure) and 4.5 mg Gd-DTPA-BSA were dispersed in a 16 mL polymer solution containing 40 ppm MEH-PPV in DCM by stirring for 10 minutes. Then, the polymer solution was added to a beaker containing 20 mL water under high shear (35kHz ultrasound bath). After 1 minute, an electric mixer was introduced and the solution was mixed vigorously under ultrasound exposure. This setting was maintained until the solution turned from milky orange to clear red (within minutes) indicating the full evaporation of DCM and the formation of the particles. The particles solution was then filtered through filter paper and centrifuged (10,000 rpm ~ 5,600xg) for 10 minutes to remove the large particles and any dispersed bulk polymer.

The synthesis method described above produced a system of different nanoparticles which were not all perfectly spherical in shape as shown in the TEM images in Figure 31 (A and B). The nanoparticles were of dimensions ranging between a few nanometers and a micron. Many of the formed particles were also not densely packed as seen in Figure 31 (A), and a good amount of polymer was dispersed without forming a defined shape as shown in Figure 31 (C). Figure 31 (D) is a magnified section of the bundled and dispersed polymers with the sub-nanometer sized dark

dots possibly representing the semiconducting segments of the chains or representing non-capped nanoparticles formed from single polymer chains which collapsed and precipitated due to the vigorous and abrupt mixing in the synthesis method. It is probable that with the increase in the centrifugational time, most of the dispersed polymers would have been removed. However, prolonged centrifugation was shown to break down most of the particles in the majority of our syntheses.

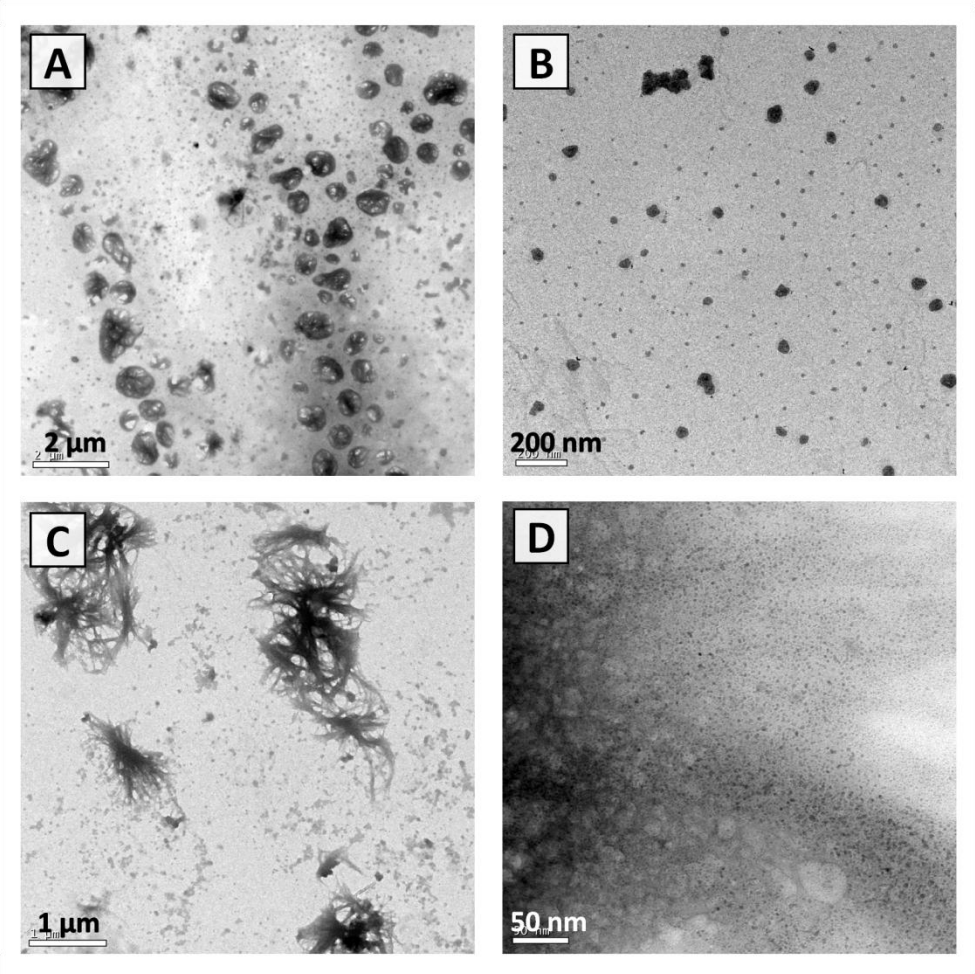

Figure 31 TEM images of the first synthesis of Gd-SPNs.

In an attempt to reduce the nanoparticles' sizes and obtain a better nanoparticle suspension, the same synthesis method was repeated but with half the amount of polymer solution (a ratio of 8 mL to 20 mL emulsified solution to water instead of 16 mL to 20 mL). The isolated nanoparticles of three repetitions of the synthesis are presented in Figure 32 (first synthesis in (A and B), second synthesis in (C and D), and third synthesis in (E and F)). Despite the fact that all three syntheses produced very small SPNs similar to those produced in the first synthesis (dark dots in the images), each synthesis also produced a different system. Figure 32 (A), for example, shows a system of large nanoparticles most probably stabilised by the lipids used, while Figure 32 (C) shows a micellar system with QD-sized SPNs attached to the surfaces of the micelles. Figure 32 (E) shows

a liposomic structure with empty bubble-like areas filled with one or a few nanoparticles. With such a huge variation in the systems produced, the synthesis method had to be further revised. Other synthesis attempts, this time using exactly the same method as that used in the synthesis of PEG capped/entwined QD-sized SPNs (presented in Chapter 2), were also not successful.

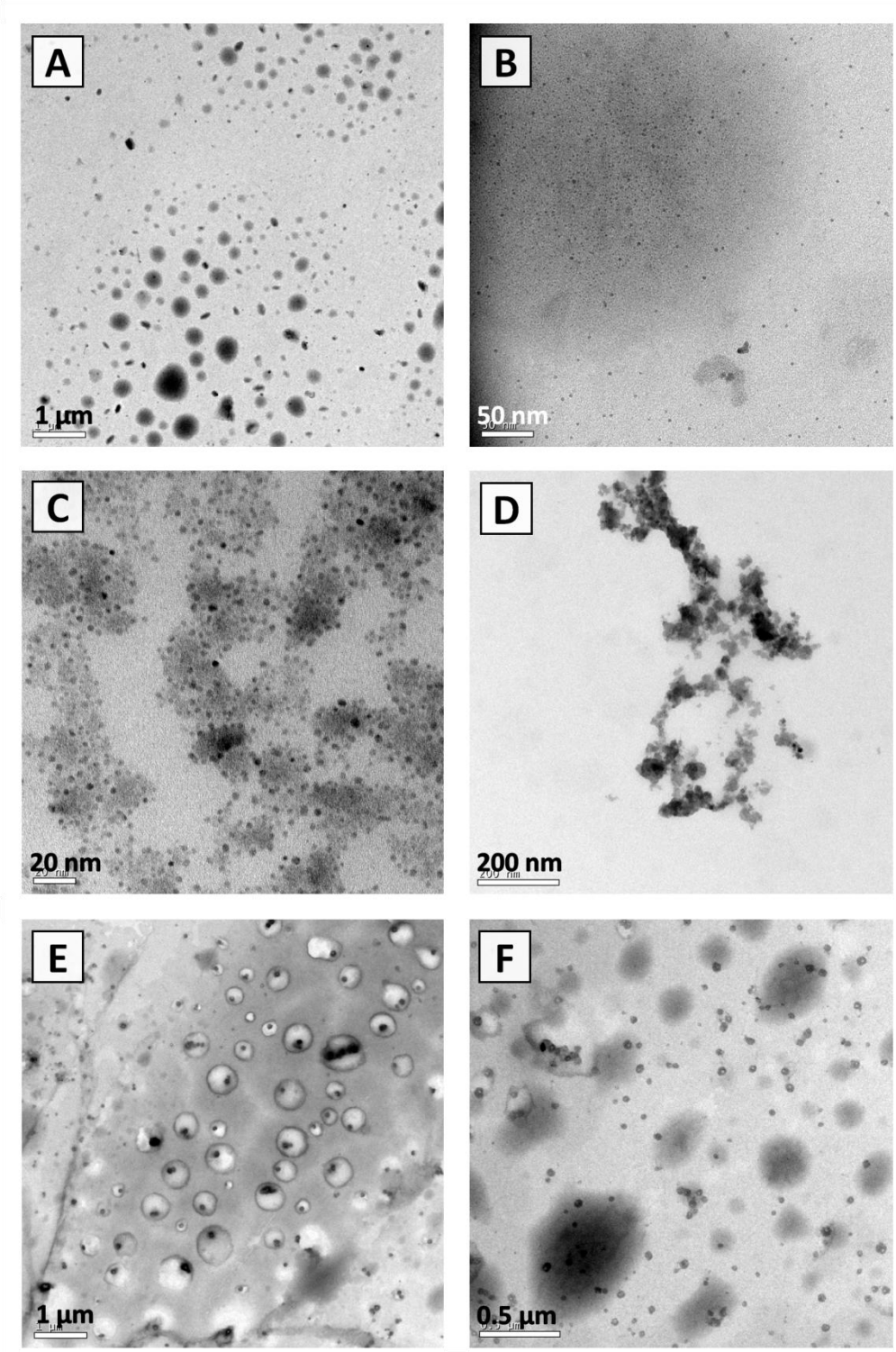

Figure 32 TEM images of three syntheses of MEH-PPV Gd-SPNs using the same synthesis method as in the first synthesis but with half the volume of polymer solution.

3.2.2 A Modified Synthesis Method for Reproducible MEH-PPV Gd-SPNs with Large Sizes

Further investigations revealed that the main reasons behind the non-reproducible Gd-SPNs systems were both the robust synthesis method used and the low concentrations of the lipids in the emulsified system. This conclusion coincided with a publication by Liu *et al.* [251] who synthesised biodegradable polymer nanoparticles capped with 1,2-dilauroylphosphatidylocholine (DLPC) lipids using a very high concentration of lipids compared to our first trials. The lipids were first dispersed in water under four cycles of ultrasound exposure in an ice bath (60 seconds exposure followed by 30 seconds rest), then the polymer in DCM solution was stirred in the aqueous solution and the mixture was sonicated with an ultrasonicating probe in an ice bath. The emulsion was then stirred to evaporate DCM.

In our modified synthesis, we used a similar synthesis method as that described above. In the synthesis, 38.2 mg PEG2000-PE, 10.5 mg DPPC, and 15.3 mg Gd-DTPA-BSA were suspended in 25 mL of deionised water in a round-bottom flask similar to Liu *et al.* [251]. The lipid suspension was then magnetically stirred for 1 minute and 1.6 mL of the polymer solution was introduced with a syringe over a period of 60 seconds. The volume of polymer solution to the volume of water was also the same as that used by Liu *et al.* (they used 16 mL polymer solution in 250 mL water) and similar to the volume ratio used in our final synthesis of QD-sized SPNs (section 2.3.5). The flask was covered and stirred vigorously for 10 minutes to initiate the emulsion. Then it was sonicated in an ultrasound ice water bath for 90 seconds. Finally, the created miniemulsion was gently stirred overnight to form the nanoparticles by full evaporation of DCM.

Figure 33 shows TEM images of the produced Gd-SPNs. The nanoparticles were perfectly spherical in shape and a large number of them were of sub-microns in size. Figure 33 (B) also shows that there was a large amount of excess lipids which were not associated with the nanoparticles. The smaller the nanoparticles, the larger their surface areas, and the more lipids are needed to cover these surfaces. Therefore, if the nanoparticles were decreased in size, it is suggested that less excess lipids will be present at the end of the synthesis.

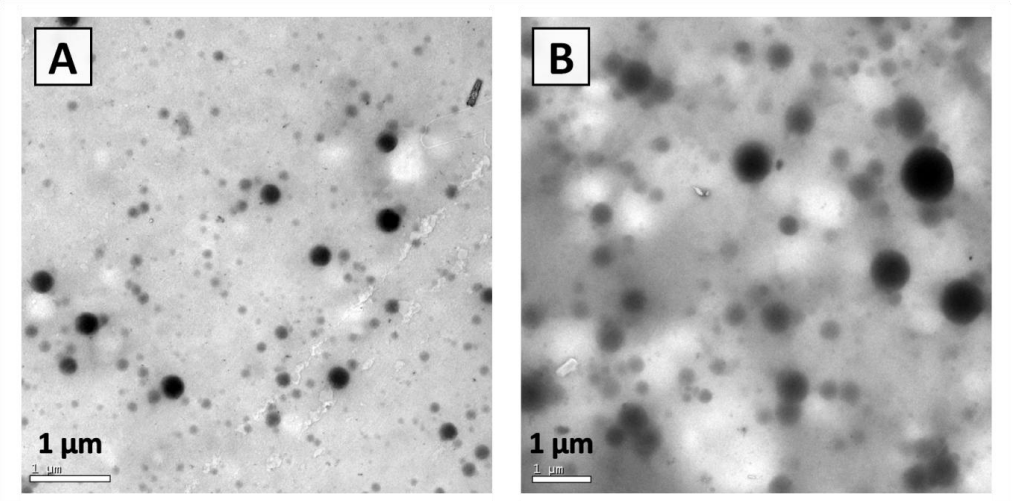

Figure 33 TEM images of the first MEH-PPV Gd-SPNs prepared with the modified synthesis method.

3.3 The Final Synthesis of MEH-PPV Gd-SPNs

To reduce the average nanoparticles' diameters in the above synthesis, half the amount of polymer solution was used (a ratio of 0.8 mL to 25 mL emulsified solution to water instead of 1.6 mL to 25 mL). The produced nanoparticles shown in Figure 34 were similar in shape to the previous nanoparticles (Figure 33) but were of smaller diameters. The observed conservation of the spherical shapes of the nanoparticles in both syntheses proved that the modified synthesis was successful in reproducing the desired Gd-SPNs system.

Most of the SPNs in this final synthesis were of diameters below 50 nm as shown in Figure 34 (A, B and C), with a few larger SPNs with diameters around 100 nm (Figure 34 (D)). All the nanoparticles were densely packed (Figure 34 (B)) compared to the SPNs prepared in our first attempts (Figure 31(A)). Figure 34 (D) also shows that the samples contained some excess lipids which were not attached to the nanoparticles (the medium grey between the dark grey which represents the nanoparticles and the light grey which represents the background). However, the excess lipids were less than those in the previous synthesis (Figure 33 (B)). The remaining lipids were necessary at the beginning of the synthesis to stabilise all the polymer-containing DCM droplets in water, as the reduction in the amount of lipids with the use of the same method was found to precipitate bulk polymer on the flask at the end of the synthesis.

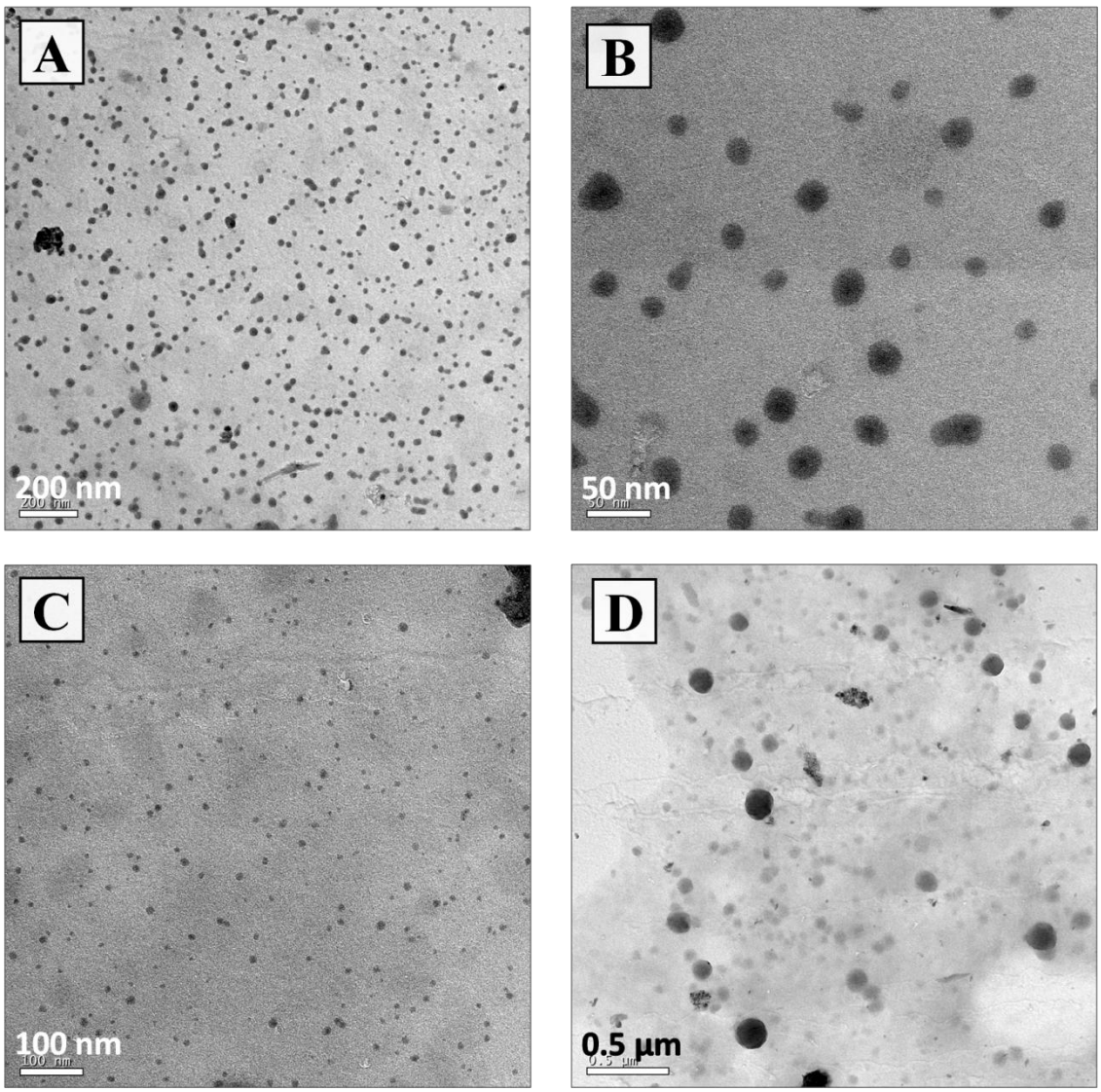

Figure 34 TEM images of the final MEH-PPV Gd-SPNs.

3.4 The Synthesis and Characterisation of Gd-SPNs with Different Fluorescent Colours

3.4.1 Synthesis of the Final Gd-SPNs

The final synthesis described in the previous section (section 3.3) which is a similar miniemulsion-evaporation technique to that used in the synthesis of the QD-sized SPNs (see Chapter 2) was used here, and four colloidally stable gadolinium-containing conjugated polymer nanoparticles (Gd-SPNs) in aqueous media were successfully synthesised from the following polymers; MEH-PPV, F8BT, PPE, and ADS108GE. Again, three lipids were used as the emulsion emulsifier in the synthesis; PEG2000-PE, DPPC, and Gd-DTPA-BSA.

In a typical synthesis, 25 mg of the conjugated polymer was dissolved in 8 mL of

dichloromethane (DCM). 11.2 mg DPPC, 37.4 mg PEG2000-PE, and 13.9 mg Gd-DTPA-BSA were suspended homogeneously in 25 mL of deionised water in a round-bottom flask, (section 5.2.3 for details). The lipid suspension was then magnetically stirred for 1 minute and 0.8 mL of the polymer solution was introduced with a syringe over a period of 60 seconds. The flask was covered, stirred vigorously for 10 minutes to initiate the emulsion, then sonicated for 90 seconds at 7°C to complete the miniemulsion. Finally, the miniemulsion was gently stirred overnight to promote full DCM evaporation and nanoparticle formation. The excess lipids were removed *via* dialysis and the Gd-SPNs solution was filtered through 0.2 µm cellulose acetate filters and stored in glass vials at 4°C, refer to section 5.3 for details. The polymers formed the inner cores of the nanoparticles while the lipids formed the outer shells. A schematic of the Gd-SPNs is presented in Figure 35 (A).

3.4.2 Optical Properties of the Gd-SPNs

The optical properties of the Gd-SPNs are presented in Table 5. The absorption and emission spectra of the four aqueous Gd-SPNs produced in this study are presented in Figure 35 (B and C). They were found to be similar to the spectra of the free polymers in organic solvents and of previously reported SPNs [36, 182, 244]. Photographs of the Gd-SPNs under ambient light and exposed to the excitation of a 365 nm UV lamp in the dark are shown in Figure 35 (D and E).

The brightness of the nanoparticles is very important in fluorescence cell imaging. Brightness depends on two factors; the fluorescence quantum yield (QY) and the wavelength-dependent extinction coefficient. The higher those two values are, the greater the brightness. The quantum yields of the purified Gd-SPNs are shown in Table 5. They are slightly lower than the QY of the same Gd-SPNs before purification and considerably lower than the QY of the constituent polymers dissolved in DCM, also shown in Table 5. It has been noted previously [244] that the increased bending and twisting of the polymer chains in the SPNs in general and with the decrease in their size, results in a decrease in their QY. The slight decrease in QY of the SPNs after purification can therefore be attributed to the removal of bulk polymer and nanoparticles larger than 200 nm. Furthermore, the QYs of the Gd-SPNs are comparable to the QYs of the non-gadolinium-containing SPNs prepared previously by our group [36] (also shown in Table 5) verifying that the inclusion of gadolinium onto the nanoparticles surfaces in the manufacturing process is not detrimental to the fluorescence properties of the bimodal SPNs in comparison to the bimodal SPNs imbedded with iron oxide nanoparticles which suffered from a substantial fluorescence quenching [182]. The QYs of three of the four Gd-SPNs prepared here also confirm that the higher the QY of the polymer in its free configuration form, the higher its QY in its nanoparticle form, similar to our observation in the QYs of the QD-sized SPNs (section 2.3.6.1) [244].

In addition to QY, the second factor which affects brightness is the wavelength-dependent

extinction coefficient. In order to calculate the extinction coefficient from Beer-Lambert's Law, the concentration of the polymer in the sample after purification and filtration must be determined. Therefore, a method for determining the final polymer concentration was developed (section 5.5.3). To this end, the nanoparticles had to be dissolved in a solution which perfectly dissolves both the polymers and the lipids. Dissolving the nanoparticles means unpacking them gently from their nanoparticle form to their neat (free) form. This required full evaporation of water and then the introduction of the ultimate solution $CHCl_3$ + 1% methanol. DLS was used to determine full dissolution before the measurement of the concentration was conducted. The extinction coefficients of the dissolved polymers from the Gd-SPN suspensions were calculated and are presented in Table 5. The high extinction coefficients combined with the considerable QYs of the Gd-SPNs yield high brightness as observed under the UV-light in Figure 35 (E).

Table 5 A summary of the optical properties of the Gd-SPNs:

Property	PPE Gd-SPNs	ADS108GE Gd-SPNs	F8BT Gd-SPNs	MEH-PPV Gd-SPNs
Absorption peak (nm)	388	450	460	495
Emission peak (nm)	470 & 440	508	539	592
Quantum yield of purified Gd-SPNs (%)	22.01	6.98	33.15	1.50
Quantum yield of non-purified Gd-SPNs (%)	25.59	6.90	35.81	1.71
Quantum Yield of polymer in DCM (%)	59.2	92	68.6	15.9
Quantum Yield of reference SPNs [36]	18.98	-	26.9	1.3
Extinction coefficient ($L.g^{-1}.cm^{-1}$) at wavelength (nm)	65.98 ± 0.35 at $\lambda = 390$	91.32 ± 0.57 at $\lambda = 450$	41.36 ± 0.15 at $\lambda = 450$	74.47 ± 0.17 at $\lambda = 490$

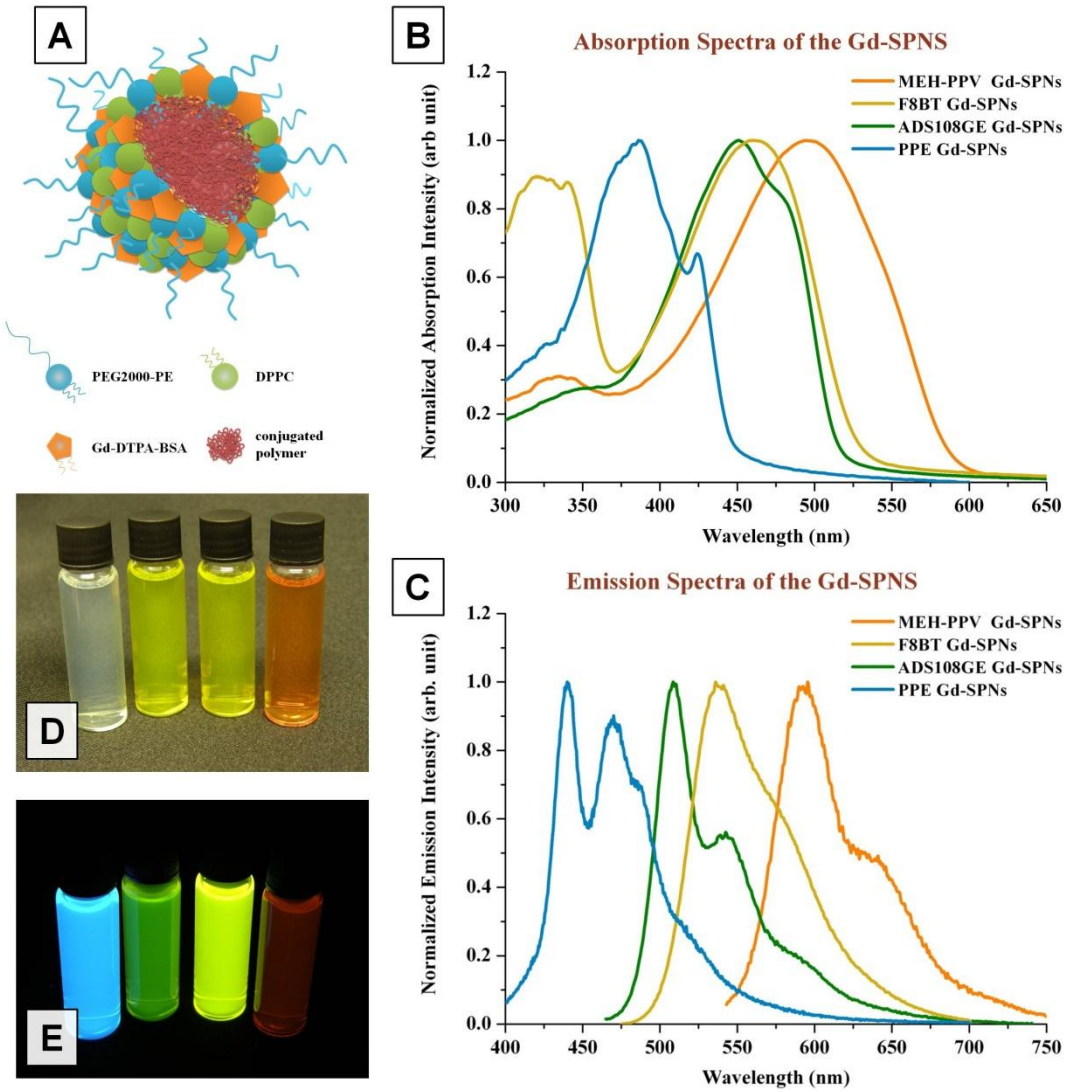

Figure 35 (A) A schematic representing a Gd-SPN. The (B) absorption and (C) emission spectra of the four aqueous Gd-SPN solutions, and two photographs of the SPN solutions under (D) ambient light and (E) 365 nm UV-lamp.

3.4.3 Nanoparticle Size and Colloidal Stability

TEM images of the purified Gd-SPNs are presented in Figure 36 (A – D), and a TEM image of non-purified MEH-PPV Gd-SPNs prepared using double the volume of polymer solution (i.e. 1.6 mL instead of 0.8 mL) is presented in Figure 36 (E). The initial volume of the polymer solution was found to be one of the crucial factors affecting the final particle diameter. Decreasing volumes of polymer solution were found to produce corresponding decreases in nanoparticle diameters. The use of 1.6 mL polymer solution in the pre-final synthesis produced polymer nanoparticles with diameters ~200 nm as shown in Figure 36 (E). By using half that volume in the final syntheses presented here, one ensures that most of the nanoparticles were below 200 nm in diameter before the purification process. During purification, 0.2 µm filters were used to remove any dust, bulk

polymer, or remaining large nanoparticles. This is very important because the samples were exposed to the air overnight during synthesis, and is also important for the DLS measurements which are very sensitive to large particulates. The suspensions were found to pass through the filters smoothly which is another observation that suggested smaller nanoparticles.

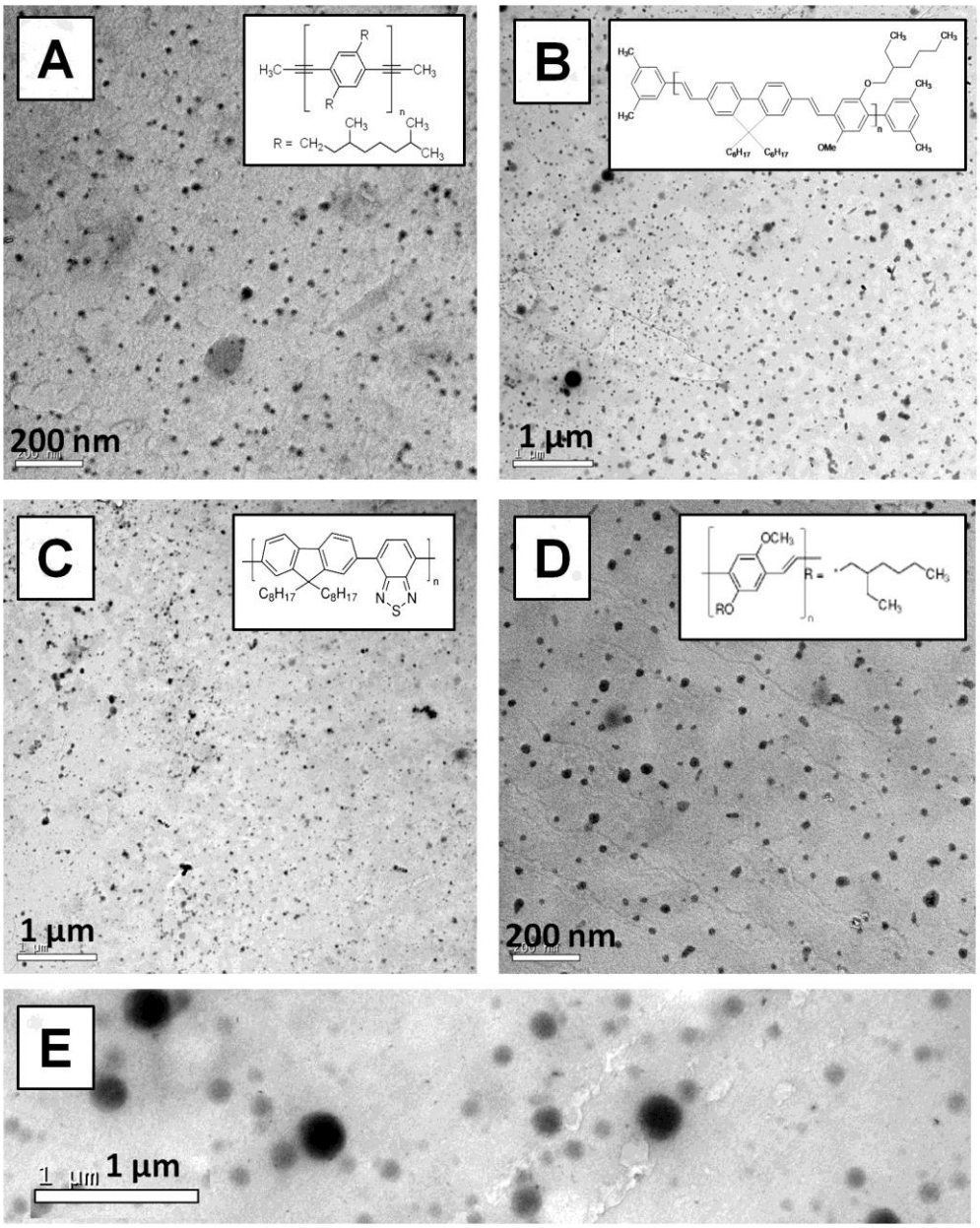

Figure 36 TEM images of purified (A) PPE Gd-SPNs, (B) ADS108GE Gd-SPNs, (C) F8BT Gd-SPNs, (D) MEH-PPV Gd-SPNs, and non-purified (E) MEH-PPV Gd-SPNs. Bar-scales are 200 nm in (A, D), and 1 µm in (B, C, E).

The number-based particle size distributions of the purified Gd-SPNs as derived from the TEM images are shown in Figure 37. For all four Gd-SPN systems, diameters varied between 6 - 140 nm, with average diameters below 35 nm and standard deviation values between 7 - 22 nm (Table

6). Table 6 also shows the average diameters of the nanoparticles in water measured using DLS (cumulant results). The randomly measured diameters using DLS for all four particle types were found to be similar (~111-117 nm) with low standard deviations. The average hydrodynamic diameters which also take into account the non-TEM visible lipidic shells of the Gd-SPNs, measured using NanoSight nanoparticle tracking analysis (NTA) (by Ms. Agnieszka Siupa, NanoSight NTA Company), ranged between 66 – 128 nm (also shown in Table 6). Similar to the average diameters measured from TEM, the average hydrodynamic diameters of the Gd-SPNs also had low standard deviations (27 – 39 nm).

The polydispersity index (PDI), measured by DLS, gives an insight of how polydisperse a nanoparticle system is, with 0 PDI being an ideally monodisperse system and 1 PDI being a highly polydisperse system. The PDI of the Gd-SPNs, also shown in Table 6, was found to be around 0.2. This correlates well with the low standard deviations and the TEM images where nanoparticles' diameters of a few nanometres up to 140 nm were observed.

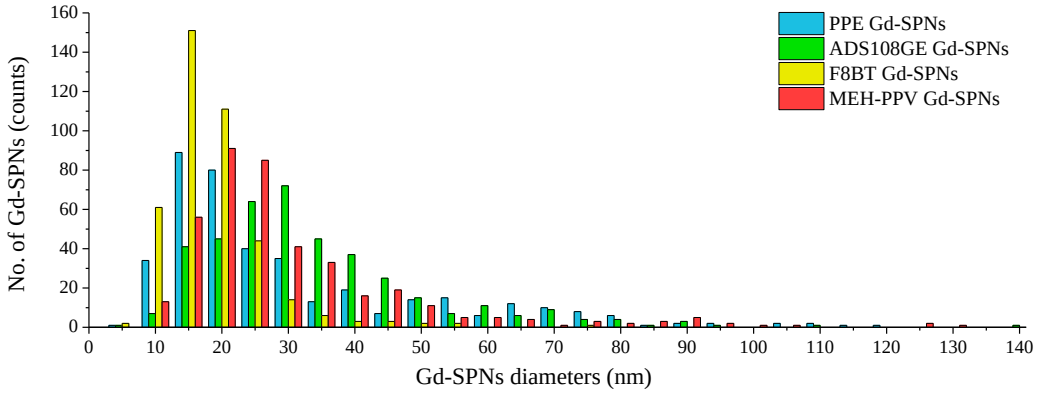

Figure 37 Gd-SPNs' number distributions measured from TEM images.

Table 6 A summary of the Gd-SPNs diameters and polydispersity indices as measured from TEM images, DLS, and NTA:

Property	PPE Gd-SPNs	ADS108GE Gd-SPNs	F8BT Gd-SPNs	MEH-PPV Gd-SPNs
TEM mean diameter (nm)	31.50	34.61	18.96	30.34
TEM standard deviation of diameters (nm)	21.53	17.23	7.48	18.00
DLS cumulants diameter in water (nm)	119.6	110.8	111.9	117
DLS poly-dispersity index	0.259	0.191	0.238	0.179
NTA (mean ± SD) (nm)	128 ± 37	66 ± 28	70 ± 27	118 ± 39

The nanoparticles were also found to be colloidally stable in more complex media. This was concluded from a study measuring the hydrodynamic diameters of similarly synthesised MEH-PPV Gd-SPNs in water and in cell culture medium (CCM) over a period of 24 hours (Figure 38). The colloidal stability of the nanoparticles in more complex media is especially important in bio-imaging applications since an aggregation state may influence their fluorescence properties, as well as the cells interactions.

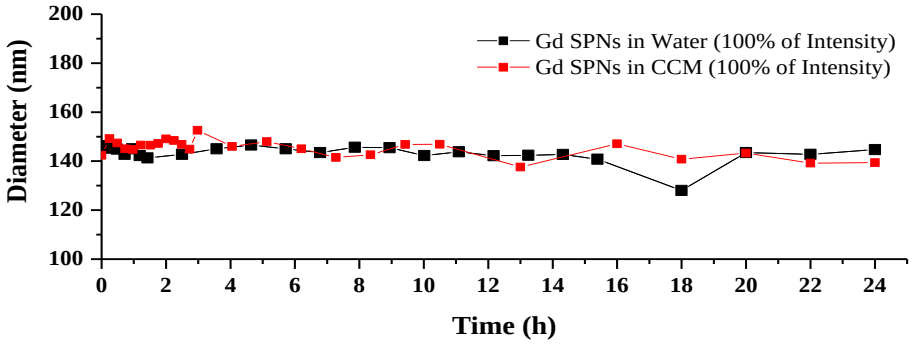

Figure 38 Diameters of MEH-PPV Gd-SPNs, measured by DLS (cumulant results) in water and in cell culture medium (CCM) over a period of 24 hours.

3.5 Bio-imaging *In-vitro* and Cellular Uptake of MEH-PPV Gd-SPNs

The uptake of MEH-PPV Gd-SPNs in two different cell lines was investigated using confocal laser scanning fluorescence imaging: the human epithelial-like cell line, HeLa (performed by Dr Pei-Hua Chung, King's College London) shown in Figure 39, and the murine macrophage-like cell line, J774 (performed by Raha Ahmadkhanbeigi, King's College London) shown in Figure 40, (section 5.8.1 for methods, and Appendix 2 for definitions). As is typical for interactions between PEGylated particles approximately 100 nm in diameter and epithelial-like cells [42, 252], a limited internalisation of MEH-PPV Gd-SPNs was observed in HeLa cells after overnight incubation of the particles with the cells. The diffuse green fluorescence observed in the optical sectioning of the HeLa cells in Figure 39 is indicative of endocytic (see Appendix 2 for definition) uptake of very small particles, while the brighter spots of fluorescence denoted by arrows may be indicative of the uptake of aggregated particles or vesicular fusion within the cell. In contrast, a qualitative comparison of the uptake of MEH-PPV Gd-SPNs in the macrophage-like cell line, J774, shows a much higher internalisation of particles after only two hours of incubation. This is typical of professional phagocytic cells (see Appendix 2 for definition), such as macrophages, which unlike epithelial cells, are designed to efficiently ingest large amounts of particulate matter (even when PEGylated) [253-254]. As expected, the pattern of Gd-SPN derived fluorescence (pseudo-coloured golden-red) in the J774 cells is indicative of vesicular uptake; however, in contrast to the HeLa epithelial-like cells, the fluorescence signal is much sharper, possibly indicating a greater number of particles per vesicle.

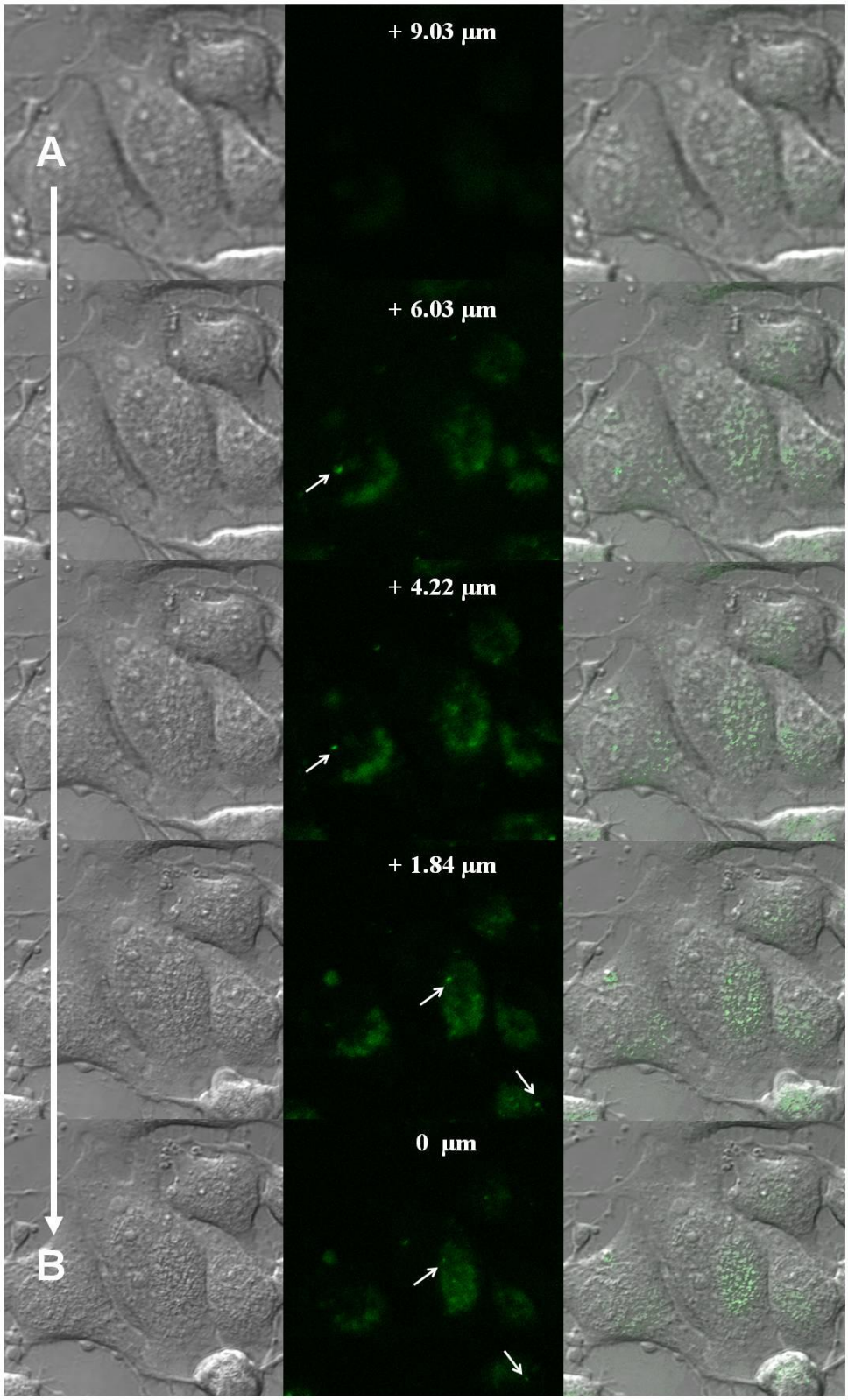

Figure 39 A cross-sectional scan of live epithelial-like HeLa cells incubated overnight with 0.05 mg/mL MEH-PPV Gd-SPNs under bright field (left column) and fluorescence excitation (middle column). The right column is an overlay of the bright field and fluorescent images. Optical sections of the cells were taken from the top (A) to the bottom (B) of the cell monolayer.

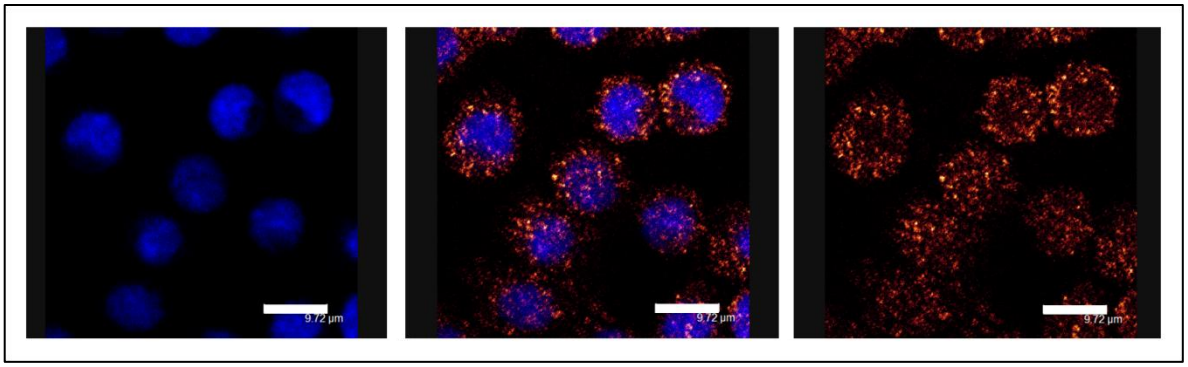

Figure 40 A cross-sectional scan of fixed J774 macrophage-like cells after a two hour incubation period with 0.2 mg/mL MEH-PPV Gd-SPNs. The left image shows the nuclear stain fluorescence (DAPI; pseudo-coloured blue), the right image shows fluorescence from the MEH-PPV Gd-SPN (pseudo-coloured golden-red), and the middle image is an overlay of the two. The optical plane was set at the midpoint between the top and bottom of the cell monolayer. Scale bars are 9.72 µm.

Both images in Figure 39 and Figure 40 demonstrate that Gd-SPNs are suitable for cellular fluorescence imaging applications in different cell types and behave similarly to other types of nanoparticles of a similar size with a PEGylated surface chemistry [255-257]. As with other types of particulate imaging agents, the surface of Gd-SPNs may be modified to target specific cell types or intracellular structures. Further, Gd-SPNs are superior to a variety of fluorescent particles or small molecule fluorescent dyes due to their highly stable fluorescence with little to no photo-bleaching after multiple image acquisitions or long storage periods [34].

Other than the fluorescence intensity used to obtain the images in the imaging technique described above, fluorescence lifetime, which is the average time a fluorophore maintains its excited state before emitting a photon, is another fluorescence parameter which can be used to obtain optical images in a technique called fluorescence lifetime imaging microscopy (FLIM).[225, 258] The fluorescence lifetime of a fluorophore can vary according to its geometrical conformation, internal rotation, and twisting, and its interactions with its surroundings such as nearby molecules [258]. Therefore, the fluorescence lifetimes of the nanoparticles prepared in this study are expected to be different from the fluorescence lifetimes of their constituent polymers. The fluorescence lifetime of MEH-PPV Gd-SPNs in solution (water) was measured (by Dr Pei-Hua Chung, King's College London) to be 0.12 ns (89.4 %), 0.55 ns (9.3 %) and 1.67 ns (1.3 %) yielding an average lifetime of 180 ps (amplitude-weighted) and 429 ps (intensity-weighted) as seen in Figure 41 (section 5.6.6 for method). The increased coiling up and packing of the polymer chains in the nanoparticles was expected to cause an increase in the fluorescence lifetime of the polymer. Zhang *et al.* reported the fluorescence lifetime of MEH-PPV in a good solvent was 0.35

ns (single exponential fit), and in a good and poor solvent mixture was 1.29 ns (7.2%) and 0.57 ns (92.8%) [259], yielding an average lifetime of 662 ps (intensity-weighted) for the coiled up polymer in the solvent mixture (Figure 41 Insert). However, this was not the case in the fluorescence lifetime measurements of the Gd-SPNs where the lifetime was found to be substantially lower than that reported for MEH-PPV in its neat form. Compared to QDs (lifetimes between 10 – 30 ns and up to 500 ns) [258], the fluorescence lifetime of MEH-PPV Gd-SPNs is much shorter.

Despite the fact that dyes with longer fluorescence lifetimes are desired in some applications, such as for finger-print detection, where the background fluorescence is comparably strong [258], the ability to detect the fluorescence lifetime of MEH-PPV Gd-SPNs, which is very short, enables their use as dyes for FLIM imaging which is an imaging technique preferred for its independence on the fluorophor's concentration [260].

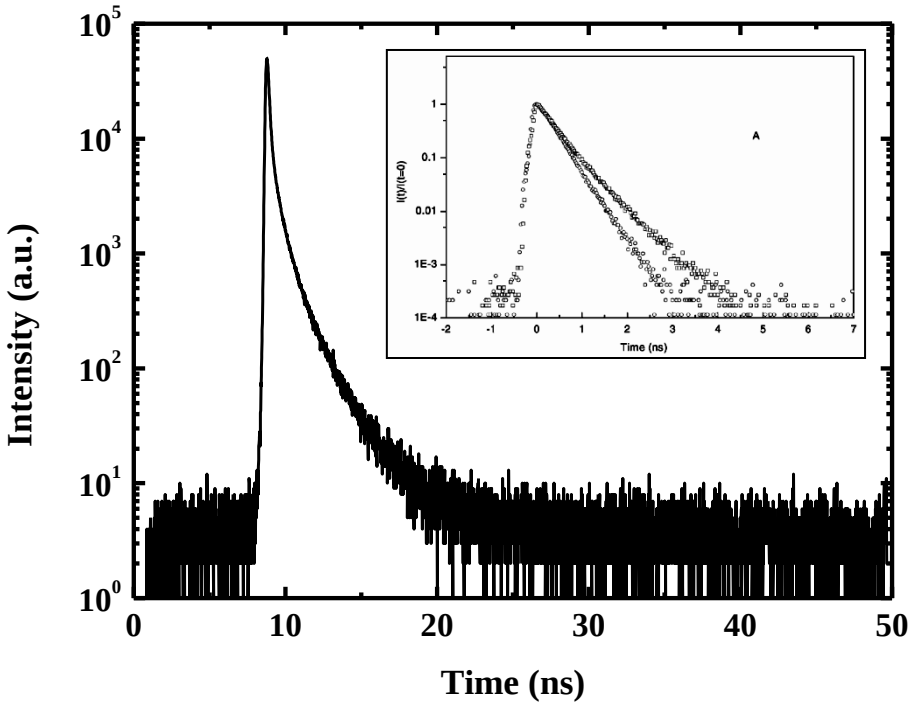

Figure 41 The fluorescence lifetime of MEH-PPV Gd-SPNs. The decay is fitted by a three-exponential function using B&H SPCImage software. The insert is the fluorescence decay of MEH-PPV in two solvents: a good solvent, and a mixture of a good and a poor solvent. Insert copied from reference [259].

3.6 Assessment of Nanoparticle-Antibody Conjugation for Future In-vivo Administration and Specific Ligand Targeting

To conjugate the nanoparticles with any type of antibody, the nanoparticles must include conjugation sites (such as carboxylic groups) on their surfaces. Carboxylation can be introduced to the nanoparticle surfaces by substituting the non-carboxylated PEGylated lipid (PEG2000-PE) with a carboxylated PEGylated lipid (1,2-distearoyl-*sn*-glycero-3-phosphoethanolamine-N-[carboxy(polyethylene glycol)-2000] (ammonium salt)) (DSPE-PEG2000, see Appendix 1 for chemical structure) in the synthesis process. To this end, carboxylated MEH-PPV Gd-SPNs were synthesised and purified from excess lipids with the same method as the non-carboxylated Gd-SPNs prepared in this chapter (sections 5.2.4 and 5.3 for methods). Then, conjugation with IgG (Immunoglobulin G; an immunoglobulin molecule; a plasma or cell-bound glycoprotein with antibody activity; IgG has two antigen binding cites [261]) was performed by linking the carboxylic groups on the nanoparticles surfaces to the amine groups of the antibodies (method similar to Howes *et al.* [36]). Successful conjugation was confirmed by gel filtration and fluorescence detection from washed (Gd-SPNs)-IgG-coated plates but not from washed unconjugated-IgG-coated plates (section 5.8.2). With a simple indirect enzyme-linked immunosorbent assay (ELISA) test, the bound nanoparticles were found not to affect the antibodies' ability to bind to their target ligands (also section 5.8.2). (Antibody linking and post-antibody-linking investigations were performed by Nicola J. Commander, DSTL, Salisbury, UK).

3.7 Assessment of Nanoparticle Fluorescence Against Tissue Auto-Fluorescence

In an assessment of Gd-SPNs' fluorescence against animal tissue's auto-fluorescence, 100 µL F8BT Gd-SPNs (yellow emitting; QY ~ 33% , initial concentration = 110 µg/mL) was injected subcutaneously into an euthanized rat's scruff (performed by Jo Scott, DSTL, Salisbury, UK), and the rat was imaged under an Elmer IVIS spectrometer (see section 5.8.3). The Gd-SPNs' fluorescence was found to be visible through the rat's tissue and distinguishable from the tissue's auto-fluorescence, as shown in Figure 42, which provides promising preliminary results for future *in-vivo* investigations.

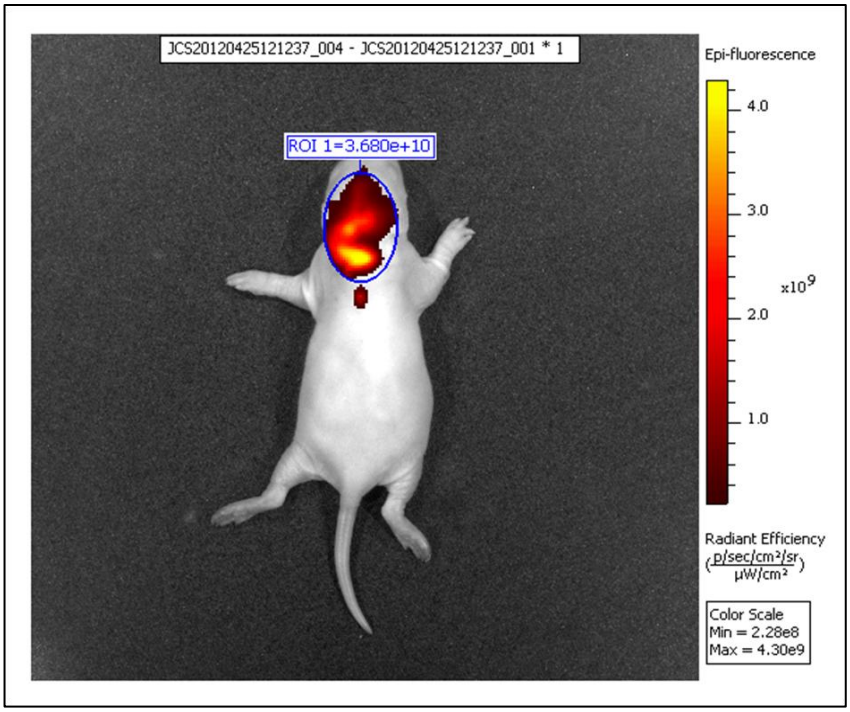

Figure 42 The fluorescence of F8BT Gd-SPNs in an euthanized rat, after subcutaneous injection and auto-fluorescence subtraction. The region of interest (ROI) shows a radiant efficiency of 3.680×10^{10}.

In a further investigation, mouse cadavers were injected (by Nicola J. Commander, DSTL, Salisbury, UK) at three locations with either antibody-conjugated MEH-PPV Gd-SPNs or unconjugated MEH-PPV Gd-SPNs (red emitting; QY ~ 1.5%; concentration ~ 35.6 µg/mL); 100 µL MEH-PPV (Gd-SPNs)-IgG solution (neat concentration which contained ~ l000x diluted Gd-SPNs) was injected into the quadriceps muscle of an euthanized mouse, 100 µL MEH-PPV Gd-SPNs suspension (concentration ~ 35.6 µg/mL) was injected subcutaneously on the ventral surface, and 100 µL MEH-PPV Gd-SPNs suspension (concentration ~ 35.6 µg/mL) was injected deep into the chest cavity (section 5.8.4). Figure 43 shows fluorescence and ambient images of the mice. Considerably high fluorescence intensity was detected from the nanoparticles injected just under the skin (located by (A) in Figure 43) which suggests that the MEH-PPV nanoparticles could emit through the skin layer and could be distinguished from the mouse's auto-fluorescence. The antibody-conjugated nanoparticles which were injected into the quadricep muscles of the mouse, and were ~1000x more diluted in terms of nanoparticle concentration, could also be detected but with a lower fluorescence intensity ((B) in Figure 43), which also means that the fluorescence could migrate through several tissue layers of the mouse. Finally, injecting the nanoparticles deep into the chest cavity resulted in a lost fluorescence signal ((C) in Figure 43). This is because the fluorescence of the nanoparticles is attenuated as it passes through the animal tissues, and the deeper they are injected, the more the fluorescence is attenuated and eventually lost. The detectable nanoparticle fluorescence also depends on their concentration; for a detectable signal from the

antibody-conjugated nanoparticles, it was necessary to inject a relatively large amount of conjugated antibodies into a certain area within the mouse's body. If that same amount of conjugated (Gd-SPNs)-IgG was to diffuse within the body of a live animal in an *in-vivo* investigation for example, the nanoparticles signal would probably be lost.

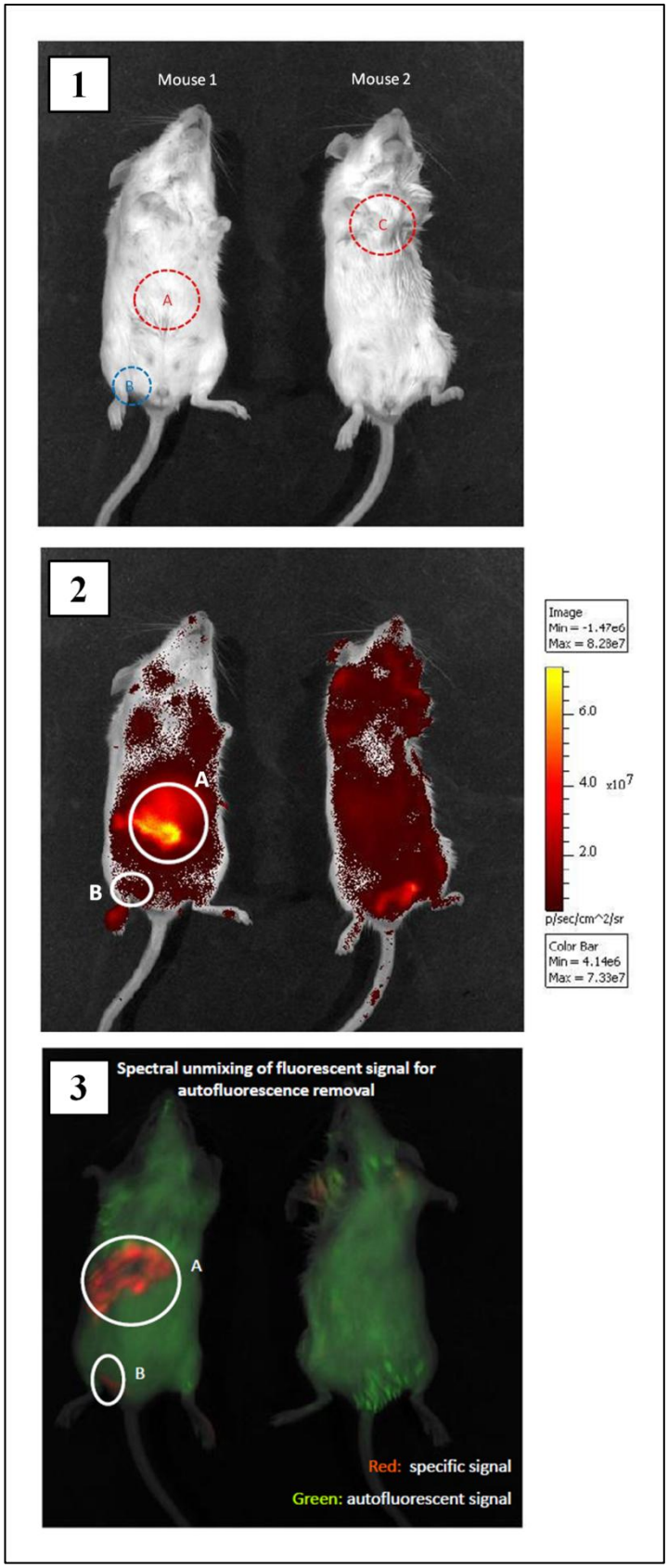

Figure 43 Images of two euthanized mice injected in three locations with (A) 100 µl MEH-PPV Gd-SPNs subcutaneously on the ventral surface, (B) 100 µl MEH-PPV (Gd-SPNs)-IgG intramuscular into the quadricep muscle (~1000x less nanoparticle

concentration), and (C) 100 µl MEH-PPV Gd-SPNs deep into the chest cavity. Image (1) is a photograph of the mice in ambient conditions, image (2) is an IVIS image showing the collected fluorescence intensity image against the mice ambient image, and image (3) is an IVIS processed image that shows the fluorescence from the nanoparticles (red) and the mice's auto-fluorescence (green).

Furthermore, MEH-PPV Gd-SPNs injected into the spleen of an euthanized mouse were successfully imaged after histology. Figure 44 shows spleen tissue imaged after snap freezing the aseptically removed spleen (section 5.8.5). The nanoparticles were readily visible in the tissue and were found not to be quenched or destroyed by the fixation process. However, fixing the spleen with paraformaldehyde was found to cause a total disappearance of the nanoparticle fluorescence which could indicate some interactions between the nanoparticles and the fixing substance. However, this cannot be certain without further investigations.

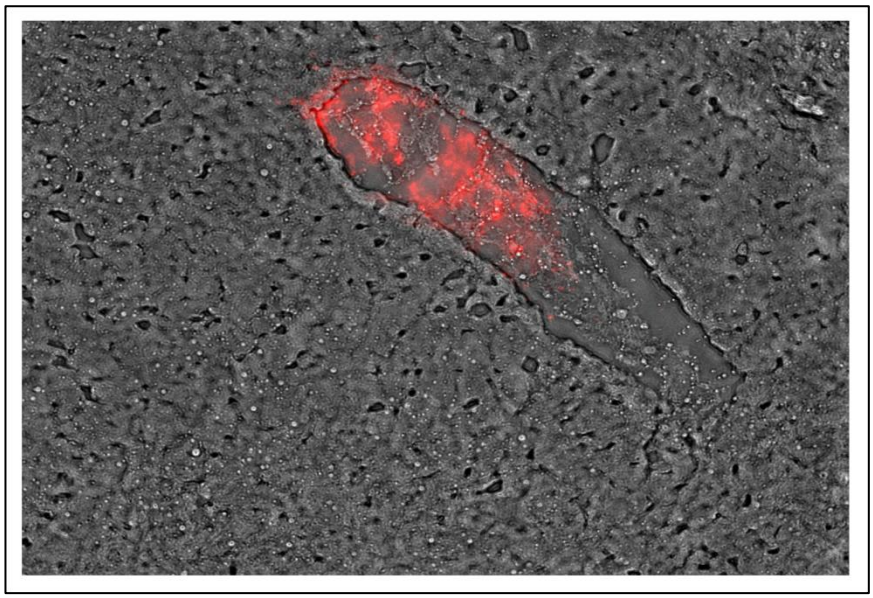

Figure 44 A bio-image of mouse-spleen tissue after MEH-PPV Gd-SPNs injection into the euthanized mouse's spleen and fixing by snap freezing. The red colour indicates the fluorescence signal from the nanoparticles after tissue auto-fluorescence subtraction.

To summarize, two differently emitting Gd-SPNs (MEH-PPV Gd-SPNs; red emitting; with QY ~ 1.5%, and F8BT Gd-SPNs; yellow emitting; QY ~ 33%) were used in an investigation to assess nanoparticle visibility through animal tissue. The nanoparticle fluorescence was distinguishable from the animal's auto-fluorescence, however, it was found to be attenuated with injections deeper into the animal tissues. Also, the final concentration of the nanoparticles within the area of interest was found to be pivotal for success of detection within a whole animal, with a relatively high concentration needed for a strong signal. Moreover, preliminary histological tests with MEH-PPV

Gd-SPNs revealed that the nanoparticles could be used as tissue-staining substances in such applications. However, their successful detection was found to depend on the fixation method used.

3.8 Nanoparticle Relaxivity Measurements in T1–weighted Magnetic Resonance Imaging

The component in the Gd-SPNs which gives the nanoparticles an MRI active property is gadolinium. The concentrations of gadolinium in the purified Gd-SPNs measured by mass spectrometry (performed by Mr Andrew Cakebread, Mass Spectrometry Facility in King's College London) are presented in Table 7.

Table 7 The concentrations of gadolinium, in the purified Gd-SPNs samples, measured by mass spectrometry:

Property	PPE Gd-SPNs	ADS108GE Gd-SPNs	F8BT Gd-SPNs	MEH-PPV Gd-SPNs
Gadolinium concentration in a non-concentrated sample (μM)	51.28	74.34	77.15	119.34

Compared to Gd-QDs prepared with similar lipids (gadolinium concentrations between 0.1 – 0.4 mM) [97], these concentrations were very low (highest being 0.119 mM in the non-concentrated MEH-PPV Gd-SPNs sample). Therefore, the MEH-PPV Gd-SPNs sample was concentrated further to a final gadolinium concentration of 0.3 mM. The relaxation time values (T1) of this concentration and two successive dilutions (0.2 and 0.1 mM) under two magnetic field strengths (3 Tesla and 7 Tesla) were measured and used to calculate the relaxivity (r_1) of the Gd-SPNs in both fields. The measurements were performed by Dr Andrea Protti and Dr Alkystis Phinikaridou, Cardiovascular Division and Division of Imaging Sciences and Biomedical Engineering, King's College London (section 5.8.6 for method). The results, reported in Table 8 and Figure 45, highlight the linear correlation between Gd concentrations and the relaxation rate values (R1) which are the reciprocals of the T1 values. The relaxivity (r_1), is calculated for the MEH-PPV Gd-SPNs in Figure 45 as the slope of the linear relationship, and is determined to be $r_1 = 20.75 \pm 0.57\ mM^{-1}.s^{-1}$ at 3T, and $r_1 = 17.21 \pm 0.50\ mM^{-1}.s^{-1}$ at 7T.

Table 8 MRI T1–weighted relaxation times and their corresponding R1 values measured for different Gd concentrations (i.e. different MEH-PPV Gd-SPNs concentrations), determined using 3T and 7T magnets:

3T			7T		
Gd concentration (mM)	mean T1 values (s)	R1values (s^{-1})	Gd concentration (mM)	mean T1 values (s)	R1 values (s^{-1})
water	2.62	0.38	water	2.933	0.34
0.1	0.40	2.5	0.1	0.474	2.11
0.2	0.29	3.46	0.2	0.28	3.57
0.3	0.21	4.68	0.3	0.262	3.82
2	0.024	41.38	2	0.029	34.48

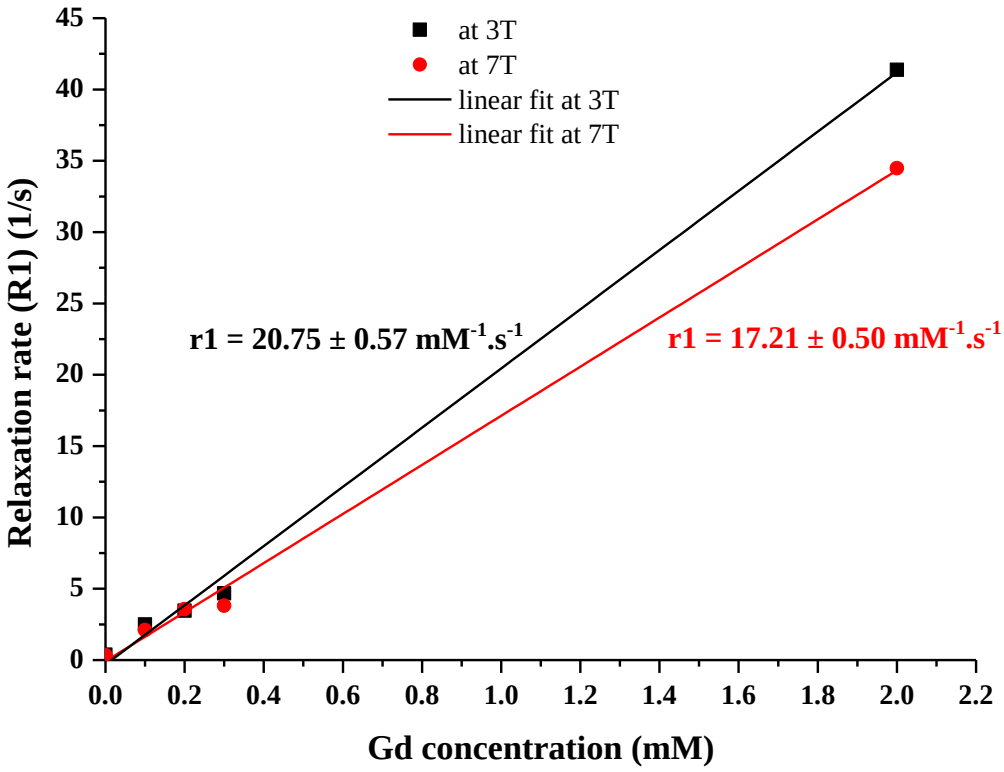

Figure 45 The relaxation rates (R1) versus gadolinium concentration of MEH-PPV Gd-SPNs at 3T and 7T. The relaxivities (r_1) are calculated as the slopes of the linear fittings.

3.9 Conclusions:

Bimodal nanosystems have several advantages over conventional imaging agents in the biological and medical fields. This led to an increase in the interest in the synthesis of bimodal nanoparticles. QDs were previously investigated as bimodal MRI-optical imaging agents [97]. However, because of the increased concerns about the health and safety issues associated with the use of QDs within living systems (due to their usual toxic compositions), the search for alternative nanoparticles was due to be investigated. In an attempt to provide suitable alternatives, we synthesised four fluorescent organic bimodal nanoparticles (Gd-SPNs), with outstanding fluorescence properties, such as high fluorescence stability with little to no photo-bleaching after multiple cell image acquisitions or long storage periods, which make them excellent imaging agents.

The Gd-SPNs manufactured in this study had average core diameters around 30 nm with standard deviations of 7 – 22 nm as measured from TEM images, and hydrodynamic diameters around 66 – 128 nm with standard deviations of 27 – 39 nm as measured by NTA. Compared to the iron oxide/SPNs [182] these Gd-SPNs showed smaller diameters and also higher quantum yields. Their MRI T1–weighted relaxation times were measured revealing a gadolinium concentration dependence with a relaxivity of $r_1 = 20.75 \pm 0.57\, mM^{-1}.s^{-1}$ at 3T, and $r_1 = 17.21 \pm 0.50\, mM^{-1}.s^{-1}$ at 7T.

Moreover, the Gd-SPNs were found to be taken up by live cells, which is desirable in cell imaging applications. Also, their fluorescence was found to be visible through animal tissue when injected subcutaneously into euthanized mice and a rat pup. The auto-fluorescence-distinguishable nanoparticle signal was dependent on both nanoparticle concentration and how deep the injection into the tissue. This observation which can limit the nanoparticle usefulness in the future could probably be solved by using Gd-SPNs with different optical properties such as infra-red emitting Gd-SPNs. Therefore, these Gd-SPNs, which were colloidally stable in different biological media, have potential as bimodal MRI-optical imaging contrast agents in a variety of biomedical applications.

4 Interactions of Semiconducting Polymer Nanospheres and Quantum Dots with Components of Human Blood: Effects of Surface Coatings

4.1 Introduction

Safety assessment of new nanomaterials [114] has become an increasingly important issue worldwide [114, 262-267]. Nanoparticles are being synthesised extensively and are already incorporated into many applications in science and industry. 'The Project on Emerging Nanotechnologies' website identified 1317 commercial products (up until 10th March 2011) which included (or claimed to include) nanoscale materials.[268] Examples are food plastic storage bags infused with silver nanoparticles [269], and cosmetic aluminium oxide nanopowders [270]. These nanomaterials have different chemical compositions, sizes, surface chemistries and coatings, and other properties which make them unique and desirable by the medical, educational, food and commercial industries. The study of the short and long term effects of such novel nanomaterials on human health and the environment is still immature. Therefore, there is an increased interest in safety assessment studies for nanomaterials, especially if the applications involve deliberate exposure to the human body, for example as in pharmaceutical and bio-imaging applications.

The fate of any type of nanoparticle administered into the body depends on its properties. For example, the size distribution of nanoparticles, which can vary from a few nanometres to sub-microns in diameter, has a direct influence on their ability to cross different biological barriers. Small nanoparticles, with a few nanometres in diameter, can cross the blood brain barrier [266, 271], while other nanoparticles with diameters up to 240 nm can cross the human placental barrier [272]. Further, nanoparticles with hydrodynamic diameters larger than 5.5 nm cannot cross the renal barrier and achieve renal clearance in mice [116]. Nanoparticles trapped within the body can be dangerous, as some accumulating nanoparticles were found to be deposited on the walls of blood vessels and in some organs [266] causing organ failure and dysfunction [114].

The chemical properties of the nanoparticles such as their composition and surface chemistries are also important factors governing their safety profile and interactions with physiological systems. Nanoparticles composed of toxic chemicals and metals can be very toxic if degraded within the body [105, 273]. Moreover, nanoparticles have amplified surface related properties, due to the increase in their surface area per unit volume with the decrease in their size. This increases the magnitude of their reaction with their surrounding cellular environment [114]. Nanoparticles with highly reactive surfaces cause an increased oxidative stress within the body and can stimulate the body's inflammatory response [274]. Inflammation can also be triggered by extremely hydrophobic nanoparticle surfaces [275]. Surface modifications with cationic and anionic chemical

groups, which are in some cases necessary for the nanoparticles' use in specific applications, also affect their behaviour and therefore change their toxicological profile [107, 262]. Nanoparticle surfaces can also be modified *in-vivo* by the adsorption of proteins to the surface in a process called opsonisation or protein corona formation [276]. Opsonisation not only increases nanoparticle diameters, but also alters their physio-chemical properties, which can influence their safety profile [276-277]. The surface charge (zeta potential) which is also associated with the surface chemistry of the nanoparticles as well as the pH of their surrounding also plays a role in influencing the total toxicity of any given nanoparticle species [107, 278].

4.1.1 Concerns Over Quantum Dot Safety and Rationale for the Development of Semiconducting Polymer Nanospheres as Safer Alternatives

Inorganic quantum dots (QDs) have received much attention in the nanotoxicity and safety assessment field, because of safety concerns associated with their chemical composition, specifically the potential of cadmium-related toxicity [104-109]. Cadmium has been identified as a human carcinogen since 1997 [279-280]; it was reported to interfere with DNA repair processes increasing the risk for tumour formation [281]. Targets of cadmium were found to include the lungs, thyroids, liver, kidneys, and cardiovascular, immune, and reproductive systems [279, 282-283] where acute exposures to medium-high doses *in-vivo* resulted in hemorrhagic injury, organ damage, dysfunction, and failure [282-283]. Cadmium is stored in different body organs for years (biological half life = 15 – 30 years) [282]. Its accumulation with chronic exposure to low doses (blood levels range of 10–100 nM) through inhaling airborn cadmium (e.g. from cigarette smoke) and/or eating contaminated foods can therefore result in a long term toxicity (dependent on the dose, route, and duration of exposure [282]). Deliberately exposing the body to cadmium, by the use of cadmium containing QDs for diagnostic purposes, will therefore increase the body's burden, and can result in cadmium poisoning with clinical misuse or dose mistakes. Moreover, other constituents of QDs, such as selenium and tellurium, were also found to cause acute toxicities if ingested with high doses [284-286].

As noted previously, QDs have excellent optical properties, which make them attractive imaging agents. They have small diameters and are known to be less polydisperse than organic nanoparticles, which provides the possibility of renal clearance as confirmed by *in-vivo* studies in mice [116, 287]. Further, many QDs are commercially available and are therefore easy to study. Due to the fact that QDs are typically composed of toxic materials, they need to be encapsulated with biocompatible materials for use in biological applications [110-111, 114-115]. The addition of the capping shells or molecules substantially increases the hydrodynamic diameters of the particles. Additionally, the risk from the presence of non-capped quantum dots, or the aggregation and decomposition of the particles in the body (such as the uptake and decomposition of intravenously

injected CdSe QDs by/in the liver, spleen, and kidneys of mice [288]) cannot be neglected, and long term toxicity will always be a concern.

Due to their lack of heavy metal constituents, it has been hypothesized that SPNs could be a highly effective, yet safer alternative to QDs. It has been established that organic SPNs have comparable optical properties to QDs [36, 182, 244], but demonstrate significantly longer shelf-lifetimes in terms of fluorescence. For example, the fluorescence of QDs can be quenched within days or weeks, however, the fluorescence of the SPNs which we synthesised was conserved for several years to date, (refer to section 1.2.2.2 for further details). However, in order to evaluate whether SPNs are suitable for use in biological and clinical applications, rigorous safety assessment must first be conducted. As diagnostic agents, SPNs are likely to be administered to patients intravenously. This means that they will first come into contact with blood plasma and the cellular components of blood. Therefore, understanding the interactions between blood components and the nanoparticles by performing *ex-vivo* tests to evaluate whether the nanoparticles promote any of these interactions is a vital component in the broader safety assessment of such new diagnostic agents. This is especially important, as some nanoparticles are known to negatively affect blood clotting pathways [277, 289] as discussed in detail in the following section.

4.1.2 Effects of Nanoparticles on Blood Components after Intravenous Administration

Human blood is composed of red blood cells, white blood cells (leukocytes: lymphocytes, monocytes, and neutrophils are the three main types), platelets, and blood plasma which contains proteins, other biomolecules, and ions. Blood circulates within blood vessels lined with endothelial cells, all of which interact together to achieve one goal: delivering oxygen and nutrients to cells, removing carbon dioxide and cell waste, coagulating in response to vessel injury, and fighting infections *via* the foreign-body triggered inflammatory response.[290]

Platelets are disk shaped blood components which originate from the bone marrow in humans and play an important role in blood clotting. In healthy humans, platelets adhere together and aggregate in the site of injury to stop the bleeding and aid in recovery.[291] In many cardiovascular disorders, however, non-favourable platelet aggregation appears to happen. This dangerous phenomenon causes fatal diseases such as acute coronary artery diseases, embolism and strokes.[292-293] The aggregation of platelets involves platelet activation, adhesion, and secretion in a synergetic and multistep process.[291] Endogenous agonists, such as adenosine diphosphate (ADP) and thrombin released from activated platelets cause platelet-platelet adhesion and hence aggregation.[291]

Platelet activation not only causes platelet-platelet adhesion as described in the previous paragraph, but also causes the platelets to interact with their surroundings and adhere to endothelial cells lining the blood vessels and to white blood cells such as monocytes and neutrophils. An

increase in platelet activation accompanies and amplifies inflammation, with platelets binding to the endothelium and to leukocytes causing leukocytes activation, facilitating their migration through endothelial cells to underlying and nearby tissues, and promoting monocyte differentiation into macrophages.[294-296] Platelets adhering to monocytes form circulating platelet-monocyte complexes which are found to be important factors in disease pathogenesis.[294-295] Likewise, platelets adhering to neutrophils form circulating platelet-neutrophil complexes which also have similar roles.[297] It was also reported that platelet-neutrophil adhesion can be caused by the activation of one of the two species or by both.[298]

Many nanoparticle types have been found to be treated as intruding foreign objects by the blood defence components when introduced to the blood system (e.g. by intravenous injection). They are generally opsonised by plasma proteins and cleared away from the blood very quickly to the liver and spleen by activated leukocytes such as neutrophils [299-300]. Some nanoparticles have also been found to trigger platelet activation leading to platelet-leukocyte interactions and platelet aggregation which results in thrombus formation. Examples of such activation events are the enhancement of platelet coagulant activity in response to the presence of silver nanoparticles in the blood stream [301] and the dysfunction of endothelial cells, platelet activation, and leukocyte activation towards atherosclerosis disease with the migration of combustion-derived nanoparticles into the cardiovascular system [302].

The surface chemistries of nanoparticles and hence their surface charges were reported to be the main influencers of such cell responses [303], with positive charged or highly negative charged nanoparticles reported to cause amplified cell-cell and particle-cell interactions in comparison to neutrally charged nanoparticles.[278, 289] An example is the increased platelet aggregation *in-vitro* by the incubation of the platelets with carboxylated QDs (which are highly negatively charged; zeta potential ~ -57.7 mV in deionised water) as opposed to non-functionalised QDs [278].

To increase nanoparticle circulation time, it is necessary to camouflage the nanoparticle surfaces through modification so that they are not recognized by the blood components as foreign intruders.[304] One surface modification which has been demonstrated to have such an effect is PEGylation. PEGylation of nanoparticle surfaces with certain chain lengths of PEG and certain surface percentage coverage [305] has been shown to decrease particle-cell interactions resulting in an increased circulation time as well as a decrease in undesired adverse events.[306-310] For example, a decreased platelet coagulant activity and platelet-monocyte binding of PEGylated amorphous silica nanoparticles was observed in contrast to nanoparticles without PEGylation [311]. Similar effects have also been observed with a variety of other nanoparticle species that have been surface-modified with PEG.[312] For these reasons, in addition to the excellent colloidal stability conferred by PEGylated nanoparticles, the majority of systems described in this thesis have varying degrees of PEG surface coverage.

4.1.3 Study Aims and Hypotheses

Three main study components are presented in this chapter. First, the physiochemical behaviours of the nanoparticles in different control and physiologically relevant media are assessed. Secondly, nanoparticle interactions with isolated human platelets are studied, and finally, nanoparticle interactions with human whole blood components are evaluated. All studies were conducted using the bimodal Gd-SPNs introduced in chapter 3 and on similarly prepared monomodal SPNs. Further, to investigate whether CdSe/ZnS QDs with similar surface morphologies have any acute effects on whole blood, two QD species were included as comparisons in the study: a neutral (QD) and a partially carboxylated surface modification (cQDs) (Figure 46). The partially carboxylated surface modification was introduced to investigate whether an elevated negative surface charge will enhance nanoparticle effects on blood cells, such as platelet activation and platelet-monocyte adhesion. This phenomenon has been previously observed with both cationic, amine-modified and anionic, carboxy-modified polystyrene beads [107, 278, 289]. To benchmark to the literature, commercially available carboxylated polystyrene beads (cPS; 50 nm) were also included in the study as a positive control.

Because all four nanoparticles in this study were partially PEGylated, we hypothesised that they will have minimum interactions with the blood, and that they will have minimum non-specific binding and opsonisation of proteins on their surfaces, they will not cause any platelet aggregation or activation in isolated platelet rich plasma, and they will not cause any platelet-monocyte adhesion or neutrophil activation in whole blood.

4.2 Synthesis and Optical Characterisation of the SPNs, Gd-SPNs, QDs, and cQDs

SPNs and Gd-SPNs with average core diameters of 30 ± 18 nm, as measured from TEM images, were synthesised, concentrated, and purified (section 5.2.5 for details). Both polymer nanoparticles were composed of a hydrophobic polymeric core of MEH-PPV polymer chains packed into a spherical conformation. The hydrophobic core of the SPNs was stabilized in aqueous suspension by a phospholipid surface coating composed of a ~1:2 molar ratio of PEG2000-PE and DPPC, while the Gd-SPNs were stabilised by a surface coating of ~1:1:1 PEG2000-PE/DPPC/Gd-DTPA-BSA. Thus, the overall hydrophilic nature of both SPN species, as conferred by the PEGylated surface coating, is similar. Importantly, all SPNs maintained the fluorescence properties (Figure 47) of their constituent polymers [36], making them suitable for use in fluorescence bio-imaging applications.

In addition to the two species of SPNs chosen for this study, QDs with similar optical and semi-conductive properties, as well as surface coatings were investigated. This was to determine whether the surface coating only or also the particle core exert an acute influence on the interactions

between nanoparticles designed for optical imaging agents and components of blood. CdSe/ZnS quantum dots with 4 nm diameters were coated with PEG2000-PE and DPPC (2:1) to imitate the SPNs. Also CdSe/ZnS QDs were coated with PEG2000-PE, DPPC, and DSPE-PEG2000 (1:1:1), forming partially carboxylated nanoparticles (cQDs) (preparation technique the same as Dubertret *et al.*[47] in section 5.2.6). Preliminary hydrodynamic diameter measurements of the PEGylated QDs and cQDs resulted in two size distributions, with one peak at~15 nm and the second at ~100 nm. Therefore, we hypothesized that both QD systems included a mixture of single, coated QDs and micellar structures which contained multiple QDs. A schematic of the cross-sectional conformations of the nanoparticles is provided in Figure 46.

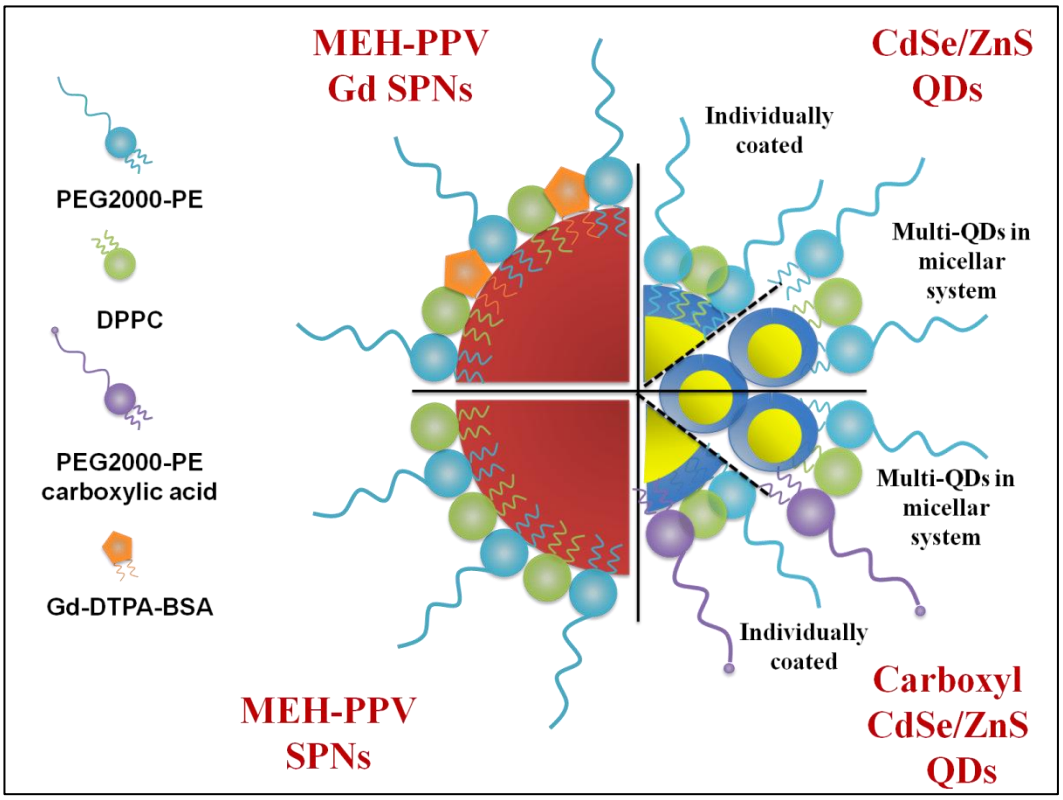

Figure 46 A schematic of the four nanoparticles under study: SPNs, Gd-SPNs, QDs and cQDs.

The absorption and emission spectra of the Gd-SPNs and the QDs are shown in Figure 47. The spectra of the SPNs and cQDs were not measured, however, they are expected to have the same spectra as their counterparts as, from our experience and as reported by others, the lipids used did not affect the absorption and emission spectra of the nanoparticles in the 400 – 900 nm region [36, 244, 313]. As shown in Figure 47, the QDs and polymer nanoparticles under study have similar absorption and emission spectra; both systems absorb light with wavelengths below 600 nm, and both emit light with an emission peak of ~595 nm. The absorption spectra of the QDs do not have a defined peak, while the polymer nanoparticles have a strong absorption peak around 495 nm. Moreover, the emission spectra of the polymer nanoparticles are broader than those of the QDs and

have an extra shoulder at 650 nm. The broadening of the emission peak and the occurrence of the secondary peak in the SPNs emission are characteristic of the polymer used and are influenced more by the proximity of the polymer chains in the compact nanoparticle configuration [244]. The similar photo-characteristics of the quantum dots to the semiconducting polymer nanospheres make them suitable comparison candidates in the nanoparticle-cell interaction investigations which follow, especially since some of the assays involved an optical component to the analysis, such as turbidity in the platelet aggregation experiments, light scattering in the nanoparticle stability studies, and fluorescence in the platelet activation experiments by flow cytometry.

The concentrations of the prepared nanoparticles were measured and adjusted to a final concentration of 4 mg/mL prior to the experiments.

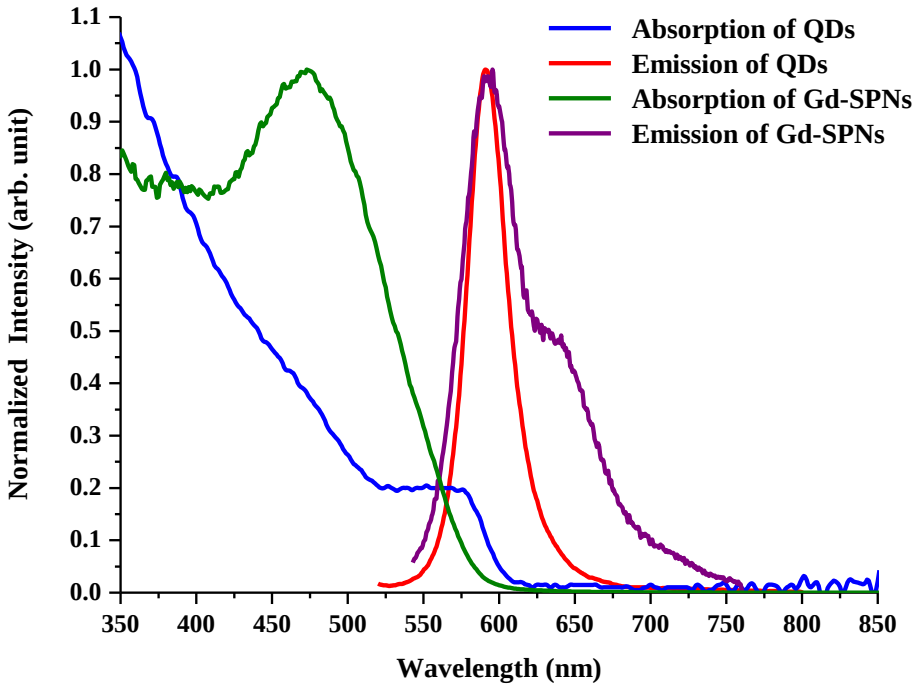

Figure 47 Normalised absorption and emission spectra of the Gd-SPNs and QDs.

4.3 Physiochemical Characterisation of the Nanoparticles

4.3.1 Nanoparticle Surface Charge

The nanoparticle zeta potential was measured using laser Doppler anemometry (Nanosizer, Malvern Instruments, UK, refer to section 5.9.3 for methods). All four nanoparticle species were found to be negatively charged in Chelex®-treated pH adjusted (NaOH and HCl) water with zeta potentials varying between – 17.90 mV and – 10.70 mV, as seen in Table 9. It is known that the higher the magnitudes of the zeta potential values for a particular system, the more colloidally

stable it is in aqueous media, where the nanoparticles repel each other and therefore nanoparticle – nanoparticle aggregation is minimised [314]. However, it is also well documented that highly charged colloids are more sensitive to the presence of counter ions in media which approach physiological tonicity. Through adsorption of counter ions to the charged surface, neutralisation can occur, which reduces charge repulsion and can promote particle aggregation or flocculation. This sensitivity of charged particles to the ionic strength of the media can be prevented by surface coating with hydrophilic polymers such as PEG, which provide a hydrophilic, steric barrier against particle-particle forces of attraction.[315-316] With regard to the four nanoparticle systems studied in this chapter, the magnitude of zeta potential values measured, which are only moderately negative, accurately reflect the combination of charged species on the particle surface and non-ionic PEG chains. This will be discussed in greater detail below.

The two common surface coating/entwining lipids in the four nanoparticles studied in this chapter were DPPC and PEG2000-PE. It was observed that increasing the molar content of PEG2000-PE resulted in a slight decrease in zeta potential. In general, the incorporation of PEGylated lipids (or increase in their percentage of total lipids) has been shown in the literature, for example in phospholipid liposomes, to decrease the magnitude of their zeta potential [317]. In that same study, the liposomes which were prepared using 80% DPPC and a varying percentage of PEG2000-PE with a third lipid (phosphatidylinositol) were found to have zeta potentials of (– 12 mV to – 4 mV, for 0 – 9 % PEG2000-PE) in 10% PBS in water at 25ºC [317]. These values, which were of empty liposomes cannot be compared directly to the zeta potentials of the nanoparticles prepared here because of the difference in the core materials and because of the different parameters used in the zeta potential measurements (temperature and medium). However, the results in general fit well with the zeta potential values measured in our study.

Both SPNs and Gd-SPNs contained the same core material, and almost the same percentage of PEG2000-PE (~30% of total). The difference was in the remaining 70% DPPC, where half of it was substituted with Gd-DTPA-BSA in the Gd-SPNs. With a fixed PEG content on both surfaces, the introduction of 35% Gd-DTPA-BSA to the surface contributed to a final increase (by ~ -4 mV) in the magnitude of the negative zeta potential. DTPA contains three carboxylic groups, which are used to complex the gadolinium ions. Any free carboxylic groups, i.e. those not involved in complex formation, are therefore responsible for this modest increase in surface charge.

Likewise, both quantum dots contained the same core content, the same percentage of PEGylated lipids, and the same percentage of DPPC, with one quarter of the total PEGylated lipids in the cQDs containing carboxylic groups. Introducing carboxylation to the surfaces of the cQDs resulted in an increase in their negative zeta potential (by ~ -7 mV), an effect that is similar to that of Gd-SPNs.

When it comes to interactions of the nanoparticles with other objects/molecules present in the aqueous medium such as biological species, it has been reported that the more negative the surface

charge of the nanosystem, the greater the adsorption of biomolecules to the nanosystem's surface [317-318]. Biomolecule adsorption to particle surfaces may be indirectly monitored by evaluating changes to the zeta potential of nanoparticles after incubation with physiologically relevant media. In this study, nanoparticles were incubated with phosphate buffered saline containing 8% human blood plasma (i.e. platelet-poor plasma; PPP) and the changes to the zeta potential were compared with their original values in water (Table 9). Exposure of the nanoparticles to dilute PPP which contains human serum proteins did not significantly alter the zeta potential of the SPNs and QDs, which were the two nanoparticles species lacking carboxylated moieties in their surface coating. However, the zeta potentials of Gd-SPNs and cQDs were found to decrease slightly in 8% PPP, which suggests adsorption of some PPP components, likely proteins, onto the nanoparticle surface and a neutralisation of some of the surface charge. This observation suggests that the presence of anionic groups, such as free carboxyl groups, on the surface of the Gd-SPNs and cQDs attracted proteins from the serum and produced some form of protein corona. The implications of this opsonisation are that both Gd-SPNs and cQDs may potentially have an altered biodistribution or differences in cell interactions compared to their comparator formulations (SPNs or QDs) when administered in the body via the intravenous route or if they came into contact with biological samples in *in-vitro* bio-imaging applications.

Table 9 Zeta potential of the nanoparticles in both water and diluted PPP:

Nanoparticles	Zeta Potential in water (mV)	Zeta Potential in 8% PPP (mV)
SPNs	- 12.8 ± 2.0	- 10.7 ± 0.2
Gd-SPNs	- 16.5 ± 1.2	- 8.9 ± 0.7
QDs	- 10.7 ± 2.0	- 9.3 ± 0.2
cQDs	- 17.9 ± 1.5	- 10.4 ± 0.6

4.3.2 Nanoparticle Colloidal Stability in Physiological and Synthetic Media

Figure 48 and Figure 49 show example size distributions of the SPNs, Gd-SPNs, QDs, and cQDs in (1) Chelex® treated/pH adjusted water, (2) cell culture medium (CCM) with 2% foetal bovine serum (FBS) supplementation, and (3) 8% human platelet poor plasma (PPP) at 37°C over a 24 hour period (the data of only six time points, from a total of 30, are shown). Platelet poor plasma and CCM contain nanometer sized biological species (proteins and protein aggregates) which are DLS detectable. Therefore, the size distributions of a blank sample in dilute PPP (8% PPP in a buffer of 20% PBS in distilled water) were also measured (also present in Figure 48 and Figure 49).

Both SPNs and Gd-SPNs were very stable in water and in CCM with little to no aggregation in

both media (showing almost the same single peaked size distribution profile over the 24 hours of monitoring, Figure 48). The average diameters of both nanoparticles in water and in CCM were very similar (mean z-average of SPNs in water = 117.5 ± 1.12 nm, SPNs in CCM $_{2\%FBS}$ = 113.0 ± 4.75 nm, Gd-SPNs in water = 117.0 ± 1.45 nm, Gd-SPNs in CCM $_{2\%FBS}$ = 110.8 ± 0.85 nm; n=24 measurements). The values are consistent with previous results from the extensive colloidal stability studies performed by Howes *et al.* on the same SPNs (prepared in a slightly different method).[319]

The dispersion of the SPNs and Gd-SPNs in 8 % PPP were difficult to interpret due to a significant amount of polydisperse colloidal material (~10-100 nm) present in the PPP (SPNs/Gd-SPNs in 8 % PPP compared to blank in 8 % PPP in Figure 48). Since the hydrodynamic diameters of the SPNs were ~120 nm, it was initially hypothesized that the nanoparticle peak would be distinguishable over the PPP background signal. At some measurement time points these peaks can be observed (peaks 100-1000 nm), however at others the nanoparticle peak seems to merge with the background signal, which makes it difficult to interpret the findings regarding particle stability. Further in-depth studies need to be conducted to identify the nature of the interactions involved and provide more detailed information on particle stability in human serum. These investigations may be carried out using a different analytical technique, such as particle tracking analysis, which is not sensitive to media composition in the same way that DLS is.

Similar to the SPNs, the QDs were stable in water; showing a bimodal size distribution in every measurement (see Figure 49). The increase in the diameters of the capped QDs in comparison to their original 4 nm diameters when non-capped (data given by the manufacturer) is pronounced, with the larger peaks situated around the same diameters as those of the SPNs/Gd-SPNs. As discussed in the introduction to this chapter, the bimodal size distribution of the QDs in water suggests that one fraction of the suspension may be composed of single, capped QDs and the remaining fraction comprises micellar systems containing an uneven number of non-capped QDs. In water, there was also a non-significant shift of the size distributions to the larger diameters with elapsed time (average diameter =92 nm (at t = 0 h), 104 nm (at t = 24 h)).

Interestingly, Figure 49 shows that the cQDs were not as stable as the QDs in water indicating that they tend to interact to some extent and undergo slight instantaneous aggregations. This is unexpected since carboxylation of the surface should theoretically prevent nanoparticle aggregation by the mechanism of enhanced repulsion of like charges [314].

The behaviour of both QDs and cQDs in cell culture medium was not significantly different than that in water (Figure 49). For example, both QD species again showed a bimodal distribution in CCM, and aggregation or consolidation to larger particle sizes was observed over 24 h. In dilute PPP, the nanoparticle signal was also very difficult to detect and the colloidal stability difficult to interpret using this method. Therefore, similar to the SPNs, further studies must be performed in ordered to truly characterise the colloidal stability of nanoparticles in human serum.

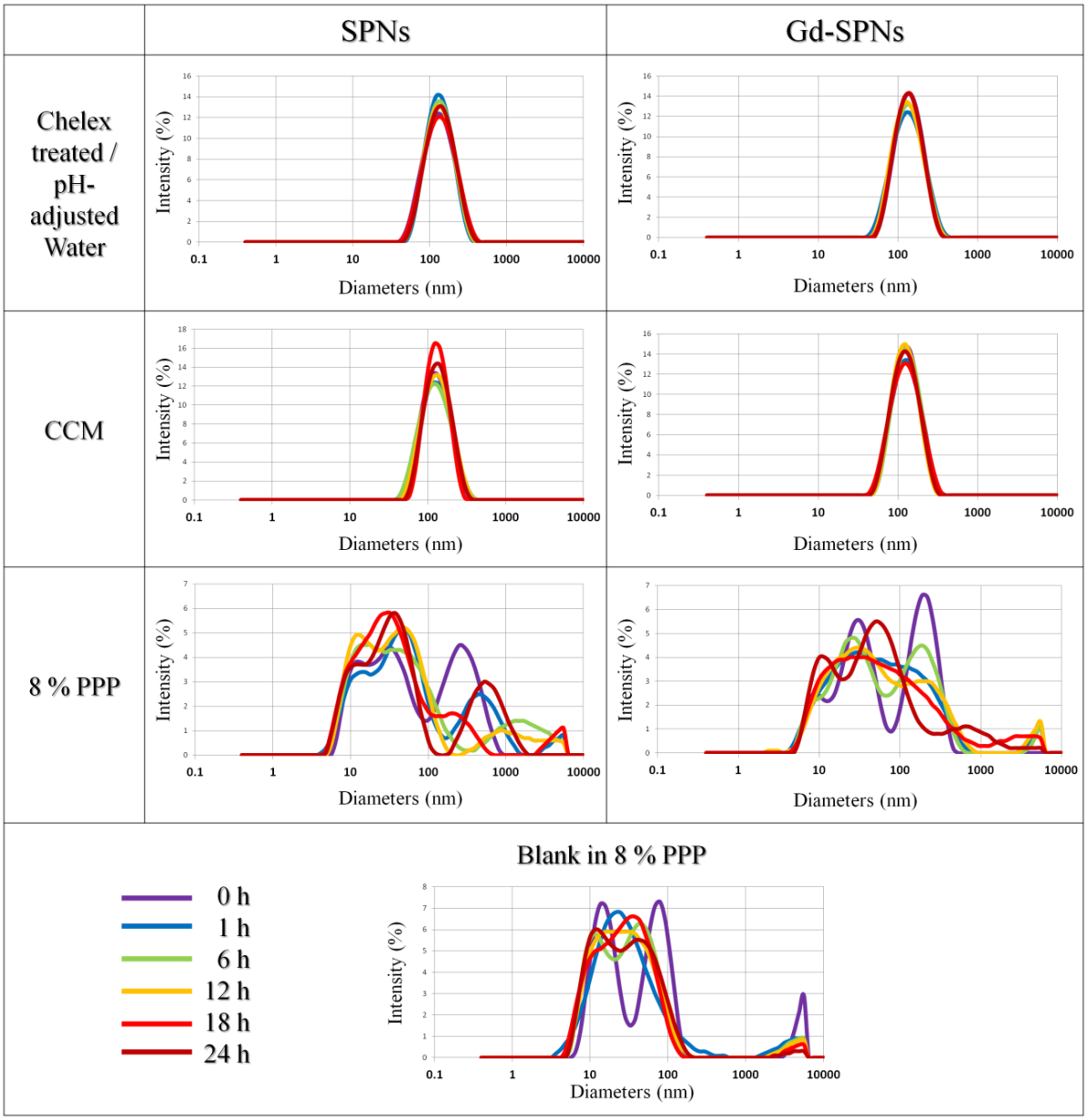

Figure 48 SPN and Gd-SPN size distribution profiles over a period of 24-hours at 37°C after dispersion in Chelex® treated/pH-adjusted water, cell culture medium (CCM) containing 2% FBS, and dilute human platelet poor plasma (8% PPP in 20% PBS, n = 1). The size distribution profiles of 8% PPP, n = 1 with a blank sample are also presented.

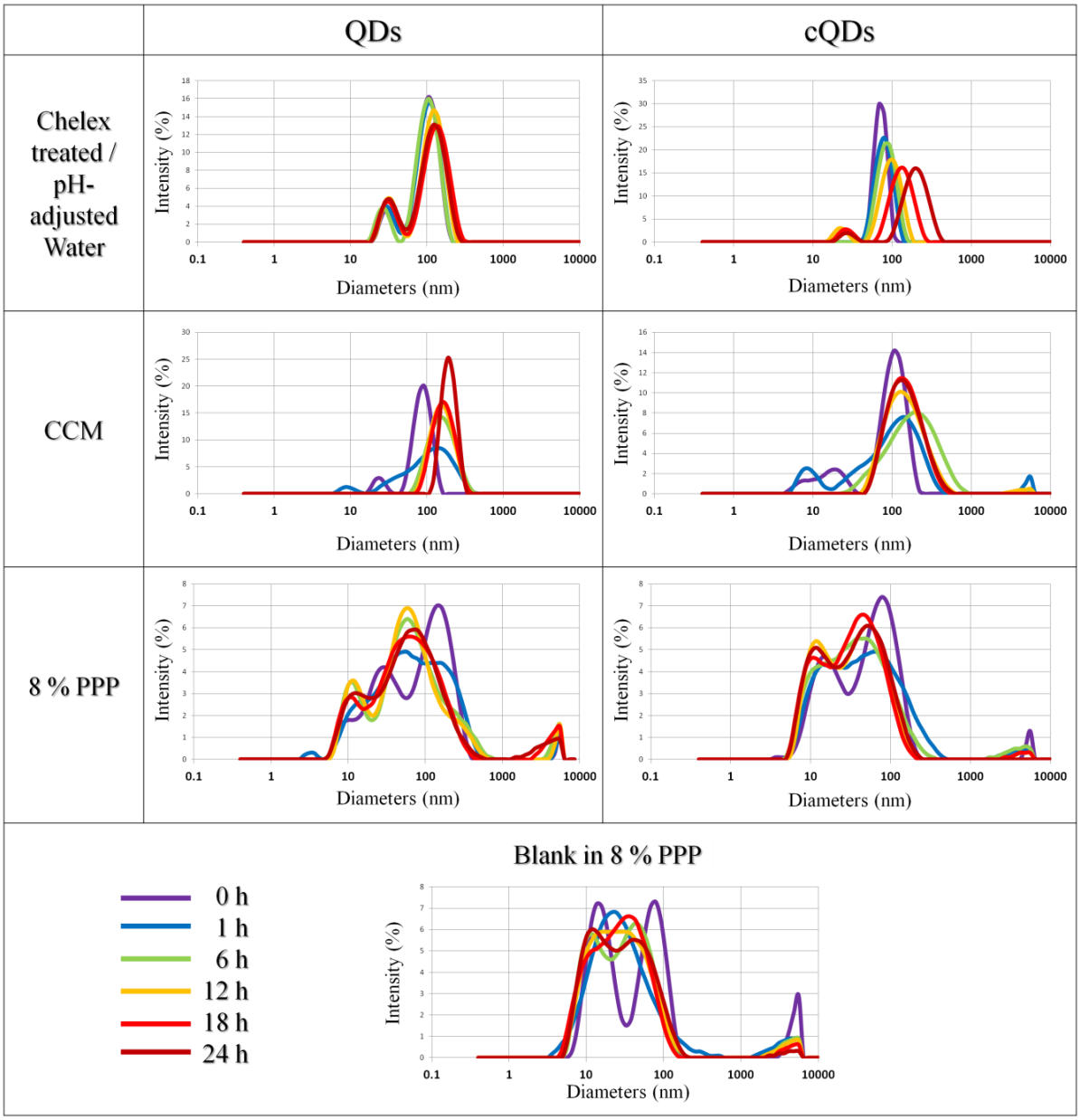

Figure 49 QD and cQD size distribution profiles over a period of 24-hours at 37°C after dispersion in Chelex® treated/pH-adjusted water, cell culture medium, and dilute human platelet poor plasma (8% PPP in 20% PBS, n = 1) . The size distribution profiles of 8% PPP, n = 1 with a blank sample are also presented.

4.3.3 Nanoparticle-Induced Oxidative Stress and Free Radicals

The reactivity of substances and oxidation within the living organism has been reported to be an important cause of aging and disease.[320] Oxidation and an increase in free radicals within the human body was found to damage cells, tissues, and DNA, causing tumour development and influencing many illnesses such as cancer, rheumatoid arthritis, intestinal inflammatory diseases, and neurodegenerative diseases.[320] The measurement of the oxidative stress of the nanoparticles is therefore important in the assessment of their safety.

The oxidative stress induced by the four nanoparticles in this study, plus a positive and negative nanoparticle control, were assessed at 37°C by two methods; ascorbic acid (AA) depletion assay [321] and electron paramagnetic resonance (EPR) of DMPO which is a free-radical spin trap [322] (see Appendix 1 for chemical structures of ascorbic acid and DMPO). Ascorbic acid is an antioxidant, it reacts with free metals, reactive oxygen species or light and is oxidised to form dehydroascorbic acid. A decrease in the reduced form of ascorbic acid, can be detected and quantified by monitoring the UV absorption of a sample at 265 nm. This assay was used to determine whether the nanoparticle species included in this study were redox active or contained redox active impurities. Titanium dioxide (TiO_2) nanoparticles, which do not induce oxidative stress or generate free radicals were used as a negative control. Copper oxide (CuO) nanoparticles, which are known to induce oxidative stress through release of Cu^+ ions was included in the study as a positive control.

Preliminary assay development tests were carried out to determine the optimal number of UV scans during a given experiment and to check for sources of heavy metal contaminants in the system (Figure 50 and Figure 51). It was interesting to observe that ascorbic acid was depleted more quickly if the UV absorption was measured more frequently over a given time period in the same sample (Figure 50). Therefore, in all final studies, a low frequency of 4 measurements per experiment was chosen. In a second experiment, DTPA was added to a fresh sample of SPNs, which had been previously observed to induce a high rate of AA depletion (i.e. the sample was unexpectedly highly redox active). DTPA is a metal chelator which, if added to the nanoparticle suspensions prior to the addition of the ascorbate, can chelate any free metal ions in the solutions and inhibit their interaction with the ascorbate. The decrease in the ascorbic acid depletion rate with the presence of DTPA in the SPN suspension shown in Figure 51 suggests that the nanoparticles were metal contaminated. Prior to this test, the SPNs had been synthesised with old glassware and equipment and in normal de-ionised water. The same SPN suspension was then purified (by successive washing, which entailed dilution of 1.5 mL SPN suspension in 10 mL of Chelex® treated water, filtration through a Millipore Amico Ultra-15 3,000 Dalton MWCO centrifugal filter and repetition of this process four times), and the AA depletion rate test repeated. The AA depletion rate, shown in Figure 51, was found to decrease by 4 fold after SPN purification. However, it was still higher than that of the SPN suspension with DTPA. This lead to the decision that the nanoparticles prepared for all future biological studies should be synthesised with new glassware, in Chelex® treated and pH adjusted water, as well as extensively purified.

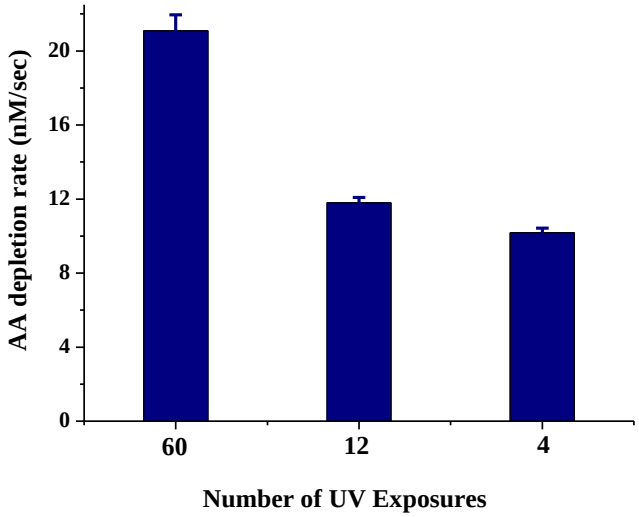

Figure 50 Ascorbic acid (AA) depletion rate of aqueous SPNs with different exposure times to the excitation of the absorption spectrometer over a period of two hours. Values represent the mean ± standard deviation of n = 3 replicate measurements.

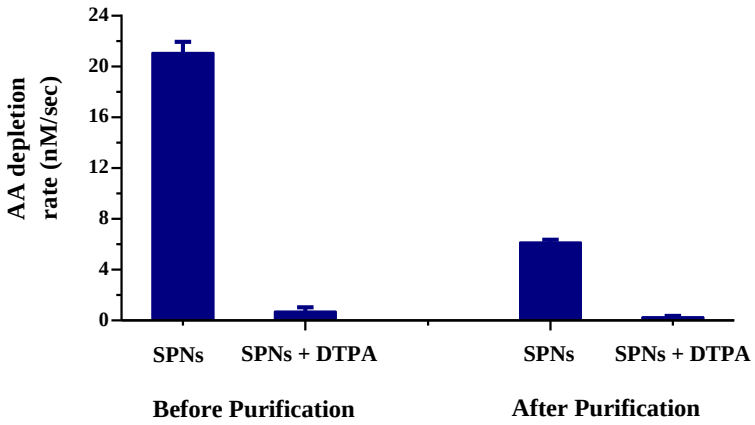

Figure 51 Ascorbic acid depletion rate of purified and non-purified SPNs in the presence and absence of DTPA.

Figure 52 shows the AA depletion rates for all nanoparticle suspensions tested, and Table 10 states the statistical significance p-values between each of the nanoparticles with or without DTPA and the controls (using a Student's paired t-test with a two tailed distribution). As expected, all AA depletion rates for SPNs and QDs, which were prepared with the precautions mentioned above and extensively purified, were significantly lower than that of CuO nanoparticles, indicating that both the SPNs and QDs were not as reactive as the positive control. Interestingly, though, all SPNs and QDs showed a slightly, but significantly elevated AA depletion rates compared with TiO_2,

implying that they did have a slightly higher surface reactivity than the negative control. This reactivity could be a result of gadolinium, cadmium or selenium released in small quantities due to the fact that Gd-SPN, QDs and cQDs all showed a slight, but significant reduction in AA depletion in the presence of the heavy metal chelator, DTPA. Both SPNs and TiO_2, however, did not show significant differences in AA depletion with or without DTPA, which suggests that the SPNs samples, similar to the negative control, did not contain significant amounts of heavy metals. As all four nanoparticles were incident to the same metal contamination precautions in their syntheses and handling, and they had undergone the exact same purification process as the SPNs, it is well understood that the metal contamination is therefore generated by the nanoparticles themselves other than any outer cause.

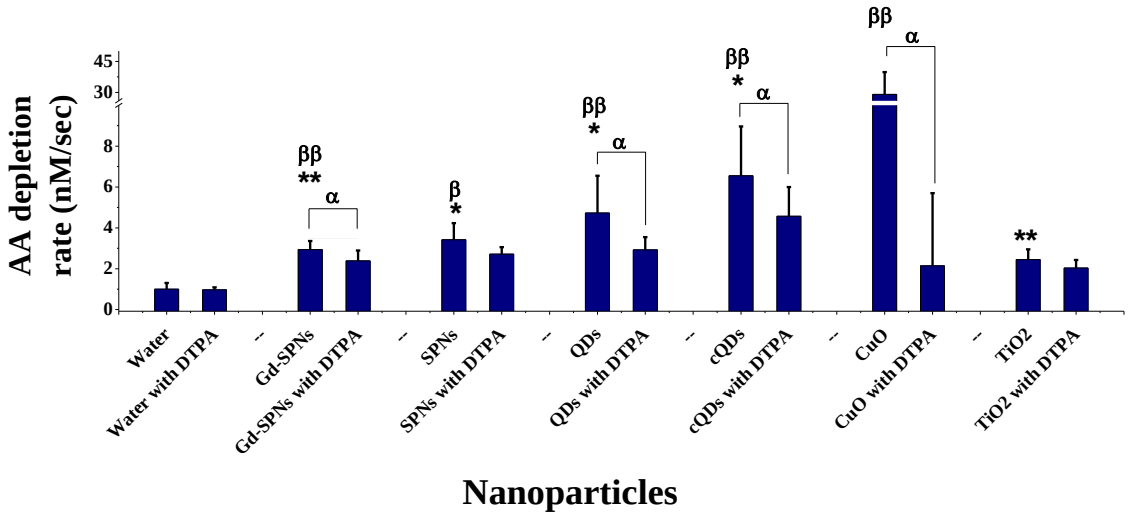

Figure 52 Ascorbic acid depletion assay of the nanoparticles, compared to a blank sample, with/without DTPA. CuO and TiO_2 are positive and negative controls respectively. Statistical significance is noted by (α) for significant difference between nanoparticles with/out DTPA, (*) for significant difference between nanoparticles and CuO, and (β) for significant difference between nanoparticles and TiO_2. Single notation = p-values < 0.05, and double notations = p-values < 0.005.

Table 10 Statistical p-values, obtained using a Student's paired t-test with a two tailed distribution, stating the statistical significance between the nanoparticles with or without DTPA in comparison to the positive and negative controls; p-values < 0.05 denote a significant difference, while p-values > 0.05 (highlighted with red) denote a non-significant difference:

Nanoparticle	p-value with CuO	p-value with TiO2	p-value (nanoparticle with/out DTPA)
SPNs	0.005375615	0.018048586	0.33461921
Gd-SPNs	0.003816073	0.00319423	0.007136606
QDs	0.01338112	0.002116387	0.009910223
cQDs	0.018205062	0.002626244	0.032592427
CuO	N/A	0.00323474	0.006810687
TiO2	0.00323474	N/A	0.27420867
Nanoparticle + DTPA	p-value with (CuO + DTPA)	p-value with (TiO2 + DTPA)	p-value (nanoparticle with/out DTPA)
SPNs with DTPA	0.129290758	0.08113347	As above
Gd-SPNs with DTPA	0.067023518	0.445262924	As above
QDs with DTPA	0.121544655	0.147254984	As above
cQDs with DTPA	0.243471244	0.158481537	As above
CuO with DTPA	N/A	0.070693544	As above
TiO2 with DTPA	0.070693544	N/A	As above

Electron paramagnetic resonance was performed (by Mr David Parker, King's College London) to compliment the AA depletion assay. DMPO which is initially EPR silent, acts as a spin trap for short-lived free radicals such as •OH and •OOH. Upon contact with a free hydroxyl radical, DMPO reacts with it and becomes EPR active with a half-lifetime of minutes (< 2.9 min for •OH and 1 min for •OOH) [322]. No free radicals were detected with DMPO in the four different nanoparticle suspensions under study (section 5.9.6 for experimental procedures). Also no free radicals were detected in a more highly concentrated MEH-PPV SPN suspension (*ca.* 180 µg/mL), which reflected the higher concentrations used in the following biological assays. Moreover, exciting the nanoparticles at 254 nm and 365 nm prior measurements did not generate any detectable free radicals.

In summary, both the EPR measurements and the AA depletion assay performed with/out the

presence of DTPA suggest a low oxidative potential of the SPNs, Gd-SPNs, QDs, and cQDs after manufacture (when using manufacturing conditions that reduce heavy metal impurities). EPR also suggests that the depletion of the ascorbic acid in the non-DTPA containing nanoparticle solutions is most probably attributed to leaching cadmium from the cores of the QDs [86] and escaping gadolinium atoms from the surfaces of the Gd-SPNs [226] rather than due to any free radical production. Therefore, this study suggests that all four nanoparticles have a low propensity to induce oxidative stress following manufacture.

4.4 Nanoparticle Interactions with Human Blood Components

4.4.1 Interactions of Nanoparticles with Platelets and their Effect on ADP-induced Platelet Aggregation in Isolated Platelets

Platelet aggregation in isolated human platelet rich plasma (PRP) was assessed using a PAP-4 Bio-Data Corporation platelet aggregometer, which measures the changes in the optical density of 100% PRP over time following the addition of the substance of interest. The instrument was calibrated by measuring the (high) optical density of each individual donor sample of 100% PRP and assigning this value as "0% platelet aggregation". Next, a sample of platelet poor plasma (PPP) was produced from each donor by removing all platelets through centrifugation and measuring the (low) optical density of the sample, which is designated by the instrument as "100% platelet aggregation". To perform a sample measurement, the possible agonist, in this case, the nanoparticles, was then added to a fresh PRP sample and changes in the optical density of the continuously-stirred PRP were monitored over time.

Three concentrations of nanoparticles were chosen for the assessment of potential to induce platelet aggregation (300, 30, and 3 µg/mL PRP), with the highest concentration chosen to reflect a concentration of Gd-SPNs which has a considerable relaxation time that is useful in MRI applications [97] (section 3.8). In preliminary tests, the addition of nanoparticle suspensions to PRP was not observed to induce significant aggregation over a 5 minute time period at the doses tested (example in Figure 53). However, because the nanoparticle suspensions of the higher concentrations were also optically dense, changes in the measured turbidity may not only reflect platelet aggregation, but also particle aggregation. This is a significant disadvantage of the standard platelet aggregometer assessment technique when applied to test nanomaterial interactions. Of the few studies in the literature, most have not reported direct assessment of nanoparticle-induced platelet aggregation, at least at high concentrations, with this technique. However, some studies have reported nanoparticle-induced changes to the platelet response to endogenous agonists, such as ADP.[278] Therefore, this experiment was also performed.

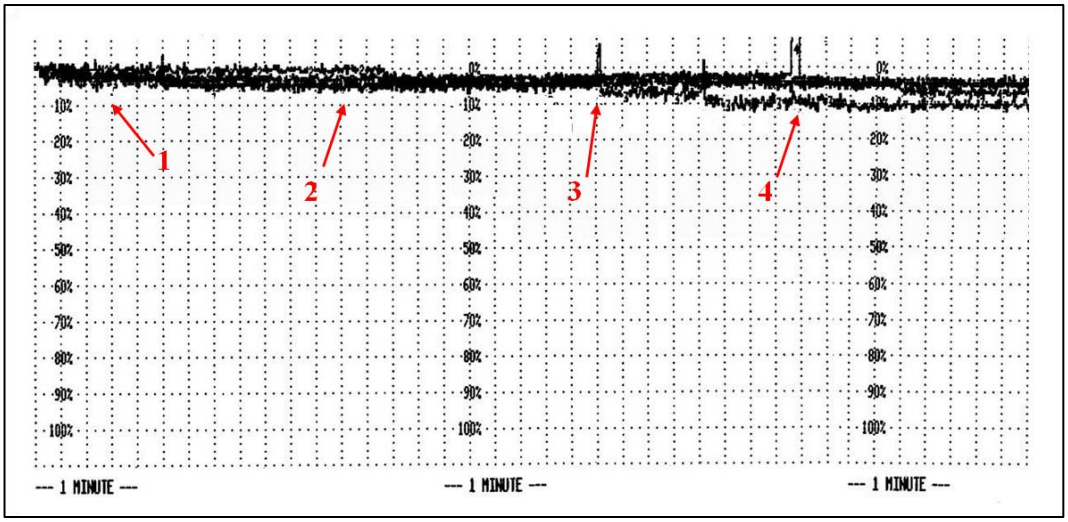

Figure 53 Example of platelet aggregation profiles (Aggregometer raw data of one of the donors) with the addition of (1) a blank sample, a final concentration of 0.2 µg/mL of (2) QDs, (3) SPNs, and (4) Gd-SPNs.

Figures 54 - 56 show the individual response profiles of platelets isolated from three different donors (D1-D3) to 10 µM ADP after incubation with 0, 3, 30 and 300 µg/mL SPNs, Gd-SPNs, QDs, and cQDs. The aggregation profiles from each donor are depicted to highlight the natural inter-experiment and inter-individual variation in platelet response to any given agonist. For example, platelets of the same donor may show approximately 20% variation in the maximum aggregation levels achieved in response to 10 µM ADP, as is depicted by the top panels in Figures 54 - 56. It is also noticeable that the maximum response between donors is highly variable, with 80-100% platelet aggregation observed for D1 platelets, 40-60% observed for D2 and only 10-30% observed for D3. This means that any influence of nanoparticles on the platelets, must be considered as normalised to each individual blood donor.

The bottom panels of Figures 54 - 56 depict platelet responses to ADP in the presence of increasing nanoparticle concentrations (3, 30, and 300 µg/mL PRP). These platelet aggregation profiles, although again showing both inter-experiment and inter-individual variation, are similar to those of the blank sample, suggesting that the nanoparticles did not influence ADP-induced platelet aggregation in a dose-dependent manner. Figure 57 depicts the maximum % platelet aggregation of the three donors combined. Values for each nanoparticle dose were normalised by subtracting the average of the three maximum response values to ADP alone. The normalised results of the three donors were then regarded as three replicates of one experiment (n = 3), these values were averaged, and the resulting change in % maximum platelet aggregation was plotted in Figure 57. The summarized data show no obvious change in platelet % aggregation *vs.* increased concentration, and the high standard deviations which extend across the baseline for most data, suggest that there is no obvious effect of the nanoparticles to the ADP-induced platelet aggregation.

These results differ from reports published previously, which will be discussed in greater detail below.

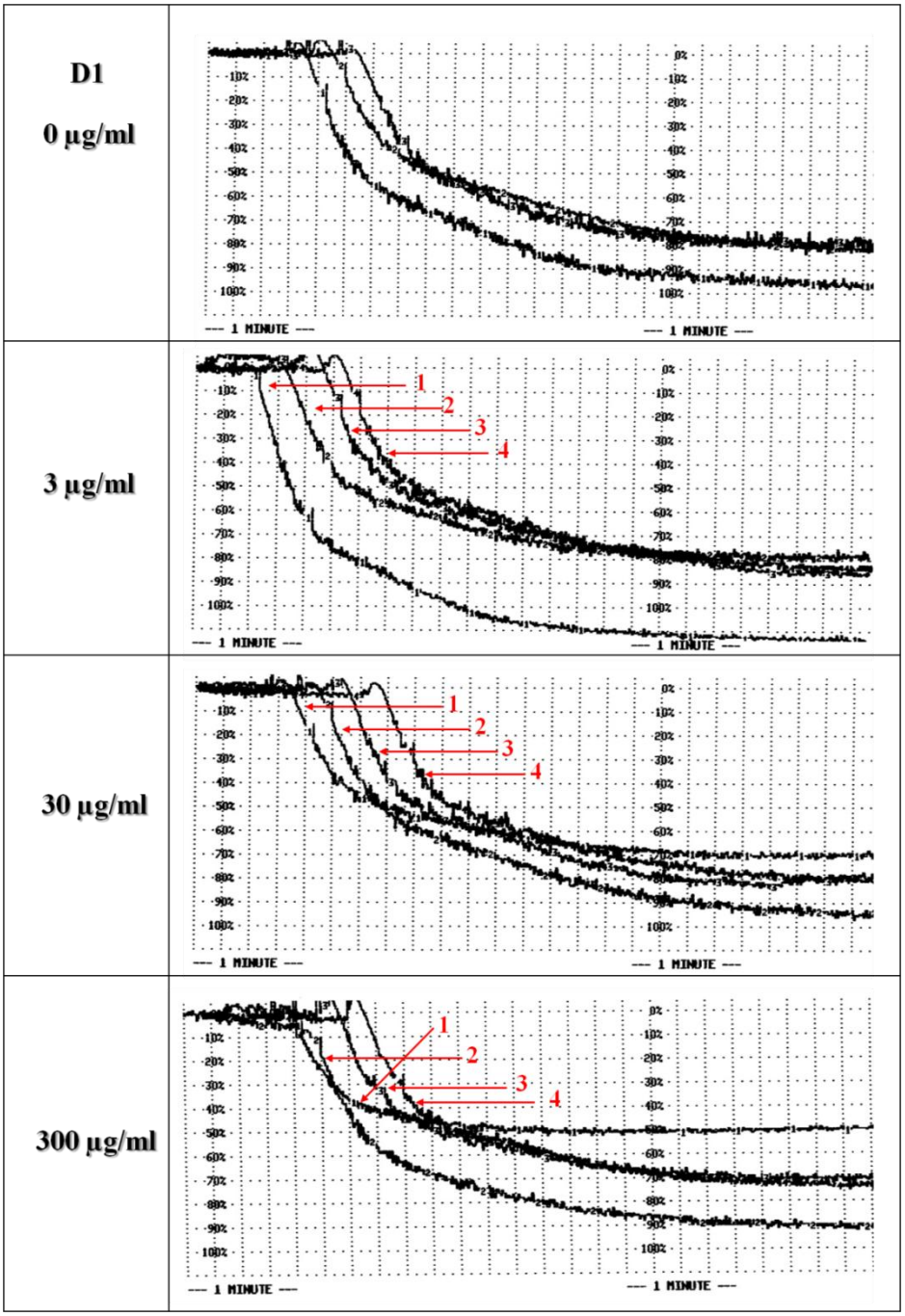

Figure 54 Traces from Donor 1 (D1) showing platelet responses to different concentrations of nanoparticles (i.e. baseline values over ~ the first minute of the measurement profile), and to the addition of 10 µM ADP to platelets in the presence of the nanoparticles (i.e. initiation of platelet aggregation curves). The top panel (0 µg/mL nanoparticles) represents the donor response to 10 µM ADP alone (n = 3 repetitions). In each graph where nanoparticles are present in the sample, the red notations denote (1) SPNs, (2) Gd-SPNs, (3) QDs, and (4) cQDs.

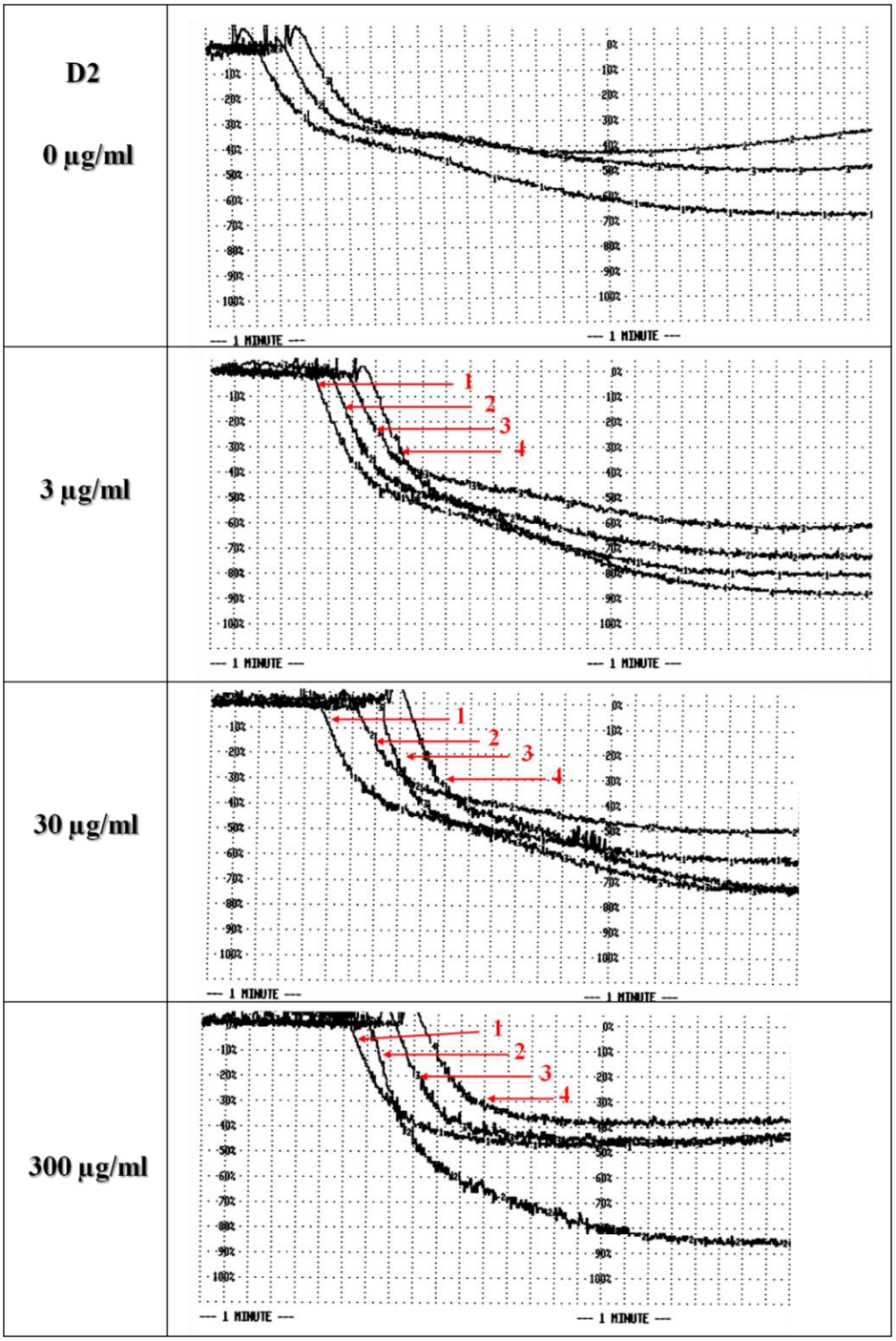

Figure 55 Traces from Donor 2 (D2) showing platelet responses to different concentrations of nanoparticles (i.e. baseline values over ~ the first minute of the measurement profile), and to the addition of 10 µM ADP to platelets in the presence of the nanoparticles (i.e. initiation of platelet aggregation curves). The top panel (0 µg/mL nanoparticles) represents the donor response to 10 µM ADP alone (n = 3 repetitions). In each graph where nanoparticles are present in the sample, the red notations denote (1) SPNs, (2) Gd-SPNs, (3) QDs, and (4) cQDs.

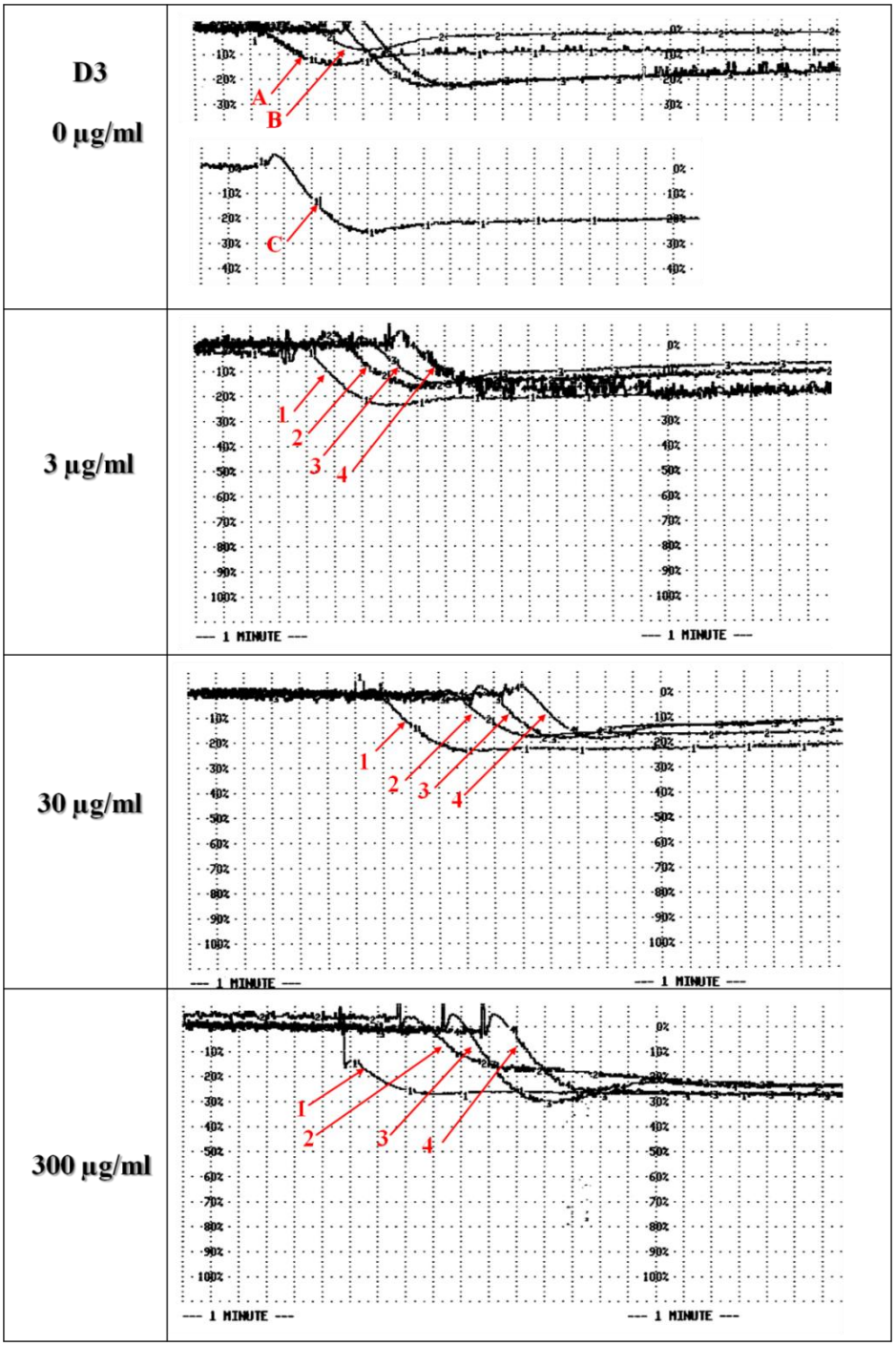

Figure 56 Traces from Donor 3 (D3) showing platelet responses to different concentrations of nanoparticles (i.e. baseline values over ~ the first minute of the measurement profile), and to the addition of 10 µM ADP to platelets in the presence of the nanoparticles (i.e. initiation of platelet aggregation curves). The top panel (0 µg/mL nanoparticles) represents the donor response to 10 µM ADP alone (A, B, and C are n = 3 repetitions). In each graph where nanoparticles are present in the sample, the red notations denote (1) SPNs, (2) Gd-SPNs, (3) QDs, and (4) cQDs.

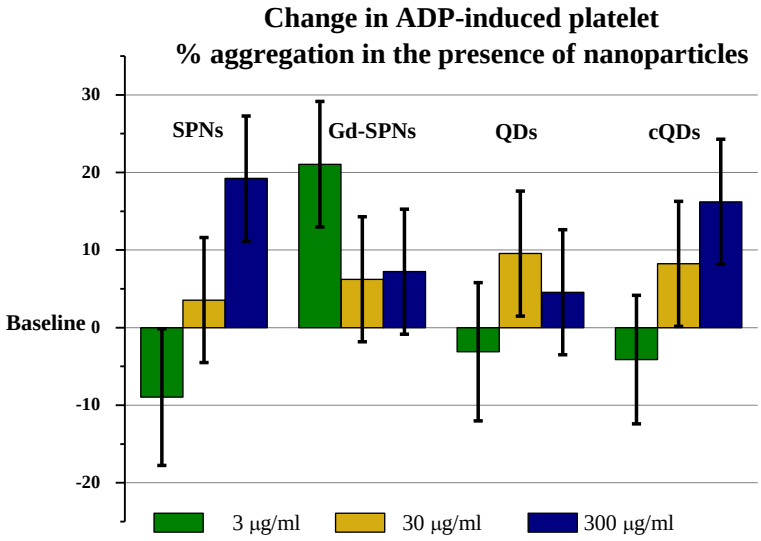

Figure 57 Percentage change in ADP-induced maximum % platelet aggregation in the presence of the nanoparticles at three different concentrations (3 µg/mL, 30 µg/mL, and 300 µg/mL; n = 3) normalised to the average ADP-induced maximum % platelet aggregation of each donor when no nanoparticles are present (baseline value which is set at a value of 0).

In previous studies, Geys *et al.* and McGuinnes *et al.* used carboxyl/amine capped nanoparticles and reported changes in platelet aggregation profiles with comparably high concentrations of their surface functionalised nanoparticles [278, 289]. The major difference between these systems and the results from this study is that the cQDs used here have a significantly lower negative zeta potential and are also partially PEGylated. As previously mentioned, PEG was reported to significantly reduce interactions between nanoparticles and biological species such as proteins and cells [210]. Further, it seems that a substantial positive or negative zeta potential value is required to activate platelets and induce aggregation. Thus, the moderate number of carboxylic groups introduced into the cQD surface coating in this study did not seem sufficient to influence platelet aggregation directly. Another important observation from the current study was that the four nanoparticles did not indirectly influence the endogenous platelet aggregation pathway in response to ADP, as has been demonstrated for other types of nanomaterials including functionalised QDs [278]. In summary, the desired passive behaviour of the platelets to the nanoparticles in the isolated platelets assays supports their profile as bio-compatible nanomaterials [323].

4.4.2 Interactions of SPNs and QDs with Human Whole Blood Components

Due to the limitations of assessing nanoparticle-induced platelet aggregation using turbidity-based methods, such as the conventional platelet aggregometer, alternative methods for assessing

interactions between nanoparticles and blood components may be useful. For example, fluorescence activated cell sorting (FACS) analysis has also been used to assess the activation of platelets, neutrophils, and monocytes in response to the presence of nanoparticles [289]. A flow cytometer is used to selectively detect and quantify cell surface proteins which are known to be upregulated in specific blood cells when they become activated in response to either an endogenous or exogenous stimulant. Using FACS analysis, three major questions were addressed in this study:

1. Do SPNs and QDs activate platelets?
2. Do SPNs and QDs promote adhesion of platelets to circulating monocytes?
3. Do SPNs and QDs activate neutrophils?

4.4.2.1 Do SPNs and QDs Activate Platelets?

Platelets are coated with different glycoproteins which play an important role in platelet activation and thus reaction with its surroundings (adhesion and aggregation). For example, platelets adhere to collagen (available on the cell membranes of endothelial cells) through glycoprotein Ia (GPIa) available on their membranes. Platelets also bind to fibrinogen (a soluble plasma protein which is converted by the enzyme (thrombin) to fibrin monomers which in turn polymerise and cross-link to form insoluble fibrin polymer which leads to blood clotting) and to Von Willebrand Factor (VWF - which is an adhesion molecule mostly produced by the endothelial cells) through glycoproteins Ib and IIb/IIIa (GPIb and GPIIb/IIIa) also available on the platelets' surface. Non-activated platelets have about 50 – 80 000 GPIIb/IIIa receptors (also called CD41a proteins) which do not bind to VWF or fibrinogen, etc. However, upon activation, platelets undergo an increase in these glycoprotein receptors which then enable platelet cross-linking with fibrinogen bridges. Also, when platelets are activated, other proteins located in their storage granules migrate and translocate to their surface facilitating their different interactions. One of these expressed proteins on the surface of activated platelets is called P selectin platelet alpha-granule membrane protein (CD62P).[261, 324]

Platelet activation can be detected by the measure of CD62P expression against the measure of CD41a. This can be performed by the use of fluorescently labelled animal antibodies which recognise the specific human proteins as antigens (i.e. foreign bodies) and therefore bind to them.[261] Mouse anti-human CD41a-FITC conjugate (fluorescein isothiocyanate; λ_{ex} = 488 nm, λ_{em} = 520 nm; BD Biosciences) can be used to label platelets in a blood sample, and mouse anti-human CD62P-PE conjugate (R-phycoerythrin; λ_{ex} = 496 nm, λ_{em} = 578 nm; BD Biosciences) can be used to label activated platelets in the same sample (each antibody is selectively labelled with a fluorophor of different wavelength). The FACS analysis will detect the fluorescence intensity of the total labelled antibodies adhering to each platelet surface and provides quantitative information on the percentage of activated platelets within a given cell population.

Because of the passive behaviour of the human platelets in the presence of the nanoparticles in the previous investigation (platelet aggregation in section 4.4.1), it was hypothesised that the nanoparticles would not induce upregulation of platelet activation markers. To test this, platelets were isolated from four healthy human donors (n = 4) and incubated with 300 µg/mL of the different nanoparticle suspension, 0.9% NaCl in water (negative control) or 300 µg/mL carboxylated polystyrene beads (cPS; 50 nm; [289]; positive control) prior to incubation with the labelled antibodies, CD41a and CD62P. To account for the possibility of fluorescence overlap between the nanoparticles and the CD62P signal, it was important that fluorescence from the background control samples was subtracted from the fluorescence of each sample containing antibodies. Elevated fluorescence levels of the background-corrected (i.e. normalised) CD62P signal denoted platelet activation. Figure 58 depicts the percentage of platelets from a population of 100,000 cells which exhibited elevated levels (above the designated threshold value) of CD62P.

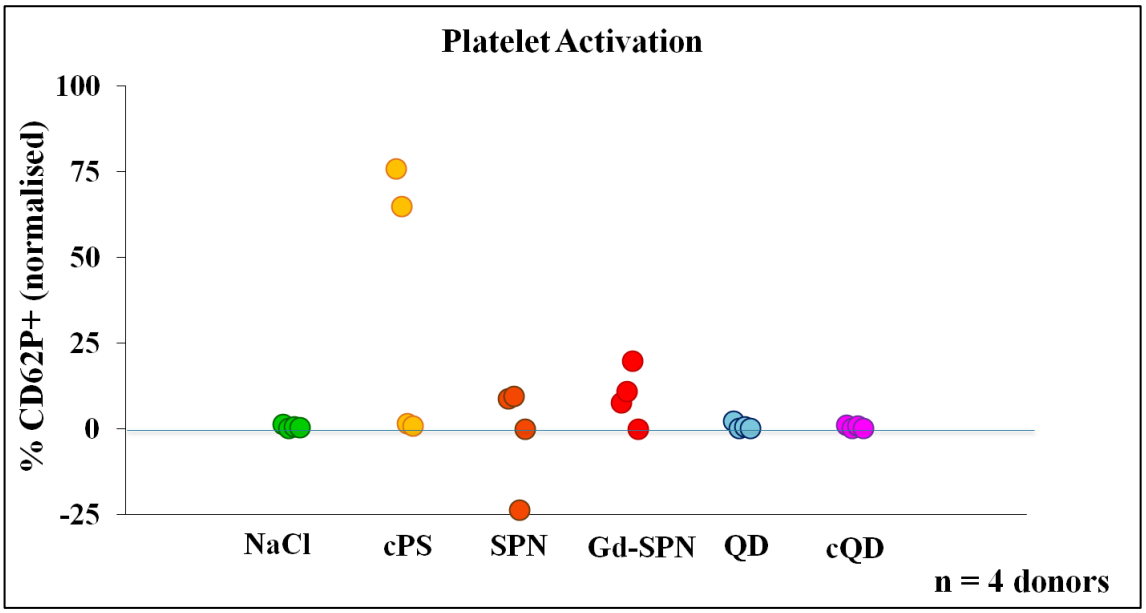

Figure 58 The percentage of activated platelet cells from a population of 100,000 after incubation with nanoparticles, the negative (0.9% NaCl in water) or positive (cPS) controls (data points represent the values from n = 4 donors).

Figure 58 shows that incubation of the isolated platelets of all four donors with NaCl did not show any CD62P expression, which is what was expected from a negative control. However, incubating the platelets with cPS (the positive control) only showed an increased CD62P expression in the platelets of two donors (from n = 4). This shows the natural variation of platelet activation in the platelets of different humans, similar to the variation of ADP-induced platelet aggregation investigated previously (section 4.4.1). Because 50% of the donors in this investigation did not react positively to cPS, it is advisable to repeat the experiment with a greater number of donors in the future to obtain a more significant result. However, because cPS was reported in the literature to cause platelet activation [289], the initiation of platelet activation in half the donors in

this study is arguably significant, and cPS was still considered a working positive control.

There was an overlap between the fluorescence spectra of the SPNs and the antibodies used. Therefore, it was important to subtract the fluorescence of the SPNs (as background) from the fluorescence of the samples containing both SPNs and antibodies. However, this approach did not solve the problem adequately since the background fluorescence (platelets + SPNs) varied considerably, possibly due to a random distribution of SPNs adhering to the platelet surface. This variability resulted in non-reliable CD62P expression values. To overcome this problem, this fluorescence overlap has to be avoided entirely, probably by the use of SPNs which emit in a different wavelength range than the antibodies such as PPE SPNs, or vice versa.

The fluorescence of the QDs, on the other hand, did not interfere with the results as their fluorescence was adequately quenched in these experiments. Therefore, the results of the QDs (shown in Figure 58) are reliable and show that both QDs and cQDs did not activate platelets. It is again interesting to note that the moderate carboxylation of the cQD surface in combination with the PEGylation, did not induce CD62P upregulation as was observed for the carboxylated polystyrene nanoparticles both in this study and the study of McGuinnes *et al.* [289] As stated in the previous section, this is most likely due to the combined effect of steric shielding of PEG and the moderately low overall surface charge. In summary, these results correspond well with the platelet aggregation study from the previous section and demonstrate that the PEGylated phospholipid coating of the nanoparticles under investigation is effective in preventing platelet activation and aggregation events. Although the results from the SPNs were inconclusive at this point, further studies with a different core material will likely confirm the hypothesis that the coating material effectively prevents platelet activation and aggregation. However, it is valuable to note that compared to the QDs, the SPN fluorescence was not quenched in the biological environment, but rather was extremely stable and bright, indicating again the potential usefulness of the system for bio-imaging applications.

4.4.2.2 Do SPNs and QDs Promote Platelet-Monocyte Adhesion?

Similar to the membranes of platelets, monocyte membranes contain specific glycoproteins which if detected, can be used to distinguish them from the rest of the blood cells. CD14 is one of these glycoproteins. It is a glycosylphosphatidylinositol (GPI)-anchored cell surface glycoprotein expressed on monocytes, macrophages, and more weakly on neutrophils.[261]

Platelet-monocyte adhesion can be detected by the measure of CD41a and CD14 in the same population. Mouse anti-human CD14-PE-Cy7 conjugate (R-phycoerythrin; λ_{ex} = 488 nm, λ_{em} = 775 nm; BD Biosciences) can be used to detect monocytes in a blood sample[289], while mouse anti-human CD41a-FITC conjugate (fluorescein isothiocyanate; λ_{ex} = 488 nm, λ_{em} = 520 nm; BD Biosciences) can be used to detect platelets in the same sample.With the use of FACS analysis, the

counted population which emits in the wavelengths of both labels is then considered a population of platelet-monocyte aggregates.

In this component of the analysis, platelet-monocyte adhesion was evaluated in whole blood from four healthy human donors (n = 4) also after incubation with the nanoparticles. Again, 0.9% NaCl in water was used as a negative control and commercially available carboxylated polystyrene beads (cPS; 50 nm; [289]) were used as a positive control. Briefly, whole blood was incubated for five minutes with each nanoparticle or control suspension and divided into two equal volumes. One volume was mixed with fluorescently-tagged antibodies against CD41a (the platelet marker) and CD14 (the monocyte marker) and the second volume was processed without antibodies as a background control (section 5.9.9 for details). FACS was then used to count individual monocytes (or monocyte-platelet aggregates) which displayed the CD14 fluorescence signal. The CD41a fluorescence signal was measured simultaneously. As discussed previously, to account for the possibility of fluorescence overlap between the nanoparticle and the CD41a (platelet) signal, it was important that fluorescence from the background control samples was subtracted from each sample containing antibodies. Elevated fluorescence levels of the background-corrected (i.e. normalised) CD41a signal denoted that one or more platelets had adhered to the surface of the individual monocytes counted. Figure 59 depicts the percentage of monocytes with platelets detected on their surface from a population of 3,000 cells.

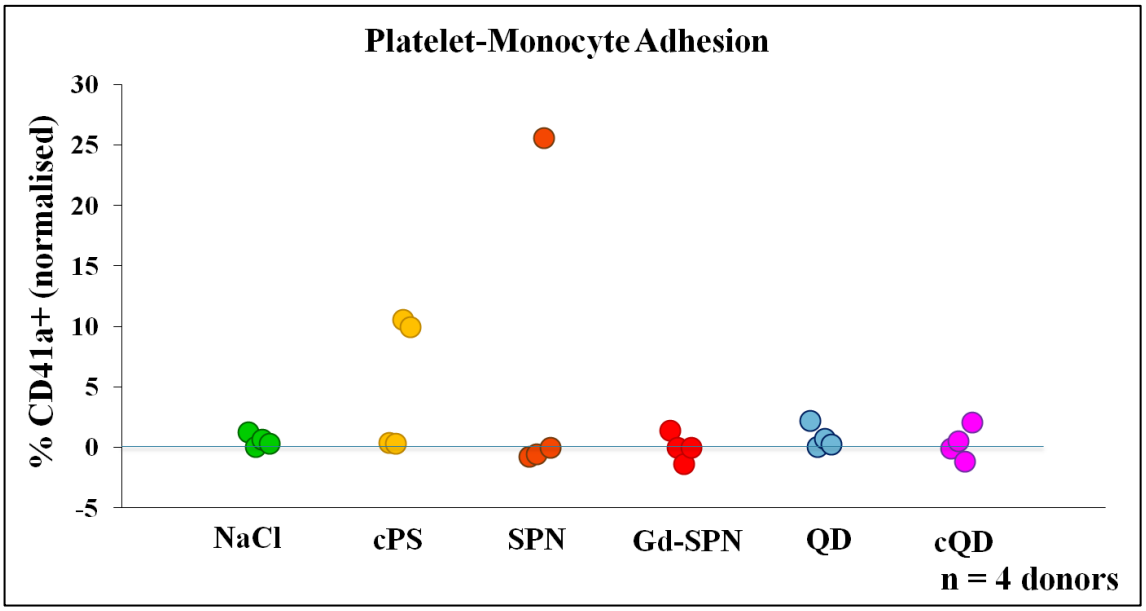

Figure 59 The percentage of monocytes (from 3,000 cells counted) with one or more platelets adhered to the surface after incubation with nanoparticles, the negative (0.9% NaCl in water) or positive (cPS) control (n = 4 donors).

Incubating whole blood with NaCl showed no detectable platelets within the population of monocytes (see Figure 59) as expected. As for the positive control, it is well understood that platelet-monocyte adhesion is initiated by platelet activation. Therefore, the results obtained from

incubation with cPS in this section must follow the results obtained in the previous section. As expected, two out of four donors did show an increased CD41a expression within the monocyte population (see Figure 59), which means that 50% of the donors showed platelet-monocyte adhesion after incubation with cPS. Again, the use of a greater number of replicates (more than n=4) is necessary for more significant results for cPS to be considered as a strong positive control.

The problem of fluorescence overlap in the SPN samples was also apparent here. Therefore, the results shown in Figure 59 for both SPNs and Gd-SPNs are not reliable. This was not the case with the QDs and cQDs which were already quenched prior to the experiment. Figure 59 shows that there was no noticeable CD41a expression within the monocyte population after incubation with the QDs and cQDs. This means that both QDs did not cause any platelet-monocyte adhesion. This result is comparable to the results of McGuinnes *et al.* [289] which reported that there was no significant difference between their surface modified and non-modified nanoparticles in terms of platelet-monocyte aggregate formation. However, McGuinnes *et al.* did detect platelet-monocyte aggregates with all three types of nanoparticles, while we here did not detect any aggregates at all. Again, the stealth effect of the partial PEGylation of the QDs and cQDs here could be the reason behind this passive behaviour of the blood components.

4.4.2.3 Do SPNs and QDs Activate Neutrophils?

Similar to platelets and monocytes, neutrophils have specific glycoproteins which are readily expressed on their surfaces. One of which is CD16 (a glycosylphosphatidylinositol (GPI)-anchored integral membrane protein expressed on T-cells, neutrophils, and macrophages). Another glycoprotein which is upregulated in activated neutrophils is CD11b (α_M integrin chain, MAC-1 or complement receptor 3). CD11b is a cell surface receptor found on activated (pro-inflammatory) neutrophils, which acts as an adhesion molecule to help neutrophils 'stick' to the endothelium and migrate to inflamed tissues. CD11b is weakly expressed on non-activated neutrophils, but is strongly expressed on activated ones.[261] Therefore, the measure of CD11b (with the use of mouse anti-human CD11b–Alexa Fluor 700 conjugate (λ_{ex} = 633 nm, λ_{em} = 723 nm; EBiosciences)) against CD16 (with the use of mouse anti-human CD16-PE-Cy7 conjugate (R-phycoerythrin; λ_{ex} = 488 nm, λ_{em} = 775 nm; BD Biosciences)) can give a measure of the percentage of activated neutrophils within a blood sample.

In this experiment, neutrophil activation was evaluated in whole blood from four healthy human donors (n = 4) after incubation with the nanoparticles. Briefly, whole blood was incubated for five minutes with each nanoparticle or control suspension and divided into two equal volumes. One volume was mixed with fluorescently-tagged antibodies against CD11b (the neutrophil activation marker) and CD16 (the neutrophil marker) and the second volume was processed without antibodies as a background control (section 5.9.10 for details). FACS was then used to count

individual neutrophils which displayed the CD16 fluorescence signal. Expression of CD11b was measured simultaneously. Elevated fluorescence levels of the background-corrected (i.e. normalised) CD11b signal denoted neutrophil activation. Figure 60 depicts the percentage of activated neutrophils from a population of 3,000 cells.

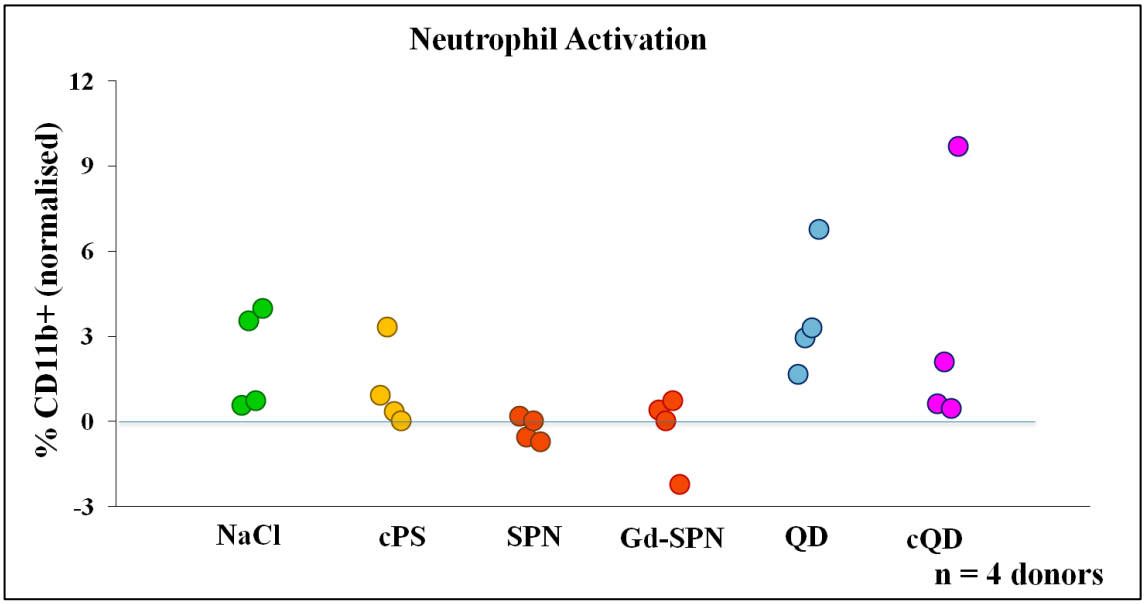

Figure 60 The percentage of activated neutrophils (from 3,000 cells counted) with elevated levels of CD11b after incubation with nanoparticles, the negative (0.9% NaCl in water) or positive (cPS) control (n = 4 donors).

Minor variations in CD11b were detected after incubating the blood samples with both NaCl and cPS (Figure 60), with the amount of expressed CD11b with the cPS samples not elevated in comparison to NaCl. This suggests that highly carboxylated polystyrene nanoparticles did not activate neutrophils and therefore could not be used as a positive control.

Again, with the overlap of fluorescence problem with the SPN samples which also caused a calculated negative response in most of the samples (compared to NaCl – the negative control), no reliable information could be depicted about the effect of the SPNs and Gd-SPNs on neutrophil activation.

The QDs however, did showed a possible trend towards a slight elevation in CD11b expression. With the lack of fluorescence overlap (because the fluorescence of the QDs was already quenched in this experiment), this suggests that the QDs and cQDs might have caused a moderate increase in neutrophil activation. However, it is necessary to repeat this experiment with a greater number of donors before making a solid conclusion about the QDs' tendency towards neutrophil activation. This was not investigated by McGuinnes *et al.* [289] nor has been reported elsewhere in the literature.

4.4.3 Evidence of SPN Interactions with Blood Cells

As described above, the experiments revealed a very high signal to noise in the detected fluorescence from isolated platelets and whole blood after incubation with the SPNs or Gd-SPNs. Fluorescence microscope imaging (performed by Dr Lea Ann Dailey, section 5.9.11 for details) of platelets, neutrophils, and monocytes incubated with SPNs or Gd-SPNs revealed that the nanoparticles were either internalised or adhered to the surfaces of many of the blood components (some of the obtained images are shown in Figure 61). We therefore concluded that the high and variable fluorescence signal from the SPN interactions with the cells made the process of background correction unreliable. Extensive method optimisation was performed to try to overcome this issue, without great success. Thus, in order to robustly assess the questions from this chapter, future studies must either use alternative semi-conducting polymers with emission spectra that do not overlap with the chosen fluorophores of the detection antibodies, or non-fluorescence based analytical methods must be employed.

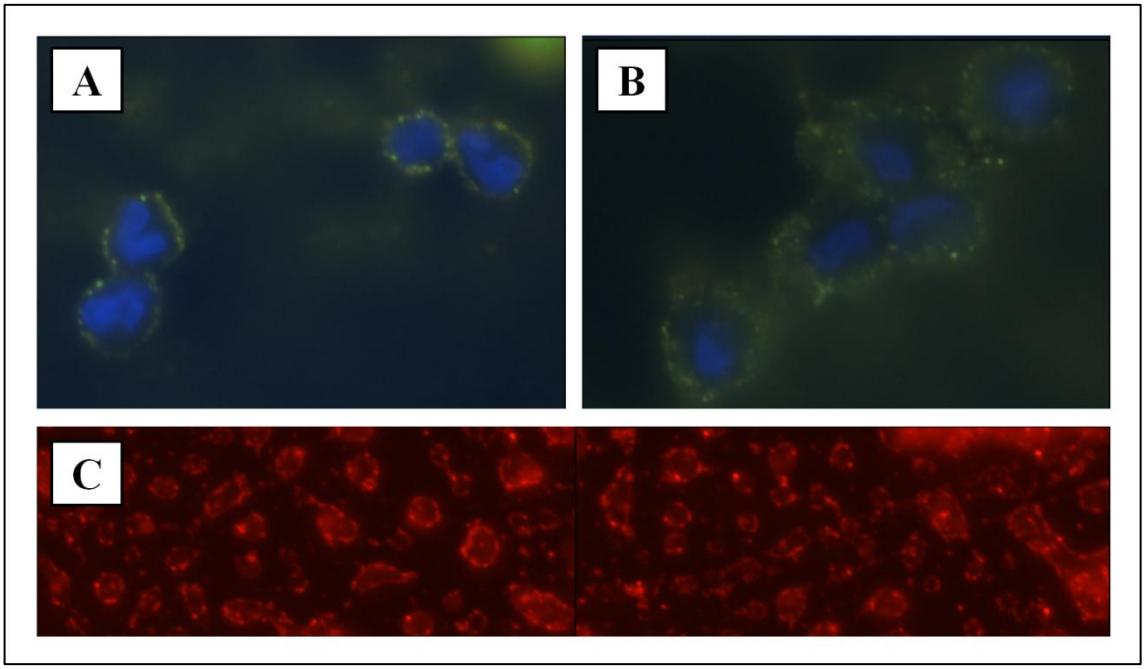

Figure 61 Fluorescence microscope images (20x magnification) of blood components incubated with SPNs or Gd-SPNs; (A) SPN fluorescence (λ_{ex} = 488 nm, λ_{em} = 520 nm; pseudo-coloured green) is detected at the cell membrane of blood neutrophils. (B) Gd-SPN fluorescence (λ_{ex} = 488 nm, λ_{em} = 520 nm; pseudo-coloured green) is detected both at the cell membrane and in internal compartments of blood monocytes. (C) SPN fluorescence (λ_{ex} = 488 nm, λ_{em} = 520 nm; pseudo-coloured red) is detected at the cell membrane of blood platelets.

A surprising and notable observation from the images in Figure 61 is the extent to which SPNs interact with different types of blood cells. According to the literature, the PEGylated coating

should reduce nanoparticle internalisation by phagocytic cells, such as monocytes and neutrophils [306-310]. Further, it is unexpected to see nanoparticles adhering to cell surfaces of both leukocytes and platelets. This adhesion may have also interfered with antibody binding to cell surface markers in the FACS experiments and should be investigated further in future. However, it will also be worthwhile to investigate the impact of PEG density and chain length on the interactions between SPNs and blood cells, as this factor may greatly influence nanoparticle circulation times and clearance after intravenous administration.

4.5 Conclusions

To achieve clinical use of any nanoparticles in the bio-imaging and medical fields, it is necessary to assess their safety. In this chapter, selected exploratory investigations were performed to assess the interactions of the Gd-SPNs we prepared in chapter 3 along with non-gadolinium containing SPNs and similar-lipid coated QDs and carboxylated QDs (cQDs) with components of human blood.

The nanoparticles were synthesised under controlled conditions to avoid metal contamination and their optical properties after synthesis were characterised. Then they went through several investigations to answer the following questions:

(a) What surface charge do they have? How does this surface charge change when they are exposed to different biological media?
(b) Are the nanoparticles colloidally stable in different biological and synthetic media?
(c) What is the status of their oxidative stress? Do they generate any free radicals?
(d) How do the nanoparticles interact with the different blood components?
    1. Do they cause any platelet aggregation?
    2. Do they affect ADP-induced platelet aggregation?
    3. Do they cause any platelet activation?
    4. Do they cause any platelet-monocyte adhesion?
    5. Do they cause any neutrophil activation?

In more detail, zeta potential measurements were performed to determine the nanoparticle surface charges. Their surfaces were found to be moderately negatively charged, with the negative charge increasing on the surfaces of both Gd-SPNs and cQDs. The negative charge was found to decrease in dilute platelet poor plasma which indicated adsorption of species on the surfaces of the nanoparticles in general and increasingly on the surfaces of both Gd-SPNs and cQDs.

Nanoparticle colloidal stability in different biological and synthetic media at 37°C was monitored for 24 hours. Both SPNs and Gd-SPNs were stable in water and in cell culture medium. The QDs were also stable in water, however, the cQDs were not. The cQDs showed evidence of aggregation over time which is not what was expected from carboxylated nanoparticles. Adding the

QDs and cQDs to cell culture medium (CCM) resulted in a shift of the small distribution towards the larger distribution which suggested that CCM acted as a colloidal stabilisers adsorbing on the surfaces of the smaller nanoparticles increasing their diameters. Finally, no information was gathered from adding the nanoparticles to dilute platelet poor plasma (PPP) as the detected diameters had a fluctuating distribution in all samples similar to that of the dilute PPP.

The nanoparticles were found not to induce platelet aggregation nor affect ADP-induced platelet aggregation. Furthermore, FACS analysis showed that both QDs and cQDs did not induce platelet activation nor platelet-monocyte adhesion. However, it did show that they do have a tendency to activate neutrophils. More experimentation with a greater number of donors is needed to strengthen this conclusion. Moreover, there was a significant overlap between the fluorescence of the SPNs/Gd-SPNs and the antibodies used in the FACS analysis. With the detection of a variable background, it was not possible to depict any reliable information about the SPNs/Gd-SPNs effects on the blood components in the three investigations conducted with this anaylsis technique (platelet activation, platelet-monocyte adhesion, and neutrophil activation).

The SPNs and Gd-SPNs were also found to adhere to blood components. The adhesion of the organic nanoparticles to the surfaces of the blood components could find an application in the future. However, from a safety assessment prospective using fluorescence related detection methods such as FACS, such highly fluorescent adhesive nanoparticles are problematic, therefore, ways to avoid their interference with the analysis results need to be explored. One way to compensate for this problem in the future is to use a different detection method which does not depend on optical properties, another way is to use SPNs which do not overlap at the same emission region of the markers (such as the blue emitting PPE SPNs), or vice versa.

Finally, the studies conducted in this chapter represent only a very preliminary approach to begin the evaluation of safety necessary for development of these nanoparticles as medical diagnostic tools. However, the results and conclusions in this chapter show an encouraging lack of reactivity with regard to platelet activation and aggregation events, as well as neutrophil activation. Future studies will explore the relationship between surface coating and nanoparticle adherence or internalisation into a variety of cells. Furthermore, cell viability studies and *in-vivo* safety testing must be carried out in the future. However, this study does highlight how useful it can be to perform parallel investigations of nanoparticle manufacture, physicochemical characterisation and evaluation with biological systems, with the aim of advancing the development of SPNs as potentially safer, more effective alternatives to quantum dots for biomedical imaging applications.

5 Methods

5.1 Chemicals for the Nanoparticles Syntheses

5.1.1 Conjugated Polymers and Quantum Dots

The five commercially available polymers used in the syntheses were:

1. BEHP-PPV: Poly[2-(2',5'-bis(2''-ethylhexyloxy)phenyl)-1,4-phenylenevinylene] (minimum MW 30000 g/mol).
2. MEH-PPV: Poly[2-methoxy-5-(2-ethylhexyloxy)-1,4-phenylenevinylene] (MW 40000 – 70000 g/mol).
3. F8BT: Poly[(9,9-di-*n*-octylfluorenyl-2,7-diyl)-*alt*-(benzo[2,1,3]thiadiazol-4,8-diyl)] (MW 5000 – 8000 g/mol).
4. PPE: Poly[2,5-di(3',7'-dimethyloctyl)phenylene-1,4-ethynylene] (MW 4122 g/mol).
5. ADS108GE: Poly[(9,9-dioctyl-2,7-divinylene-fluorenylene)-alt-co-(2-methoxy-5-(2-ethyl-hexyloxy)-1,4-phenylene)] (MW 111000 g/mol).

All polymers were obtained from Sigma-Aldrich, except for ADS108GE which was obtained from American Dye Source, Inc. All polymers were used as received.

The quantum dots used in the nanoparticle-cell interaction studies in chapter 4 were (Lumidot^{TM} CdSe/ZnS 590), which were obtained from Sigma-Aldrich.

5.1.2 Surfactants

The surfactants used in the syntheses of the QD-sized PEG capped/entwined SPNs were:

1. PEG: Poly(ethylene glycol) (a range of MWs; 300, 200, 8000 g/mol), obtained from Sigma-Aldrich.
2. PEG-dithiol: Poly(ethylene glycol) dithiol (MW 1530 g/mol) obtained from Sigma-Aldrich.

The lipids used in the syntheses of the SPNs, Gd-SPNs, QDs, and cQDs were:

1. PEG2000-PE: 1,2-dipalmitoyl-sn-glycero-3-phosphoethanolamine-N-[methoxy(polyethyleneglycol)-2000] (ammonium salt), obtained from Avanti Polar Lipids.
2. DPPC: 1,2-dipalmitoyl-sn-glycero-3-phosphocholine, obtained from Avanti Polar Lipids.
3. Gd-DTPA-BSA: (diethylenetriaminepentaacetic acid)-bis(stearylamide) (gadolinium salt), obtained from IQsynthesis, Inc.

4. DSPE-PEG2000 carboxylic acid: (1,2-distearoyl-*sn*-glycero-3-phosphoethanolamine-N-[carboxy(polyethylene glycol)-2000] (ammonium salt)), obtained from Avanti Polar Lipids.

All surfactants were used as received.

5.2 Nanoparticles Syntheses

5.2.1 Final Miniemulsion-Evaporation Synthesis of the PEG Capped/Entwined QD-sized SPNs

Five polymers were used to form the nanoparticles; BEHP-PPV, MEH-PPV, F8BT, PPE, and ADS108GE.

In a typical synthesis, 0.424 mg of the conjugated polymer was dissolved in 8 mL of dichloromethane (DCM) to form a 40 ppm (by weight) solution. 0.01 g PEG300 was added to 20 mL of deionised water and stirred in a covered conical flask for ten minutes. The 40 ppm conjugated polymer solution was then added drop-wise to the aqueous PEG solution while stirring vigorously. The mixture was covered and left to stir vigorously for 10 minutes. Next, the conical flask was suspended in a 35 kHz ultrasound bath for 20 minutes. The mixture was covered for the first 5 minutes then uncovered. Finally, the emulsified solution was transferred to a beaker and stirred rapidly to evaporate the remaining DCM. The solution was then filtered through filter paper and centrifuged at 5,600 rcf (10000 rpm) for 10 minutes. The purified aqueous solutions were stored in glass vials under light exclusion at room temperature.

5.2.2 Synthesis of QD-sized SPNs Capped/Entwined with PEG-dithiol

0.051 g PEG-dithiol was used instead of 0.01 PEG300 in the same synthesis described in section 5.2.1 to prepare PEG-dithiol capped/entwined QD-sized MEH-PPV SPNs.

5.2.3 Final Synthesis of the Bimodal Gd-SPNs

Four polymers were used to form the nanoparticles; MEH-PPV, F8BT, PPE, and ADS108GE. Three lipids were used in the outer shell of the nanoparticles; PEG2000-PE, DPPC, and Gd-DTPA-BSA.

In a typical synthesis, 25 mg of the conjugated polymer was dissolved in 8 mL of dichloromethane (DCM). 11.2 mg DPPC, 37.4 mg PEG2000-PE, and 13.9 mg Gd-DTPA-BSA were added to 25 mL of deionised water in a round-bottom flask. To achieve a homogenous lipid suspension in water, the flask was covered and sonicated in a 35 kHz ultrasound water bath which was maintained at a temperature below 7°C using ice. All samples were subjected to four sonication cycles of 60 seconds each, with 30 second rest periods in between each cycle. The lipid

suspension was then magnetically stirred for 1 minute and 0.8 mL of the polymer solution was introduced with a syringe over a period of 60 seconds. The flask was covered, stirred vigorously for 10 minutes, then sonicated for 90 seconds at 7°C. Finally, the open flask was gently stirred overnight to promote full DCM evaporation and nanoparticle formation. The nanoparticles suspensions were stored in glass vials at 4°C.

5.2.4 Synthesis of Carboxylated MEH-PPV Gd-SPNs for IgG Linkage

Carboxylated MEH-PPV Gd-SPNs were synthesised as follows: 25 mg of MEH-PPV was dissolved in 8 mL of dichloromethane (DCM). 11.2 mg DPPC, 37.4 mg DSPE-PEG2000, and 13.9 mg Gd-DTPA-BSA were added to 25 mL of deionised water in a round-bottom flask. To achieve a homogeneous lipid suspension in water, the flask was covered and sonicated in a 35 kHz ultrasound water bath which was maintained at a temperature below 7°C using ice. All samples were subjected to four sonication cycles of 60 seconds each, with 30 second rest periods in between each cycle. The lipid suspension was then magnetically stirred for 1 minute and 0.8 mL of the polymer solution was introduced with a syringe over a period of 60 seconds. The flask was covered, stirred vigorously for 10 minutes, then sonicated for 90 seconds at 7°C. Finally, the open flask was gently stirred overnight to promote full DCM evaporation and nanoparticle formation.

5.2.5 Synthesis of the SPNs and Gd-SPNs for the Nanoparticles' Interactions with Human Blood Studies

SPNs and Gd-SPNs were prepared as in section 5.2.3. MEH-PPV was used to form the polymeric core, and two lipids were used in the outer shell of the SPNs: PEG2000-PE and DPPC. In the Gd-SPNs, a third lipid, Gd-DTPA-BSA, was also used.

In a typical synthesis, 25 mg of the conjugated polymer was dissolved in 8 mL of dichloromethane (DCM). For the SPNs: 35.5 mg PEG2000-PE and 20.4 mg DPPC were added to 25 mL of Chelex® 100-treated water in a round-bottom flask. For the Gd-SPNs: 40.4 mg PEG2000-PE, 9.7 mg DPPC, and 14.1 mg Gd-DTPA-BSA were used. To achieve a homogeneous lipid suspension in water, the flask was covered and sonicated in a 35 kHz ultrasound water bath which was maintained at a temperature below 7°C using ice. All samples were subjected to four sonication cycles of 60 seconds each, with 30 second rest periods in between each cycle. The lipid suspension was then magnetically stirred for 1 minute and 0.8 mL of the polymer solution was introduced with a syringe over a period of 60 seconds. The flask was covered, stirred vigorously for 10 minutes, then sonicated for 90 seconds at 7°C. Finally, the open flask was gently stirred overnight to promote full DCM evaporation. The resulting aqueous nanoparticle suspensions were concentrated (section 5.4 and 5.5), purified (section 5.3), and stored in glass vials at 4°C.

5.2.6 Preparation of the Quantum Dots for the Nanoparticles' Interactions with Human Blood Studies

QDs and cQDs were prepared similar to Dubertret *et al.* [47] as follows: 200 µL CdSe/ZnS QDs in toluene (Lumidot™ CdSe/ZnS 590) was precipitated using 1 mL acetone and 5 minutes centrifugation at 3214 G (5000 rpm). For the QDs: 8 mg PEG2000-PE, 2.6 mg DPPC, and 2 mL chloroform were stirred in a round-bottom flask for 3 minutes. For the cQDs: 4.3 mg DSPE-PEG2000 carboxylic acid, 6 mg PEG2000-PE, and 2.8 mg DPPC were used. The lipidic suspension was used to dissolve the precipitated QDs and then they were transferred back to the flask and stirred for 3 minutes. Chloroform was then evaporated under vacuum, and the flask was dipped in an 80°C water bath where the solid material became gel-like. Then, 2 mL Chelex® 100-treated water was added and the solution was stirred for 10 minutes. The resulting red-coloured aqueous QDs suspensions were then purified (section 5.3) and stored in glass vials at 4°C.

5.3 Purification Techniques

Excess PEG-dithiol molecules in the QD-sized PEG-dithiol capped/entwined SPNs were removed via dialysis with a 2,000 Dalton dialysis membrane (obtained from Sigma-Aldrich). The dialysis membrane was filled with 2 mL of the aqueous micellar MEH-PPV SPNs solution and was placed in 350 mL of deionised water which was continuously stirred. The dialysis system was kept in the dark and the water was changed every two days over a period of 10 days.

Excess lipids in the SPNs, Gd-SPNs, QDs, and cQDs were removed via dialysis with Spectra/Por Float-A-Lyzer G2 MWCO 3.5 – 5 kDa cellulose ester membrane tubes (manufactured by Spectrum Laboratories, Inc.) and Chelex® 100-treated water. The tubes were immersed in 1 L deionised water which was stirred and changed every 24 hours for three days.

The purified aqueous nanoparticle suspensions were then filtered through 0.2 µm cellulose acetate filters to remove any dust or large nanoparticles and stored in glass vials at 4°C.

5.4 Concentration Techniques

Concentration of the nanoparticle suspensions was performed using Spectra/Por Float-A-Lyzer G2 MWCO 0.1 – 0.5 kDa (cellulose ester membrane tubes) and Spectra/Gel absorbent made of polyacylate-polyalcohol (manufactured by Spectrum Laboratories, Inc.). Tubes were filled with purified nanoparticle suspensions, covered, and surrounded by the absorbent which gradually extracted the aqueous phase. In this manner, 75 mL suspensions were concentrated in subsequent steps to 1 mL for the nanoparticle-cell investigation studies in chapter 4.

5.5 Concentration Determination Techniques

5.5.1 Mass Spectrometry to Determine the Concentrations of PEG-dithiol and Gd-DTPA-BSA

Before the determination of the concentration of either PEG-dithiol or Gd-DTPA-BSA in the SPNs samples, the samples were excessively purified, using the same dialysis techniques described in section 5.3.

An inductively coupled plasma / mass spectrometer (ICP/MS) (Elan 6100 DRC+, Perkin Elmer) was used to determine the concentration of sulfur in the purified PEG-dithiol capped/entwined QD-sized SPNs and the concentration of gadolinium in the purified Gd-SPNs. The concentration of PEG-dithiol in the samples was then calculated as half the detected concentration of sulfur since each PEG-dithiol molecule contains two sulfur atoms. The concentration of Gd-DTPA-BSA in the samples is the same as that of gadolinium because each Gd-DTPA-BSA lipid contains only one gadolinium atom.

5.5.2 Calculations to Determine the Percentage of Surfactant Associated with the SPNs after Synthesis

The above determined concentrations, in section 5.5.1, could not be compared to the initial surfactant concentrations used because the dialysis method which was used to purify the samples caused an uncontrolled change in the nanoparticles concentration as water molecules were freely travelling in to and out of the dialysis tubes. Therefore, to determine the percentage of the surfactant of interest associated with the nanoparticles after synthesis (PEG-dithiol in the QD-sized SPNs and Gd-DTPA-BSA in the Gd-SPNs), a method which does not require the determination of the final nanoparticles concentration was developed as follows:

The change in concentration can be estimated by comparing the aqueous SPNs' absorbances before/after purification (at the same wavelength) using the absorbance equation in Beer Lambert Law:

$$A = \varepsilon C L$$

where A is the absorbance, ε is the wavelength dependant extinction coefficient, L is the path length, and C is the concentration of the sample.

The two equations *i* (before dialysis) and *f* (after dialysis) are therefore:

$$A_i = \varepsilon C_i L$$

$$A_f = \varepsilon C_f L$$

Dividing both equations leads to:

$$\frac{A_f}{A_i} = \frac{C_f}{C_i}$$

For the above relation to be true, the absorbances should be measured under the same conditions.

If all the gadolinium atoms/lipids were associated with and attached to the nanoparticles, then the number of gadolinium atoms in the dialysed sample will be the same before and after dialysis. In this case, the change in the concentration of gadolinium should be equal to the change in the concentration of the nanoparticles (polymer), so that:

$$\left(\frac{C_f}{C_i}\right)_{Gd} = \left(\frac{C_f}{C_i}\right)_{Polymer} \Rightarrow \quad \left(\frac{C_f}{C_i}\right)_{Gd} = \left(\frac{A_f}{A_i}\right)_{Polymer}$$

The concentration of gadolinium before and after dialysis can be measured by mass spectrometry, and the absorbances of the nanoparticles at the same wavelength, before and after dialysis, can be determined by absorption spectroscopy.

The percentage of Gd atoms/lipids incorporated in the Gd micellar SPNs after purification can then be calculated by the equation:

$$\left(\frac{C_f}{C_i}\right)_{Gd} \div \left(\frac{A_f}{A_i}\right)_{Polymer} \times 100 = \%\ of\ Gd\ atoms\ incorporated\ in\ the\ Gd\ micellar\ SPNs$$

The same argument applies to the PEG-dithiol percentage in the PEG-dithiol capped/entwined QD-sized SPNs.

5.5.3 A Developed Method to Determine the Final Polymer Concentrations in the Aqueous SPNs Samples

The concentrations of the final polymer nanoparticle suspensions were determined by evaporating the water and dissolving the nanoparticles in chloroform ($CHCl_3$) with 1% methanol. Using the absorbance/concentration relation given by the Beer-Lambert Law and the specific extinction coefficient values of the polymer in $CHCl_3$ + 1% methanol (measured in lab) at the wavelength of absorption peaks, the concentrations were determined.

5.5.4 Concentration Determination of the QDs used in the Nanoparticles' Interactions with Human Blood Studies

The concentrations of the purified QDs were calculated directly from Beer-Lambert Law after measuring their absorbances, and by using their extinction coefficient provided by their manufacturer.

5.6 Optical Characterisation and Analysis Techniques

5.6.1 Absorption Spectroscopy

The solutions were placed in quartz cuvettes (path length = 1 cm), and their absorption spectra were analysed (200-800 nm) using a Hitachi U-4100 Spectrophotometer (Hitachi).

5.6.2 Fluorescence Emission Spectroscopy

The solutions were placed in quartz cuvettes (path length = 1 cm), and their emission spectra were obtained using a LS50B Luminescence Spectrometer (Perkin Elmer).

5.6.3 Photographs and Excitation with a UV-lamp

The aqueous nanoparticle solutions were placed in glass vials and were exposed to a 365 nm UV-lamp under ambient light exclusion. Their fluorescence was observed and photographed with a hand-held 7.1 megapixel SP-55OUZ Olympus camera. Photographs of the nanoparticles in ambient light were also captured with the same camera.

5.6.4 Fluorescence Quantum Yield (QY) Calculations

The quantum yields (QY) were measured by comparison with suitable fluorescent standards:

1. Fluorescein in water (QY = 93% [325]) for F8BT and ADS108GE.
2. Atto 390 in water (QY = 90% [326]) for BEHP-PPV and PPE.
3. Rhodamine 6G in water (QY = 95% [325]) for MEH-PPV.

The measurements were carried out with dilute samples (absorbances of absorption peaks below 0.1) to avoid any concentration related fluorescence quenching such as re-absorption. The absorbances at a fixed wavelength (for both sample and standard) and their related emission spectra (under excitation with that same wavelength) were taken for successive dilutions (8 – 10 different concentrations) under the exact same measurement conditions and settings. A graph was plotted for each sample/standard, with the integrals of the emission intensity spectra (y-axis) against their relevant absorbances (x-axis). The slopes of the linear fittings were then obtained and the quantum yields of the samples were calculated by the equation:

$$(QY)_{sample} = (QY)_{standard} \times \left(\frac{slope\ of\ sample}{slope\ of\ standard}\right)$$

5.6.5 Extinction Coefficient Measurements

The extinction coefficients were estimated using the absorbance values at the peaks of the absorption spectra of the nanoparticles in Beer-Lambert Law. The Beer-Lambert Law is given by

$$I = I_o e^{-\varepsilon CL}$$

where I is the transmitted light intensity, I_o is the incident light intensity, ε is the extinction coefficient of the sample in ($mg^{-1}.cm^{-1}.ml$), C is its concentration in ($mg.ml^{-1}$), and L is the pathlength in (cm).

5.6.6 Fluorescence Lifetime Measurements

The fluorescence lifetime of MEH-PPV Gd-SPNs was measured by time-correlated single photon counting using a Leica TCS SP2 inverted scanning confocal microscope coupled with a Becker & Hickl SPC830 card in a 3-GHz, Pentium IV, 1-GB RAM computer running Microsoft Windows XP. A pulsed diode laser (Hamamatsu PLP10) with wavelength of 470 nm, pulse duration 90 ps, and a repetition rate of 20 MHz was used as the excitation source. The emission was collected through a bandpass filter onto a cooled PMC 100-01 photomultiplier detector Becker & Hickl, a hybrid detector based on a Hamamatsu H5772P-01 photomultiplier. The fluorescence decay was then fitted by a triple exponential decay model using Becker & Hickl SPCImage software. The intensity-weighted and amplitude-weighted average fluorescence lifetimes were calculated from the multi-exponential decay (by both Dr Klaus Suhling and Dr Pei-Hua Chung).[260, 327]

5.7 Size Measurement Techniques

5.7.1 Transmission Electron Microscopy (TEM)

Transmission electron microscopy (TEM) was performed on an FEI Tecnai G2 F20 FE-TEM. For TEM imaging of the nanoparticles, the aqueous SPN suspensions were dropcast onto carbon coated copper TEM grids. Nanoparticle diameters were measured using ImageJ from at least five different TEM images and 400 counts for each sample.

5.7.2 Dynamic Light Scattering (DLS) for Hydrodynamic Diameters

In many attempts to measure the true hydrodynamic diameters of the nanoparticles in water both Beckman Coulter DelsaTM Nano C Particle Analyser and Malvern Zetasizer Nano ZS were used. In both devices, a dynamic light scattering (DLS) technique is used to determine the hydrodynamic diameters of the nanoparticles in a substance. Nanoparticles dispersed in any solvent undergo Brownian motion which is a random movement of the nanoparticles caused by their interaction with the solvent they are dispersed in. The nanoparticles' velocity in their Brownian motion is defined by the translational diffusion coefficient (D) which is related to the nanoparticles' hydrodynamic diameter by the Stokes-Einstein equation:

$$d(H) = \frac{kT}{3\pi\eta D}$$

Where k is the Boltzmann constant and T and η are the absolute temperature and viscosity of the solvent respectively.

The translational diffusion coefficient is dependent on the surface structure of the nanoparticles, their concentration and the types of ions present in the solvent. The hydrodynamic diameter is therefore always larger that the physical diameter of the nanoparticle due to the above factors.

In DLS, a laser beam is directed towards the cuvette which contains the nanoparticle liquid suspensions. The scattered light detected, which is scattered from the surfaces of the moving particles, fluctuates due to their Brownian motion. The fluctuations are detected by a digital auto correlator and a correlation curve is obtained. The correlation function of the correlation curve is directly related to the translational diffusion coefficient, and therefore, it can be used to estimate the nanoparticle size distribution.

By fitting a single exponential to the correlation function, a general z-average diameter (cumulant diameter) and an estimation of the width of the size distribution (polydispersity index) are obtained. The above results are the most reproducible. However, the cumulants diameter is not a true representation of the average hydrodynamic diameters in the sample, but is a general indicator of the presence of nanoparticles.

By fitting multiple exponentials to the correlation curve, a size distribution graph is obtained (called the intensity distribution). The intensity distribution is a true representation of the intensities of the scattered light from the nanoparticles in the samples. With particles much smaller than the wavelength of the used light (less than λ/10), Rayleigh scattering happens. In Rayleigh approximation, the intensity of scattered light is relative to six orders of magnitude of the nanoparticle's diameter ($I \propto d^6$). This means that a much higher intensity of light is scattered from the larger nanoparticles in a polydispersed system. Therefore, the intensity distribution suggests the presence of much more of the larger particles than there really is.

The intensity distribution can be converted into a volume distribution using the Mie Theory which requires a pre-knowledge of the nanoparticles refractive index. With an unknown or estimated refractive index, an accurate volume distribution cannot be obtained.

The volume distribution can then be converted to a number distribution assuming that the nanoparticles are spherical in shape. If the assumptions and estimations made in the previous calculation steps are correct, then the number distribution will be a true representation of the size distribution of the hydrodynamic diameters of the nanoparticles and their averages.

Figure 62 shows that with a sample containing the same number of two sizes of nanoparticles (5 and 50 nm), the larger particles are detected one million times more than the smaller nanoparticles in the intensity distribution, while in the volume distribution they are detected a thousand times more. This is really important in polydispersed systems, as the presence of just a few larger

particles dramatically skews the results towards the larger species.

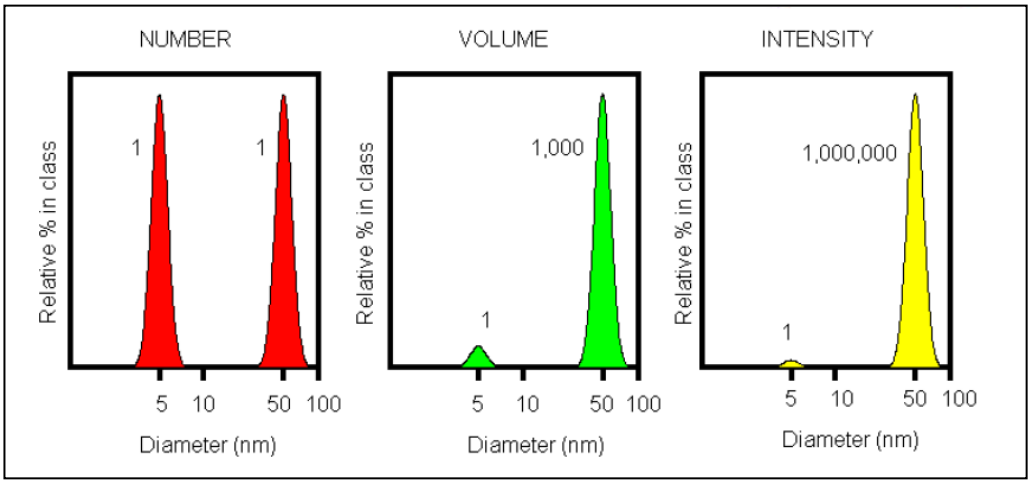

Figure 62 The number, volume, and intensity distributions determined by DLS of a sample containing the same number of 5 and 50 nm diameter nanoparticles.[328]

In the DLS measurements conducted for this project, quartz cuvettes were used with freshly prepared samples, and three replicates were taken for each sample (n = 3).

Because the refractive indecies of the nanoparticles are not known, only the cumulants diameter, the polydispersity index, and the intensity distribution results could be used. However, as discussed earlier, both the cumulants diameter and the intensity distribution average diameters are not the real average hydrodynamic diameters of the nanoparticles in the samples. Therefore, we could only use those results to identify the presence of nanoparticles, to get a general idea of how polydispersed the nanoparticles are, and to study the colloidal stability of the nanoparticles in the same sample.

In most of our measurements, the DLS intensity distribution average diameter was considered instead of the commonly reported cumulants diameter because the measured samples did not undergo excessive purification as they were not centrifuged to remove any large particles or dust. The large particles were found to skew the cumulants results towards larger diameters giving a faulty determination of a significantly larger population than that of the actual, as shown in Figure 63.

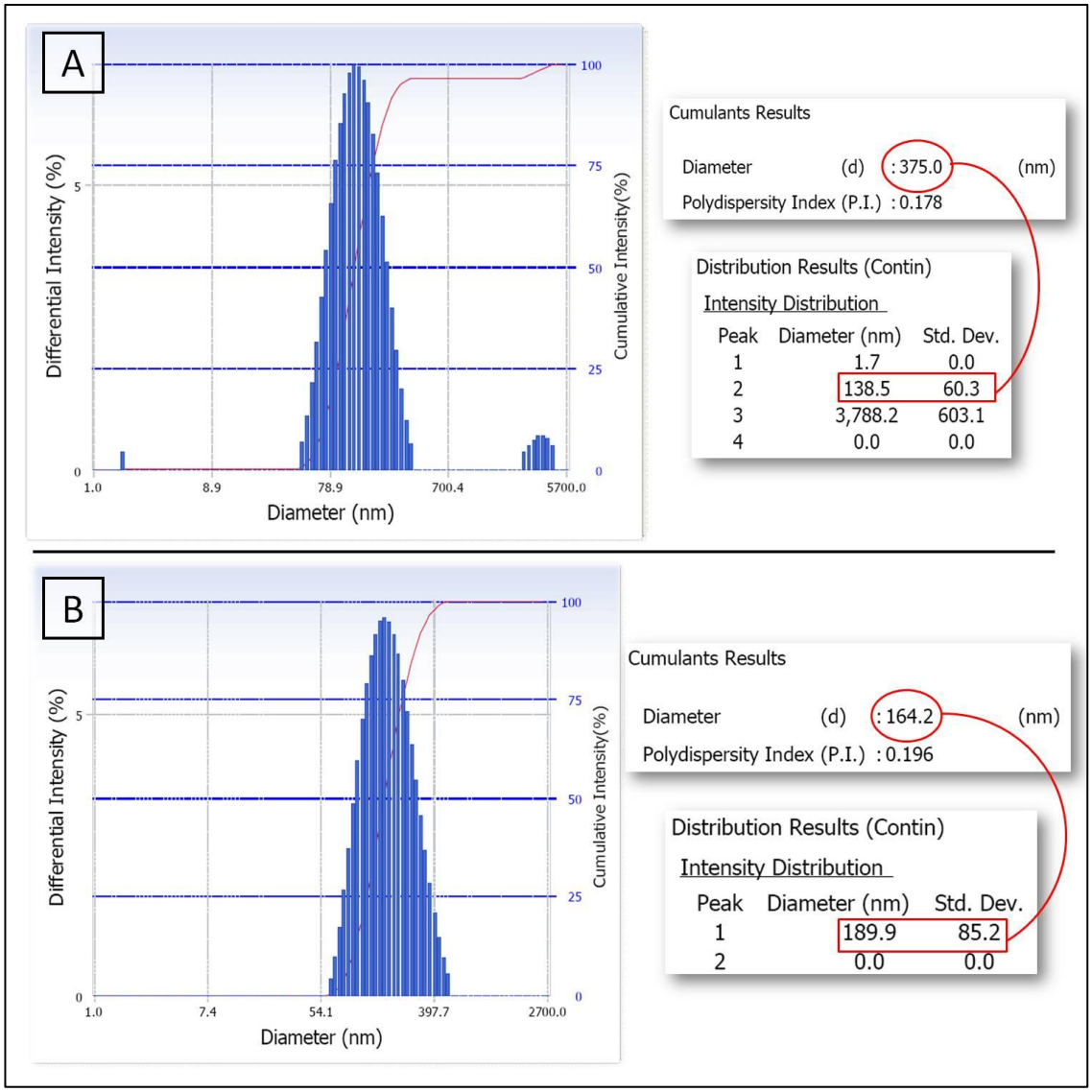

Figure 63 DLS cumulants results compared to the average diameters of their intensity distributions (A) with and (B) without the presence of a second peak with larger diameters.

5.7.3 Nanosight Nanoparticle Tracking Analysis (NTA) for Hydrodynamic Diameter

A NanoSight LM10 Nanoparticle Tracking Analysis system was used to determine the hydrodynamic diameters of the Gd-SPNs. The samples were diluted before measurements, and the measurements were carried out by Ms. Agnieszka Siupa in the labs of the NanoSight company.

5.8 Applications of the Gd-SPNs

5.8.1 Fluorescence Biomaging and Cellular Uptake Measurements of the Gd-SPNs

Live cell confocal laser scanning fluorescence microscopy of MEH-PPV Gd-SPNs was

performed using the human HeLa cell line (American Type Culture Collection). HeLa cells were cultured in phenol red Dulbecco's modified eagle's medium (DMEM) supplemented with 10% fetal bovine serum (FBS), 1% non essential amino acids, 1 mM sodium-pyruvate and 0.1 % penicillin/streptomycin at 37°C and 5% CO_2. The cells were seeded in a 6-well glass bottom plate (WaferGen Smartslide-6^{TM} micro-incubator) 24 hours prior to the addition of 20 µl MEH-PPV Gd-SPNs (initial concentration = 0.05 mg/mL). After overnight incubation, cells were washed 4-5 times with phenol red-free DMEM to remove Gd-SPNs, which were not associated with or internalised by the cells. During imaging, cells were maintained in phenol red-free DMEM at 37°C. Image acquisition was carried out using an inverted Leica TCS SP2 confocal microscope. Fluorescence excitation was stimulated by the 488 nm line of a continuous wave Ar^+ laser through a 63x water immersion objective (HCX PL APO, NA = 1.2), with a line scan speed of 400 Hz. Emitted fluorescence at 570 – 650 nm was collected through the same objective, dispersed through a prism and detected using a photomultiplier. Transmitted light images were collected simultaneously. Gd-SPNs were pseudo-coloured green and images are representative of at least three separate experiments.

Fixed cell confocal laser scanning fluorescence microscopy of MEH-PPV Gd-SPNs was performed using the murine macrophage-like J774 cell line (American Type Culture Collection). J774 cells were cultured in phenol red Dulbecco's modified eagle's medium (DMEM) supplemented with 10% fetal bovine serum (FBS), 1% L-glutamine, 1% sodium-pyruvate and 1% penicillin/streptomycin at 37°C and 5% CO_2. The cells were seeded at $1x10^6$ cells/cm^2 in 8-well glass chamber slides (LabTek^{TM} Chamber Slides^{TM}) 24 hours prior to the addition of 50 µl MEH-PPV Gd-SPNs suspended in cell culture medium (initial concentration = 0.2 mg/mL). Gd-SPNs were incubated with J774 cells for two hours and were subsequently washed 4-5 times with phosphate buffered saline (PBS) pH 7.4 to remove Gd-SPNs which were not associated with or internalised by the cells. Cells were fixed with 4% paraformaldehyde in PBS and the nuclei stained 30 min under light exclusion with 4',6-diamidino-2-phenylindole (DAPI). The cells were then mounted in glycerine: PBS (1:1) and visualised using a Leica DMIR E2 confocal microscope (Leica Microsystems, Milton Keynes, UK). Fluorescent emissions from DAPI (λ_{ex} = 205 nm; λ_{em} = 430-480 nm) and Gd-SPNs (λ_{ex} = 488 nm; λ_{em} = 570-650 nm) were collected using separate channels at a magnification of 63x and at an optical plane selected at half the cell height. Instrument gain and offset values were adjusted using the negative control and remained constant for all subsequent experiments. Images obtained from each scan were pseudo-colored blue (DAPI) and gold-red (Gd-SPNs), then overlapped afterwards to obtain a multicolored composite image. The presented results depict a representative image from at least three experiments.

5.8.2 Assessment of MEH-PPV Gd-SPNs Conjugation to IgG Antibodies

Carboxylated MEH-PPV Gd-SPNs were synthesised (section 5.2.4) and purified from excess lipids (section 5.3). Conjugation of the nanoparticles with IgG was performed (by Nicola J. Commander, DSTL, Salisbury, UK) using a standard Sulpho-NHS and EDC method (as described by Howes *et al.* [36]). Successful conjugation was confirmed by gel filtration and fluorescence detection from washed antibody-coated plates as follows; 100 µl (Gd-SPNs)-IgG solution was added to the wells of an immunosorb assay plate. Also 100 µl unconjugated IgG was added to separate wells as a negative control. The plate was incubated overnight at 4ºC. Then, it was washed 5 times with PBS to remove the unbound materials. Fluorescence from the washed wells was then analysed at λ_{ex} = 485 nm and λ_{em} = 536 nm. Fluorescence was detected from the wells of the (Gd-SPNs)-IgG but not from the wells of unconjugated IgG, which means that the nanoparticles were tightly bound to the antibodies.

A simple indirect ELISA test was used to demonstrate that the bound nanoparticles to the antibodies did not adversely affect their ability to bind to their target ligands as follows; immunosorb plates were coated with diluted antigen (in carbonate buffer) by overnight incubation at 4ºC, then blocking with 1% skimmed milk PBS solution for 1 hour at room temperature. Plates were then washed in PBS and blotted dry before use. MEH-PPV (Gd-SPNs)-IgG or non-conjugated IgG were diluted in 1% skimmed milk PBS-T solution and added to the plates at a range of dilutions. The plates were incubated for 1 hour at 37ºC then washed five times in PBS. Diluted goat anti-mouse IgG horse raddish peroxidase conjugate (obtained from AbD Serotec; diluted 1/4000 in 1% Skimmed milk PBS) was then added to the plates and they were incubated at 37ºC for a further hour then washed in PBS. 100 µl TMB chromogen / substrate (obtained from Sigma) was added to each well in the plates, and the plates were left at room temperature for 10 minutes. The colour development was stopped with a stopper solution (also obtained from Sigma), and finally, the absorbance of the plates' wells were detected at 450nm within 30 minutes of stopping. The fluorescence intensities were also detected at λ_{ex} = 485 nm and λ_{em} = 536 nm. The strength of the antigen-antibody reaction was determined by the intensity of the absorbance of the dye used.

5.8.3 Assessment of F8BT Gd-SPNs Fluorescence Against Animal Auto-Fluorescence

A rat pup was euthanized and 100 µL F8BT Gd-SPNs solution was injected subcutaneously into its scruff (initial concentration = 110 µg/mL). The rat was then imaged using an IVIS Spectrum (Caliper LS, Perkin Elmer) using a range of excitation and emission filters. The image obtained from the most optimum settings (excitation filter 465 nm and emission filter 540 nm) was then processed using the IVIS Spectrum analytical 'Image Math' tool and the background auto-fluorescence was subtracted resulting in an image detailing the fluorescence solely from the Gd-SPNs' emission. (This work was done by Jo Scott, DSTL, Salisbury, UK).

5.8.4 Assessment of the Fluorescence of Antibody-Conjugated and Unconjugated MEH-PPV Gd-SPNs Against Animal Auto-Fluorescence

Mouse cadavers were injected (by Ms. Nicola J. Commander, DSTL, Salisbury, UK) at three locations with either antibody-conjugated MEH PPV Gd-SPNs or unconjugated MEH-PPV Gd-SPNs as follows: 100 µL MEH-PPV (Gd-SPNs)-IgG solution (neat concentration ~ 1000x diluted Gd-SPNs with an initial concentration of ~ 35.6 µg/mL)) was injected into the quadriceps muscle of an euthanized mouse, 100 µL MEH-PPV Gd-SPNs solution (concentration ~ 35.6 µg/mL) was injected subcutaneously on the ventral surface, and 100 µL MEH-PPV Gd-SPNs solution (concentration ~ 35.6 µg/mL) was injected deep into the chest cavity. The mice were transferred to the IVIS isolator and were imaged using an IVIS Spectrum (Caliper LS, Perkin Elmer) using a range of excitation and emission filters.

5.8.5 Histopathology of MEH-PPV Gd-SPNs Injected into the Spleens of Euthanized Mice

Two mouse cadavers were injected with MEH-PPV Gd-SPNs into the spleen (by Ms. Nicola J. Commander, DSTL, Salisbury, UK). The spleens were then aseptically removed. One spleen was placed into paraformaldehyde fixative and the second one was placed into liquid nitrogen for snap freezing. Then both were processed for histopathology.

5.8.6 MRI T1–weighted Relaxivity Measurements of Gd-SPNs in Water

MRI was performed at a clinical 3T (Philips, Germany) and at a pre-clinical 7T (Agilent, Oxford UK) magnet. The sequence used at the 3T employed two non-selective inversion pulses with inversion times ranging from 20ms to 2000ms, followed by eight segmented readouts for eight individual images. The two imaging trains result in a set of 16 images per slice with increasing inversion times. For T1 mapping the acquisition parameters were: FOV=36x22x8, matrix=192x102, in-plane resolution=0.18x0.22mm, measured slice thickness=0.5mm, slices=16, TR/TE=9.6/4.9ms, flip angle=10°. The method used at 7T was a Look-Locker [329]. The sequence used a 180 degrees pulse to invert the magnetization of the samples. The acquisition started 10ms after the application of inversion pulse; TR = 100ms; TReff = 3700ms; 30 repetitions during the TReff; TE = 1.5 ms; FOV=30x30mm^2, 1mm thickness, matrix size = 96x96; 1 average; 1 slice; 4 phase encoding steps per pulse; scan time ~ 2min. The inversion pulse consisted of a non-selective adiabatic 180º of 8 ms while the flip angle of the turbo-FLASH imaging sequence was 20º.

The R1 values of the samples were calculated using ImageJ software (NIH, Bethesda, MD). The images were loaded and fitted for a T1 relaxation curve. R1 values were consequently associated to the concentration values using Microsoft Excel. T1 values were computed on a pixel-by-pixel basis using an in-house Matlab software [330].

5.9 Interactions with Components of Human Blood

5.9.1 Nanoparticle Manufacture for Biological Studies

New glassware, magnetic beads, spatulas, distilled/ metal free filters and membranes, and pH-adjusted Chelex®-treated distilled water were used in the preparation and handling of the nanoparticles to minimise heavy metal contamination. Water treatment with Chelex® 100 was performed as follows: 30 g of Chelex® 100 mesh (Chelex® 100 sodium salt, Sigma Aldrich) were added to 1 L water in a plastic beaker. The water was stirred for at least one hour with non-metallic stirring beads and filtered through 0.45 µm cellulose nitrate membrane filter paper. The pH was adjusted to 7.0 using concentrated NaOH and HCl solutions (also prepared with the filtered Chelex® 100-treated water). The treated water was then stored in non-metallic, non-glass containers at room temperature until further use. All nanoparticle suspensions were purified and concentrated to 4 mg/mL prior to use in biological studies.

5.9.2 Human Blood Collection and Processing

Human whole blood samples were collected in citrate buffer from consenting, healthy, aspirin-free volunteers aged 25-45 years old. Informed consent from all blood donors was obtained and procedures were approved by the King's College London Research Ethics Committee. To separate the platelet rich plasma (PRP) from the remaining blood components, 5 mL aliquots were centrifuged at 100xg for 20 minutes. To separate the platelet poor plasma (PPP) from PRP, PRP aliquots were centrifuged at 1400xg for 10 minutes. Whole blood, PRP and PPP samples were stored at room temperature and utilized within 4 hours of collection.

5.9.3 Nanoparticle Zeta Potential

Particle zeta potentials were measured using a Zetasizer Nano ZS (Malvern Instruments). Zeta potentials were measured both in Chelex® treated, pH adjusted water (using NaOH and HCl) and in 8% human PPP diluted in a buffer containing 20% phosphate buffered saline (PBS, obtained from Oxoid Limited), 80% distilled water, and 0.018% sodium azide (NaN_3, obtained from Fluka)). Measurements were performed in triplicate.

5.9.4 Nanoparticle Colloidal Stability Assessment in Physiological and Synthetic Media

The hydrodynamic diameters of all nanoparticle suspensions were measured at 37°C, over a period of 24 hours using the Zetasizer Nano ZS (Malvern Instruments). Nanoparticle stock suspensions (4 mg/mL) were diluted to 12.5 µg/mL either in water, phenol-red-free Dulbecco's Modified Eagle Medium (DMEM, obtained from Invitrogen) with 2% serum, or 8% human PPP

(see section 5.9.3 for 8% human PPP preparation). Size measurements were taken at 10 minute intervals for the first hour, then at 1 or 2 hour intervals for the remainder of 24 hours. The following instrument settings were used for each measurement: Temperature: 37°C, detection angle: 90°, $viscosity_{CCM}$: 0.738 cP, $refractive\ index_{ccm}$: 1.337, $viscosity_{water}$: 0.6864 cP, $refractive\ index_{water}$: 1.330.

5.9.5 Oxidative Potential Measured by Ascorbic Acid Depletion

To assess the oxidative potential of the nanoparticle suspension and confirm that suspensions were free of heavy metal contaminants, an *in vitro* ascorbic acid depletion assay was conducted. All SPN and QD nanoparticle suspensions, plus two control nanoparticle species, i.e. copper oxide nanoparticles (CuO, positive control; NanoScale Material Inc., USA) and titanium dioxide nanoparticles (TiO_2, negative control; NanoScale Material Inc., USA) were diluted to a concentration of 10 µg/mL in Chelex® 100-treated water. A blank sample of Chelex® 100-treated water was also used as a media control. L-ascorbic acid (Sigma-Aldrich), prepared in Chelex® 100-treated water and adjusted to pH 7, was added to the particle suspensions in a UV flat-bottom 96-well plate to achieve a final concentration of 0.2 mM. Four wells were allocated for each nanoparticle type including one background well (which contained no ascorbic acid). On the same plate, an identical set of experiments was conducted in the presence of 0.2 mM DTPA (diethylenetriaminepentaacetic acid; a heavy metal chelator). All plates were equilibrated to 37°C before measurement of the ascorbic acid absorbance (SpectraMax 190 Microplate Reader, Molecular Devices, USA), at 265 nm. Measurements were taken every 30 minutes for 2 hours. The concentration of ascorbic acid at each time point was calculated by subtracting the background absorbance values from the control wells and then conversion using a calibration curve. All experimental results are presented as the mean and standard deviation of the ascorbic acid depletion rate (n = 3 separate experiments).

5.9.6 Electron Paramagnetic Resonance for Free Radicals Detection

Spin trap (5-*tert*-butoxy carbonyl-5-methyl-1-pyrroline-*N*-oxide) (DMPO, Sigma Aldrich) was dissolved in Chelex® 100-treated water and was added to each particle suspension resulting in a final concentration of 100 mM DMPO and 12.5 µg/mL nanoparticles. Suspensions were equilibrated at 37°C and electron paramagnetic resonance (EPR) was performed under light exclusion using an EMX Bruker EPR spectrometer. Measurements were carried out with (1) no excitation, (2) excitation at 365 nm for 1 minute, and (3) excitation at 254 nm for 1 minute. As a negative control, DMPO was added to a blank sample (Chelex® 100-treated water), and EPR was performed under the same three conditions. Experiments were also repeated at room temperature. For a further investigation, the EPR experiment was also performed with a final concentration of

180 µg/mL of the SPNs.

5.9.7 Platelet Aggregation

Platelet rich plasma (PRP) and platelet poor plasma (PPP) of three healthy human volunteers were collected and processed as previously described (section 5.9.2). The concentrations of platelets in the PRP were adjusted to 2.6 x 10^8 platelets/mL using PPP from the same donor. To determine whether the presence of nanoparticles will induce aggregation in isolated platelets a PAP-4 Bio-Data Corporation Platelet Aggregometer was calibrated to 100% aggregation using PPP and 0% aggregation using PRP from each individual donor. Using nanoparticle suspensions with concentrations of 4, 0.4 and 0.04 mg/mL, 25 µL of the appropriate suspension (or 0.9% saline solution as the negative control) was mixed with 225 µL PRP (final nanoparticle concentrations tested were 300, 30 and 3 µg/mL) and turbidity was monitored for 5 minutes at 37°C under constant stirring.

A second experiment was performed to determine whether the presence of nanoparticles will influence pathways of platelet aggregation after pharmacological induction. PRP was first exposed to nanoparticles (or saline control) at the same concentrations as described above. After stirring for 1 minute, 6 µL adenosine diphosphate (ADP; final concentration: 10 µM) were added to induce platelet aggregation and turbidity was monitored for 5 minutes. The aggregation profiles for each donor, as represented by percentage aggregation after 5 minutes were normalised by dividing the sample results by the results of the blank sample and the mean value was calculated from the results of the three donors.

5.9.8 Platelet Activation

PRP of four donors was isolated as described in section 5.9.2 and diluted to a concentration of 10^7 cells/mL in PBS containing 1% bovine serum albumin and 0.1% sodium azide. Platelets were allowed to recover at room temperature for 45 minutes prior to addition of the four particle types achieving a final concentration of 300 µg/mL nanoparticles. 0.9% saline was used as a negative control and 300 µg/mL carboxylated polystyrene nanoparticles (50 nm in diameter; ThermoScientific) were used as positive controls. After 5 min of incubation with the particles, platelets were fixed with 100 µL PBS containing 1% bovine serum albumin, 0.5% paraformaldehyde and 0.1% sodium azide. Platelets were sedimented via centrifugation (1400xg for 10 minutes), resuspended in 100 µL PBS containing 1% bovine serum albumin and 0.1% sodium azide, and separated into two 50 µL aliquots. One aliquot (control) was mixed with 1.25 µL mouse anti-human CD41a-FITC conjugate (fluorescein isothiocyanate; λ_{ex}=488 nm, λ_{em}=520 nm; BD Biosciences). The second aliquot (sample) was mixed with 1.25 µL mouse anti-human CD41a-FITC conjugate and 1.25 µL mouse anti-human CD62P-PE conjugate (R-phycoerythrin;

λ_{ex}=496 nm, λ_{em}=578 nm; BD Biosciences). Isotype controls were conducted for both antibodies. CD41a is the alpha integrin chain gpIIb/IIIa transmembrane complex recognized on the surface of human platelets and is stably expressed in platelets, making it a suitable platelet marker. CD62P (P-selectin) functions as a cell adhesion molecule and translocates to the surface of activated platelets, making it a suitable marker for platelet activation. Following 20 minutes incubation under light exclusion at room temperature, 500 µL PBS containing 1% bovine serum albumin and 0.1% sodium azide was added to the samples.

Platelet activation was measured using a Cytomics FC500 MPL flow cytometer (Beckman Coulter). Platelets were discriminated from free particles by setting the forward scatter threshold to 10 (side scatter to 0) and gating for CD41a-positive events (threshold fluorescence intensity >1 arbitrary units). 10,000 CD41a-positive events were counted for each sample and the fluorescence intensity (FI) of the FITC-marker was plotted against the FI of the CD62P (PE)-marker. The percentage platelets from each particle and isotype control showing a FI > 1 (a.u.) for the CD62P (PE)-marker were subtracted from the percentage of platelets showing a FI > 1 (a.u.) for the CD41a (PE)-marker in each sample. Data from n = 4 separate donors are reported.

5.9.9 Platelet-Monocyte Adhesion

In a procedure similar to that described in the previous section, the percentage of platelet – monocyte adhesion was quantified as follows: the four nanoparticles were added to 100 µL of blood achieving a final concentration of 300 µg/mL nanoparticles. 0.9% saline was used as a negative control and 300 µg/mL carboxylated polystyrene nanoparticles (50 nm in diameter; ThermoScientific) were used as positive controls. The nanoparticle-blood mixture was then separated into two aliquots. One aliquot (control) was mixed with 1.25 µL mouse anti-human CD14-PE-Cy7 conjugate (R-phycoerythrin; λ_{ex}=488 nm, λ_{em}=775 nm; BD Biosciences). The second aliquot (sample) was mixed with 1.25 µL mouse anti-human CD41a-FITC conjugate (fluorescein isothiocyanate; λ_{ex}=488 nm, λ_{em}=520 nm; BD Biosciences) and 1.25 µL mouse anti-human CD14-PE-Cy7 conjugate. Isotype controls were conducted for both antibodies. CD41a is the alpha integrin chain gpIIb/IIIa transmembrane complex recognized on the surface of human platelets and is stably expressed in platelets, making it a suitable platelet marker. CD14 is a glycosylphosphatidylinositol (GPI)-anchored cell surface glycoprotein recognized on the surface of human monocytes and is stably expressed in monocytes, making it a suitable monocyte marker. Following 20 minutes incubation under light exclusion at room temperature, 500 µL OptiLyse C solution (Beckman Coulter) was added to the samples.

Platelet-monocyte adhesion was measured using a Cytomics FC500 MPL flow cytometer (Beckman Coulter). Monocytes were discriminated from free particles by setting the forward scatter threshold to 150 (side scatter to 0) and gating for CD14-positive events (threshold

fluorescence intensity >1 arbitrary units). 3,000 CD14-positive events were counted for each sample and the fluorescence intensity (FI) of the PE-Cy7-marker was plotted against the FI of the CD41a (FITC)-marker. The percentage cells from each particle and isotype control showing a FI > 1 (a.u.) for the CD41a (FITC)-marker were subtracted from the percentage of cells showing a FI > 1 (a.u.) for the CD14 (PE-Cy7)-marker in each sample. Data from n = 4 separate donors are reported.

5.9.10 Neutrophil Activation

In a procedure similar to that described in the previous section, the percentage of activated neutrophils was quantified as follows: the four nanoparticles and carboxylated polystyrene nanoparticles (50 nm in diameter; ThermoScientific) were added to 100 µL of blood achieving a final concentration of 300 µg/mL nanoparticles. 0.9% saline was used as a negative control and carboxylated polystyrene beads were investigated as a positive control. The nanoparticle-blood mixture was then separated into two aliquots. One aliquot (control) was mixed with 1.25 µL mouse anti-human CD16-PE-Cy7 conjugate (R-phycoerythrin; λ_{ex}=488 nm, λ_{em}=775 nm; BD Biosciences). The second aliquot (sample) was mixed with 1.25 µL mouse anti-human CD11b–Alexa Fluor 700 conjugate (λ_{ex} = 633 nm, λ_{em} = 723 nm; EBiosciences) and 1.25 µL mouse anti-human CD16-PE-Cy7 conjugate. Isotype controls were conducted for both antibodies. CD16 (PE-Cy7) is a glycosylphosphatidylinositol (GPI)-anchored integral membrane protein expressed on T-cells, neutrophils, and macrophages, making it a suitable neutrophil marker. CD11b functions as a cell adhesion molecule and translocates to the surface of activated neutrophils, making it a suitable activated neutrophil marker. Following 20 minutes incubation under light exclusion at room temperature, 500 µL OptiLyse C solution (Beckman Coulter) was added to the samples.

Neutrophil activation was measured using a Cytomics FC500 MPL flow cytometer (Beckman Coulter). Neutrophils were discriminated from free particles by setting the forward scatter to 150 (side scatter to 0) and gating for CD16 (PE-Cy7)-positive events (threshold fluorescence intensity >1 arbitrary units). 3,000 CD16-positive events were counted for each sample and the fluorescence intensity (FI) of the CD16 (PE-Cy7)-marker was plotted against the FI of the CD11b-marker. The percentage cells from each particle and isotype control showing a FI > 1 (a.u.) for the CD11b-marker were subtracted from the percentage of cells showing a FI > 1 (a.u.) for the CD16 (PE-Cy7)-marker in each sample. Data from n = 4 separate donors are reported.

5.9.11 Confocal Laser Scanning Microscope Imaging of Blood Cells Incubated with SPNs and Gd-SPNs

Whole blood was incubated with the SPNs and Gd-SPNs (a final concentration of 300 µg/mL nanoparticles) for 20 minutes at room temperature. Then 500 µL OptiLyse C solution ((Beckman

Coulter) was added to the samples to fix the cells and the nuclei stained 30 min under light exclusion with 4',6-diamidino-2-phenylindole (DAPI). Cells were deposited onto glass slides using a cytospin centrifuge, embedded in FluorSave® (Merck Millipore), and visualised using a Leica DMIR E2 confocal microscope (Leica Microsystems, Milton Keynes, UK). Fluorescent emissions from DAPI (λ_{ex} = 205 nm; λ_{em} = 430 - 480 nm) and SPNs/Gd-SPNs (λ_{ex} = 488 nm; λ_{em} = 570 - 650 nm) were collected using separate channels at a magnification of 20x and at an optical plane selected at half the cell height. Instrument gain and offset values were adjusted using the negative control (i.e. NaCl treated whole blood) and remained constant for all subsequent experiments. Images obtained from each scan were pseudo-colored blue (DAPI) and red or green (SPNs/Gd-SPNs), then overlapped afterwards to obtain a multi-colored composite image. The presented results depict representative images from n = 4 different donors.

6 Conclusions

In this thesis, the synthesis, characterisation, and preliminary nanoparticle-cell interaction investigations of monomodal and bimodal semiconducting polymer nanospheres was discussed. These organic nanoparticles could be proposed as alternatives to inorganic quantum dots specifically for bio-imaging applications, as they demonstrate superior optical brightness and fluorescence stability. Preliminary investigations of SPN interactions with human whole blood components show some promise for enhanced biocompatibility, but further studies must be carried out before making more conclusive statements about SPN safety. More details are presented in the Summary and Evaluation section followed by Future Work.

6.1 Summary and Evaluation

According to the literature, quantum dots (QDs) have been extensively investigated as bio-imaging agents due to the fact that the nanoparticles are a few nanometers in diameter with a narrow size distribution, are available in the commercial market, and their optical properties which surpass those of conventional imaging agents. However, many toxicological issues were raised about the safety of their use in such applications because of their composition. Therefore, alongside the work done in modifying the quantum dots to overcome this problem, other types of nanoparticles emerged such as semiconducting polymer nanoparticles (SPNs).

SPNs are newly emerging nanomaterials which are synthesised from conjugated polymers, and are reported to have larger diameters than QDs with relatively broader size distributions. To be suitable alternatives to QDs, the size problem had to be addressed and SPNs with QD-sizes had to be prepared. This problem was studied thoroughly in the first part of this thesis; with modifications to the miniemulsion-evaporation synthesis method used by our group and by others, PEG capped/entwined SPNs with diameters as small as 2 nm were prepared from five commercially available conjugated polymers. The concentration and molecular weight of PEG was found to greatly influence the reaction yield, and the prohibition of DCM evaporation during the miniemulsion process was found to be an important factor in the control and success of the synthesis outcomes. PEG-dithiol was also used in one variant of the syntheses, allowing the purified sample to be examined by mass spectrometry (using sulfur as a reporter), confirming the inclusion of a significant number of PEG molecules in the nanoparticles. The nanoparticles were characterized by TEM, absorption and emission spectroscopy, and were found to be stable in solution for months. Although those QD-sized SPNs had desirable size distributions, they suffered from great fluorescence quenching. However, due to their estimated high extinction coefficients, they were still considered bright.

In the second part of this thesis, another imaging functionality was added to the SPNs by

capping/entwining them with gadolinium containing amphiphilic molecules. The approximately 30 nm diameter bimodal nanoparticles (Gd-SPNs) had better size distributions and better fluorescent properties in comparison to the bimodal iron-oxide SPNs prepared previously by our group. They were readily taken up by both the human cell line, HeLa, and murine macrophage-like J774 cells as demonstrated by confocal laser scanning microscopy. The nanoparticles had desirable fluorescence properties, such as high fluorescence stability with little or no photo-bleaching after multiple cell image acquisitions or long storage periods. Their fluorescence was also found to be distinguishable from the auto-fluorescence of animal tissue, which makes them excellent imaging agents. However, this was dependent on both nanoparticle concentration and depth within the animal. The nanoparticles were also found to be MRI active generating a linear relationship between T1–weighted relaxation rates and gadolinium concentrations with calculated relaxivities of $r_1 = 20.75 \pm 0.57\, mM^{-1}.s^{-1}$ at 3T, and $r_1 = 17.21 \pm 0.50\, mM^{-1}.s^{-1}$ at 7T.

The third and final part of this thesis investigated interactions between human whole blood components and both monomodal and bimodal SPNs in comparison to QDs capped with similar capping agents. These studies are an excellent starting point to examine the safety of SPNs as alternatives to QDs in the biological and medical fields, as they represent a relevant biological environment into which nanoparticle imaging agents may be administered. Our preliminary studies revealed that organic and inorganic nanoparticles with exposed pendant carboxyl groups attracted protein adsorption to the particle surface, as suggested by decreases to their zeta potential values. In contrast, surface coatings without carboxyl groups were not altered measurably by incubation with media containing proteins. Moreover, the nanoparticles did not generate any DMPO-detectable free radicals, and were found to have little-to-no oxidative stress in comparison to CuO nanoparticles. Introducing the nanoparticles to isolated human platelets was found not to induce any aggregation nor affect ADP-induced aggregation. Also, introducing the inorganic nanoparticles to whole blood was found, by flow cytometry (FACS), not to induce any platelet activation nor platelet-monocyte adhesion, but a possible tendency to activate neutrophils was seen. Interestingly, while the fluorescence of the inorganic nanoparticles was substantially quenched by all biological media, SPN fluorescence remained bright and stable throughout.

6.2 Future Work

Now that the synthesis methods in preparation of PEG-capped SPNs and SPNs capped/entwined with amphiphilic molecules were refined, syntheses using different polymers and surfactants can be tested. By using infra-red emitting polymers, for example, the problem of tissue auto-fluorescence interference with the nanoparticles' emission *in-vivo* can be resolved. Also, by combining different functional surfactants, the synthesis of trifuctional SPNs might be achieved. However, the results of this study demonstrate that it is important to control surface charge with all modifications, as highly

negative or positive charges will promote non-specific binding of biological species to the nanoparticles. In the future, a continuation of SPN safety investigations should be conducted on the organic nanoparticles before making any conclusions about their safety for use in the medical and bio-imaging fields. With regard to the inconclusive results generated from the FACS analysis of platelet and neutrophil activation described in this thesis, experiments are currently underway with the PPE polymer, which has already been shown to avoid fluorescence interference with common antibody labels, thus overcoming the methodological challenges identified in this study. Preliminary results from these new investigations indicate that, as expected, no platelet activation, platelet-monocyte adhesion or neutrophil activation is observed. Finally, the SPNs synthesised in fulfilment of this thesis were mainly proposed for medical and biological use. However, SPNs can be prepared and tested in other non-medical applications such as the newly growing organic electronics field.

7 Bibliography

1. *Nanoscience and nanotechnologies: opportunities and uncertainties*. 2004, The Royal Society: Royal Academy of Engineering.
2. Franks, A., *Nanotechnology.* Journal of Physics E-Scientific Instruments, 1987. **20**(12): p. 1442-1451.
3. Asiyanbola, B. and W. Soboyejo, *For the surgeon: An introduction to nanotechnology.* Journal of Surgical Education, 2008. **65**(2): p. 155-161.
4. Buot, F.A., *Mesoscopic Physics and Nanoelectronics - Nanoscience and Nanotechnology.* Physics Reports-Review Section of Physics Letters, 1993. **234**(2-3): p. 73-174.
5. Tolles, W.M., *Nanoscience and nanotechnology: A perspective with chemistry examples*, in *Nanotechnology: Molecularly Designed Materials*, G.M. Chow and K.E. Gonsalves, Editors. 1996. p. 1-18.
6. De, M., P.S. Ghosh, and V.M. Rotello, *Applications of Nanoparticles in Biology.* Advanced Materials, 2008. **20**(22): p. 4225-4241.
7. Raki, L., J. Beaudoin, R. Alizadeh, J. Makar, and T. Sato, *Cement and Concrete Nanoscience and Nanotechnology.* Materials, 2010. **3**(2): p. 918-942.
8. Traykova, T., C. Aparicio, M.P. Ginebra, and J.A. Planell, *Bioceramics as nanomaterials.* Nanomedicine, 2006. **1**(1): p. 91-105.
9. Tolles, W.M., *Nanoscience and nanotechnology in Europe.* Nanotechnology, 1996. **7**(2): p. 59-105.
10. Sahoo, S.K., S. Parveen, and J.J. Panda, *The present and future of nanotechnology in human health care.* Nanomedicine-Nanotechnology Biology and Medicine, 2007. **3**(1): p. 20-31.
11. Khemtong, C., C.W. Kessinger, and J.M. Gao, *Polymeric nanomedicine for cancer MR imaging and drug delivery.* Chemical Communications, 2009(24): p. 3497-3510.
12. Sharifi, S., S. Behzadi, S. Laurent, M.L. Forrest, P. Stroeve, and M. Mahmoudi, *Toxicity of nanomaterials.* Chemical Society Reviews, 2012. **41**(6): p. 2323-2343.
13. Eustis, S. and M.A. El-Sayed, *Why gold nanoparticles are more precious than pretty gold: Noble metal surface plasmon resonance and its enhancement of the radiative and nonradiative properties of nanocrystals of different shapes.* Chemical Society Reviews, 2006. **35**(3): p. 209-217.
14. Drummen, G.P.C., *Quantum Dots-From Synthesis to Applications in Biomedicine and Life Sciences.* International Journal of Molecular Sciences, 2010. **11**(1): p. 154-163.
15. *PAS71:2011 Nanoparticles - Vocabulary*. 2011, British Standards Institution.
16. Buzea, C., Pacheco, II, and K. Robbie, *Nanomaterials and nanoparticles: Sources and toxicity.* Biointerphases, 2007. **2**(4): p. MR17-MR71.
17. Saunders, J.A., D.L. Unger, G.D. Kamenov, M. Fayek, W.E. Hames, and W.C. Utterback, *Genesis of Middle Miocene Yellowstone hotspot-related bonanza epithermal Au-Ag deposits, Northern Great Basin, USA.* Mineralium Deposita, 2008. **43**(7): p. 715-734.
18. Hornyak, G.L., J. Dutta, H.F. Tibbals, and A.K. Rao, *Introduction to Nanoscience*. 2008, United States: Taylor and Francis Group, LLC.
19. Kim, J.H., X.J. Huang, and Y.K. Choi, *Controlled synthesis of gold nanocomplex arrays by a combined top-down and bottom-up approach and their electrochemical behavior.* Journal of Physical Chemistry C, 2008. **112**(33): p. 12747-12753.
20. Lin, T.C., S.C. Lee, and H.H. Cheng, *Silicon-germanium spherical quantum dot infrared photodetectors prepared by the combination of bottom-up and top-down technologies.* Journal of Vacuum Science & Technology B, 2004. **22**(1): p. 109-115.
21. Euliss, L.E., J.A. DuPont, S. Gratton, and J.M. DeSimone, *Imparting size, shape, and composition control of materials for nanomedicine.* Chemical Society Reviews, 2006. **35**(11): p. 1095-1104.
22. Foelske-Schmitz, A., A. Peitz, V.A. Guzenko, D. Weingarth, G.G. Scherer, A. Wokaun, and R. Kotz, *In situ electrochemical STM study of platinum nanodot arrays on highly oriented pyrolythic graphite prepared by electron beam lithography.* Surface Science,

2012. **606**(23-24): p. 1922-1933.
23. Prabakar, S., A. Shiohara, S. Hanada, K. Fujioka, K. Yamamoto, and R.D. Tilley, *Size Controlled Synthesis of Germanium Nanocrystals by Hydride Reducing Agents and Their Biological Applications.* Chemistry of Materials, 2010. **22**(2): p. 482-486.
24. Higuchi, T., A. Tajima, H. Yabu, and M. Shimomura, *Spontaneous formation of polymer nanoparticles with inner micro-phase separation structures.* Soft Matter, 2008. **4**(6): p. 1302-1305.
25. Bahrami, K., P. Nazari, Z. Sepehrizadeh, B. Zarea, and A.R. Shahverdi, *Microbial synthesis of antimony sulfide nanoparticles and their characterization.* Annals of Microbiology, 2012. **62**(4): p. 1419-1425.
26. Landfester, K., *Miniemulsion Polymerization and the Structure of Polymer and Hybrid Nanoparticles.* Angewandte Chemie-International Edition, 2009. **48**(25): p. 4488-4507.
27. Kelsall, R., I. Hamley, and M. Geoghegan, *Nanoscale Science and Technology*. 2005, John Wiley & Sons Ltd.
28. Yang, H., Y.M. Zhuang, H. Hu, X.X. Du, C.X. Zhang, X.Y. Shi, H.X. Wu, and S.P. Yang, *Silica-Coated Manganese Oxide Nanoparticles as a Platform for Targeted Magnetic Resonance and Fluorescence Imaging of Cancer Cells.* Advanced Functional Materials, 2010. **20**(11): p. 1733-1741.
29. Ballou, B., B.C. Lagerholm, L.A. Ernst, M.P. Bruchez, and A.S. Waggoner, *Noninvasive imaging of quantum dots in mice.* Bioconjugate Chemistry, 2004. **15**(1): p. 79-86.
30. Yang, Y., Y. Yan, W. Wang, and J.R. Li, *Precise size control of hydrophobic gold nanoparticles using cooperative effect of refluxing ripening and seeding growth.* Nanotechnology, 2008. **19**(17).
31. Yoffe, A.D., *Low-dimensional systems: quantum size effects and electronic properties of semiconductor microcrystallites (zero-dimensional systems) and some quasi-two-dimensional systems.* Advances in Physics, 2002. **51**(2): p. 799-890.
32. Odenbach, S., *Magnetic fluids - Suspensions of magnetic dipoles and their magnetic control.* Journal of Physics-Condensed Matter, 2003. **15**(15): p. S1497-S1508.
33. Liu, W.T., *Nanoparticles and their biological and environmental applications.* Journal of Bioscience and Bioengineering, 2006. **102**(1): p. 1-7.
34. Wu, C., B. Bull, C. Szymanski, K. Christensen, and J. McNeill, *Multicolor Conjugated Polymer Dots for Biological Fluorescence Imaging.* ACS Nano, 2008. **2**(11): p. 2415-2423.
35. Kim, H.J., J. Lee, T.H. Kim, T.S. Lee, and J. Kim, *Highly emissive self-assembled organic nanoparticles having dual color capacity for targeted immunofluorescence labeling.* Advanced Materials, 2008. **20**(6): p. 1117.
36. Howes, P., M. Green, J. Levitt, K. Suhling, and M. Hughes, *Phospholipid Encapsulated Semiconducting Polymer Nanoparticles: Their Use in Cell Imaging and Protein Attachment.* Journal of the American Chemical Society, 2010. **132**(11): p. 3989-3996.
37. Kacenka, M., O. Kaman, J. Kotek, L. Falteisek, J. Cerny, D. Jirak, V. Herynek, K. Zacharovova, Z. Berkova, P. Jendelova, J. Kupcik, E. Pollert, P. Veverka, and I. Lukes, *Dual imaging probes for magnetic resonance imaging and fluorescence microscopy based on perovskite manganite nanoparticles.* Journal of Materials Chemistry, 2011. **21**(1): p. 157-164.
38. Koktysh, D., V. Bright, and W. Pham, *Fluorescent magnetic hybrid nanoprobe for multimodal bioimaging.* Nanotechnology, 2011. **22**(27).
39. Shkilnyy, A., E. Munnier, K. Herve, M. Souce, R. Benoit, S. Cohen-Jonathan, P. Limelette, M.L. Saboungi, P. Dubois, and I. Chourpa, *Synthesis and Evaluation of Novel Biocompatible Super-paramagnetic Iron Oxide Nanoparticles as Magnetic Anticancer Drug Carrier and Fluorescence Active Label.* Journal of Physical Chemistry C, 2010. **114**(13): p. 5850-5858.
40. Hai, T.H., L.H. Phuc, D.T.K. Dung, N.T. Le Huyen, B.D. Long, L.K. Vinh, N.T.T. Kieu, and M. Abe, *Contrast agents for magnetic resonance imaging based on ferrite nanoparticles synthesized by using a wet-chemical method.* Journal of the Korean Physical Society, 2008. **53**(2): p. 772-775.

41. Rosenberg, J.T., J.M. Kogot, D.D. Lovingood, G.F. Strouse, and S.C. Grant, *Intracellular Bimodal Nanoparticles Based on Quantum Dots for High-Field MRI at 21.1 T.* Magnetic Resonance in Medicine, 2010. **64**(3): p. 871-882.
42. Mahon, E., A. Salvati, F. Baldelli Bombelli, I. Lynch, and K.A. Dawson, *Designing the nanoparticle-biomolecule interface for "targeting and therapeutic delivery".* J Control Release, 2012.
43. Feng, X.L., F.T. Lv, L.B. Liu, H.W. Tang, C.F. Xing, Q.O. Yang, and S. Wang, *Conjugated Polymer Nanoparticles for Drug Delivery and Imaging.* ACS Applied Materials & Interfaces, 2010. **2**(8): p. 2429-2435.
44. Ghosh, P., G. Han, M. De, C.K. Kim, and V.M. Rotello, *Gold nanoparticles in delivery applications.* Advanced Drug Delivery Reviews, 2008. **60**(11): p. 1307-1315.
45. Kannan, R., A. Zambre, N. Chanda, R. Kulkarni, R. Shukla, K. Katti, A. Upendran, C. Cutler, E. Boote, and K.V. Katti, *Functionalized radioactive gold nanoparticles in tumor therapy.* Wiley Interdisciplinary Reviews-Nanomedicine and Nanobiotechnology, 2012. **4**(1): p. 42-51.
46. Tholouli, E., F. Sweeney, E. Barrow, V. Clay, J.A. Hoyland, and R.J. Byers, *Quantum dots light up pathology.* Journal of Pathology, 2008. **216**(3): p. 275-285.
47. Dubertret, B., P. Skourides, D.J. Norris, V. Noireaux, A.H. Brivanlou, and A. Libchaber, *In vivo imaging of quantum dots encapsulated in phospholipid micelles.* Science, 2002. **298**(5599): p. 1759-1762.
48. Michalet, X., F.F. Pinaud, L.A. Bentolila, J.M. Tsay, S. Doose, J.J. Li, G. Sundaresan, A.M. Wu, S.S. Gambhir, and S. Weiss, *Quantum dots for live cells, in vivo imaging, and diagnostics.* Science, 2005. **307**(5709): p. 538-544.
49. Larson, D.R., W.R. Zipfel, R.M. Williams, S.W. Clark, M.P. Bruchez, F.W. Wise, and W.W. Webb, *Water-soluble quantum dots for multiphoton fluorescence imaging in vivo.* Science, 2003. **300**(5624): p. 1434-1436.
50. Weiss, S., *Fluorescence spectroscopy of single biomolecules.* Science, 1999. **283**(5408): p. 1676-1683.
51. Bustamante, C., *In singulo biochemistry: When less is more.* Annual Review of Biochemistry, 2008. **77**: p. 45-50.
52. Parak, W.J., T. Pellegrino, and C. Plank, *Labelling of cells with quantum dots.* Nanotechnology, 2005. **16**(2): p. R9-R25.
53. Sano, K., M. Mitsunaga, T. Nakajima, P.L. Choyke, and H. Kobayashi, *In vivo breast cancer characterization imaging using two monoclonal antibodies activatably labeled with near infrared fluorophores.* Breast Cancer Research, 2012. **14**(2).
54. Delehanty, J.B., H. Mattoussi, and I.L. Medintz, *Delivering quantum dots into cells: strategies, progress and remaining issues.* Analytical and Bioanalytical Chemistry, 2009. **393**(4): p. 1091-1105.
55. Bruchez, M., M. Moronne, P. Gin, S. Weiss, and A.P. Alivisatos, *Semiconductor nanocrystals as fluorescent biological labels.* Science, 1998. **281**(5385): p. 2013-2016.
56. Alivisatos, A.P., W.W. Gu, and C. Larabell, *Quantum dots as cellular probes.* Annual Review of Biomedical Engineering, 2005. **7**: p. 55-76.
57. Erogbogbo, F., K.T. Yong, I. Roy, G.X. Xu, P.N. Prasad, and M.T. Swihart, *Biocompatible luminescent silicon quantum dots for imaging of cancer cells.* ACS Nano, 2008. **2**(5): p. 873-878.
58. Kim, B.Y.S., W. Jiang, J. Oreopoulos, C.M. Yip, J.T. Rutka, and W.C.W. Chan, *Biodegradable Quantum Dot Nanocomposites Enable Live Cell Labeling and Imaging of Cytoplasmic Targets.* Nano Letters, 2008. **8**(11): p. 3887-3892.
59. Gao, J.H. and B. Xu, *Applications of nanomaterials inside cells.* Nano Today, 2009. **4**(1): p. 37-51.
60. Roca, M. and A.J. Haes, *Probing cells with noble metal nanoparticle aggregates.* Nanomedicine, 2008. **3**(4): p. 555-565.
61. Kumar, S.A., Y.A. Peter, and J.L. Nadeau, *Facile biosynthesis, separation and conjugation of gold nanoparticles to doxorubicin.* Nanotechnology, 2008. **19**(49).
62. Fuller, J.E., G.T. Zugates, L.S. Ferreira, H.S. Ow, N.N. Nguyen, U.B. Wiesner, and R.S.

Langer, *Intracellular delivery of core-shell fluorescent silica nanoparticles.* Biomaterials, 2008. **29**(10): p. 1526-1532.
63. Santra, S., P. Zhang, K.M. Wang, R. Tapec, and W.H. Tan, *Conjugation of biomolecules with luminophore-doped silica nanoparticles for photostable biomarkers.* Analytical Chemistry, 2001. **73**(20): p. 4988-4993.
64. Du, W.J., Z.Q. Xu, A.M. Nystrom, K. Zhang, J.R. Leonard, and K.L. Wooley, *F-19- and Fluorescently Labeled Micelles as Nanoscopic Assemblies for Chemotherapeutic Delivery.* Bioconjugate Chemistry, 2008. **19**(12): p. 2492-2498.
65. El-Sayed, M.A., *Small Is Different: Shape-, Size-, and Composition-Dependent Properties of Some Colloidal Semiconductor Nanocrystals.* Accounts of Chemical Research, 2004. **37**(5): p. 326-333.
66. Waser, R.E. *Nanoelectronics and Information Technology*. 2005.
67. Ruhle, S., M. Shalom, and A. Zaban, *Quantum-Dot-Sensitized Solar Cells.* Chemphyschem, 2010. **11**(11): p. 2290-2304.
68. Osedach, T.P., N. Zhao, T.L. Andrew, P.R. Brown, D.D. Wanger, D.B. Strasfeld, L.Y. Chang, M.G. Bawendi, and V. Bulovic, *Bias-Stress Effect in 1,2-Ethanedithiol-Treated PbS Quantum Dot Field-Effect Transistors.* ACS Nano, 2012. **6**(4): p. 3121-3127.
69. Medintz, I.L., H. Mattoussi, and A.R. Clapp, *Potential clinical applications of quantum dots.* International Journal of Nanomedicine, 2008. **3**(2): p. 151-167.
70. Mulder, W.J.M., A.W. Griffioen, G.J. Strijkers, D.P. Cormode, K. Nicolay, and Z.A. Fayad, *Magnetic and fluorescent nanoparticles for multimodality imaging.* Nanomedicine, 2007. **2**(3): p. 307-324.
71. *The Penguin Dictionary of Physics*. 3rd ed. 2000, England: Penguin Group.
72. Park, J.H., D.H. Shin, C.O. Kim, S.H. Choi, and K.J. Kim, *Photovoltaic and luminescence properties of Sb- and P-doped Si quantum dots.* Journal of the Korean Physical Society, 2012. **60**(10): p. 1616-1619.
73. Xue, G., W. Chao, N. Lu, and X.G. Su, *Aqueous synthesis of Cu-doped ZnSe quantum dots.* Journal of Luminescence, 2011. **131**(7): p. 1300-1304.
74. Roy, S., C. Tuinenga, F. Fungura, P. Dagtepe, V. Chikan, and J. Jasinski, *Progress toward Producing n-Type CdSe Quantum Dots: Tin and Indium Doped CdSe Quantum Dots.* Journal of Physical Chemistry C, 2009. **113**(30): p. 13008-13015.
75. He, Y., Y.L. Zhong, F. Peng, X.P. Wei, Y.Y. Su, Y.M. Lu, S. Su, W. Gu, L.S. Liao, and S.T. Lee, *One-Pot Microwave Synthesis of Water-Dispersible, Ultraphoto- and pH-Stable, and Highly Fluorescent Silicon Quantum Dots.* Journal of the American Chemical Society, 2011. **133**(36): p. 14192-14195.
76. Heath, J.R., J.J. Shiang, and A.P. Alivisatos, *Germanium Quantum Dots - Optical-Properties and Synthesis.* Journal of Chemical Physics, 1994. **101**(2): p. 1607-1615.
77. Howes, P., M. Green, C. Johnston, and A. Crossley, *Synthesis and shape control of mercury selenide (HgSe) quantum dots.* Journal of Materials Chemistry, 2008. **18**(29): p. 3474-3480.
78. Glaser, E.R., B.R. Bennett, B.V. Shanabrook, and R. Magno, *Photoluminescence studies of self-assembled InSb, GaSb, and AlSb quantum dot heterostructures.* Applied Physics Letters, 1996. **68**(25): p. 3614-3616.
79. Liu, J., S.J. Gu, K.Y. Pan, B.L. Gu, H.J. Lai, H.L. Zhou, C.Q. He, and H.J. Zhang, *Synthesis and photoluminescence properties of high-quality CdSe quantum dot in liquid paraffin.* Micro & Nano Letters, 2011. **6**(11): p. 964-966.
80. Reiss, P., M. Protiere, and L. Li, *Core/Shell Semiconductor Nanocrystals.* Small, 2009. **5**(2): p. 154-168.
81. Taniguchi, S., M. Green, S.B. Rizvi, and A. Seifalian, *The one-pot synthesis of core/shell/shell CdTe/CdSe/ZnSe quantum dots in aqueous media for in vivo deep tissue imaging.* Journal of Materials Chemistry, 2011. **21**(9): p. 2877-2882.
82. Pelucchi, E., V. Dimastrodonato, L.O. Mereni, G. Juska, and A. Gocalinska, *Semiconductor nanostructures engineering: Pyramidal quantum dots.* Current Opinion in Solid State & Materials Science, 2012. **16**(2): p. 45-51.
83. Jun, Y.W., J.E. Koo, and J. Cheon, *One-step synthesis of size tuned zinc selenide quantum*

dots via a temperature controlled molecular precursor approach. Chemical Communications, 2000. **14**: p. 1243-1244.

84. Deng, D.W., W.H. Zhang, X.Y. Chen, F. Liu, J. Zhang, Y.Q. Gu, and J.M. Hong, *Facile Synthesis of High-Quality, Water-Soluble, Near-Infrared-Emitting PbS Quantum Dots.* European Journal of Inorganic Chemistry, 2009. **23**: p. 3440-3446.
85. Sykora, M., A.Y. Koposov, J.A. McGuire, R.K. Schulze, O. Tretiak, J.M. Pietryga, and V.I. Klimov, *Effect of Air Exposure on Surface Properties, Electronic Structure, and Carrier Relaxation in PbSe Nanocrystals.* ACS Nano, 2010. **4**(4): p. 2021-2034.
86. Brunetti, V., H. Chibli, R. Fiammengo, A. Galeone, M.A. Malvindi, G. Vecchio, R. Cingolani, J.L. Nadeau, and P.P. Pompa, *InP/ZnS as a safer alternative to CdSe/ZnS core/shell quantum dots: in vitro and in vivo toxicity assessment.* Nanoscale, 2013. **5**(1): p. 307-317.
87. Manner, V.W., A.Y. Koposov, P. Szymanski, V.I. Klimov, and M. Sykora, *Role of Solvent-Oxygen Ion Pairs in Photooxidation of CdSe Nanocrystal Quantum Dots.* ACS Nano, 2012. **6**(3): p. 2371-2377.
88. Veeranarayanan, S., A.C. Poulose, M.S. Mohamed, Y. Nagaoka, S. Iwai, Y. Nakagame, S. Kashiwada, Y. Yoshida, T. Maekawa, and D.S. Kumar, *Synthesis and application of luminescent single CdS quantum dot encapsulated silica nanoparticles directed for precision optical bioimaging.* International Journal of Nanomedicine, 2012. **7**: p. 3769-3786.
89. Rafailov, E.U., M.A. Cataluna, and W. Sibbett, *Mode-locked quantum-dot lasers.* Nat Photon, 2007. **1**(7): p. 395-401.
90. McWilliam, A., *Quantum-dot-based saturable absorber for femtosecond mode-locked operation of a solid-state laser.* Opt. Lett., 2006. **31**: p. 1444-1446.
91. Ray, S.K., *Broad-band superluminescent light-emitting diodes incorporating quantum dots in compositionally modulated quantum wells.* IEEE Photon. Technol. Lett., 2006. **18**: p. 58-60.
92. Rossetti, M., *High-power quantum-dot superluminescent diodes with p-doped active region.* IEEE Photon. Technol. Lett., 2006. **18**: p. 1946-1948.
93. van Tilborg, G.A.F., W.J.M. Mulder, P.T.K. Chin, G. Storm, C.P. Reutelingsperger, K. Nicolay, and G.J. Strijkers, *Annexin A5-conjugated quantum dots with a paramagnetic lipidic coating for the multimodal detection of apoptotic cells.* Bioconjugate Chemistry, 2006. **17**(4): p. 865-868.
94. Yong, K.T., H. Ding, I. Roy, W.C. Law, E.J. Bergey, A. Maitra, and P.N. Prasad, *Imaging Pancreatic Cancer Using Bioconjugated InP Quantum Dots.* ACS Nano, 2009. **3**(3): p. 502-510.
95. Jaiswal, J.K., H. Mattoussi, J.M. Mauro, and S.M. Simon, *Long-term multiple color imaging of live cells using quantum dot bioconjugates.* Nature Biotechnology, 2003. **21**(1): p. 47-51.
96. Jaiswal, J.K. and S.M. Simon, *Potentials and pitfalls of fluorescent quantum dots for biological imaging.* Trends in Cell Biology, 2004. **14**(9): p. 497-504.
97. Mulder, W.J.M., R. Koole, R.J. Brandwijk, G. Storm, P.T.K. Chin, G.J. Strijkers, C.D. Donega, K. Nicolay, and A.W. Griffioen, *Quantum dots with a paramagnetic coating as a bimodal molecular imaging probe.* Nano Letters, 2006. **6**(1): p. 1-6.
98. Chan, W.C.W. and S.M. Nie, *Quantum dot bioconjugates for ultrasensitive nonisotopic detection.* Science, 1998. **281**(5385): p. 2016-2018.
99. Michalet, X., F. Pinaud, T.D. Lacoste, M. Dahan, M.P. Bruchez, A.P. Alivisatos, and S. Weiss. *Properties of fluorescent semiconductor nanocrystals and their application to biological labeling*. in *Les Houches Spring School on Optical Spectroscopy and Microscopy of Single Objects*. 2001. Les Houches, France.
100. Wu, X.Y., H.J. Liu, J.Q. Liu, K.N. Haley, J.A. Treadway, J.P. Larson, N.F. Ge, F. Peale, and M.P. Bruchez, *Immunofluorescent labeling of cancer marker Her2 and other cellular targets with semiconductor quantum dots.* Nature Biotechnology, 2003. **21**(1): p. 41-46.
101. Zhang, Y., L. Mi, R.L. Xiong, P.N. Wang, J.Y. Chen, W.L. Yang, C.C. Wang, and Q. Peng, *Subcellular Localization of Thiol-Capped CdTe Quantum Dots in Living Cells.*

Nanoscale Research Letters, 2009. **4**(7): p. 606-612.
102. Zaman, M.B., T.N. Baral, J.B. Zhang, D. Whitfield, and K. Yu, *Single-Domain Antibody Functionalized CdSe/ZnS Quantum Dots for Cellular Imaging of Cancer Cells.* Journal of Physical Chemistry C, 2009. **113**(2): p. 496-499.
103. Cai, W.B., A.R. Hsu, Z.B. Li, and X.Y. Chen, *Are quantum dots ready for in vivo imaging in human subjects?* Nanoscale Research Letters, 2007. **2**(6): p. 265-281.
104. Bottrill, M. and M. Green, *Some aspects of quantum dot toxicity.* Chemical Communications, 2011. **47**(25): p. 7039-7050.
105. Rzigalinski, B.A. and J.S. Strobl, *Cadmium-containing nanoparticles: Perspectives on pharmacology and toxicology of quantum dots.* Toxicology and Applied Pharmacology, 2009. **238**(3): p. 280-288.
106. Pelley, J.L., A.S. Daar, and M.A. Saner, *State of Academic Knowledge on Toxicity and Biological Fate of Quantum Dots.* Toxicological Sciences, 2009. **112**(2): p. 276-296.
107. Slaveykova, V.I., K. Startchev, and J. Roberts, *Amine- and Carboxyl- Quantum Dots Affect Membrane Integrity of Bacterium Cupriavidus metallidurans CH34.* Environmental Science & Technology, 2009. **43**(13): p. 5117-5122.
108. Kirchner, C., T. Liedl, S. Kudera, T. Pellegrino, A.M. Javier, H.E. Gaub, S. Stolzle, N. Fertig, and W.J. Parak, *Cytotoxicity of colloidal CdSe and CdSe/ZnS nanoparticles.* Nano Letters, 2005. **5**(2): p. 331-338.
109. Vieira, C.S., D.B. Almeida, A.A. de Thomaz, R.F.S. Menna-Barreto, J.R. dos Santos-Mallet, C.L. Cesar, S.A.O. Gomes, and D. Feder, *Studying nanotoxic effects of CdTe quantum dots in Trypanosoma cruzi.* Memorias Do Instituto Oswaldo Cruz, 2011. **106**(2): p. 158-165.
110. Derfus, A.M., W.C.W. Chan, and S.N. Bhatia, *Probing the cytotoxicity of semiconductor quantum dots.* Nano Letters, 2004. **4**(1): p. 11-18.
111. Hoshino, A., K. Fujioka, T. Oku, M. Suga, Y.F. Sasaki, T. Ohta, M. Yasuhara, K. Suzuki, and K. Yamamoto, *Physicochemical properties and cellular toxicity of nanocrystal quantum dots depend on their surface modification.* Nano Letters, 2004. **4**(11): p. 2163-2169.
112. Liang, J.G., Z.K. He, S.S. Zhang, S. Huang, X.P. Ai, H.X. Yang, and H.Y. Han, *Study on DNA damage induced by CdSe quantum dots using nucleic acid molecular "light switches" as probe.* Talanta, 2007. **71**(4): p. 1675-1678.
113. Anas, A., H. Akita, H. Harashima, T. Itoh, M. Ishikawa, and V. Biju, *Photosensitized breakage and damage of DNA by CdSe-ZnS quantum dots.* Journal of Physical Chemistry B, 2008. **112**(32): p. 10005-10011.
114. Medina, C., M.J. Santos-Martinez, A. Radomski, O.I. Corrigan, and M.W. Radomski, *Nanoparticles: pharmacological and toxicological significance.* British Journal of Pharmacology, 2007. **150**(5): p. 552-558.
115. Hardman, R., *A toxicologic review of quantum dots: Toxicity depends on physicochemical and environmental factors.* Environmental Health Perspectives, 2006. **114**(2): p. 165-172.
116. Choi, H.S., W. Liu, P. Misra, E. Tanaka, J.P. Zimmer, B.I. Ipe, M.G. Bawendi, and J.V. Frangioni, *Renal clearance of quantum dots.* Nature Biotechnology, 2007. **25**(10): p. 1165-1170.
117. Hines, M.A. and P. Guyot-Sionnest, *Synthesis and characterization of strongly luminescing ZnS-Capped CdSe nanocrystals.* Journal of Physical Chemistry, 1996. **100**(2): p. 468-471.
118. Green, M., P. Howes, C. Berry, O. Argyros, and M. Thanou, *Simple conjugated polymer nanoparticles as biological labels.* Proceedings of the Royal Society a-Mathematical Physical and Engineering Sciences, 2009. **465**(2109): p. 2751-2759.
119. Holzapfel, V., M. Lorenz, C.K. Weiss, H. Schrezenmeier, K. Landfester, and V. Mailander, *Synthesis and biomedical applications of functionalized fluorescent and magnetic dual reporter nanoparticles as obtained in the miniemulsion process.* Journal of Physics-Condensed Matter, 2006. **18**(38): p. S2581-S2594.
120. van Schooneveld, M.M., D.P. Cormode, R. Koole, J.T. van Wijngaarden, C. Calcagno, T. Skajaa, J. Hilhorst, D.C. t Hart, Z.A. Fayad, W.J.M. Mulder, and A. Meijerink, *A*

fluorescent, paramagnetic and PEGylated gold/silica nanoparticle for MRI, CT and fluorescence imaging. Contrast Media & Molecular Imaging, 2010. **5**(4): p. 231-236.

121. Brandwijk, R., W.J.M. Mulder, K. Nicolay, K.H. Mayo, V. Thijssen, and A.W. Griffioen, *Anginex-conjugated liposomes for targeting of angiogenic endothelial cells.* Bioconjugate Chemistry, 2007. **18**(3): p. 785-790.
122. van Tilborg, G.A.F., W.J.M. Mulder, N. Deckers, G. Storm, C.P.M. Reutelingsperger, G.J. Strijkers, and K. Nicolay, *Annexin A5-functionalized bimodal lipid-based contrast agents for the detection of apoptosis.* Bioconjugate Chemistry, 2006. **17**(3): p. 741-749.
123. Pu, K.Y., K. Li, J.B. Shi, and B. Liu, *Fluorescent Single-Molecular Core-Shell Nanospheres of Hyperbranched Conjugated Polyelectrolyte for Live-Cell Imaging.* Chemistry of Materials, 2009. **21**(16): p. 3816-3822.
124. Raymond B. Seymour, *Seymour/Carraher's polymer chemistry*. 6th ed. rev. and expanded, ed. J. Charles E. Carraher. c2003, New York: Marcel Dekker Inc.
125. S. S. Dara , A.K.S., *Basics of Engineering Chemistry*. Revised ed. 2008, New Delhi: S. Chand & Company Ltd.
126. Johansson, N., *Thesis: (Conjugated Luminescent Molecular Materials: An Experimental and Theoretical Study of Electronic, Optical and Chemical Properties of some Conjugated Molecules, Polymers and Interfaces)*, in *Department of Physics and Measurement Technology*. 1998, Linkoping University, S-581 83 Linkoping: Sweden Linkoping.
127. Burroughes, J.H., D.D.C. Bradley, A.R. Brown, R.N. Marks, K. Mackay, R.H. Friend, P.L. Burns, and A.B. Holmes, *Light-Emitting-Diodes Based on Conjugated Polymers.* Nature, 1990. **347**(6293): p. 539-541.
128. Wandelt, B., P. Turkewitsch, S. Wysocki, and G.D. Darling, *Fluorescent molecularly imprinted polymer studied by time-resolved fluorescence spectroscopy.* Polymer, 2002. **43**(9): p. 2777-2785.
129. Chen, F., S.J. Zhang, W.B. Bu, X.H. Liu, Y. Chen, Q.J. He, M. Zhu, L.X. Zhang, L.P. Zhou, W.J. Peng, and J.L. Shi, *A "Neck-Formation" Strategy for an Antiquenching Magnetic/Upconversion Fluorescent Bimodal Cancer Probe.* Chemistry-a European Journal, 2010. **16**(37): p. 11254-11260.
130. Szymanski, C., C.F. Wu, J. Hooper, M.A. Salazar, A. Perdomo, A. Dukes, and J. McNeill, *Single molecule nanoparticles of the conjugated polymer MEH-PPV, preparation and characterization by near-field scanning optical microscopy.* Journal of Physical Chemistry B, 2005. **109**(18): p. 8543-8546.
131. Traiphol, R., P. Sanguansat, T. Srikhirin, T. Kerdcharoen, and T. Osotchan, *Spectroscopic study of photophysical change in collapsed coils of conjugated polymers: Effects of solvent and temperature.* Macromolecules, 2006. **39**(3): p. 1165-1172.
132. Lee, R.H. and L.W. Liu, *Electroluminescence and photovoltaic properties of light-emitting devices and solar cells comprising 2-pyran-4-ylidene-malononitrile conjugated polymers.* Dyes and Pigments, 2010. **84**(2): p. 190-202.
133. Braun, D. and A.J. Heeger, *Visible-Light Emission From Semiconductiong Polymer Diodes.* Applied Physics Letters, 1991. **58**(18): p. 1982-1984.
134. Schwartz, B.J., *Conjugated polymers as molecular materials : How chain conformation and film morphology influence energy transfer and interchain interactions.* Annual Review of Physical Chemistry, 2003. **54**: p. 141-172.
135. Howes, P., *Synthesis of Organic and Inorganic Semiconductor Nanoparticles*, in *School of Physical Sciences and Engineering - Department of Physics*. 2010, King's College London - University of London: London.
136. Moon, J.H., P. MacLean, W. McDaniel, and L.F. Hancock, *Conjugated polymer nanoparticles for biochemical protein kinase assay.* Chemical Communications, 2007(46): p. 4910-4912.
137. Wu, C.F., C. Szymanski, and J. McNeill, *Preparation and encapsulation of highly fluorescent conjugated polymer nanoparticles.* Langmuir, 2006. **22**(7): p. 2956-2960.
138. Grimland, J.L., C.F. Wu, R.R. Ramoutar, J.L. Brumaghim, and J. McNeill, *Photosensitizer-doped conjugated polymer nanoparticles with high cross-sections for one- and two-photon excitation.* Nanoscale, 2011. **3**(4): p. 1451-1455.

139. Landfester, K., R. Montenegro, U. Scherf, R. Guntner, U. Asawapirom, S. Patil, D. Neher, and T. Kietzke, *Semiconducting polymer nanospheres in aqueous dispersion prepared by a miniemulsion process.* Advanced Materials, 2002. **14**(9): p. 651-655.
140. Moon, J.H., R. Deans, E. Krueger, and L.F. Hancock, *Capture and detection of a quencher labeled oligonucleotide by poly(phenylene ethynylene) particles.* Chemical Communications, 2003(1): p. 104-105.
141. Ko, Y.J., E. Mendez, and J.H. Moon, *Controlled Aggregation in Conjugated Polymer Nanoparticles via Organic Acid Treatments.* Macromolecules, 2011. **44**(13): p. 5527-5530.
142. Chen, Z. and X. Li, *Water-Soluble Fluorescent Particle Comprising Entangled Fluorescent Polymer and Amphiphilic Molecule.* Patent Number: WO 2007/027159, 2007.
143. Wu, C.F., C. Szymanski, Z. Cain, and J. McNeill, *Conjugated polymer dots for multiphoton fluorescence imaging.* Journal of the American Chemical Society, 2007. **129**(43): p. 12904-+.
144. Wu, C.F., T. Schneider, M. Zeigler, J.B. Yu, P.G. Schiro, D.R. Burnham, J.D. McNeill, and D.T. Chiu, *Bioconjugation of Ultrabright Semiconducting Polymer Dots for Specific Cellular Targeting.* Journal of the American Chemical Society, 2010. **132**(43): p. 15410-15417.
145. Wu, C.F., S.J. Hansen, Q.O. Hou, J.B. Yu, M. Zeigler, Y.H. Jin, D.R. Burnham, J.D. McNeill, J.M. Olson, and D.T. Chiu, *Design of Highly Emissive Polymer Dot Bioconjugates for In Vivo Tumor Targeting.* Angewandte Chemie-International Edition, 2011. **50**(15): p. 3430-3434.
146. Zhang, K., Z. Gui, D. Chen, and M. Jiang, *Synthesis of small polymeric nanoparticles sized below 10 nm via polymerization of a cross-linker in a glassy polymer matrix.* Chem Commun (Camb), 2009(41): p. 6234-6.
147. Taylor, J.R., C.D. Zafiratos, and M.A. Dubson, *Modern Physics for Scientists and Engineers*. 2nd ed. 2004, New Jersy: Prentice Hall, Inc. Pearson Education.
148. Wade, L.G., *Conjugated Systems, Orbital Symmetry, and Ultraviolet Spectroscopy*, in *Organic Chemistry*. 1999, Prentice-Hall, Inc.: New Jersey. p. 647 - 689.
149. G. Solomons, C.F., *Organic Chemistry*. Seventh ed. 2000, New York: John Wiley & Sons, Inc.
150. Petty, M.C., *Molecular Electronics: From Principles to Practice*. 2007, John Wiley & Sons, Ltd.: West Sussex. p. 96 - 106.
151. Scheblykin, I.G., A. Yartsev, T. Pullerits, V. Gulbinas, and V. Sundstrom, *Excited state and charge photogeneration dynamics in conjugated polymers.* Journal of Physical Chemistry B, 2007. **111**(23): p. 6303-6321.
152. Barbara, P.F., A.J. Gesquiere, S.J. Park, and Y.J. Lee, *Single-molecule spectroscopy of conjugated polymers.* Accounts of Chemical Research, 2005. **38**(7): p. 602-610.
153. Friend, R.H., R.W. Gymer, A.B. Holmes, J.H. Burroughes, R.N. Marks, C. Taliani, D.D.C. Bradley, D.A. Dos Santos, J.L. Bredas, M. Logdlund, and W.R. Salaneck, *Electroluminescence in conjugated polymers.* Nature, 1999. **397**(6715): p. 121-128.
154. *Luminescence in Chemistry*, ed. E.J. Bowen. 1968, London: D. Van Nostrand Company, Ltd.
155. Grey, J.K., D.Y. Kim, B.C. Norris, W.L. Miller, and P.F. Barbara, *Size-dependent spectroscopic properties of conjugated polymer nanoparticles.* Journal of Physical Chemistry B, 2006. **110**(51): p. 25568-25572.
156. Piok, T., C. Gadermaier, F.P. Wenzl, S. Patil, R. Montenegro, K. Landfester, G. Lanzani, G. Cerullo, U. Scherf, and E.J.W. List, *The photophysics of organic semiconducting nanospheres: a comprehensive study.* Chemical Physics Letters, 2004. **389**(1-3): p. 7-13.
157. Li, H.W. and W.T.S. Huck, *Polymers in nanotechnology.* Current Opinion in Solid State & Materials Science, 2002. **6**(1): p. 3-8.
158. Kreuter, J. and E. Liehl, *Long-Term Studies of Microencapsulated and Adsorbed Influenza Vaccine Nanoparticles.* Journal of Pharmaceutical Sciences, 1981. **70**(4): p. 367-371.
159. Ryan, A.J., *Nanotechnology Squaring up with polymers.* Nature, 2008. **456**(7220): p. 334-336.
160. Kim, D., Z.G. Gao, E.S. Lee, and Y.H. Bae. *In Vivo Evaluation of Doxorubicin-Loaded*

Polymeric Micelles Targeting Folate Receptors and Early Endosomal pH in Drug-Resistant Ovarian Cancer. in *NanoMedicine Summit on Nanoparticles for Imaging, Diagnosis, and Therapeutics*. 2008. Cleveland, OH.

161. Guari, Y., J. Larionova, M. Corti, A. Lascialfari, M. Marinone, G. Poletti, K. Molvinger, and C. Guerin, *Cyano-bridged coordination polymer nanoparticles with high nuclear relaxivity: toward new contrast agents for MRI.* Dalton Transactions, 2008(28): p. 3658-3660.
162. Venugopal, J., M.P. Prabhakaran, S. Low, A.T. Choon, G. Deepika, V.R.G. Dev, and S. Ramakrishna, *Continuous Nanostructures for the Controlled Release of Drugs.* Current Pharmaceutical Design, 2009. **15**(15): p. 1799-1808.
163. Jagur-Grodzinski, J., *Polymers for targeted and/or sustained drug delivery.* Polymers for Advanced Technologies, 2009. **20**(7): p. 595-606.
164. Dimonie, D., C. Radovici, R.M. Coserea, S. Garea, and M. Teodorescu, *The Polymer Molecular Weight and Silicate Treatment Influence Upon the Morphology of Nanocomposites for Food Packaging.* Revue Roumaine De Chimie, 2008. **53**(11): p. 1017.
165. Kim, H.C., S.M. Park, and W.D. Hinsberg, *Block Copolymer Based Nanostructures: Materials, Processes, and Applications to Electronics.* Chemical Reviews, 2010. **110**(1): p. 146-177.
166. Gunes, S., H. Neugebauer, and N.S. Sariciftci, *Conjugated polymer-based organic solar cells.* Chemical Reviews, 2007. **107**(4): p. 1324-1338.
167. Piok, T., S. Gamerith, C. Gadermaier, H. Plank, F.P. Wenzl, S. Patil, R. Montenegro, T. Kietzke, D. Neher, U. Scherf, K. Landfester, and E.J.W. List, *Organic light-emitting devices fabricated from semiconducting nanospheres.* Advanced Materials, 2003. **15**(10): p. 800.
168. Kuroda, K. and T.M. Swager, *Synthesis of a nonionic water soluble semiconductive polymer.* Chemical Communications, 2003(1): p. 26-27.
169. Guimard, N.K., N. Gomez, and C.E. Schmidt, *Conducting polymers in biomedical engineering.* Progress in Polymer Science, 2007. **32**(8-9): p. 876-921.
170. Peng, H., L.J. Zhang, C. Soeller, and J. Travas-Sejdic, *Conducting polymers for electrochemical DNA sensing.* Biomaterials, 2009. **30**(11): p. 2132-2148.
171. Foulds, N.C. and C.R. Lowe, *Enzyme Entrapment in Electrically Conducting polymers - Immobilization of Glucose-Oxidase in Polypyrrole and its Application in Amperometric Glucose Sensors.* Journal of the Chemical Society-Faraday Transactions I, 1986. **82**: p. 1259-1264.
172. Wong, J.Y., R. Langer, and D.E. Ingber, *Electrically Conducting Polymers can Noninvasively Control the Shape and Growth of Mammalian-cells.* Proceedings of the National Academy of Sciences of the United States of America, 1994. **91**(8): p. 3201-3204.
173. Heeger, P.S. and A.J. Heeger, *Making sense of polymer-based biosensors.* Proceedings of the National Academy of Sciences of the United States of America, 1999. **96**(22): p. 12219-12221.
174. Thomas, S.W., S. Yagi, and T.M. Swager, *Towards chemosensing phosphorescent conjugated polymers: cyclometalated platinum(II) poly(phenylene)s.* Journal of Materials Chemistry, 2005. **15**(27-28): p. 2829-2835.
175. Disney, M.D., J. Zheng, T.M. Swager, and P.H. Seeberger, *Detection of bacteria with carbohydrate-functionalized fluorescent polymers.* Journal of the American Chemical Society, 2004. **126**(41): p. 13343-13346.
176. Gaylord, B.S., A.J. Heeger, and G.C. Bazan, *DNA detection using water-soluble conjugated polymers and peptide nucleic acid probes.* Proceedings of the National Academy of Sciences of the United States of America, 2002. **99**(17): p. 10954-10957.
177. Liu, B. and G.C. Bazan, *Interpolyelectrolyte complexes of conjugated copolymers and DNA: Platforms for multicolor biosensors.* Journal of the American Chemical Society, 2004. **126**(7): p. 1942-1943.
178. Peng, H., C. Soeller, and J. Travas-Sejdic, *A novel cationic conjugated polymer for homogeneous fluorescence-based DNA detection.* Chemical Communications, 2006(35): p. 3735-3737.

179. Tian, Z.Y., J.B. Yu, C.F. Wu, C. Szymanski, and J. McNeill, *Amplified energy transfer in conjugated polymer nanoparticle tags and sensors.* Nanoscale, 2010. **2**(10): p. 1999-2011.
180. Wu, C.F., B. Bull, K. Christensen, and J. McNeill, *Ratiometric Single-Nanoparticle Oxygen Sensors for Biological Imaging.* Angewandte Chemie-International Edition, 2009. **48**(15): p. 2741-2745.
181. Yu, J.B., C.F. Wu, S.P. Sahu, L.P. Fernando, C. Szymanski, and J. McNeill, *Nanoscale 3D Tracking with Conjugated Polymer Nanoparticles.* Journal of the American Chemical Society, 2009. **131**(51): p. 18410-18414.
182. Howes, P., M. Green, A. Bowers, D. Parker, G. Varma, M. Kallumadil, M. Hughes, A. Warley, A. Brain, and R. Botnar, *Magnetic Conjugated Polymer Nanoparticles as Bimodal Imaging Agents.* Journal of the American Chemical Society, 2010. **132**(28): p. 9833-9842.
183. Dönüs Tuncel, D. and H. Demir, *Conjugated Polymer Nanoparticles.* Nanoscale, 2010. **2**: p. 484 - 494.
184. Vauthier, C. and K. Bouchemal, *Methods for the Preparation and Manufacture of Polymeric Nanoparticles.* Pharmaceutical Research, 2009. **26**(5): p. 1025-1058.
185. Baier, M.C., J. Huber, and S. Mecking, *Fluorescent Conjugated Polymer Nanoparticles by Polymerization in Miniemulsion.* Journal of the American Chemical Society, 2009. **131**(40): p. 14267-14273.
186. Tomalia, D.A., *Birth of a new macromolecular architecture: dendrimers as quantized building blocks for nanoscale synthetic polymer chemistry.* Progress in Polymer Science, 2005. **30**(3-4): p. 294-324.
187. Quintanar-Guerrero, D., E. Allemann, H. Fessi, and E. Doelker, *Preparation techniques and mechanisms of formation of biodegradable nanoparticles from preformed polymers.* Drug Development and Industrial Pharmacy, 1998. **24**(12): p. 1113-1128.
188. Mecerreyes, D., V. Lee, C.J. Hawker, J.L. Hedrick, A. Wursch, W. Volksen, T. Magbitang, E. Huang, and R.D. Miller, *A novel approach to functionalized nanoparticles: Self-crosslinking of macromolecules in ultradilute solution.* Advanced Materials, 2001. **13**(3): p. 204-208.
189. Rosety, M., F.J. Ordonez, M. Rosety-Rodriguez, J.M. Rosety, I. Rosety, C. Carrasco, and A. Ribelles, *Acute toxicity of anionic surfactants sodium dodecyl sulphate (SDS) and linear alkylbenzene sulphonate (LAS) on the fertilizing capability of gilthead (Sparus aurata L.) sperm.* Histology and Histopathology, 2001. **16**(3): p. 839-843.
190. Chen, J., D.P. Wang, A. Turshatov, R. Munoz-Espi, U. Ziener, K. Koynov, and K. Landfester, *One-pot fabrication of amphiphilic photoswitchable thiophene-based fluorescent polymer dots.* Polymer Chemistry, 2013. **4**(3): p. 773-781.
191. Wu, C.F., C. Szymanski, Z. Cain, and J. McNeill, *Conjugated polymer dots for multiphoton fluorescence imaging.* Journal of the American Chemical Society, 2007. **129**(43): p. 12904.
192. Howes, P., R. Thorogate, M. Green, S. Jickells, and B. Daniel, *Synthesis, characterisation and intracellular imaging of PEG capped BEHP-PPV nanospheres.* Chemical Communications, 2009(18): p. 2490-2492.
193. Yu, J.B., C.F. Wu, Z.Y. Tian, and J. McNeill, *Tracking of Single Charge Carriers in a Conjugated Polymer Nanoparticle.* Nano Letters, 2012. **12**(3): p. 1300-1306.
194. Howes, P., M. Green, J. Levitt, K. Suhling, and M. Hughes, *Phospholipid encapsulated semiconducting polymer nanoparticles: their use in cell imaging and protein attachment.* J Am Chem Soc, 2010. **132**(11): p. 3989-96.
195. Vuu, K., J.W. Xie, M.A. McDonald, M. Bernardo, F. Hunter, Y.T. Zhang, K. Li, M. Bednarski, and S. Guccione, *Gadolinium-rhodamine nanoparticles for cell labeling and tracking via magnetic resonance and optical imaging.* Bioconjugate Chemistry, 2005. **16**(4): p. 995-999.
196. Rahim, N.A.A., W. McDaniel, K. Bardon, S. Srinivasan, V. Vickerman, P.T.C. So, and J.H. Moon, *Conjugated Polymer Nanoparticles for Two-Photon Imaging of Endothelial Cells in a Tissue Model.* Advanced Materials, 2009. **21**(34): p. 3492.
197. Sarkar, P., S. Sridharan, R. Luchowski, S. Desai, B. Dworecki, M. Nlend, Z. Gryczynski, and I. Gryczynski, *Photophysical properties of a new DyLight 594 dye.* Journal of

Photochemistry and Photobiology B-Biology, 2010. **98**(1): p. 35-39.
198. Landfester, K., *Synthesis of colloidal particles in miniemulsions.* Annual Review of Materials Research, 2006. **36**: p. 231-279.
199. Tadros, T.F., *Emulsion Science and Technology*. 2009, Weinheim: Wiley-VCH.
200. Qiu, G.H., Q. Wang, C. Wang, W. Lau, and Y.L. Guo, *Polystyrene/Fe(3)O(4)magnetic emulsion and nanocomposite prepared by ultrasonically initiated miniemulsion polymerization.* Ultrasonics Sonochemistry, 2007. **14**(1): p. 55-61.
201. Landfester, K. and L.P. Ramirez, *Encapsulated magnetite particles for biomedical application.* Journal of Physics-Condensed Matter, 2003. **15**(15): p. S1345-S1361.
202. Bechthold, N., F. Tiarks, M. Willert, K. Landfester, and M. Antonietti, *Miniemulsion polymerization: Applications and new materials.* Macromolecular Symposia, 2000. **151**: p. 549-555.
203. Siegwart, D.J., A. Srinivasan, S.A. Bencherif, A. Karunanidhi, J.K. Oh, S. Vaidya, R. Jin, J.O. Hollinger, and K. Matyjaszewki, *Cellular Uptake of Functional Nanogels Prepared by Inverse Miniemulsion ATRP with Encapsulated Proteins, Carbohydrates, and Gold Nanoparticles.* Biomacromolecules, 2009. **10**(8): p. 2300-2309.
204. Chen, J., F. Zeng, S.Z. Wu, J. Su, and Z. Tong, *Photoreversible Fluorescent Modulation of Nanoparticles via One-Step Miniemulsion Polymerization.* Small, 2009. **5**(8): p. 970-978.
205. Barrere, M. and K. Landfester, *High molecular weight polyurethane and polymer hybrid particles in aqueous miniemulsion.* Macromolecules, 2003. **36**(14): p. 5119-5125.
206. Landfester, K., *The generation of nanoparticles in miniemulsions.* Advanced Materials, 2001. **13**(10): p. 765-768.
207. Zhang, Y., S.Y. Zhu, L.C. Yin, F. Qian, C. Tang, and C.H. Yin, *Preparation, characterization and biocompatibility of poly(ethylene glycol)-poly(n-butyl cyanoacrylate) nanocapsules with oil core via miniemulsion polymerization.* European Polymer Journal, 2008. **44**(6): p. 1654-1661.
208. Kietzke, T., D. Neher, K. Landfester, R. Montenegro, R. Guntner, and U. Scherf, *Novel approaches to polymer blends based on polymer nanoparticles.* Nature Materials, 2003. **2**(6): p. 408-U7.
209. Veronese, F.M., A. Mero, and G. Pasut, *Protein PEGylation, basic science and biological applications*. PEGylated Protein Drugs: Basic Science and Clinical Applications, ed. F.M. Veronese. 2009: Birkhauser Verlag Ag. 11-31.
210. Zheng, M., F. Davidson, and X.Y. Huang, *Ethylene glycol monolayer protected nanoparticles for eliminating nonspecific binding with biological molecules.* Journal of the American Chemical Society, 2003. **125**(26): p. 7790-7791.
211. Landfester, K., N. Bechthold, F. Tiarks, and M. Antonietti, *Formulation and stability mechanisms of polymerizable miniemulsions.* Macromolecules, 1999. **32**(16): p. 5222-5228.
212. van Zyl, A.J.P., D. de Wet-Roos, R.D. Sanderson, and B. Klumperman, *The role of surfactant in controlling particle size and stability in the miniemulsion polymerization of polymeric nanocapsules.* European Polymer Journal, 2004. **40**(12): p. 2717-2725.
213. Wu, M., E. Dellacherie, A. Durand, and E. Marie, *Poly(n-butyl cyanoacrylate) nanoparticles via miniemulsion polymerization. 2. PEG-based surfactants.* Colloids and Surfaces B-Biointerfaces, 2009. **69**(1): p. 147-151.
214. Traiphol, R., N. Charoenthai, T. Srikhirin, T. Kerdeharoen, T. Osotchan, and T. Maturos, *Chain organization and photophysics of conjugated polymer in poor solvents: Aggregates, agglomerates and collapsed coils.* Polymer, 2007. **48**(3): p. 813-826.
215. Nguyen, T.Q., V. Doan, and B.J. Schwartz, *Conjugated polymer aggregates in solution: Control of interchain interactions.* Journal of Chemical Physics, 1999. **110**(8): p. 4068-4078.
216. Nguyen, T.Q., R.Y. Yee, and B.J. Schwartz, *Solution processing of conjugated polymers: the effects of polymer solubility on the morphology and electronic properties of semiconducting polymer films.* Journal of Photochemistry and Photobiology a-Chemistry, 2001. **144**(1): p. 21-30.
217. Nguyen, T.Q., I.B. Martini, J. Liu, and B.J. Schwartz, *Controlling interchain interactions*

in conjugated polymers: The effects of chain morphology on exciton-exciton annihilation and aggregation in MEH-PPV films. Journal of Physical Chemistry B, 2000. **104**(2): p. 237-255.

218. Traiphol, R., N. Charoenthai, P. Manorat, T. Pattanatornchai, T. Srikhirin, T. Kerdcharoen, and T. Osotchan, *Photophysical change of poly(9,9-di(2-ethylhexyl)fluorene) and its copolymer with anthracene in solvent-non-solvent: Roles of interchain interactions on the formation of non-emissive and emissive aggregates.* Synthetic Metals, 2009. **159**(12): p. 1224-1233.
219. Johansson, D.M., M. Theander, G. Srdanov, G. Yu, O. Inganas, and M.R. Andersson, *Influence of polymerization temperature on molecular weight, photoluminescence, and electroluminescence for a phenyl-substituted poly(p-phenylenevinylene).* Macromolecules, 2001. **34**(11): p. 3716-3719.
220. Striolo, A., J. Ward, J.M. Prausnitz, W.J. Parak, D. Zanchet, D. Gerion, D. Milliron, and A.P. Alivisatos, *Molecular weight, osmotic second virial coefficient, and extinction coefficient of colloidal CdSe nanocrystals.* Journal of Physical Chemistry B, 2002. **106**(21): p. 5500-5505.
221. Janczewski, D., Y. Zhang, G.K. Das, D.K. Yi, P. Padmanabhan, K.K. Bhakoo, T.T.Y. Tan, and S.T. Selvan, *Bimodal Magnetic-Fluorescent Probes for Bioimaging.* Microscopy Research and Technique, 2011. **74**(7): p. 563-576.
222. Jennings, L.E. and N.J. Long, *'Two is better than one'-probes for dual-modality molecular imaging.* Chemical Communications, 2009(24): p. 3511-3524.
223. Koole, R., W.J.M. Mulder, M.M. van Schooneveld, G.J. Strijkers, A. Meijerink, and K. Nicolay, *Magnetic quantum dots for multimodal imaging.* Wiley Interdisciplinary Reviews-Nanomedicine and Nanobiotechnology, 2009. **1**(5): p. 475-491.
224. Suhling, K., P.M.W. French, and D. Phillips, *Time-resolved fluorescence microscopy.* Photochemical & Photobiological Sciences, 2005. **4**(1): p. 13-22.
225. Levitt, J.A., D.R. Matthews, S.M. Ameer-Beg, and K. Suhling, *Fluorescence lifetime and polarization-resolved imaging in cell biology.* Current Opinion in Biotechnology, 2009. **20**(1): p. 28-36.
226. Weishaupt, D., V.D. Kochli, and B. Marincek, *How Does MRI Work? An Introduction to the Physics and Function of Magnetic Resonance Imaging*. Corrected 2nd ed. 2008: Springer-Verlag Berlin Heidelberg.
227. Kim, H.K., G.H. Lee, T.J. Kim, and Y.M. Chang, *Determination of Correlation Times of New Paramagnetic Gadolinium MR Contrast Agents by EPR and O-17 NMR.* Bulletin of the Korean Chemical Society, 2009. **30**(4): p. 849-852.
228. Weinmann, H.J., R.C. Brasch, W.R. Press, and G.E. Wesbey, *Characteristics of Gadolinium-DTPA Complex - A Potential NMR Contrast Agent.* American Journal of Roentgenology, 1984. **142**(3): p. 619-624.
229. Carr, D.H., J. Brown, G.M. Bydder, R.E. Steiner, H.J. Weinmann, U. Speck, A.S. Hall, and I.R. Young, *Gadolinium-DTPA as a Contrast Agent in MRI - Initial Clinical-Experience in 20 Patients.* American Journal of Roentgenology, 1984. **143**(2): p. 215-224.
230. Strijkers, G.J., W.J.M. Mulder, G.A.F. van Tilborg, and K. Nicolay, *MRI contrast agents: Current status and future perspectives.* Anti-Cancer Agents in Medicinal Chemistry, 2007. **7**(3): p. 291-305.
231. Kamaly, N. and A.D. Miller, *Paramagnetic Liposome Nanoparticles for Cellular and Tumour Imaging.* International Journal of Molecular Sciences, 2010. **11**(4): p. 1759-1776.
232. Kamaly, N., T. Kalber, A. Ahmad, M.H. Oliver, P.W. So, A.H. Herlihy, J.D. Bell, M.R. Jorgensen, and A.D. Miller, *Bimodal paramagnetic and fluorescent liposomes for cellular and tumor magnetic resonance imaging.* Bioconjugate Chemistry, 2008. **19**(1): p. 118-129.
233. Bitounis, D., R. Fanciullino, A. Iliadis, and J. Ciccolini, *Optimizing Druggability through Liposomal Formulations: New Approaches to an Old Concept.* ISRN Pharmaceutics, 2012. **2012**.
234. Torchilin, V.P., *Recent advances with liposomes as pharmaceutical carriers.* Nature Reviews Drug Discovery, 2005. **4**(2): p. 145-160.
235. Kabalka, G.W., E. Buonocore, K. Hubner, M. Davis, and L. Huang, *Gadolinium-Labeled*

Liposomes Containing Paramagnetic Amphipathic Agents - Targeted MRI Contrast Agents for the Liver. Magnetic Resonance in Medicine, 1988. **8**(1): p. 89-95.

236. Kabalka, G.W., M.A. Davis, E. Holmberg, K. Maruyama, and L. Huang, *Gadolinium-Labeled Liposomes Containing Amphiphilic Gd-DTPA Derivatives of Varying Chain-Length - Targeted MRI Contrast Enhancement Agents for the Liver.* Magnetic Resonance Imaging, 1991. **9**(3): p. 373-377.
237. Murray, A.R., E. Kisin, S.S. Leonard, S.H. Young, C. Kommineni, V.E. Kagan, V. Castranova, and A.A. Shvedova, *Oxidative stress and inflammatory response in dermal toxicity of single-walled carbon nanotubes.* Toxicology, 2009. **257**(3): p. 161-171.
238. Wang, F., X.L. Chen, Z.X. Zhao, S.H. Tang, X.Q. Huang, C.H. Lin, C.B. Cai, and N.F. Zheng, *Synthesis of magnetic, fluorescent and mesoporous core-shell-structured nanoparticles for imaging, targeting and photodynamic therapy.* Journal of Materials Chemistry, 2011. **21**(30): p. 11244-11252.
239. van Tilborg, G.A.F., E. Vucic, G.J. Strijkers, D.P. Cormode, V. Mani, T. Skajaa, C.P.M. Reutelingsperger, Z.A. Fayad, W.J.M. Mulder, and K. Nicolay, *Annexin A5-Functionalized Bimodal Nanoparticles for MRI and Fluorescence Imaging of Atherosclerotic Plaques.* Bioconjugate Chemistry, 2010. **21**(10): p. 1794-1803.
240. Liu, G., H.X. Wu, H.R. Zheng, L.H. Tang, H. Hu, H. Yang, and S.P. Yang, *Synthesis and applications of fluorescent-magnetic-bifunctional dansylated Fe(3)O(4)@SiO(2) nanoparticles.* Journal of Materials Science, 2011. **46**(18): p. 5959-5968.
241. Liu, Y.L., K.L. Ai, Q.H. Yuan, and L.H. Lu, *Fluorescence-enhanced gadolinium-doped zinc oxide quantum dots for magnetic resonance and fluorescence imaging.* Biomaterials, 2011. **32**(4): p. 1185-1192.
242. Wang, K., J. Ruan, Q.R. Qian, H. Song, C.C. Bao, X.Q. Zhang, Y.F. Kong, C.L. Zhang, G.H. Hu, J. Ni, and D.X. Cui, *BRCAA1 monoclonal antibody conjugated fluorescent magnetic nanoparticles for in vivo targeted magnetofluorescent imaging of gastric cancer.* Journal of Nanobiotechnology, 2011. **9**.
243. Corr, S.A., Y.P. Rakovich, and Y.K. Gun'ko, *Multifunctional magnetic-fluorescent nanocomposites for biomedical applications.* Nanoscale Research Letters, 2008. **3**(3): p. 87-104.
244. Hashim, Z., P. Howes, and M. Green, *Luminescent quantum-dot-sized conjugated polymer nanoparticles-nanoparticle formation in a miniemulsion system.* Journal of Materials Chemistry, 2011. **21**(6): p. 1797-1803.
245. Vaidya, A., Y.G. Sun, Y. Feng, L. Emerson, E.K. Jeong, and Z.R. Lu, *Contrast-Enhanced MRI-Guided Photodynamic Cancer Therapy with a Pegylated Bifunctional Polymer Conjugate.* Pharmaceutical Research, 2008. **25**(9): p. 2002-2011.
246. Xu, Q., L. Liu, L. Zhu, M. Yu, Q. Yang, and S. Wang, *A conjugated polymer-Gd (III) complex as pH sensitive contrast agent in magnetic resonance imaging.* Frontiers of Chemistry in China, 2010. **5**(2): p. 166-170.
247. Mulder, W.J.M., G.J. Strijkers, A.W. Griffioen, L. van Bloois, G. Molema, G. Storm, G.A. Koning, and K. Nicolay, *A liposomal system for contrast-enhanced magnetic resonance imaging of molecular targets.* Bioconjugate Chemistry, 2004. **15**(4): p. 799-806.
248. Mulder, W.J.M., G.J. Strijkers, J.W. Habets, E.J.W. Bleeker, D.W.J. van der Schaft, G. Storm, G.A. Koning, A.W. Griffioen, and K. Nicolay, *MR molecular imaging and fluorescence microscopy for identification of activated tumor endothelium using a bimodal lipidic nanoparticle.* Faseb Journal, 2005. **19**(12): p. 2008.
249. Mulder, W.J.M., G.J. Strijkers, G.A.F. van Tilborg, A.W. Griffioen, and K. Nicolay, *Lipid-based nanoparticles for contrast-enhanced MRI and molecular imaging.* Nmr in Biomedicine, 2006. **19**(1): p. 142-164.
250. Valencia, P.M., P.A. Basto, L.F. Zhang, M. Rhee, R. Langer, O.C. Farokhzad, and R. Karnik, *Single-Step Assembly of Homogenous Lipid - Polymeric and Lipid - Quantum Dot Nanoparticles Enabled by Microfluidic Rapid Mixing.* Acs Nano, 2010. **4**(3): p. 1671-1679.
251. Liu, Y.T., J. Pan, and S.S. Feng, *Nanoparticles of lipid monolayer shell and biodegradable polymer core for controlled release of paclitaxel: Effects of surfactants on particles size, characteristics and in vitro performance.* International Journal of Pharmaceutics, 2010.

395(1-2): p. 243-250.
252. Kumari, S., M.G. Swetha, and S. Mayor, *Endocytosis unplugged: multiple ways to enter the cell.* Cell Research, 2010. **20**(3): p. 256-275.
253. Aderem, A. and D.M. Underhill, *Mechanisms of phagocytosis in macrophages.* Annual Review of Immunology, 1999. **17**: p. 593-623.
254. Khanbeigi, R.A., A. Kumar, F. Sadouki, C. Lorenz, B. Forbes, L.A. Dailey, and H. Collins, *The delivered dose: Applying particokinetics to in vitro investigations of nanoparticle internalization by macrophages.* Journal of Controlled Release, 2012. **162**(2): p. 259-266.
255. Dailey, L.A., E. Kleemann, T. Merdan, H. Petersen, T. Schmehl, T. Gessler, J. Hanze, W. Seeger, and T. Kissel, *Modified polyethylenimines as non viral gene delivery systems for aerosol therapy: effects of nebulization on cellular uptake and transfection efficiency.* Journal of Controlled Release, 2004. **100**(3): p. 425-436.
256. Chang, E., W.W. Yu, V.L. Colvin, and R. Drezek, *Quantifying the Influence of Surface Coatings on Quantum Dot Uptake in Cells.* Journal of Biomedical Nanotechnology, 2005. **1**(4): p. 397-401.
257. Bentzen, E.L., I.D. Tomlinson, J. Mason, P. Gresch, M.R. Warnement, D. Wright, E. Sanders-Bush, R. Blakely, and S.J. Rosenthal, *Surface modification to reduce nonspecific binding of quantum dots in live cell assays.* Bioconjugate Chemistry, 2005. **16**(6): p. 1488-1494.
258. Berezin, M.Y. and S. Achilefu, *Fluorescence Lifetime Measurements and Biological Imaging.* Chemical Reviews, 2010. **110**(5): p. 2641-2684.
259. Zhang, H.R., X.F. Lu, Y. Li, X.C. Ai, X.K. Zhang, and G.Q. Yang, *Conformational transition of poly 2-methoxy-5-(2 '-ethylhexoxy)-p-phenylene vinylene in solutions: solvent-induced emitter change.* Journal of Photochemistry and Photobiology a-Chemistry, 2002. **147**(1): p. 15-23.
260. Fiserova, E. and M. Kubala, *Mean fluorescence lifetime and its error.* Journal of Luminescence, 2012. **132**(8): p. 2059-2064.
261. Bain, B.J. and R. Gupta, *A - Z of Haematology*. 2003, Oxford: Blackwell Publishing Ltd.
262. Fadeel, B. and A.E. Garcia-Bennett, *Better safe than sorry: Understanding the toxicological properties of inorganic nanoparticles manufactured for biomedical applications.* Advanced Drug Delivery Reviews, 2010. **62**(3): p. 362-374.
263. Marquis, B.J., S.A. Love, K.L. Braun, and C.L. Haynes, *Analytical methods to assess nanoparticle toxicity.* Analyst, 2009. **134**(3): p. 425-439.
264. Seaton, A., L. Tran, R. Aitken, and K. Donaldson, *Nanoparticles, human health hazard and regulation.* Journal of the Royal Society Interface, 2010. **7**: p. S119-S129.
265. Lewinski, N., V. Colvin, and R. Drezek, *Cytotoxicity of nanoparticles.* Small, 2008. **4**(1): p. 26-49.
266. Li, J.J., S. Muralikrishnan, C.T. Ng, L.Y.L. Yung, and B.H. Bay, *Nanoparticle-induced pulmonary toxicity.* Experimental Biology and Medicine, 2010. **235**(9): p. 1025-1033.
267. Hillegass, J.M., A. Shukla, S.A. Lathrop, M.B. MacPherson, N.K. Fukagawa, and B.T. Mossman, *Assessing nanotoxicity in cells in vitro.* Wiley Interdisciplinary Reviews-Nanomedicine and Nanobiotechnology, 2010. **2**(3): p. 219-231.
268. *The Project on Emerging Nanotechnologies*. 2013 [cited 2013 28 March 2013]; Available from: http://www.nanotechproject.org/.
269. *FresherLonger™ Plastic Storage Bags*. 15 June 2009 [cited 2013 28 March 2013]; Available from: http://www.nanotechproject.org/inventories/consumer/browse/products/fresherlonger_plastic_storage_bags/.
270. *Alusion™ Alumina Powders*. 12 June 2009 [cited 2013 28 March 2013]; Available from: http://www.nanotechproject.org/inventories/consumer/browse/products/alusion_alumina_powders/.
271. Oberdorster, G., Z. Sharp, V. Atudorei, A. Elder, R. Gelein, W. Kreyling, and C. Cox, *Translocation of inhaled ultrafine particles to the brain.* Inhalation Toxicology, 2004. **16**(6-7): p. 437-445.
272. Wick, P., A. Malek, P. Manser, D. Meili, X. Maeder-Althaus, L. Diener, P.-A. Diener, A.

Zisch, H.F. Krug, and U. von Mandach, *Barrier Capacity of Human Placenta for Nanosized Materials.* Environmental Health Perspectives, 2010. **118**(3): p. 432-436.
273. Gagne, F., M. Fortier, L. Yu, H.L. Osachoff, R.C. Skirrow, G. van Aggelen, C. Gagnon, and M. Fournier, *Immunocompetence and alterations in hepatic gene expression in rainbow trout exposed to CdS/CdTe quantum dots.* Journal of Environmental Monitoring, 2010. **12**(8): p. 1556-1565.
274. Park, E.J. and K. Park, *Oxidative stress and pro-inflammatory responses induced by silica nanoparticles in vivo and in vitro.* Toxicology Letters, 2009. **184**(1): p. 18-25.
275. Maynard, A.D., D.B. Warheit, and M.A. Philbert, *The New Toxicology of Sophisticated Materials: Nanotoxicology and Beyond.* Toxicological Sciences, 2011. **120**: p. S109-S129.
276. Fischer, H.C. and W.C.W. Chan, *Nanotoxicity: the growing need for in vivo study.* Current Opinion in Biotechnology, 2007. **18**(6): p. 565-571.
277. Dobrovolskaia, M.A., P. Aggarwal, J.B. Hall, and S.E. McNeil, *Preclinical studies to understand nanoparticle interaction with the immune system and its potential effects on nanoparticle biodistribution.* Molecular Pharmaceutics, 2008. **5**(4): p. 487-495.
278. Geys, J., A. Nemmar, E. Verbeken, E. Smolders, M. Ratoi, M.F. Hoylaerts, B. Nemery, and P.H.M. Hoet, *Acute Toxicity and Prothrombotic Effects of Quantum Dots: Impact of Surface Charge.* Environmental Health Perspectives, 2008. **116**(12): p. 1607-1613.
279. Fowler, B.A., *Monitoring of human populations for early markers of cadmium toxicity: A review.* Toxicology and Applied Pharmacology, 2009. **238**(3): p. 294-300.
280. Satoh, M., H. Koyama, T. Kaji, H. Kito, and C. Tohyama, *Perspectives on cadmium toxicity research.* Tohoku Journal of Experimental Medicine, 2002. **196**(1): p. 23-32.
281. Giaginis, C., E. Gatzidou, and S. Theocharis, *DNA repair systems as targets of cadmium toxicity.* Toxicology and Applied Pharmacology, 2006. **213**(3): p. 282-290.
282. Prozialeck, W.C., J.R. Edwards, and J.M. Woods, *The vascular endothelium as a target of cadmium toxicity.* Life Sciences, 2006. **79**(16): p. 1493-1506.
283. Wade, M.G., S. Parent, K.W. Finnson, W. Foster, E. Younglai, A. McMahon, D.G. Cyr, and C. Hughes, *Thyroid toxicity due to subchronic exposure to a complex mixture of 16 organochlorines, lead, and cadmium.* Toxicological Sciences, 2002. **67**(2): p. 207-218.
284. Spallholz, J.E., *On the Nature of Selenium Toxicity and Carcinostatic Activity.* Free Radical Biology and Medicine, 1994. **17**(1): p. 45-64.
285. Tinggi, U., *Essentiality and toxicity of selenium and its status in Australia: a review.* Toxicology Letters, 2003. **137**(1-2): p. 103-110.
286. Yarema, M.C. and S.C. Curry, *Acute tellurium toxicity from ingestion of metal-oxidizing solutions.* Pediatrics, 2005. **116**(2): p. E319-E321.
287. Schipper, M.L., G. Iyer, A.L. Koh, Z. Cheng, Y. Ebenstein, A. Aharoni, S. Keren, L.A. Bentolila, J.Q. Li, J.H. Rao, X.Y. Chen, U. Banin, A.M. Wu, R. Sinclair, S. Weiss, and S.S. Gambhir, *Particle Size, Surface Coating, and PEGylation Influence the Biodistribution of Quantum Dots in Living Mice.* Small, 2009. **5**(1): p. 126-134.
288. Wang, T.H., H.A. Hsieh, Y.K. Hsieh, C.S. Chiang, Y.C. Sun, and C.F. Wang, *The in vivo biodistribution and fate of CdSe quantum dots in the murine model: a laser ablation inductively coupled plasma mass spectrometry study.* Analytical and Bioanalytical Chemistry, 2012. **404**(10): p. 3025-3036.
289. McGuinnes, C., R. Duffin, S. Brown, N.L. Mills, I.L. Megson, W. MacNee, S. Johnston, S.L. Lu, L. Tran, R.F. Li, X. Wang, D.E. Newby, and K. Donaldson, *Surface Derivatization State of Polystyrene Latex Nanoparticles Determines both Their Potency and Their Mechanism of Causing Human Platelet Aggregation In Vitro.* Toxicological Sciences, 2011. **119**(2): p. 359-368.
290. Mader, S.S., *Human Biology*. 4th ed. 1995: Wm. C. Brown Communications, Inc.
291. Ramasamy, I., *Inherited bleeding disorders: disorders of platelet adhesion and aggregation.* Critical Reviews in Oncology Hematology, 2004. **49**(1): p. 1-35.
292. Jackson, S.P., *The growing complexity of platelet aggregation.* Blood, 2007. **109**(12): p. 5087-5095.
293. Puri, R.N. and R.W. Colman, *ADP-induced platelet activation.* Critical Reviews in Biochemistry and Molecular Biology, 1997. **32**(6): p. 437-502.

294. van Gils, J.M., J.J. Zwaginga, and P.L. Hordijk, *Molecular and functional interactions among monocytes, platelets, and endothelial cells and their relevance for cardiovascular diseases.* Journal of Leukocyte Biology, 2009. **85**(2): p. 195-204.
295. Kamath, S., A.D. Blann, and G.Y.H. Lip, *Platelet activation: assessment and quantification.* European Heart Journal, 2001. **22**(17): p. 1561-1571.
296. Zarbock, A., R.K. Polanowska-Grabowska, and K. Ley, *Platelet-neutrophil-interactions: Linking hemostasis and inflammation.* Blood Reviews, 2007. **21**(2): p. 99-111.
297. Tuttle, H.A., G. Davis-Gorman, S. Goldman, J.G. Copeland, and P.F. McDonagh, *Platelet-neutrophil conjugate formation is increased in diabetic women with cardiovascular disease.* Cardiovascular Diabetology, 2003. **2**.
298. Brown, K.K., P.M. Henson, J. Maclouf, M. Moyle, J.A. Ely, and G.S. Worthen, *Neutrophil-platelet adhesion: Relative roles of platelet P-selectin and neutrophil beta(2) (CD18) integrins.* American Journal of Respiratory Cell and Molecular Biology, 1998. **18**(1): p. 100-110.
299. Jackson, J.K., C.M.K. Springate, W.L. Hunter, and H.M. Burt, *Neutrophil activation by plasma opsonized polymeric microspheres: inhibitory effect of Pluronic F127.* Biomaterials, 2000. **21**(14): p. 1483-1491.
300. Mann, E.E., L.C. Thompson, J.H. Shannahan, and C.J. Wingard, *Changes in cardiopulmonary function induced by nanoparticles.* Wiley Interdisciplinary Reviews-Nanomedicine and Nanobiotechnology, 2012. **4**(6): p. 691-702.
301. Jun, E.A., K.M. Lim, K. Kim, O.N. Bae, J.Y. Noh, K.H. Chung, and J.H. Chung, *Silver nanoparticles enhance thrombus formation through increased platelet aggregation and procoagulant activity.* Nanotoxicology, 2011. **5**(2): p. 157-167.
302. Mills, N.L., H. Tornqvist, S.D. Robinson, M.C. Gonzalez, S. Soderberg, T. Sandstrom, A. Blomberg, D.E. Newby, and K. Donaldson, *Air pollution and atherothrombosis.* Inhalation Toxicology, 2007. **19**: p. 81-89.
303. Labarre, D., *The Interactions between Blood and Polymeric Nanoparticles Depend on the Nature and Structure of the Hydrogel Covering the Surface.* Polymers, 2012. **4**(2): p. 986-996.
304. Yoo, J.W., E. Chambers, and S. Mitragotri, *Factors that Control the Circulation Time of Nanoparticles in Blood: Challenges, Solutions and Future Prospects.* Current Pharmaceutical Design, 2010. **16**(21): p. 2298-2307.
305. Gref, R., A. Domb, P. Quellec, T. Blunk, R.H. Muller, J.M. Verbavatz, and R. Langer, *The controlled intravenous delivery of drugs using PEG-coated sterically stabilized nanospheres.* Advanced Drug Delivery Reviews, 2012. **64**: p. 316-326.
306. Immordino, M.L., F. Dosio, and L. Cattel, *Stealth liposomes: review of the basic science, rationale, and clinical applications, existing and potential.* International Journal of Nanomedicine, 2006. **1**(3): p. 297-315.
307. Amoozgar, Z. and Y. Yeo, *Recent advances in stealth coating of nanoparticle drug delivery systems.* Wiley Interdisciplinary Reviews-Nanomedicine and Nanobiotechnology, 2012. **4**(2): p. 219-233.
308. Neoh, K.G. and E.T. Kang, *Functionalization of inorganic nanoparticles with polymers for stealth biomedical applications.* Polymer Chemistry, 2011. **2**(4): p. 747-759.
309. Jia, H. and S. Titmuss, *Polymer-functionalized nanoparticles: from stealth viruses to biocompatible quantum dots.* Nanomedicine, 2009. **4**(8): p. 951-966.
310. Peracchia, M.T., *Stealth nanoparticles for intravenous administration.* Stp Pharma Sciences, 2003. **13**(3): p. 155-161.
311. Tavano, R., D. Segat, E. Reddi, J. Kos, M. Rojnik, P. Kocbek, S. Iratni, D. Scheglmann, M. Colucci, I.M. Echevarria, F. Selvestrel, F. Mancin, and E. Papini, *Procoagulant properties of bare and highly PEGylated vinyl-modified silica nanoparticles.* Nanomedicine, 2010. **5**(6): p. 881-896.
312. Owens, D.E. and N.A. Peppas, *Opsonization, biodistribution, and pharmacokinetics of polymeric nanoparticles.* International Journal of Pharmaceutics, 2006. **307**(1): p. 93-102.
313. *Lumidot CdSe/ZnS 590 Product Specification Sheet*. [cited 2013 28 March 2013]; Available from:

http://www.sigmaaldrich.com/Graphics/COfAInfo/SigmaSAPQM/SPEC/694622/694622-BULK_____ALDRICH__.pdf.

314. Bagwe, R.P., L.R. Hilliard, and W.H. Tan, *Surface modification of silica nanoparticles to reduce aggregation and nonspecific binding.* Langmuir, 2006. **22**(9): p. 4357-4362.
315. Romero-Cano, M.S., A. Martin-Rodriguez, G. Chauveteau, and F.J. de las Nieves, *Colloidal stabilization of polystyrene particles by adsorption of nonionic surfactant - II. Electrosteric stability studies.* Journal of Colloid and Interface Science, 1998. **198**(2): p. 273-281.
316. Santander-Ortega, M.J., N. Csaba, M.J. Alonso, J.L. Ortega-Vinuesa, and D. Bastos-Gonzalez, *Stability and physicochemical characteristics of PLGA, PLGA : poloxamer and PLGA : poloxamine blend nanoparticles - A comparative study.* Colloids and Surfaces a-Physicochemical and Engineering Aspects, 2007. **296**(1-3): p. 132-140.
317. Ahmed, K., P.W. Muiruri, G.H. Jones, M.J. Scott, and M.N. Jones, *The effect of grafted poly(ethylene glycol) on the electrophoretic properties of phospholipid liposomes and their adsorption to bacterial biofilms.* Colloids and Surfaces a-Physicochemical and Engineering Aspects, 2001. **194**(1-3): p. 287-296.
318. Zhao, W., S. Zhuang, and X.R. Qi, *Comparative study of the in vitro and in vivo characteristics of cationic and neutral liposomes.* International Journal of Nanomedicine, 2011. **6**: p. 3087-3098.
319. Howes, P. and M. Green, *Colloidal and optical stability of PEG-capped and phospholipid-encapsulated semiconducting polymer nanospheres in different aqueous media.* Photochemical & Photobiological Sciences, 2010. **9**(8): p. 1159-1166.
320. Giammarioli, S., C. Filesi, and E. Sanzini, *Oxidative stress markers: specificity and measurement techniques.* Annali dell'Istituto superiore di sanita, 1999. **35**(4): p. 563-76.
321. Ayres, J.G., P. Borm, F.R. Cassee, V. Castranova, K. Donaldson, A. Ghio, R.M. Harrison, R. Hider, F. Kelly, I.M. Kooter, F. Marano, R.L. Maynard, I. Mudway, A. Nel, C. Sioutas, S. Smith, A. Baeza-Squiban, A. Cho, S. Duggan, and J. Froines, *Evaluating the toxicity of airborne particulate matter and nanoparticles by measuring oxidative stress potential - A workshop report and consensus statement.* Inhalation Toxicology, 2008. **20**(1): p. 75-99.
322. Spasojevic, I., *Electron Paramagnetic Resonance - A Powerful Tool of Medical Biochemistry in Discovering Mechanisms of Disease and Treatment Prospects.* Journal of Medical Biochemistry, 2010. **29**(3): p. 175-188.
323. Ramtoola, Z., P. Lyons, K. Keohane, S.W. Kerrigan, B.P. Kirby, and J.G. Kelly, *Investigation of the interaction of biodegradable micro- and nanoparticulate drug delivery systems with platelets.* Journal of Pharmacy and Pharmacology, 2011. **63**(1): p. 26-32.
324. Hoffbrand, A.V. and P.A.H. Moss, *Essential Haematology*. 6th ed. 2011: Wiley - Blackwell. .
325. Magde, D., G.E. Rojas, and P.G. Seybold, *Solvent dependence of the fluorescence lifetimes of xanthene dyes.* Photochemistry and Photobiology, 1999. **70**(5): p. 737-744.
326. *Atto 390 data sheet* [cited 2011 22 November 2011]; Available from: http://www.atto-tec.com/fileadmin/user_upload/Katalog_Flyer_Support/ATTO_390.pdf.
327. Sillen, A. and Y. Engelborghs, *The correct use of "average" fluorescence parameters.* Photochemistry and Photobiology, 1998. **67**(5): p. 475-486.
328. Malvern. *DLS Technical Sheet*. [cited 2013 28 March 2013]; Available from: http://www.malvern.com/common/downloads/campaign/MRK656-01.pdf.
329. Protti, A., A. Sirker, A.M. Shah, and R. Botnar, *Late Gadolinium Enhancement of Acute Myocardial Infarction in Mice at 7T: Cine-FLASH Versus Inversion Recovery.* Journal of Magnetic Resonance Imaging, 2010. **32**(4): p. 878-886.
330. Makowski, M.R., A.J. Wiethoff, U. Blume, F. Cuello, A. Warley, C.H.P. Jansen, E. Nagel, R. Razavi, D.C. Onthank, R.R. Cesati, M.S. Marber, T. Schaeffter, A. Smith, S.P. Robinson, and R.M. Botnar, *Assessment of atherosclerotic plaque burden with an elastin-specific magnetic resonance contrast agent.* Nature Medicine, 2011. **17**(3): p. 383-388.

Appendix 1 Chemical Structures of Some Chemicals Mentioned in the Thesis

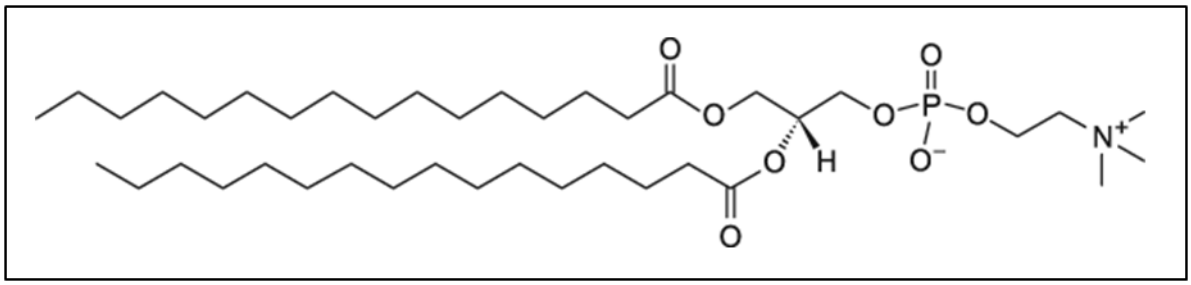

Figure 64 The chemical structure of DPPC.

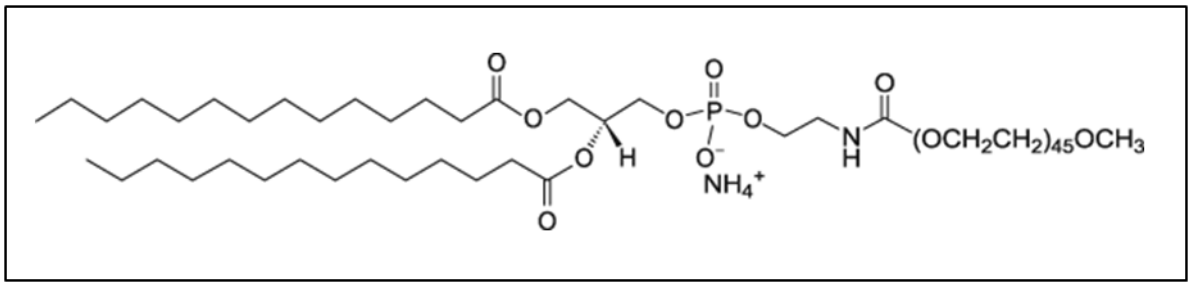

Figure 65 The chemical structure of PEG2000-PE.

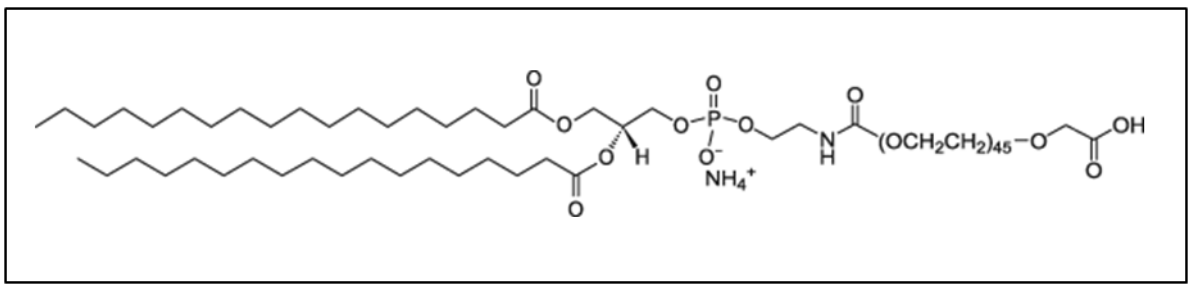

Figure 66 The chemical structure of DSPE-PEG2000.

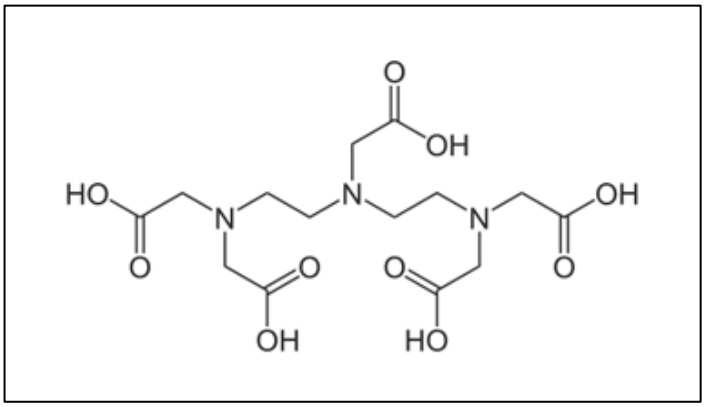

Figure 67 The chemical structure of DTPA.

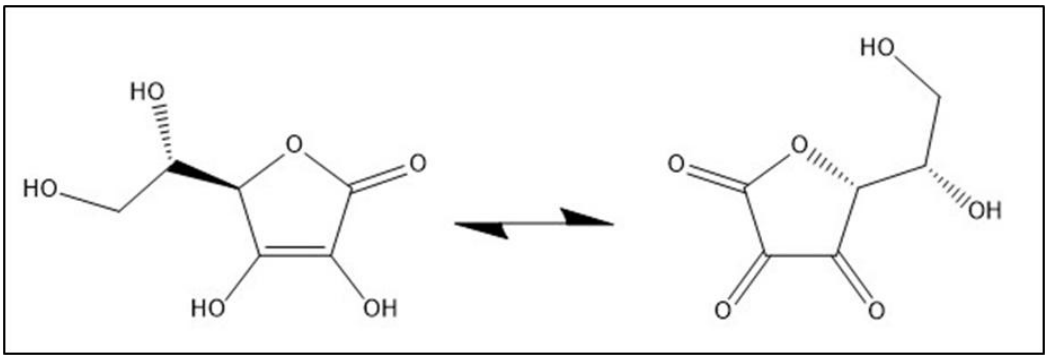

Figure 68 The chemical structure of ascorbic acid (left) and dehydroascorbic acid (right).

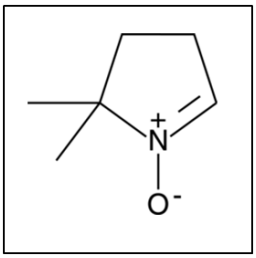

Figure 69 The chemical structure of DMPO.

Appendix 2 Definitions of Some Relevant Biological Terms

Endocytic : able to carry endocytosis.[261]

Endocytosis : is the process by which the surface membrane of a cell, usually with a specific particle bound to its receptor, is invaginated forming a vesicle containing the particle and some extracellular fluid.[261]

Epithelial cell : is the surface cell of skin or mucous membrane.[261]

Phagocytic : able to carry phagocitosis.[261]

Phagocytosis : is a specialised form of endocytosis in which larger particles and cells are engulfed and ingested.[261]

Neutrophil : is a type of leukocyte (i.e. white blood cell) with a lobed nucleus and granular cytoplasm (cytoplasm means: the part of the cell that surrounds the nucleus). Neutrophils have neutrophilic granules, i.e. granules which are neither strongly acidophilic nor strongly basophilic.[261]

Monocyte : is a type of leukocyte (i.e. white blood cell). It is a mature cell of the monocyte/macrophage lineage, and is derived from a promonocyte and matures into a tissue macrophage.[261]

Macrophage : is the end cell of a monocyte/macrophage lineage. It is found mainly in tissues and is phagocytic, acting as a defence cell against infection.[261]